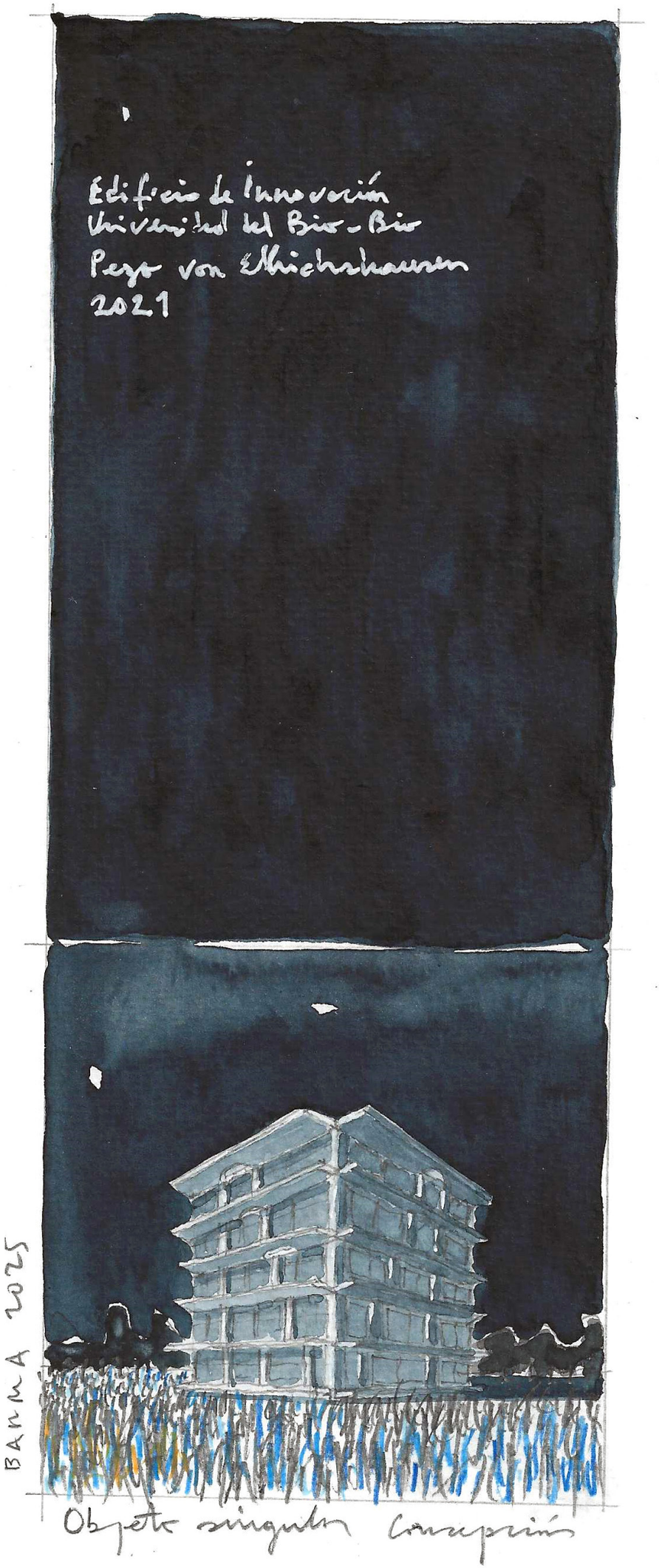


HS

Revista Hábitat Sustentable

ISSN 0719 - 0700
Vol. 16 N°. 1
jun
2026

UNIVERSIDAD DEL BIO BIO



Revista Hábitat Sustentable

ISSN 0719 - 0700
Vol. 16 N°. 1
junio
2026



UNIVERSIDAD DEL BIO BIO

HS REVISTA HÁBITAT SUSTENTABLE V16N1
Revista del Departamento Diseño y Teoría de la Arquitectura
Universidad del Bío-Bío, Concepción, Chile

ISSN 0719-6466 versión online

RECTOR:
BENITO UMAÑA HERMOSILLA

DECANO FACULTAD DE ARQUITECTURA, CONSTRUCCIÓN Y DISEÑO:
HERNÁN BARRÍA CHATEAU

EDITORA RESPONSABLE:
Maureen Trebilcock-Kelly / Departamento Diseño y Teoría de la Arquitectura, Universidad del Bío-Bío, Concepción, Chile
mtrebilc@ubiobio.cl

Rafael López-Guerrero / Departamento Ciencias de la Construcción, Universidad del Bío-Bío, Concepción, Chile
rlopez@ubiobio.cl

PRODUCTORA EDITORIAL:
JOCELYN VIDAL RAMOS / Facultad de Arquitectura, Construcción y Diseño, Universidad del Bío-Bío, Concepción, Chile
javidal@ubiobio.cl

ASISTENTE EDITORIAL:
Arq. ALMENDRA ÁLVAREZ RÍOS / Facultad de Arquitectura, Construcción y Diseño, Universidad del Bío-Bío, Concepción, Chile
calvarezr@ubiobio.cl

CORRECIÓN DE ESTILO:
TANIA VIDAL RAMOS

GESTIÓN INFORMÁTICA:
KARINA LEIVA / Universidad del Bío-Bío, Chile

DIRECTOR DE ARTE Y DIAGRAMACIÓN:
IGNACIO A. SÁEZ ARANEDA

CONSEJO EDITORIAL:
Dra. M° BEATRIZ PIDERIT MORENO / Departamento de Teoría y Diseño de la Arquitectura, Facultad de Arquitectura, Construcción y Diseño, Universidad del Bío - Bío, Concepción, Chile
Dr. RODRIGO GARCÍA ALVARADO / Universidad del Bío-Bío, Concepción, Chile
Dra. NINA HORMAZÁBAL / Universidad Técnica Federico Santa María, Valparaíso, Chile
Dr. WALDO BUSTAMANTE / Pontificia Universidad Católica de Chile, Santiago, Chile
Dr. ERNESTO KUCHEN / Instituto Regional de Planeamiento y Hábitat, San Juan, Argentina
Dra. CRISTINA ENGEL DE ALVAREZ / Universidade Federal do Espírito Santo, Brasil
Dr. OLAVO ESCORCIA OYOLA / Universidad Nacional de Colombia, Bogotá, Colombia
Dr. ALEXANDER GONZÁLEZ CASTAÑO / Universidad Pontificia Bolivariana de Medellín, Universidad Nacional de Colombia Sede Medellín, Colombia
Dr. CARLOS RUBIO-BELLIDO / Universidad de Sevilla, Sevilla, España
Dra. MARÍA DEL PILAR MERCADER MOYANO / Universidad de Sevilla, Sevilla, España
Dr. VICENTE FLORES ALÉS / Universidad de Sevilla, Sevilla, España
Dr. FLAVIO CELIS D'AMICO / Universidad de Alcalá, Madrid, España
Dr. ERNESTO ECHEVERRÍA VALIENTE / Universidad de Alcalá, Madrid, España

TRADUCCIONES:
KEVIN WRIGHT

PORTADA:
HERNAN BARRIA CHATEAU
/ Acuarela Dos torres y un sendero, Azocar Catrón, 2016

DIRECCIÓN:
Avda. Collao 1202
CP: 4081112. Concepción, Chile
TEL.(56-41)3111409

Revista **HS** indexada en Scopus, SciELO, ERIHPLUS, Emerging Source Citation Index de Clarivate Analytics, Latindex Catálogo 2.0, Avery Index, DOAJ, Dialnet, Redib, EBSCO, Rebiun, JornalTOcs y ARLA.
HS se adhiere a la Declaración de San Francisco Sobre la Evaluación de la Investigación (DORA).

Los criterios expuestos en los artículos son de exclusiva responsabilidad de sus autores y no reflejan necesariamente la opinión de la dirección de la revista.

Revista Hábitat Sustentable es editada por el Facultad de Arquitecturas Construcción y Diseño de la Universidad del Bío-Bío, es financiada por el Fondo de Publicaciones Periódicas de la Vicerrectoría Académica, la Dirección General de Investigación, Desarrollo e Innovación y la Dirección de Postgrado de la Universidad del Bío-Bío junto al Programa de Información Científica Concurso Fondos de Publicación de Revistas Científicas 2018 Proyecto Código: FP180007

04 EDITORIAL
Maureen Trebilcock-Kelly , Rafael Eduardo López-Guerrero

10 CARACTERIZACIÓN TÉRMICA DEL ENTORNO UNIVERSITARIO PARA LA PLANIFICACIÓN DE INFRAESTRUCTURA VERDE
Walter Ávila-Ruiz, Carlos Salazar-Briones, José Ruiz-Gibert, Juan Saiz-Rodríguez, Marcelo Lomelí-Banda

24 IMPLEMENTACIÓN DE UN SISTEMA PASIVO DE DESHUMIDIFICACIÓN BASADO EN LA TECNOLOGÍA DEL ATRAPANIEBLAS EN VILLA MARÍA DEL TRIUNFO - LIMA, PERÚ
Milagros Delgado-Peña, Alonzo Cardenas-Vera-Pinto, Richard Valdivia-Sisniegas

42 DISEÑO DE SISTEMA INDIRECTO DE FACHADA VERDE PARA MEJORAR EL CONFORT TÉRMICO EN VIVIENDAS MULTIFAMILIARES
Analucia Espinoza-Abarca, Alis Tasayco-Huanca, Victor Miranda-Alfaro

56 OPTIMIZACIÓN DEL CONFORT TÉRMICO DE UNA CASA ECOLOGICA: MODELAMIENTO EN OPEN FOAM DE MUROS SANDWICH CON AISLANTE DE ICHU (STIPA ICHU)
Henry Javier-Ninahuaman, Kenny Montalvo-Morales, Jose Rojas-Guillén, Grimaldo Quispe-Santivañez

70 CHAKIÑAN: RECUPERACIÓN DE INFRAESTRUCTURA ANCESTRAL Y GESTIÓN DEL TERRITORIO VIVO EN LA COMUNIDAD DE LAS LAGUNAS, SARAGURO
Flor Lozano-Guamán, Angel Lozano-Guamán

96 EVALUACIÓN SOCIOESPACIAL DE LA POBREZA ENERGÉTICA Y SU DIMENSIÓN DE GÉNERO EN ÁREAS VULNERABLES DE GRANADA
Susana Clavijo-Núñez, Antonio Aguilar-Aguilera, María De-la-Hoz-Torres, Antonio Serrano-Jiménez,David Bienvenido-Huertas

108 FIELD-VALIDATED PARAMETRIC ANALYSIS OF OUTDOOR THERMAL COMFORT IN PARKING ENVIRONMENTS IN TIRUCHIRAPPALLI, INDIA
Amalan-Sigmund Kaushik-S., Gopalakrishnan Padmanaban, Subbaiyan Gnanasambandam

126 SHADING THE GLASS FAÇADE: TEXTILE MEMBRANE STRATEGIES FOR EARLY-STAGE DESIGN FOR ENERGY EFFICIENCY OF OFFICE BUILDINGS IN HOT–HUMID CLIMATES
Chandrasekaran Chockalingam, Madhu Mathi Anbu, Mase Noguchi

142 HERMETICIDAD AL AIRE DE VIVIENDAS PRECARIAS EN BARRIOS INFORMALES DE LIMA
Martín Wieser, Ronald Mas, Enrique Barrantes, Enrique Mejía-Solis, Alessandra Gonzales, Jimena Valdivia, Luis-Ricardo Chirinos-García

156 EVALUACIÓN TÉRMICA COMPARATIVA DE UNA ESTRUCTURA DE SOMBREADO VEGETAL Y UNA MALLA DE SOMBREADO ARTIFICIAL
Nelson Arias-Jiménez, Rodrigo Figueroa-San-Martín, Diego Cárdenas-Merino

Editorial
Maureen Trebilcock-Kelly , Rafael Eduardo López-Guerrero
Revista Hábitat Sustentable Vol. 16, N°. 1. ISSN 0719 - 0700 / Págs. 04 -09
https://doi.org/10.22320/07190700.2026.16.01.00

EDITORIAL

PANORAMA TECNOLÓGICO PARA LA SUSTENTABILIDAD DEL AMBIENTE CONSTRUIDO: UNA VISIÓN EDITORIAL

La industria de la arquitectura, ingeniería y construcción (AEC) atraviesa un cambio de paradigma impulsado por la necesidad crítica de mitigar el cambio climático. Actualmente, el sector de la edificación es responsable de aproximadamente el 34% del consumo de energía global y del 37% de las emisiones de CO2 relacionadas con la energía (Ahmed et al., 2026; Oliveira et al., 2026). Ante este escenario, la sustentabilidad ya no puede ser un objetivo periférico o un mero cumplimiento normativo; debe constituir el núcleo del diseño, la construcción y la operación, gestionada a través de tecnologías emergentes que permitan una precisión y eficiencia sin precedentes (Manzoor et al., 2025).

Una de las transformaciones más significativas ocurre en la fase de diseño mediante la optimización multi-objetivo. El diseño de edificios sustentables es inherentemente complejo debido a la interacción de factores como el clima local, las propiedades de la envolvente y el comportamiento del usuario. Tradicionalmente, las simulaciones detalladas de desempeño térmico o lumínico han sido costosas en términos computacionales y de tiempo. Sin embargo, la literatura reciente destaca el uso de modelos subrogados (surrogate models) basados en Machine Learning, los cuales permiten aproximar el comportamiento de simulaciones complejas a una fracción del costo temporal (Cruz et al., 2024; Mihalakakou et al., 2025). Esta capacidad facilita la exploración de espacios de diseño masivos para encontrar soluciones óptimas que equilibren funciones a menudo contrapuestas, como el confort térmico, la eficiencia energética y el costo de ciclo de vida (Cruz et al., 2024).

El enfoque de la eficiencia energética ha evolucionado de análisis estáticos hacia modelos dinámicos de ciclo de vida. El aprendizaje automático se aplica ahora en todas las fases del ciclo edilicio, desde la concepción y la construcción hasta la operación y el retrofit (Kaya et al., 2025). En este contexto, algoritmos como las Redes Neuronales Artificiales y las Máquinas de Soporte de Vectores se han consolidado como herramientas robustas para predecir el consumo de energía y las condiciones de confort, superando las limitaciones de los métodos estadísticos tradicionales (Ahmed et al., 2026; Kaya et al., 2025). Asimismo, el acoplamiento de técnicas de simulación con algoritmos metaheurísticos, como los algoritmos genéticos y la optimización por enjambre de partículas, permite reducir sustancialmente tanto las emisiones de gases de efecto invernadero como los costos operativos (Mihalakakou et al., 2025).

En el ámbito de la gestión energética operativa, la Inteligencia Artificial (IA) juega un papel revolucionario en el control en tiempo real. Tecnologías como las Redes Neuronales Transformer, que utilizan mecanismos de auto-atención para capturar dependencias temporales complejas en los datos de sensores, han demostrado ser altamente efectivas para el pronóstico de carga a corto y mediano plazo (Ahmed et al., 2026). Estos sistemas integrados pueden lograr reducciones de hasta un 50% en la utilización de energía, optimizando sistemas de calefacción, ventilación y aire acondicionado (HVAC) sin sacrificar el bienestar del ocupante (Ahmed et al., 2026; Qiu et al., 2025). La convergencia de estos modelos con el Internet de las Cosas (IoT) y las redes inteligentes (smart grids) permite que los edificios dejen de ser consumidores pasivos para convertirse en participantes activos y flexibles en la red eléctrica (Bibri & Huang, 2025).

La envolvente del edificio, como mediadora fundamental entre el interior y el exterior, es otro foco de innovación tecnológica disruptiva. Las envolventes adaptativas y las fachadas inteligentes, que integran sistemas fotovoltaicos, sistemas de doble piel y materiales avanzados como aerogeles, vidrios electrocrómicos o termocrómicos, tienen el potencial de reducir las cargas térmicas de forma dinámica (Tahmasbi et al., 2025). Complementariamente, el uso de materiales de cambio de fase (PCM) y tecnologías de enfriamiento radiativo pasivo contribuyen a estabilizar las temperaturas internas, permitiendo ahorros energéticos significativos y facilitando el camino hacia los edificios de energía cero (Qiu et al., 2025; Tahmasbi et al., 2025). Incluso elementos de infraestructura verde, como los techos verdes, están siendo optimizados mediante modelos de aprendizaje profundo para maximizar no solo el ahorro energético, sino también la retención de agua de lluvia y la biodiversidad urbana (Mihalakakou et al., 2026).

La sostenibilidad del ambiente construido exige también una transición ineludible hacia la economía circular. Tecnologías de la Industria 4.0 introducen el concepto de "Edificios como Bancos de Materiales" (BAMB), donde el Modelado de Información de Construcción (BIM) se utiliza para rastrear y gestionar los componentes edilicios a lo largo de su vida útil (Oliveira et al., 2026). La integración de Blockchain y Pasaportes de Materiales asegura la trazabilidad y facilita la reutilización y el reciclaje al final de la vida útil, minimizando los residuos de construcción y demolición (Oliveira et al., 2026). Además, se han desarrollado sistemas robóticos operados por Deep Learning para la clasificación de residuos con una pureza promedio del 97%, haciendo viable económicamente la recuperación de recursos en la industria (Oliveira et al., 2026).

En una escala urbana y sistémica, el uso de Gemelos Digitales (Digital Twins) emerge como una herramienta poderosa. Estas réplicas virtuales permiten la monitorización predictiva del carbono y la optimización del entorno construido dentro del marco de las ciudades inteligentes (Bibri & Huang, 2025). Los Gemelos Digitales facilitan la creación de distritos de energía positiva y refuerzan la resiliencia ante desastres climáticos mediante el análisis de Big Data y simulaciones de escenarios futuros (Bibri & Huang, 2025). La resiliencia, de hecho, se ha vuelto un pilar central del diseño contemporáneo; las herramientas de diseño paramétrico y generativo deben integrar no solo métricas técnicas, sino también perspectivas de identidad cultural y necesidades sociales para asegurar que las viviendas sean equitativas y coherentes con su contexto (Kumar et al., 2026).

A pesar de estas promesas, persisten desafíos significativos para la adopción masiva de estas tecnologías. Los altos costos iniciales de inversión y la falta de marcos regulatorios estandarizados siguen siendo barreras críticas (Manzoor et al.,

2025). Asimismo, existe una necesidad imperativa de mayor transparencia y ética en el manejo de datos; la comunidad investigadora debe promover la disponibilidad de códigos y bases de datos abiertos para evitar los sesgos en los modelos de IA y asegurar la replicabilidad de los hallazgos científicos (Cruz et al., 2024; Oliveira et al., 2026).

En conclusión, la integración de IA, Machine Learning, Digital Twins y procesos avanzados de simulación no es simplemente una opción de vanguardia, sino una necesidad para crear un hábitat verdaderamente sustentable. Estas tecnologías proporcionan las herramientas necesarias para transitar de una construcción fragmentada a una gestión holística, circular y resiliente del ambiente construido. Invitamos a la comunidad científica a continuar explorando estas fronteras tecnológicas, manteniendo siempre el rigor científico y el compromiso ético que la crisis ambiental global nos demanda.

REFERENCIAS BIBLIOGRÁFICAS

Abu Jadayil, W., Alkhedher, M., Shwaheen, G., & Ramadan, M. (2026). Sustainable and efficient use of integrated technology solutions in energy management. *Energy Reports, 15*, 109319. https://doi.org/10.1016/j.egyr.2026.109319

Ahmed, N., Ding, Y., Canti, G., & Anglani, N. (2026). Sustainable building's energy management with artificial intelligence and machine learning: A decadal scoping review (2014–2024). *Energy Reports, 15*, 109082. https://doi.org/10.1016/j.egyr.2026.109082

Bibri, S. E., & Huang, J. (2025). Artificial intelligence and digital twins for environmentally sustainable smart buildings: A comprehensive systematic review. *Environmental Science and Ecotechnology, 28*, 100628. https://doi.org/10.1016/j.ese.2025.100628

Cruz, A. S., Caldas, L. R., Mendes, V. M., Mendes, J. C., & Bastos, L. E. G. (2024). Multi-objective optimization based on surrogate models for sustainable building design: A systematic literature review. *Building and Environment, 266*, 112147. https://doi.org/10.1016/j.buildenv.2024.112147

Kaya, G. N., Beyhan, F., Ilerisoy, Z. Y., & Cudzik, J. (2025). Evaluation of machine learning applications in building life cycle processes for energy efficiency: A systematic review. *Energy Reports, 13*, 4900–4916. https://doi.org/10.1016/j.egyr.2025.04.034

Kumar, R., Dekin, A., Prince, M., Froese, T., & Mukhopadhyaya, P. (2026). Integrated building form and structural strategies for sustainable and resilient residential buildings. *Sustainable Cities and Society: Advances, 2*, 100075. https://doi.org/10.1016/j.scsadv.2026.100075

Manzoor, B., Antwi-Afari, M. F., & Alotaibi, K. S. (2025). Green buildings and digital technologies: A pathway to sustainable development. *Green Technologies and Sustainability, 3*, 100243. https://doi.org/10.1016/j.grets.2025.100243

Mihalakakou, G., Giannadakis, A., Malefaki, S., Souliotis, M., Georgiou, P., Romaios, A., Antzoulatou, A., Nikolakopoulos, P., & Paravantis, J. A. (2025). Coupling simulation-based and machine learning methodologies for energy optimization and environmental impact mitigation in buildings. *Journal of Building Engineering, 112*, 113809. https://doi.org/10.1016/j.jobe.2025.113809

Mihalakakou, G., Romeos, A., Malefaki, S., Souliotis, M., Paravantis, J. A., Georgiou, P., & Giannadakis, A. (2026). From simulation to surrogates: optimizing green roofs for sustainable urban performance. *Sustainable Cities and Society, 145*, 107439. https://doi.org/10.1016/j.scs.2026.107439

Oliveira, J., Schreiber, D., & Jahno, V. D. (2026). Sustainability in civil construction through industry 4.0 and BIM technologies. *Automation in Construction, 182*, 106729. https://doi.org/10.1016/j.autcon.2025.106729

Qiu, L., Li, H., Wang, Z., Yang, Y., Lazarus, G. A., Chen, Y., & Feng, Y. (2025). Pathways to decarbonizing buildings: Harnessing energy efficiency and sustainable technologies. *Thermal Science and Engineering Progress, 66*, 103991. https://doi.org/10.1016/j.tsep.2025.103991

Tahmasbi, F., Khdair, A. I., Aburumman, G. A., Tahmasebi, M., Thi, N. H., & Afrand, M. (2025). Energy-efficient building façades: A comprehensive review of innovative technologies and sustainable strategies. *Journal of Building Engineering, 99*, 111643. https://doi.org/10.1016/j.jobe.2024.111643

Editorial
Maureen Trebilcock-Kelly , Rafael Eduardo López-Guerrero
Revista Hábitat Sustentable Vol. 16, N°. 1. ISSN 0719 - 0700 / Págs. 04 -09
https://doi.org/10.22320/07190700.2026.16.01.00

EDITORIAL

TECHNOLOGICAL OUTLOOK FOR THE BUILT ENVIRONMENT'S SUSTAINABILITY: AN EDITORIAL VIEW

The architecture, engineering, and construction (AEC) industry is going through a paradigm shift driven by the critical need to mitigate climate change. Currently, the building sector is responsible for approximately 34% of global energy consumption and 37% of energy-related CO_2 emissions (Ahmed et al., 2026; Oliveira et al., 2026). Faced with this scenario, sustainability can no longer be a peripheral objective or a mere regulatory compliance requirement; it must constitute the core of design, construction, and operation, managed through emerging technologies that provide unprecedented precision and efficiency (Manzoor et al., 2025).

One of the most significant transformations occurs in the design phase through multi-objective optimization. The design of sustainable buildings is inherently complex due to interactions among factors such as the local climate, the properties of the envelope, and user behavior. Traditionally, detailed thermal or light performance simulations have been costly both computationally and time-consuming. However, recent literature highlights the use of Machine Learning-based surrogate models, which enable the approximation of complex simulations' behavior in a fraction of the time and cost (Cruz et al., 2024; Mihalakakou et al., 2025). This capability facilitates the exploration of massive design spaces to find optimal solutions that balance often-conflicting functions such as thermal comfort, energy efficiency, and life-cycle cost (Cruz et al., 2024).

The energy-efficiency approach has evolved from static analyses to dynamic life-cycle models. Machine learning is now applied in all phases of the building cycle, from conception and construction to operation and retrofit (Kaya et al., 2025). In this context, algorithms such as Artificial Neural Networks and Vector Support Machines have established themselves as robust tools for predicting energy consumption and comfort conditions, overcoming the limitations of traditional statistical methods (Ahmed et al., 2026; Kaya et al., 2025). The coupling of simulation techniques with metaheuristic algorithms, such as genetic algorithms and particle swarm optimization, also produces substantial reductions in both greenhouse gas emissions and operating costs (Mihalakakou et al., 2025).

In the field of operational energy management, Artificial Intelligence (AI) plays a revolutionary role in real-time control. Technologies such as Transformer Neural Networks, which use self-attention mechanisms to capture complex temporal dependencies in sensor data, have proven highly effective for short- and medium-term load forecasting (Ahmed et al., 2026). These integrated systems can achieve up to 50% reductions in energy use, optimizing heating, ventilation, and air conditioning (HVAC) systems without compromising occupant well-being (Ahmed et al., 2026; Qiu et al., 2025). The convergence of these models with the Internet of Things (IoT) and smart grids enables buildings to move from passive consumers to active, flexible participants in the electricity grid (Bibri & Huang, 2025).

The building envelope, as a fundamental mediator between interior and exterior, is another focus of disruptive technological innovation. Adaptive envelopes and smart facades, which integrate photovoltaic systems, double-skin systems, and advanced materials such as aerogels, electrochromic or thermochromic glasses, have the potential to dynamically reduce thermal loads (Tahmasbi et al., 2025). In addition, the use of phase change materials (PCMs) and passive radiative cooling technologies helps stabilize indoor temperatures, producing significant energy savings and facilitating the path to zero-energy buildings (Qiu et al., 2025; Tahmasbi et al., 2025). Even green infrastructure elements, such as green roofs, are being optimized using deep learning models to maximize not only energy savings but also rainwater retention and urban biodiversity (Mihalakakou et al., 2026).

The sustainability of the built environment also requires an inescapable transition to the circular economy. Industry 4.0 technologies introduce the concept of "Buildings as Material Banks" (BAMB), where Building Information Modeling (BIM) is used to track and manage building components throughout their useful life (Oliveira et al., 2026). The integration of Blockchain and Material Passports ensures traceability and facilitates reuse and recycling at the end of the useful life, minimizing construction and demolition waste (Oliveira et al., 2026). In addition, robotic systems powered by Deep Learning have been developed to classify waste with an average purity of 97%, making resource recovery in industry economically viable (Oliveira et al., 2026).

At the urban and systemic scales, Digital Twins emerge as a powerful tool. These virtual replicas allow predictive carbon monitoring and optimization of the built environment within the framework of smart cities (Bibri & Huang, 2025). Digital Twins facilitate the creation of positive energy districts and strengthen resilience to climate disasters through Big Data analysis and simulations of future scenarios (Bibri & Huang, 2025). Resilience, in fact, has become a central pillar of contemporary design; parametric and generative design

tools must integrate not only technical metrics but also cultural identity perspectives and social needs to ensure that housing is equitable and coherent with its context (Kumar et al., 2026).

Despite these promises, significant challenges remain for the mass adoption of these technologies. High initial investment costs and lack of standardized regulatory frameworks remain critical barriers (Manzoor et al., 2025). There is also an urgent need for greater transparency and ethical practices in data management; the research community must promote the availability of open-source code and datasets to avoid biases in AI models and ensure the replicability of scientific findings (Cruz et al., 2024; Oliveira et al., 2026).

In conclusion, the integration of AI, Machine Learning, Digital Twins, and advanced simulation processes is not simply a cutting-edge option but a necessity for creating a truly sustainable habitat. These technologies provide the necessary tools to move from a fragmented construction to a holistic, circular, and resilient management of the built environment. We invite the scientific community to continue exploring these technological frontiers, always maintaining the scientific rigor and ethical commitment that the global environmental crisis demands of us.

BIBLIOGRAPHIC REFERENCES

Abu Jadayil, W., Alkhedher, M., Shwaheen, G., & Ramadan, M. (2026). Sustainable and efficient use of integrated technology solutions in energy management. *Energy Reports, 15*, 109319. https://doi.org/10.1016/j.egyr.2026.109319

Ahmed, N., Ding, Y., Canti, G., & Anglani, N. (2026). Sustainable building's energy management with artificial intelligence and machine learning: A decadal scoping review (2014–2024). *Energy Reports, 15*, 109082. https://doi.org/10.1016/j.egyr.2026.109082

Bibri, S. E., & Huang, J. (2025). Artificial intelligence and digital twins for environmentally sustainable smart buildings: A comprehensive systematic review. *Environmental Science and Ecotechnology, 28*, 100628. https://doi.org/10.1016/j.ese.2025.100628

Cruz, A. S., Caldas, L. R., Mendes, V. M., Mendes, J. C., & Bastos, L. E. G. (2024). Multi-objective optimization based on surrogate models for sustainable building design: A systematic literature review. *Building and Environment, 266*, 112147. https://doi.org/10.1016/j.buildenv.2024.112147

Kaya, G. N., Beyhan, F., Ilerisoy, Z. Y., & Cudzik, J. (2025). Evaluation of machine learning applications in building life cycle processes for energy efficiency: A systematic review. *Energy Reports, 13*, 4900–4916. https://doi.org/10.1016/j.egyr.2025.04.034

Kumar, R., Dekin, A., Prince, M., Froese, T., & Mukhopadhyaya, P. (2026). Integrated building form and structural strategies for sustainable and resilient residential buildings. *Sustainable Cities and Society: Advances, 2*, 100075. https://doi.org/10.1016/j.scsadv.2026.100075

Manzoor, B., Antwi-Afari, M. F., & Alotaibi, K. S. (2025). Green buildings and digital technologies: A pathway to sustainable development. *Green Technologies and Sustainability, 3*, 100243. https://doi.org/10.1016/j.grets.2025.100243

Mihalakakou, G., Giannadakis, A., Malefaki, S., Souliotis, M., Georgiou, P., Romaios, A., Antzoulatou, A., Nikolakopoulos, P., & Paravantis, J. A. (2025). Coupling simulation-based and machine learning methodologies for energy optimization and environmental impact mitigation in buildings. *Journal of Building Engineering, 112*, 113809. https://doi.org/10.1016/j.jobe.2025.113809

Mihalakakou, G., Romeos, A., Malefaki, S., Souliotis, M., Paravantis, J. A., Georgiou, P., & Giannadakis, A. (2026). From simulation to surrogates: optimizing green roofs for sustainable urban performance. *Sustainable Cities and Society, 145*, 107439. https://doi.org/10.1016/j.scs.2026.107439

Oliveira, J., Schreiber, D., & Jahno, V. D. (2026). Sustainability in civil construction through industry 4.0 and BIM technologies. *Automation in Construction, 182*, 106729. https://doi.org/10.1016/j.autcon.2025.106729

Qiu, L., Li, H., Wang, Z., Yang, Y., Lazarus, G. A., Chen, Y., & Feng, Y. (2025). Pathways to decarbonizing buildings: Harnessing energy efficiency and sustainable technologies. *Thermal Science and Engineering Progress, 66*, 103991. https://doi.org/10.1016/j.tsep.2025.103991

Tahmasbi, F., Khdair, A. I., Aburumman, G. A., Tahmasebi, M., Thi, N. H., & Afrand, M. (2025). Energy-efficient building façades: A comprehensive review of innovative technologies and sustainable strategies. *Journal of Building Engineering, 99*, 111643. https://doi.org/10.1016/j.jobe.2024.111643

Editorial
Maureen Trebilcock-Kelly , Rafael Eduardo López-Guerrero
Revista Hábitat Sustentable Vol. 16, N°. 1. ISSN 0719 - 0700 / Págs. 04 -09
https://doi.org/10.22320/07190700.2026.16.01.00

EDITORIAL

PANORAMA TECNOLÓGICO PARA A SUSTENTABILIDADE DO AMBIENTE CONSTRUÍDO: UMA VISÃO EDITORIAL

A indústria da arquitetura, engenharia e construção (AEC) atravessa uma mudança de paradigma impulsionada pela necessidade crítica de mitigar as mudanças climáticas. Atualmente, o setor da edificação é responsável por aproximadamente 34% do consumo global de energia e por 37% das emissões de CO_2 associadas à energia (Ahmed et al., 2026; Oliveira et al., 2026). Diante desse cenário, a sustentabilidade já não pode ser um objetivo periférico ou um mero cumprimento normativo; ela deve constituir o núcleo do projeto, da construção e da operação, sendo gerida por meio de tecnologias emergentes que proporcionem precisão e eficiência sem precedentes (Manzoor et al., 2025).

Uma das transformações mais significativas ocorre na fase de projeto, por meio da otimização multiobjetivo. O projeto de edifícios sustentáveis é inerentemente complexo devido à interação entre fatores como o clima local, as propriedades da envoltória e o comportamento do usuário. Tradicionalmente, as simulações detalhadas de desempenho térmico ou lumínico têm sido dispendiosas em termos computacionais e de tempo. Contudo, a literatura recente destaca o uso de modelos substitutos (*surrogate models*) baseados em *Machine Learning*, que permitem aproximar o comportamento de simulações complexas a uma fração do custo temporal (Cruz et al., 2024; Mihalakakou et al., 2025). Essa capacidade facilita a exploração de espaços de projeto em larga escala, em busca de soluções ideais que equilibrem funções muitas vezes contrapostas, como o conforto térmico, a eficiência energética e o custo do ciclo de vida (Cruz et al., 2024).

A abordagem da eficiência energética evoluiu das análises estáticas para modelos dinâmicos de ciclo de vida. O aprendizado de máquina é atualmente aplicado em todas as fases do ciclo edilício, desde a concepção e a construção até a operação e o *retrofit* (Kaya et al., 2025). Nesse contexto, algoritmos como as Redes Neurais Artificiais e as Máquinas de Vetores de Suporte consolidaram-se como ferramentas robustas para prever o consumo de energia e as condições de conforto, superando as limitações dos métodos estatísticos tradicionais (Ahmed et al., 2026; Kaya et al., 2025). Da mesma forma, o acoplamento de técnicas de simulação a algoritmos meta-heurísticos, como os algoritmos genéticos e a otimização por enxame de partículas, permite reduzir substancialmente tanto as emissões de gases de efeito estufa quanto os custos operacionais (Mihalakakou et al., 2025).

No âmbito da gestão energética operacional, a Inteligência Artificial (IA) desempenha um papel revolucionário no controle em tempo real. Tecnologias como as Redes Neurais *Transformer*, que utilizam mecanismos de autoatenção para capturar dependências temporais complexas nos dados de sensores, mostraram-se altamente eficazes para a previsão de carga de curto e médio prazo (Ahmed et al., 2026). Esses sistemas integrados podem alcançar reduções de até 50% no consumo de energia, otimizando os sistemas de aquecimento, ventilação e ar-condicionado (HVAC) sem sacrificar o bem-estar dos ocupantes (Ahmed et al., 2026; Qiu et al., 2025). A convergência desses modelos com a Internet das Coisas (IoT) e as redes inteligentes (*smart grids*) permite que os edifícios deixem de ser consumidores passivos e se tornem participantes ativos e flexíveis na rede elétrica (Bibri & Huang, 2025).

A envoltória do edifício, como mediadora fundamental entre o interior e o exterior, é outro foco de inovação tecnológica disruptiva. As envoltórias adaptativas e as fachadas inteligentes, que integram sistemas fotovoltaicos, sistemas de dupla pele e materiais avançados, como aerogéis, vidros eletrocrômicos ou termocrômicos, têm potencial para reduzir as cargas térmicas de forma dinâmica (Tahmasbi et al., 2025). De modo complementar, o uso de materiais de mudança de fase (PCM) e de tecnologias de resfriamento radiativo passivo contribui para estabilizar as temperaturas internas, permitindo economias energéticas significativas e facilitando o caminho rumo aos edifícios de energia zero (Qiu et al., 2025; Tahmasbi et al., 2025). Até mesmo elementos de infraestrutura verde, como os telhados verdes, vêm sendo otimizados por meio de modelos de aprendizado profundo para maximizar não apenas a economia energética, mas também a retenção de águas pluviais e a biodiversidade urbana (Mihalakakou et al., 2026).

A sustentabilidade do ambiente construído exige também uma transição incontornável rumo à economia circular. Tecnologias da Indústria 4.0 introduzem o conceito de "Edifícios como Bancos de Materiais" (BAMB), no qual a Modelagem da Informação da Construção (BIM) é utilizada para rastrear e gerir os componentes edilícios ao longo de sua vida útil (Oliveira et al., 2026). A integração de *Blockchain* e Passaportes de Materiais assegura a rastreabilidade e facilita a reutilização e a reciclagem ao final da vida útil, minimizando os resíduos de construção e demolição (Oliveira et al., 2026). Além disso, foram desenvolvidos sistemas robóticos operados por *Deep Learning* para a triagem de resíduos, com uma pureza média de 97%, tornando economicamente viável a recuperação de recursos na indústria (Oliveira et al., 2026).

Em uma escala urbana e sistêmica, o uso de Gêmeos Digitais (*Digital Twins*) desponta como uma ferramenta poderosa. Essas réplicas virtuais permitem o monitoramento preditivo do carbono e a otimização do ambiente construído no âmbito das cidades inteligentes (Bibri & Huang, 2025). Os Gêmeos Digitais facilitam a criação de distritos de energia positiva e reforçam a resiliência frente a desastres climáticos por meio da análise de *Big Data* e de simulações de cenários futuros (Bibri & Huang, 2025). A resiliência, de fato, tornou-se um pilar central do projeto contemporâneo; as ferramentas de projeto paramétrico e generativo devem integrar não apenas métricas técnicas, mas também perspectivas de identidade cultural e necessidades sociais, a fim de assegurar que as habitações sejam equitativas e coerentes com seu contexto (Kumar et al., 2026).

Apesar dessas promessas, persistem desafios significativos para a adoção em larga escala dessas tecnologias. Os altos custos iniciais de investimento e a ausência de marcos regulatórios padronizados continuam sendo barreiras críticas (Manzoor et al., 2025). Da mesma forma, há uma necessidade imperativa de maior transparência e ética no tratamento de dados; a comunidade científica deve promover a disponibilização de códigos e bases de dados abertos, a fim de evitar vieses nos modelos de IA e assegurar a replicabilidade dos achados científicos (Cruz et al., 2024; Oliveira et al., 2026).

Em conclusão, a integração de IA, *Machine Learning*, *Digital Twins* e processos avançados de simulação não é apenas uma opção de vanguarda, mas uma necessidade para criar um habitat verdadeiramente sustentável. Essas tecnologias fornecem as ferramentas necessárias para transitar de uma construção fragmentada para uma gestão holística, circular e resiliente do ambiente construído. Convidamos a comunidade científica a continuar explorando essas fronteiras tecnológicas, mantendo sempre o rigor científico e o compromisso ético que a crise ambiental global nos exige.

REFERÊNCIAS BIBLIOGRÁFICAS

Abu Jadayil, W., Alkhedher, M., Shwaheen, G., & Ramadan, M. (2026). Sustainable and efficient use of integrated technology solutions in energy management. *Energy Reports, 15*, 109319. https://doi.org/10.1016/j.egyr.2026.109319

Ahmed, N., Ding, Y., Canti, G., & Anglani, N. (2026). Sustainable building's energy management with artificial intelligence and machine learning: A decadal scoping review (2014–2024). *Energy Reports, 15*, 109082. https://doi.org/10.1016/j.egyr.2026.109082

Bibri, S. E., & Huang, J. (2025). Artificial intelligence and digital twins for environmentally sustainable smart buildings: A comprehensive systematic review. *Environmental Science and Ecotechnology, 28*, 100628. https://doi.org/10.1016/j.ese.2025.100628

Cruz, A. S., Caldas, L. R., Mendes, V. M., Mendes, J. C., & Bastos, L. E. G. (2024). Multi-objective optimization based on surrogate models for sustainable building design: A systematic literature review. *Building and Environment, 266*, 112147. https://doi.org/10.1016/j.buildenv.2024.112147

Kaya, G. N., Beyhan, F., Ilerisoy, Z. Y., & Cudzik, J. (2025). Evaluation of machine learning applications in building life cycle processes for energy efficiency: A systematic review. *Energy Reports, 13*, 4900–4916. https://doi.org/10.1016/j.egyr.2025.04.034

Kumar, R., Dekin, A., Prince, M., Froese, T., & Mukhopadhyaya, P. (2026). Integrated building form and structural strategies for sustainable and resilient residential buildings. *Sustainable Cities and Society: Advances, 2*, 100075. https://doi.org/10.1016/j.scsadv.2026.100075

Manzoor, B., Antwi-Afari, M. F., & Alotaibi, K. S. (2025). Green buildings and digital technologies: A pathway to sustainable development. *Green Technologies and Sustainability, 3*, 100243. https://doi.org/10.1016/j.grets.2025.100243

Mihalakakou, G., Giannadakis, A., Malefaki, S., Souliotis, M., Georgiou, P., Romaios, A., Antzoulatou, A., Nikolakopoulos, P., & Paravantis, J. A. (2025). Coupling simulation-based and machine learning methodologies for energy optimization and environmental impact mitigation in buildings. *Journal of Building Engineering, 112*, 113809. https://doi.org/10.1016/j.jobe.2025.113809

Mihalakakou, G., Romeos, A., Malefaki, S., Souliotis, M., Paravantis, J. A., Georgiou, P., & Giannadakis, A. (2026). From simulation to surrogates: optimizing green roofs for sustainable urban performance. *Sustainable Cities and Society, 145*, 107439. https://doi.org/10.1016/j.scs.2026.107439

Oliveira, J., Schreiber, D., & Jahno, V. D. (2026). Sustainability in civil construction through industry 4.0 and BIM technologies. *Automation in Construction, 182*, 106729. https://doi.org/10.1016/j.autcon.2025.106729

Qiu, L., Li, H., Wang, Z., Yang, Y., Lazarus, G. A., Chen, Y., & Feng, Y. (2025). Pathways to decarbonizing buildings: Harnessing energy efficiency and sustainable technologies. *Thermal Science and Engineering Progress, 66*, 103991. https://doi.org/10.1016/j.tsep.2025.103991

Tahmasbi, F., Khdair, A. I., Aburumman, G. A., Tahmasebi, M., Thi, N. H., & Afrand, M. (2025). Energy-efficient building façades: A comprehensive review of innovative technologies and sustainable strategies. *Journal of Building Engineering, 99*, 111643. https://doi.org/10.1016/j.jobe.2024.111643

Maureen Trebilcock-Kelly
Doctora en Arquitectura Sustentable
Editora Responsable Hábitat Sustentable, Profesora Titular,
Departamento Diseño y Teoría de la Arquitectura, Facultad de Arquitectura, Construcción y Diseño
Universidad del Bío-Bío, Concepción, Chile
https://orcid.org/0000-0002-1984-0259
mtrebilc@ubiobio.cl



Rafael Eduardo López-Guerrero
Doctorado en Ciencias de la Ingeniería
Co-Editor Hábitat Sustentable, Profesor Asistente,
Departamento de Ciencias de la Construcción, Facultad de Arquitectura, Construcción y Diseño,
Universidad del Bío-Bío, Concepción, Chile
https://orcid.org/0000-0002-5941-0421
rlopez@ubiobio.cl



THERMAL CHARACTERIZATION OF THE UNIVERSITY ENVIRONMENT FOR GREEN INFRASTRUCTURE PLANNING

Recibido 07/03/2026
Aceptado 24/04/2026

CARACTERIZACIÓN TÉRMICA DEL ENTORNO UNIVERSITARIO PARA LA PLANIFICACIÓN DE INFRAESTRUCTURA VERDE

CARACTERIZAÇÃO TÉRMICA DO AMBIENTE UNIVERSITÁRIO PARA O PLANEJAMENTO DE INFRAESTRUTURA VERDE

Walter Ávila-Ruiz
Magíster en Ingeniería
Estudiante de Doctorado de la Facultad de Ingeniería
Universidad Autónoma de Baja California
Mexicali, México
https://orcid.org/0009-0000-3450-1194
walter.avila@uabc.edu.mx

Carlos Salazar-Briones (autor correspondencia)
Doctor en Ciencias
Profesor investigador de la Facultad de Ingeniería
Universidad Autónoma de Baja California
Mexicali, México
https://orcid.org/0000-0002-5237-5539
csalazar86@uabc.edu.mx

José Ruiz-Gibert
Doctor en Ciencias
Profesor investigador de la Facultad de Ingeniería
Universidad Autónoma de Baja California
Mexicali, México
https://orcid.org/0000-0003-4532-7413
mizael.ruiz@uabc.edu.mx

Juan Saiz-Rodríguez
Doctor en Ciencias
Profesor investigador del Departamento de Ingeniería Civil y Minas
Universidad de Sonora
Hermosillo, México
https://orcid.org/0000-0002-0046-7298
alejandro.saiz@unison.mx

Marcelo Lomelí-Banda
Doctor en Ciencias
Profesor investigador de la Facultad de Ingeniería
Universidad Autónoma de Baja California
Mexicali, México
https://orcid.org/0000-0003-0171-9394
lomeli.marcelo@uabc.edu.mx

CC BY SA

ABSTRACT

The increase in urban temperatures, driven by climate change and the expansion of gray infrastructure, has intensified the urban heat island (UHI) phenomenon, affecting thermal comfort in outdoor spaces. This study characterized the campus thermal environment at the Autonomous University of Baja California in Mexicali, one of the world's hottest cities, to identify opportunities for green infrastructure (GI) planning. The methodology included generating a high-resolution orthomosaic using an unmanned aerial vehicle to calculate the NGRDI index, in situ measurements of land surface temperature (LST) using infrared thermometers, and geospatial analysis of both variables. The results showed higher temperatures on impervious surfaces such as concrete and asphalt, while tree-covered areas presented lower values. However, some green areas with low vegetation vigor showed limited cooling capacity, highlighting the need to strengthen GI strategies.

Keywords
urban heat islands, vegetation, NGRDI, green infrastructure, planning

RESUMEN

El incremento de las temperaturas urbanas, asociado al cambio climático y a la expansión de la infraestructura gris, ha intensificado el fenómeno de isla de calor urbana (ICU), lo que ha afectado el confort térmico en espacios exteriores. Este estudio caracterizó el entorno térmico del campus de la Universidad Autónoma de Baja California en Mexicali, una de las ciudades más calurosas del mundo, con el objetivo de identificar oportunidades para la planificación de infraestructura verde (IV). La metodología incluyó la generación de un ortomosaico de alta resolución mediante un vehículo aéreo no tripulado para el cálculo del índice NGRDI, mediciones in situ de temperatura superficial (LST) con termómetros infrarrojos y el análisis geoespacial de ambas variables. Los resultados mostraron temperaturas más elevadas en superficies impermeables, como el concreto y el asfalto, mientras que las áreas arboladas presentaron valores más bajos. No obstante, se identificaron zonas verdes con bajo vigor vegetal y capacidad de enfriamiento limitada, lo que evidencia la necesidad de fortalecer las estrategias de IV.

Palabras clave
islas de calor urbanas, vegetación, NGRDI, infraestructura verde, planeación

RESUMO

O aumento das temperaturas urbanas, associado às mudanças climáticas e à expansão da infraestrutura cinza, tem intensificado o fenômeno da ilha de calor urbana (ICU), afetando o conforto térmico em espaços externos. Este estudo caracterizou o ambiente térmico do campus da Universidade Autônoma da Baixa Califórnia em Mexicali, uma das cidades mais quentes do mundo, com o objetivo de identificar oportunidades para o planejamento de infraestrutura verde (IV). A metodologia incluiu a geração de um ortomosaico de alta resolução por meio de um veículo aéreo não tripulado para o cálculo do índice NGRDI, medições in situ da temperatura da superfície (LST) com termômetros infravermelhos e a análise geoespacial de ambas as variáveis. Os resultados mostraram temperaturas mais elevadas em superfícies impermeáveis, como o concreto e o asfalto, enquanto as áreas arborizadas apresentaram valores mais baixos. No entanto, foram identificadas zonas verdes com baixo vigor vegetal e capacidade limitada de resfriamento, o que evidencia a necessidade de fortalecer as estratégias de infraestrutura verde.

Palavras-chave
ilhas de calor urbanas, vegetação, NGRDI, infraestrutura verde, planejamento

INTRODUCTION

The global acceleration of urbanization, particularly in developing countries, has led to the concentration of population in cities, where approximately 55% of the world's population currently lives (United Nations, 2018; Valavanidis, 2024). This process, combined with climate change, has intensified the urban heat island (UHI) phenomenon, worsening environmental conditions in the built environment and directly affecting population health and thermal comfort in outdoor spaces. The adverse effects of urban overheating are manifested in both psychological well-being and the perception of heat, emotional state, and ability to concentrate, as well as in associated physiological impacts, such as sunburn and other disorders related to thermal exposure (Rony & Alamgir, 2023). In this context, thermal comfort in outdoor spaces has become increasingly relevant to the quality of urban life.

UHIs are environmental phenomena characterized by higher average temperatures in urban areas than in surrounding rural areas (Garzón et al., 2024). This phenomenon is a direct consequence of human activities and the transformation of the natural landscape, in which artificial materials predominate and alter the Earth's surface's original thermal balance, increasing heat absorption and retention (Oke, 1982).

Due to rising urban temperatures and the intensification of the UHI effect, several studies have indicated that thermal comfort in urban outdoor spaces is a key element of population well-being. In urban design processes, the need to consider the thermal impact of the built environment and to promote research to improve outdoor habitability, particularly at the microclimatic scale, has been emphasized (Mandjoupa et al., 2025). The UHI is characterized by air temperature measurements, specifically from the lowest layer of the atmosphere up to the height of trees or buildings (Arnfield, 2003; Stewart, 2011). In addition to the Urban Heat Island (UHI) phenomenon, Land Surface Temperature (LST) is a fundamental variable in analyzing the surface–atmosphere energy balance. While the air temperature characterizes the UHI, the LST represents the surface temperature and is one of the main variables used to evaluate this phenomenon from a surface perspective (Schwarz et al., 2012; Krishnan et al., 2020). In this sense, it is important to distinguish between the atmospheric Urban Heat Island (UHI), associated with air temperature within the urban canopy, and the Surface Urban Heat Island (SUHI), derived from LST analysis (Voogt & Oke, 2003). The latter enables characterization of the surface's thermal variations using remote sensing techniques, which provide spatially continuous information on urban thermal behavior.

The specialized literature indicates that for an urban space to provide adequate thermal comfort, it must meet at least three fundamental criteria: the morphological configuration of the built environment, the spatial orientation of its components, and the presence of vegetation (Yahia & Johansson, 2014). Studies such as those of Wu et al. (2024) indicate that increasing vegetation cover by 1% reduces the surface temperature of 0.099-0.1 °C in urban environments, where it has been observed that the shade generated by trees can contribute up to 80% of the total cooling effect in open spaces (Shashua-Bar & Hoffman, 2000), which consolidate vegetation as a key element in urban microclimate regulation (Declet-Barreto et al., 2013).

Vegetation plays an important role in mitigating high surface temperatures, as some of its properties, such as evapotranspiration, reduce ambient temperature. However, due to damage or stress on vegetation, environmental cooling could be reduced (Speak, 2015).

Several indices describe vegetation health, with the Normalized Difference Vegetation Index (NDVI) being the most widely used in the literature (Huang et al., 2021). Commonly, this index is obtained by using multispectral cameras mounted on Unmanned Aerial Vehicles (UAVs), also known as drones. However, this equipment tends to be expensive, and its acquisition is limited (Stamford et al., 2023). Alternatively, indices based solely on RGB bands (Red/Green/Blue) can be used to identify and distinguish vegetation and/or crops from soils or other surfaces, as well as to assess vegetation health.

Studies such as those of Macedo et al. (2025) conclude that one of the most reliable indices for detecting vegetation health based on RGB bands is the Normalized Green Red Difference Index (NGRDI), which is more readily estimated. In their study, they aimed to detect weeds in vineyards during the crop cycle. RGB images obtained from UAVs were used to evaluate several vegetation indices, with the NGRDI showing the best results since it clearly differentiated the vine and soil classes. It detected weeds more accurately than other indices.

Also, Lee & Yu (2019) conducted research to propose a method to automatically detect unhealthy and dead trees, in which the NGRDI was used as a

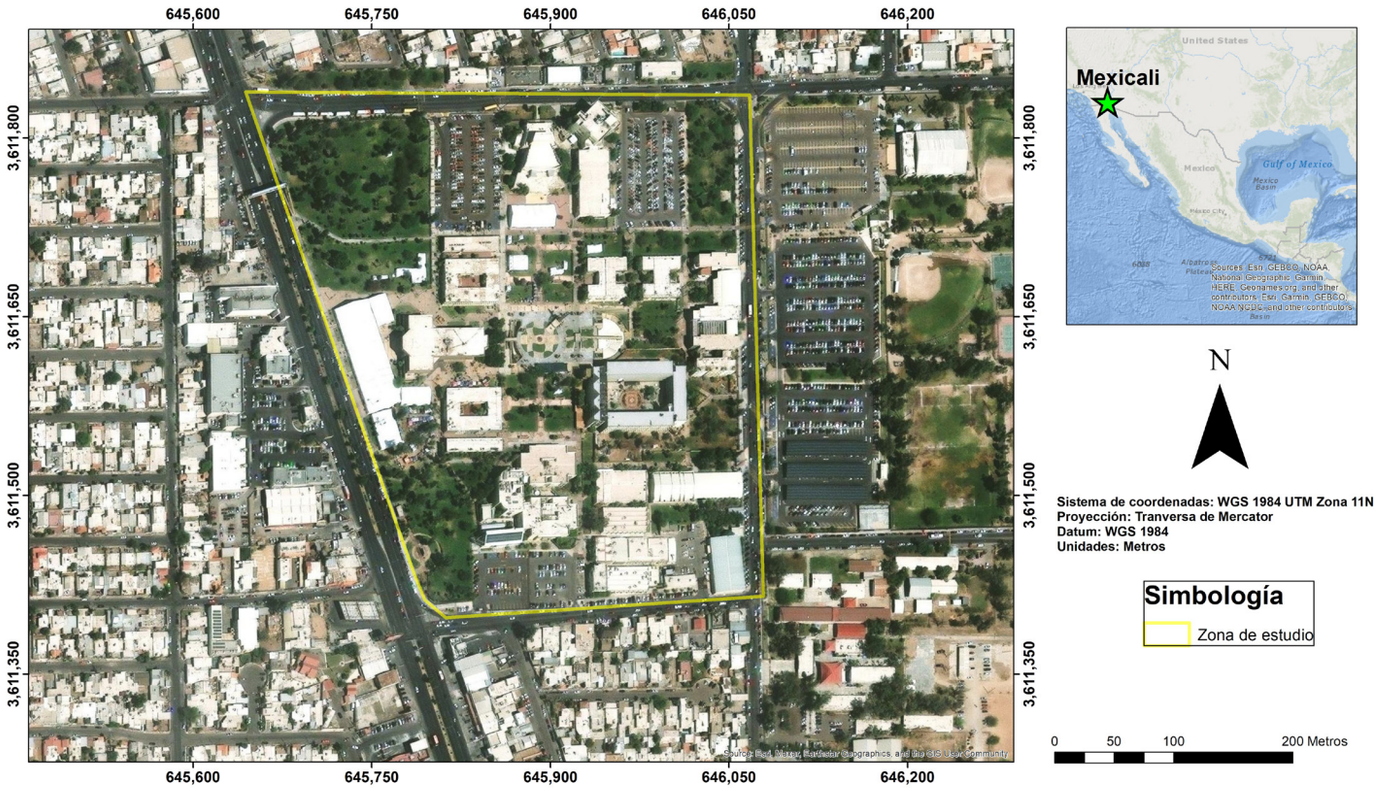


Figure 1. Location of the study area. Source: Prepared by the authors.

vegetation health index, obtaining results with a confidence level of more than 80% in the detection of dead trees, showing that the NGRDI is also an index that indicates the health of vegetation.

Therefore, this study aims to analyze the relationship between the land surface temperature (LST) and vegetation conditions using the NGRDI index on a university campus. Based on this relationship, the aim is to identify areas with high thermal stress and low plant performance to inform the planning, design, and management of green infrastructure to mitigate high LST and improve thermal comfort.

STUDY AREA

The central unit of the Autonomous University of Baja California, Mexicali campus, is located in the city of Mexicali, Baja California, Mexico, at coordinates UTM 645893 East and 3611631 North in the WGS84 coordinate system, zone 11N (Figure 1). The campus has an area of approximately 14.4 Ha, of which 24% is green area (4.3 Ha), excluding small areas such as planters. This site has extensions of key green areas for environmental well-being, which provide shade for the university community (Gutiérrez Boneo, 2025); however, the city's climatic conditions can limit vegetation health, reducing its capacity to reduce LST.

CITY CLIMATE AND SURFACE TEMPERATURE PROBLEMS

The city has a hot desert climate, with average temperatures between 41 ° and 42 °C during July and August (Mexicali City Council, 2024). However, during heat waves, temperatures can exceed 50 °C, with 52.7 °C being the highest temperature recorded historically in the city on August 7th, 2025 (Heras, 2025), making it the city with the highest temperature recorded in Mexico and thus one of the hottest cities in the world. In addition to the region's climatic characteristics, the rapid expansion of gray infrastructure has contributed to rising surface temperatures, which amplify the UHI effect (Yang et al., 2021).

The Mexicali City Council established the local regulatory framework through the Regulation of Green Areas for the municipality of Mexicali (Mexicali City Council, 2005). In its original design, Article 11 stipulated that the construction of shopping malls

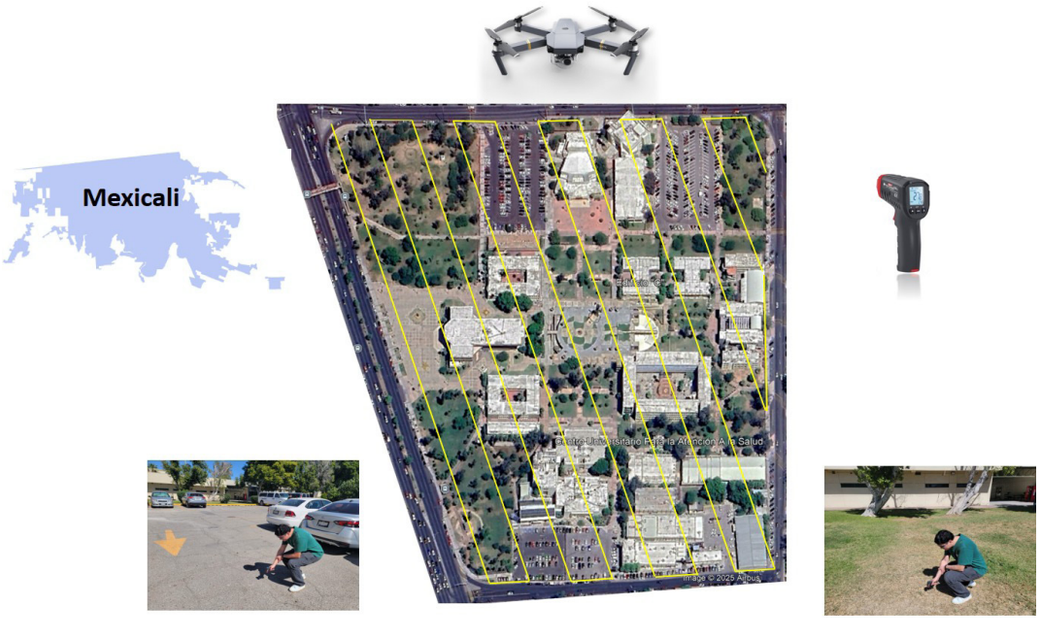


Figure 2. Work methodology. Source: Prepared by the authors.

and of construction sites with outdoor parking for more than nine cars required planting one tree for every six parking spaces. However, after the reform published in the Official Gazette of the State of Baja California in 2015, this requirement was doubled to one tree per three parking spaces, empowering the authority to deny building permits for non-compliance (Mexicali City Council, 2005; reformed in 2015). Despite this punitive measure, most parking lots in shopping malls and public spaces disregard the rule. As a result, these surfaces are directly exposed to solar radiation, which intensifies the micro-urban heat island effect and increases the thermal stress on users.

Although these regulations only establish tree planting, they do not include criteria that effectively reduce temperature and the UHI.

METHODOLOGY

In general, this project was carried out in three methodological stages (Figure 2). In the first, a high-resolution image (orthomosaic) was generated using an Unmanned Aerial Vehicle (UAV) to calculate the Red-Green Normalized Difference Index (NGRDI) and to characterize the vegetation within the university campus spatially. In the second stage, land surface temperature (LST) data were obtained via in situ measurements using infrared thermometers, following a standardized protocol to ensure consistency across records. Finally, both variables were integrated into a geospatial analysis environment to evaluate their relationship and degree of correlation, allowing the identification of spatial patterns associated with thermal stress and plant performance.

PHOTOGRAMMETRIC FLIGHT USING UAV

The photogrammetric flight was carried out using a DJI Mavic Pro UAV and the DroneDeploy application. To configure the flight plan, the parameters shown in Table 1 were used to obtain a high-resolution image (orthomosaic) of the university campus using the Agisoft Metashape version 1.8.0 program, and, with this input, also to calculate the NGRDI.

Table 1. Photogrammetric flight configuration parameters. Source: Prepared by the authors.

Photogrammetric flight configuration	
Flight surface	15 hectares
Flight time	13:55 minutes
Flight height	80 meters
Camera position angle	90°
Percentage of overlap between photographs	80%

NGRDI CALCULATION

To calculate the NGRDI, a composition of the green and red bands from the photogrammetric flight was conducted, using the following equation (Equation 1).

$$NRGDI = \frac{GREEN - RED}{GREEN + RED} \quad \text{(Equation 1)}$$

To create this band composition, ArcGIS version 10.5 and its Raster Calculator tool were used. According to the literature, this band composition yields an NGRDI index ranging from -1 to 1, with negative values associated with surfaces without vegetation cover and water bodies. In contrast, values close to 0 indicate bare soils or poor plant health. On the other hand, positive values close to 1 indicate dense and healthy vegetation (Jannoura et al., 2015).

ACQUISITION OF SURFACE TEMPERATURE DATA

To obtain surface temperature data, an in situ survey was conducted. UNI-T UT306S infrared thermometers were used. Measurements were taken at a distance of 0.10 m from the surface across the entire university campus and its different land cover types to ensure accurate data acquisition. A raster-type temperature surface was generated using ArcGIS version 10.5. The data acquisition activity was carried out on May 12th, 2025, between 1:15 pm and 2:15 pm.

EVALUATION OF THE CORRELATION BETWEEN THE NGRDI AND THE SURFACE TEMPERATURE

The Pearson correlation coefficient (r) was used to assess the statistical relationship between the NGRDI and surface temperature. This coefficient quantifies the continuous linear relationship between two numerical variables and is commonly used in remote perception studies (Rahimi et al., 2025).

The Pearson coefficient is calculated using the following expression (Equation 2):

$$r = \frac{\sum_{i=1}(x_i - \bar{x})(y_i - \bar{y})}{\sqrt{\sum_{i=1}^{n}(x_i - \bar{x})^2}\sqrt{\sum_{i=1}^{n}(y_i - \bar{y})^2}} \quad \text{(Equation 2)}$$

Where:
r: Pearson's correlation coefficient.
xi: the values of the NGRDI.
yi: the values of the surface temperature.
$\bar{x}$ and $\bar{y}$: Represent the means of each variable.
n: Total number of observations.

The values of the coefficient r range between -1 and 1 (Figure 3).

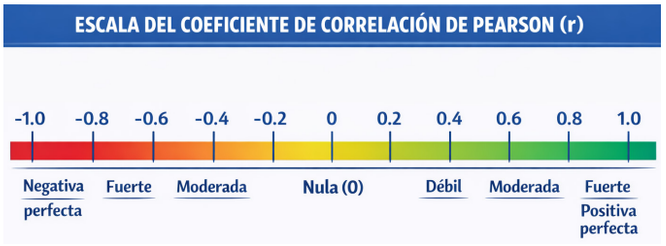


Figure 3. Pearson correlation (r) coefficient scale. Source: Prepared by the authors.

In the case study, negative values indicate an inverse relationship: the greater the vegetation health (higher NGRDI), the lower the surface temperature, whereas positive values indicate a direct relationship. Another variable considered in the analysis was the coefficient of determination (R^2), which is the square of the correlation coefficient r and represents the proportion of the variance in the dependent variable explained by the independent variable (Duke University, 2002). In this study, the dependent variable is surface temperature, while the independent variable is the NGRDI.

RESULTS

PHOTOGRAMMETRIC FLIGHT AND ORTHOMOSAIC GENERATION

A total of 297 aerial images of the university campus were obtained and processed at a flight height of 70m above ground level. With 80% overlap between photographs, an orthomosaic was generated using the Agisoft Metashape program at a spatial resolution of 5cm/pixel (Figure 4). In this image, the different materials on the campus surface are more clearly identified.

VEGETATION HEALTH ASSESSMENT BY NGRDI

By combining the RGB spectral bands, it was possible to determine the state of health of the vegetation within the university campus, as indicated by values ranging from -0.33 to 0.24, where negative values represent vegetation in poor condition and positive values represent healthier vegetation (Figure 5).

Within the campus's green areas, negative NGRDI values were identified, mainly associated with grass-covered surfaces. Field observations indicated low vegetative vigor in these areas. These areas had relatively higher surface temperatures than areas dominated by tree cover. The spatial match between negative NGRDI values and higher surface

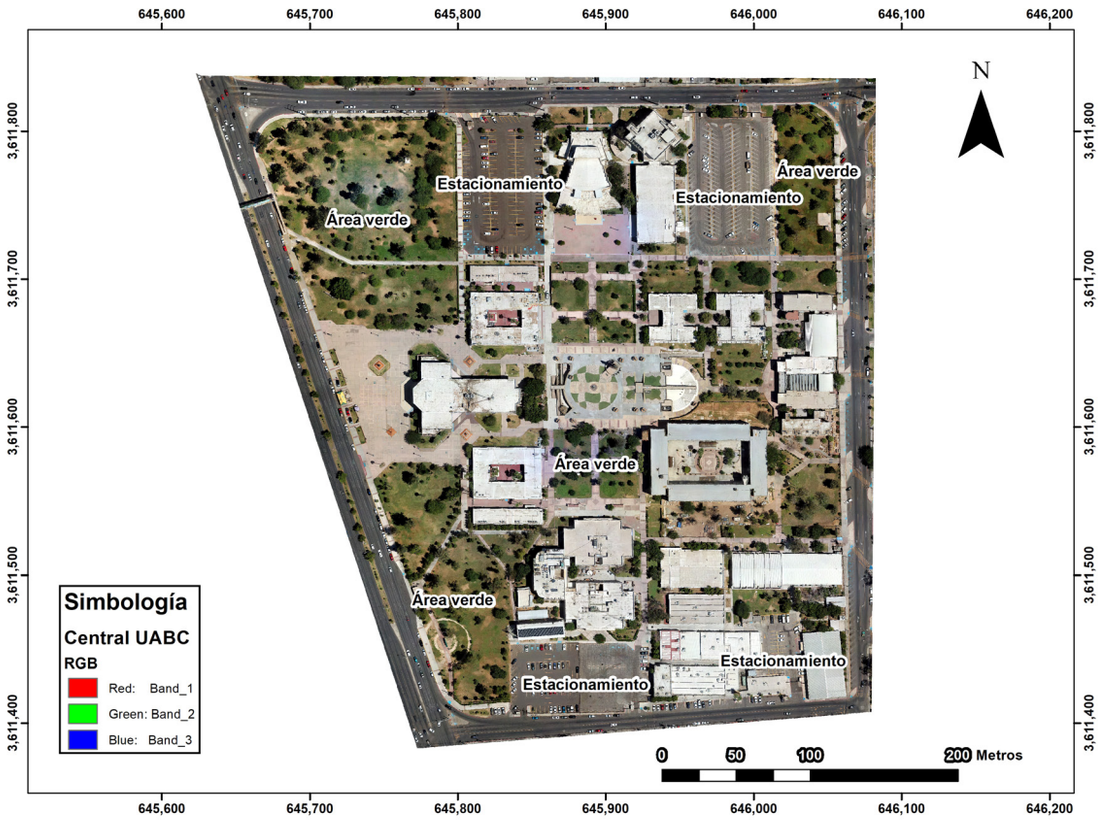


Figure 4. Orthomosaic of the university campus, spatial resolution of 5cm/pixel. Source: Prepared by the authors.

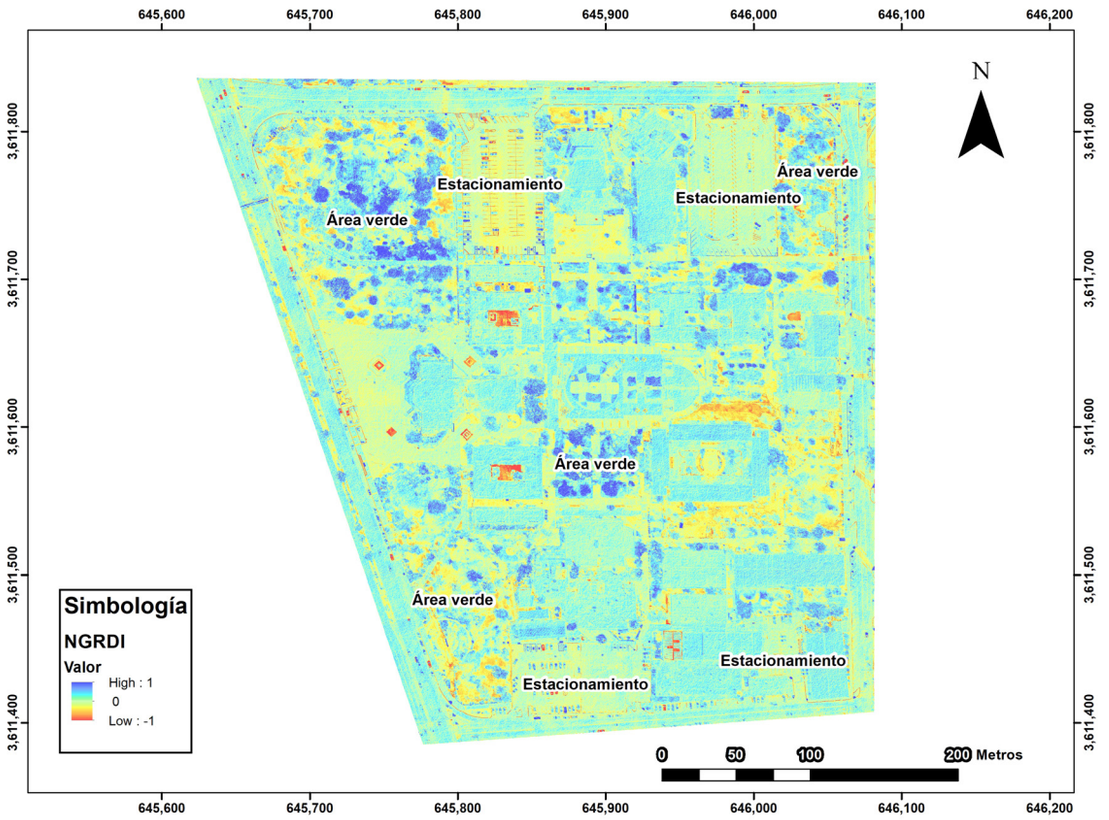


Figure 5. NGRDI map of the university campus. Source: Preparation by the authors.

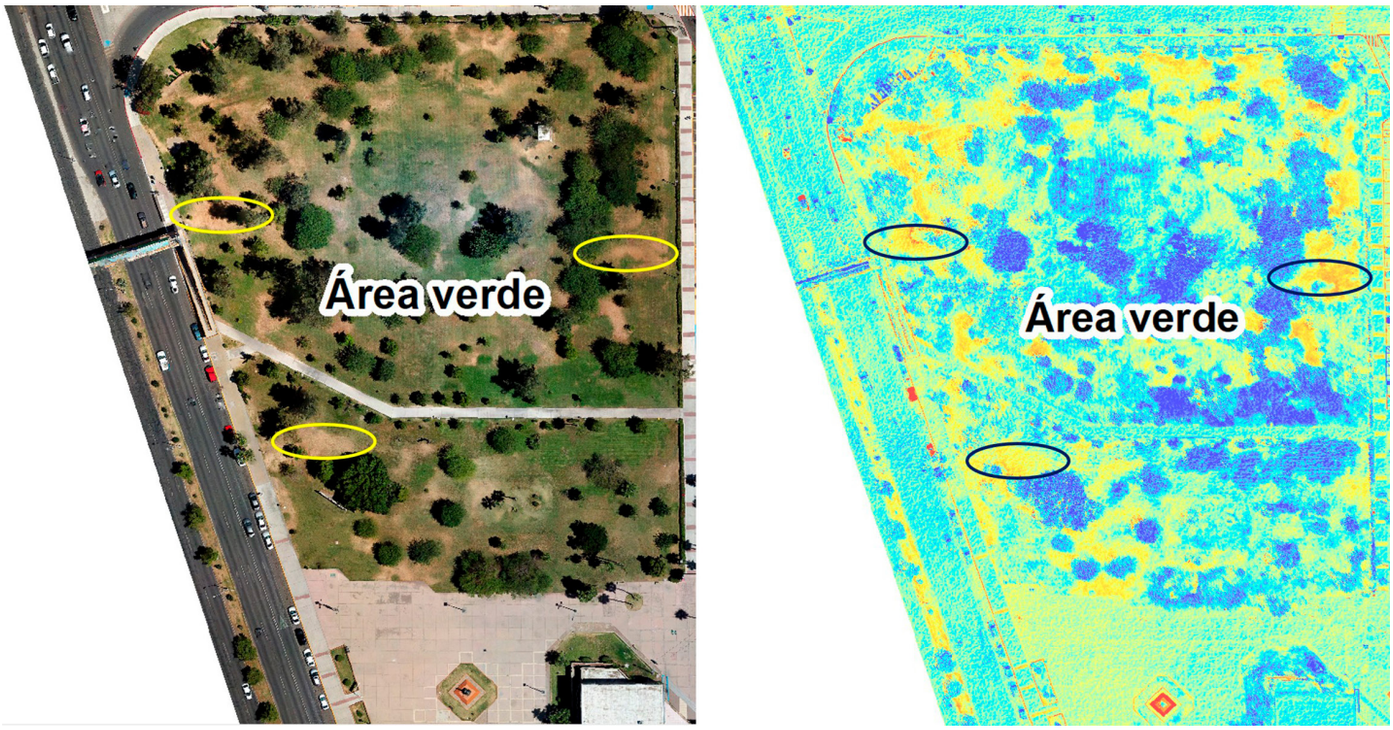


Figure 6. Example of negative NGRDI in vegetation and visual verification. Source: Prepared by the authors.

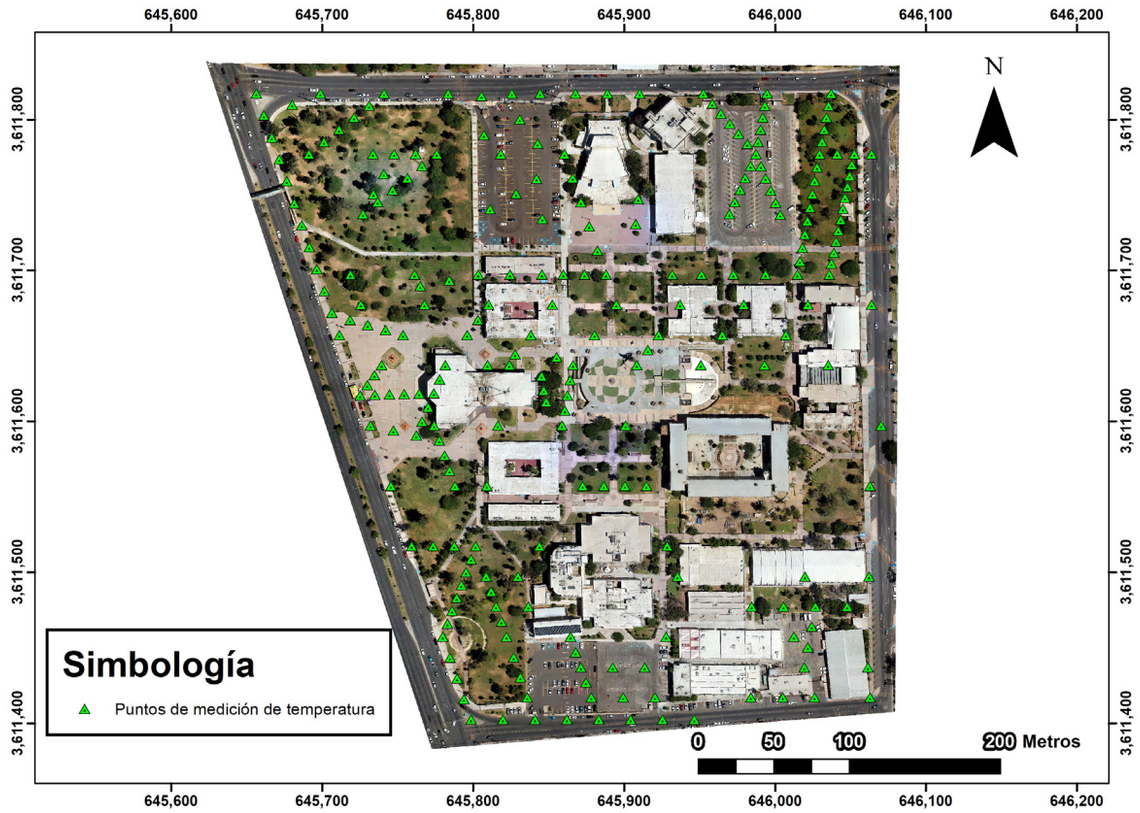


Figure 7. Distribution of temperature measurement points. Source: Prepared by the authors.

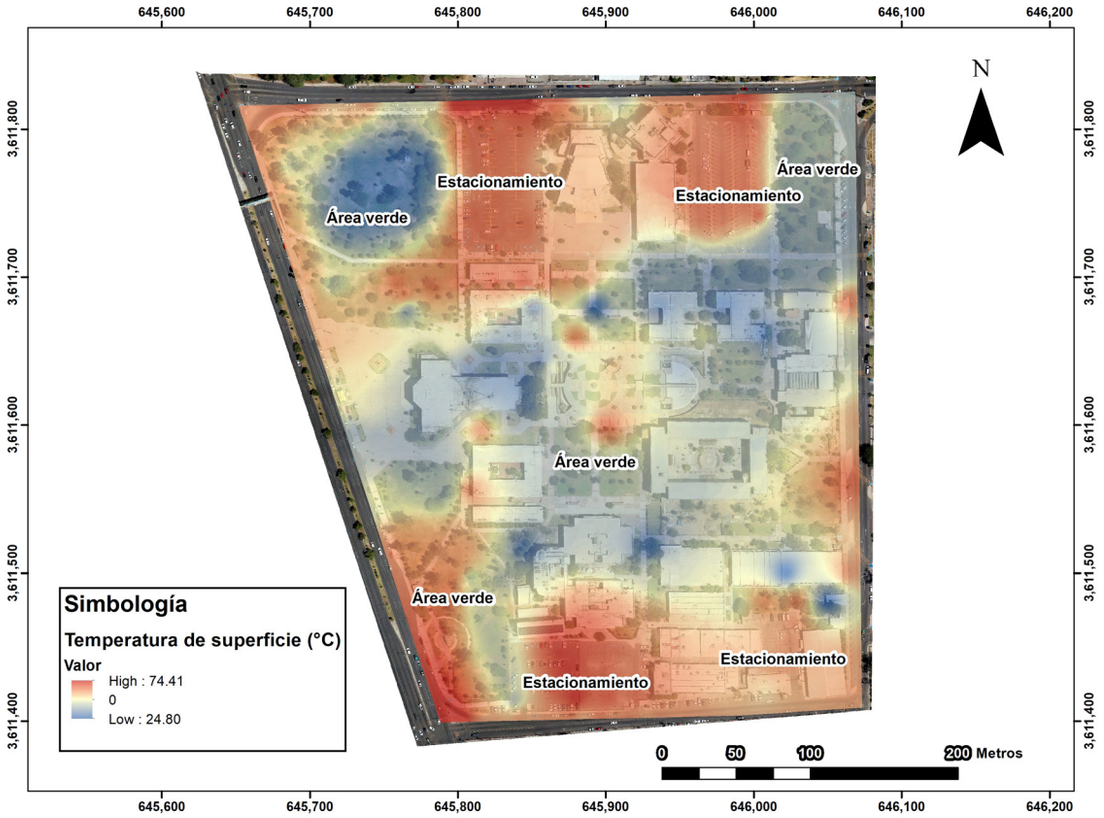


Figure 8. Surface temperature map generated using the data acquired on May 15th, 2025. Source: Prepared by the authors.

temperatures suggests reduced vegetative vigor and a limited capacity of these surfaces to mitigate thermal effects (Figure 6).

SURFACE TEMPERATURE GENERATION

A total of 246 surface temperature points of the university campus were obtained (Figure 7), and their data were used to generate a surface temperature raster. The weighted inverse distance interpolation (IDW) method was also used, resulting in a surface with a minimum temperature of around 24.8°C and a maximum of 72.4°C, as shown in Figure 8.

The minimum temperature values appeared within the green areas, specifically where the trees' shadows were. Temperature differences were observed between 5 °C and 6 °C compared to the green areas directly exposed to sunlight, which reaffirms the importance of trees for mitigating high temperatures, especially in arid and semi-arid regions.

Although the IDW method is used in spatial analysis and has been considered an effective method for temperature interpolation (Lau & Hsu, 2025), its accuracy strongly depends on the spatial distribution of the sampling points, and inaccurate results may be presented when these are irregular, especially in environmental contexts where the data density is heterogeneous (Ohlert et al., 2023). In addition, the extreme values of the interpolated surface are restricted at the measured points, which limits the detection of real maxima and minima (Longley et al., 2005). For the case study, the heterogeneity of the points was limited due to the difficulty of accessing parts of the university campus and other factors that hindered data acquisition.

CORRELATION BETWEEN THE NGRDI AND THE SURFACE TEMPERATURE

The Pearson correlation coefficient (r) between the NGRDI and the surface temperature was -0.122, indicating a weak inverse relationship between vegetation presence and surface temperature. Although vegetation helps reduce surface temperature, the results suggest that its influence is not a dominant factor in explaining thermal variability within the university campus. The coefficient of determination (R^2) was 0.0148 (Figure 9), indicating that only 1.48% of the observed thermal variability is explained by variations in the NGRDI.

Several studies have documented a negative relationship between vegetation indices, such as the NGRDI, and the Earth's surface temperature (Anand et al., 2025; Dheeraj et al., 2025). This behavior is

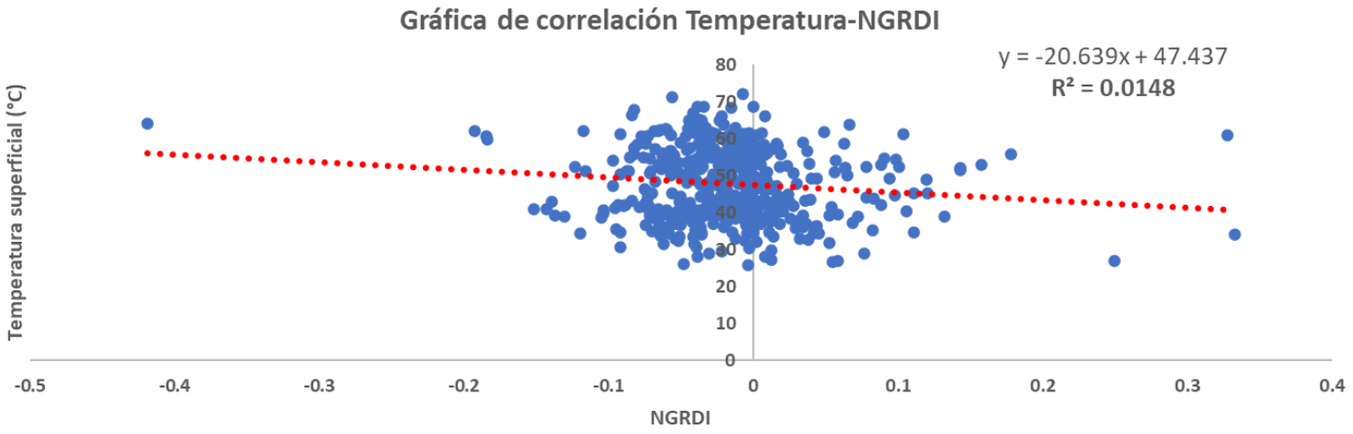


Figure 9. Comparative analysis of the correlation between surface temperature and the NGRDI. Source: Prepared by the authors.

mainly explained by the shading effects of trees and evapotranspiration processes, which influence the regulation of surface thermal storage (Yin et al., 2024). However, a weak correlation between the two variables is observed in the study area. This result could be associated with the high coverage of impermeable surfaces, such as asphalt and concrete, as well as the presence of low-vigor vegetation and bare soil. Additionally, the region's semi-arid climate may limit vegetation's ability to provide effective environmental cooling (Dashti & Khajah, 2024).

DISCUSSION

A relevant finding of this research is the identification of areas with low plant performance and high thermal stress within the university campus, particularly in the southwest and east-central areas, where negative NGRDI values close to -1 were recorded and were associated with vegetation in deficient or absent conditions. These areas coincide spatially with surfaces dominated by impermeable materials, such as parking lots, which presented the highest surface temperatures, reaching up to 71.4 °C. This behavior shows the decisive role of gray infrastructure in heat accumulation, which is also influenced by properties such as albedo, which regulates the absorption of solar radiation and contributes to increased surface temperature. In this context, several studies (Franco et al., 2025; Zhao et al., 2025) have shown that implementing permeable surfaces, combined with vegetation cover, promotes the dissipation of thermal energy through evaporative and evapotranspiration processes. However, the results obtained also show that not all vegetation contributes effectively to surface cooling. In arid environments such as Mexicali, there is a trade-off between water conservation and thermal efficiency, since, although reforestation programs and local regulations prioritize the use of endemic species (Mexicali City Council, 2020), these present physiological adaptations aimed at reducing water loss, which limits their evapotranspiration rates and, therefore, their cooling capacity. Consequently, green infrastructure planning should not focus solely on incorporating native vegetation but on selecting functional species that consider their thermal performance. It is therefore proposed to prioritize species that, within the allowed vegetable palette, have greater cooling efficiency to optimize the balance between water efficiency and thermal mitigation capacity. This approach would allow shifting from a conventional vision of reforestation to a climate design strategy that simultaneously addresses water stress and extreme temperature conditions identified in the study area.

CONCLUSIONS

This study characterized the thermal environment of the UABC campus in Mexicali and considered variables such as land use, surface materials, surface temperature, and vegetation condition. The results allowed the identification of spatial patterns of thermal behavior within the campus and their interaction with the urban environment. The highest surface temperatures were recorded on impermeable surfaces, particularly concrete and asphalt, while the lowest values were observed in green areas, especially under the shade of trees. Although the green areas showed a general trend of surface cooling, areas where vegetation did not significantly contribute to the thermal reduction were identified, mainly in those with deteriorated

lawns and low NGRDI values. The results obtained matched those reported in the literature, where the lack of vegetation cover, poor vegetation health, and the increase in gray infrastructure increase heat absorption and reduce the environment's cooling capacity.

The trend is as expected; however, the relationship is weak due to the health and layout of the vegetation space, so one opportunity is to intervene in areas of low health with IV to correct the cooling deficit these areas currently provide.

With regard to vegetation, tree shading is one of the most important factors for urban cooling, as it decreases surface temperature by 5-6 °C, yielding better results than grass, particularly at sites of low vigor. Nevertheless, water availability and climatic conditions, such as temperature and solar radiation, affect the cooling capacity of trees; therefore, the IV should be strategically planned by prioritizing factors such as planting endemic trees in regions with the highest evapotranspiration rates. Therefore, it is advisable to conduct studies on the cooling capacities of endemic vegetation in these regions and, in turn, to develop studies focused on the design and management implications of the IV, considering variables such as land cover and use, material properties, and microclimate simulations. This will allow determining thermal comfort variables, which describe the physical state and psychological well-being experienced by the individual in their environment, thus contributing to the improvement of their quality of life.

LIMITATIONS

This study is based on a thermal analysis conducted at a specific point in time, which limits the evaluation of seasonal variability in surface temperature. However, the information collection was carried out during May 2025, a period when the city of Mexicali experiences elevated temperatures that can exceed 40 °C, enabling the characterization of the campus's thermal behavior under significant heat. It is possible that during periods of greater summer thermal intensity, surface temperatures are even higher. Also, semi-arid climatic conditions can cause water stress in vegetation, which could affect its cooling capacity. In this sense, future studies could incorporate broader temporal analyses to better understand the thermal dynamics and the role of vegetation in mitigating the urban heat island.

CONTRIBUTION OF AUTHORS CRediT:

Conceptualization, C.S.B.; Data Curation, J.M.R.G., J.A.S.R.; Formal analysis, C.S.B., J.M.R.G.; Research, W.A.R.; Methodology, W.A.R., C.S.B.; Software. W.A.R., J.M.R.G., J.A.S.R.; Validation, J.M.R.G., J.A.S.R.; Visualization, M.A.L.B.; Writing - original draft, W.A.R., C.S.B.; Writing - revision and editing, C.S. B, M.A.L.B.

ACKNOWLEDGMENTS

The authors would like to thank the Secretariat of Science, Humanities, Technology and Innovation (SECIHTI) for the grant awarded for the academic training of one of the authors. This research did not receive any other funding.

BIBLIOGRAPHIC REFERENCES

Anand, V., Kaur, S., Rajput, V. D., Minkina, T., Mandzhieva, S., Kumar, S., Sharma, A., & Kumar, S. (2025). Analyzing the spatial relationship between land surface temperature and normalized difference vegetation index using remote sensing and GIS. *Discover Geoscience*, *3*(1), 65. https://doi.org/10.1007/s44288-025-00167-w

Arnfield, A. J. (2003). Two decades of urban climate research: A review of turbulence, exchanges of energy and water, and the urban heat island. *International Journal of Climatology*, *23*(1), 1–26. https://doi.org/10.1002/joc.859

Ayuntamiento de Mexicali. (2005). *Reglamento de áreas verdes para el municipio de Mexicali, Baja California*. Gobierno Municipal de Mexicali. https://www.ordenjuridico.gob.mx/Estatal/BAJA%20CALIFORNIA/Municipios/Mexicali/REG01.pdf

Ayuntamiento de Mexicali. (2020). *Guía de forestación para el municipio de Mexicali, baja California*. Gobierno Municipal de Mexicali. https://www.scribd.com/document/610318541/2021-Guia-Municipal-de-Forestacion-para-el-Municipio-de-Mexicali-2021

Ayuntamiento de Mexicali. (2024). *Atlas de Riesgos del Municipio de Mexicali, B.C. [Actualización 2023].* Universidad Autónoma de Baja California [UABC]. Unidad Municipal de Protección Civil. http://www.mexicali.gob.mx/transparencia/administracion/atlas/pdf/0.pdf

Dashti, A., & Khajah, M. (2024). Urban green areas and their impact on land surface temperature in semi-arid environments: a case study in Kuwait. *GeoJournal*, *89*, 86. https://doi.org/10.1007/s10708-024-11079-6

Declet-Barreto, J., Brazel, A. J., Martin, C. A., Chow, W. T., & Harlan, S. L. (2013). Creating the park cool island in an inner-city neighborhood: heat mitigation strategy for Phoenix, AZ. *Urban Ecosystems*, 16(3), 617-635. https://doi.org/10.1007/s11252-012-0278-8

Dheeraj, V. P., Rai, A. K., Yadav, A. K., Sonkar, S., Maurya, A., Chaudhary, A., & Chaudhary, P. (2025). Spatiotemporal analysis and correlation of surface temperature, vegetation cover, and water index using remote sensing and GIS techniques in Ambedkar Nagar, India. *Discover Environment*, 3(1), 232. https://doi.org/10.1007/s44274-025-00438-w

Duke University. (2002). *STA102: Correlation and regression – The coefficient of determination*. Department of Statistical Science, Duke University.

Jannoura, R., Brinkmann, K., Uteau, D., Bruns, C., & Joergensen, R. G. (2015). Monitoring of crop biomass using true colour aerial photographs taken from a remote controlled hexacopter. *Biosystems Engineering*, 129, 341-351. https://doi.org/10.1016/j.biosystemseng.2014.11.007

Franco, E., Ghisi, E., Vaz, I. C. M., & Thives, L. P. (2025). Permeable Pavements: An Integrative Review of Technical and Environmental Contributions to Sustainable Cities. *Water*, *17*(22), 3323. https://doi.org/10.3390/w17223323

Gutiérrez Boneo, M. M. (10 de junio de 2025). *El cuidado de áreas verdes: Clave para el bienestar ambiental*. Gaceta UABC. Universidad Autónoma de Baja California. https://gaceta.uabc.mx/el-cuidado-de-areas-verdes-clave-para-el-bienestar-ambiental

Garzón, J., Molina Sánchez, I., & Jiménez Cleves, G. (2024). Evaluación del fenómeno de la isla de calor urbano en Cartago, Colombia: tendencias de factores ambientales en los últimos 20 años. *Encuentro Internacional de Educación en Ingeniería ACOFI*. https://doi.org/10.26507/paper.3712

Heras, A. (8 de agosto de 2025). *Mexicali, BC, rompe récord de temperatura con 52.7 grados Celsius.* La Jornada. https://www.jornada.com.mx/noticia/2025/08/08/estados/mexicali-bc-rompe-record-de-temperatura-con-527-grados-celsius

Huang, S., Tang, L., Hupy, J. P., Wang, Y., & Shao, G. (2021). A commentary review on the use of normalized difference vegetation index (NDVI) in the era of popular remote sensing. *Journal of Forestry Research*, *32*(1), 1-6. https://doi.org/10.1007/s11676-020-01155-1

Krishnan, P., Meyers, T. P., Hook, S. J., Heuer, M., Senn, D., & Dumas, E. J. (2020). Intercomparison of in situ sensors for ground-based land surface temperature measurements. *Sensors*, 20(18), 5268. https://doi.org/10.3390/s20185268

Lau, T.-K., & Hsu, H.-C. (2025). Urban Heat Island Effect and Unequal Temperature-Related News Attention in Taiwan's Major Cities. *Urban Science*, *9*(10), 417. https://doi.org/10.3390/urbansci9100417

Lee, S., & Yu, B.-H. (2019). Automatic detection of dead tree from UAV imagery. *Coordinates, 15*(4), 36-39. https://mycoordinates.org/pdf/apr19.pdf

Longley, P. A., Goodchild, M. F., Maguire, D. J., & Rhind, D. W. (2005). *Geographical information systems and science*. John Wiley & Sons.

Macedo, F. L., Nóbrega, H., de Freitas, J. G., & Pinheiro de Carvalho, M. A. A. (2025). Assessment of vegetation indices derived from UAV imagery for weed detection in vineyards. *Remote Sensing*, *17*(11), 1899. https://doi.org/10.3390/rs17111899

Mandjoupa, L. K., Behera, P., Roman, K. K., Azam, H., & Denis, M. (2025). Street-Level Sensing for Assessing Urban Microclimate (UMC) and Urban Heat Island (UHI) Effects on Air Quality. *Environments, 12*(6), 184. https://doi.org/10.3390/environments12060184

Ohlert, P. L., Bach, M., & Breuer, L. (2023). Accuracy assessment of inverse distance weighting interpolation of groundwater nitrate concentrations in Bavaria (Germany). *Environmental Science and Pollution Research*, *30*(4), 9445-9455. https://doi.org/10.1007/s11356-022-22670-0

Oke, T. R. (1982). The energetic basis of the urban heat island. *Quarterly Journal of the Royal Meteorological Society, 108*(455), 1–24. https://doi.org/10.1002/qj.49710845502

Rahimi, E., Dong, P., & Jung, C. (2025). Global NDVI-LST correlation: Temporal and spatial patterns from 2000 to 2024. *Environments*, *12*(2), 67. https://doi.org/10.3390/environments12020067

Rony, M. K. K., & Alamgir, H. M. (2023). High temperatures on mental health: Recognizing the association and the need for proactive strategies—A perspective. *Health Science Reports,* 6(12), e1729. https://doi.org/10.1002/hsr2.1729

Schwarz, N., Schlink, U., Franck, U., & Großmann, K. (2012). Relationship of land surface and air temperatures and its implications for quantifying urban heat island indicators—An application for the city of Leipzig (Germany). *Ecological indicators*, *18*, 693-704. https://doi.org/10.1016/j.ecolind.2012.01.001

Shashua-Bar, L., & Hoffman, M. E. (2000). Vegetation as a climatic component in the design of an urban street: An empirical model for predicting the cooling effect of urban green areas with trees. *Energy Buildings* 31(3), 221-235. https://doi.org/10.1016/S0378-7788(99)00018-3

Speak, A. (2015). 12-Influence of vegetation damage on urban cooling effects in F. Pacheco-Torgal, J.A. Labrincha, L.F. Cabeza, C.-G. Granqvist (Eds.), E*co-Efficient Materials for Mitigating Building Cooling Needs* (pp. 325-347). Woodhead Publishing. https://doi.org/10.1016/B978-1-78242-380-5.00012-1

Stamford, J. D., Vialet-Chabrand, S., Cameron, I., & Lawson, T. (2023). Development of an accurate low cost NDVI imaging system for assessing plant health. *Plant Methods, 19*(1), 9. https://doi.org/10.1186/s13007-023-00981-8

Stewart, I. D. (2011). A systematic review and scientific critique of methodology in modern urban heat island literature. *International Journal of Climatology*, 31(2), 200–217. https://doi.org/10.1002/joc.2141

United Nations. (16 de mayo de 2018). *2018 Revision of World Urbanization Prospects*. United Nations, Department of Economic and Social Affairrs. https://www.un.org/en/desa/2018-revision-world-urbanization-prospects

Valavanidis, A. (2024). *Half of the Global Population Lives in MegaCities. Megacities are hotspots for slums, GHG emissions, toxic air pollution, climate change, deteriorating water and soil quality.* https://www.researchgate.net/publication/379655450_Half_of_the_Global_Population_Lives_in_MegaCities_Megacities_are_hotspots_for_slums_GHG_emissions_toxic_air_pollution_climate_change_deteriorating_water_and_soil_quality

Voogt, J. A., & Oke, T. R. (2003). Thermal remote sensing of urban climates. *Remote Sensing of Environment,* 86(3), 370-384. https://doi.org/10.1016/S0034-4257(03)00079-8

Wu, B., Zhang, Y., Wang, Y., He, Y., Wang, J., Wu, Y., Lin, X., & Wu, S. (2024). Mitigation of urban heat island in China (2000–2020) through vegetation-induced cooling. *Sustainable Cities and Society*, 112, 105599. https://doi.org/10.1016/j.scs.2024.105599

Yahia, M. W., & Johansson, E. (2014). Landscape interventions in improving thermal comfort in the hot dry city of Damascus, Syria—The example of residential spaces with detached buildings. *Landscape and Urban Planning*, 125, 1-16. https://doi.org/10.1016/j.landurbplan.2014.01.014

Yang, J., Ren, J., Sun, D., Xiao, X., Xia, J. C., Jin, C., & Li, X. (2021). Understanding land surface temperature impact factors based on local climate zones. *Sustainable Cities and Society*, 69, 102818. https://doi.org/10.1016/j.scs.2021.102818

Yin, Y., Li, S., Xing, X., Zhou, X., Kang, Y., Hu, Q., & Li, Y. (2024). Cooling benefits of urban tree canopy: A systematic review. *Sustainability,* 16(12), 4955. https://doi.org/10.3390/su16124955

Zhao, J., Lu, J., Ge, J., Fan, Y., Wang, H., Gu, M., Xue, Y., Zhao, Y., Lv, G., Lin, H., Zhao, K., & Luo, X. (2025). Influences of permeable pavements with different hydraulic properties on evaporative cooling and outdoor thermal environment: Field experiments. *Building and Environment*, 270, 112525. https://doi.org/10.1016/j.buildenv.2025.112525

IMPLEMENTATION OF A PASSIVE DEHUMIDIFICATION SYSTEM BASED ON FOG CATCHER TECHNOLOGY IN VILLA MARÍA DEL TRIUNFO - LIMA, PERÚ

Recibido 08/12/2025
Aceptado 19/05/2026

IMPLEMENTACIÓN DE UN SISTEMA PASIVO DE DESHUMIDIFICACIÓN BASADO EN LA TECNOLOGÍA DEL ATRAPANIEBLAS EN VILLA MARÍA DEL TRIUNFO - LIMA, PERÚ

IMPLEMENTAÇÃO DE UM SISTEMA PASSIVO DE DESUMIDIFICAÇÃO BASEADO EM TECNOLOGIA DE CAPTURA DE NÉVOA EM VILLA MARÍA DEL TRIUNFO - LIMA, PERÚ

Milagros Delgado-Peña
Arquitecta
Egresada Carrera de Arquitectura, Facultad de Ingeniería
Universidad Tecnológica del Perú
Lima, Perú
https://orcid.org/0009-0004-4678-0919
U17205052@utp.edu.pe

Alonzo Cardenas-Vera-Pinto (Autor de Correspondencia)
Arquitecto
Egresado Carrera de Arquitectura, -Facultad de Ingeniería
Universidad Tecnológica del Perú
Lima, Perú
https://orcid.org/0009-0006-5707-4475
U17102967@utp.edu.pe

Richard Valdivia-Sisniegas
Magíster de Estudios Avanzados en Arquitectura y Desarrollo Sostenible
Docente y Asesor del programa de Titulación, Carrera de Arquitectura
Universidad Tecnológica del Perú
Lima, Perú
https://orcid.org/0000-0003-0783-6831
C19165@utp.edu.pe

CC BY SA

ABSTRACT

In Lima (Peru), homes in high-relative-humidity environments face unfavorable living conditions, with surface condensation and structural deterioration when indoor RH exceeds 65%. In this context, this research evaluates the efficiency of the DESHUME passive dehumidification prototype in a highly saturated environment, such as the hills of Villa María del Triunfo (692 meters above sea level), where temperatures reached 14.04°C, and RH was 100%. The quasi-experimental, in situ methodology was based on the analysis of meteorological records (2020-2024) and the materials' technical characteristics. Validation was carried out by monitoring indoor and outdoor hygrothermal variables for 72 hours in 1:2 and 1:1-scale modules, incorporating fog-collecting technology and the Venturi effect in their design to remove water mass. This resulted in an average reduction of 0.20g/m³ in indoor RH in winter compared to the reference module, demonstrating the system's viability as a hygrothermal regulator for vulnerable high-humidity sectors.

Keywords
humidity, fog, ventilation, coastal housing

RESUMEN

En Lima (Perú), las viviendas ubicadas en entornos de alta humedad relativa enfrentan condiciones desfavorables para la habitabilidad, lo que favorece la condensación superficial y el deterioro constructivo cuando la HR interior supera el 65%. En este contexto, la investigación evalúa la eficiencia del prototipo de deshumidificación pasiva DESHUME en un entorno de alta saturación hídrica, como las lomas de Villa María del Triunfo (692 m.s.n.m.), registrando condiciones de 14,04 °C y 100% de HR. La metodología cuasiexperimental in situ partió del análisis de precedentes meteorológicos (2020-2024) y de las características técnicas de los materiales. La validación se realizó mediante el monitoreo de variables higrotérmicas interiores y exteriores durante 72 h, en módulos a escala 1:2 y 1:1, incorporando en su diseño la tecnología del atrapanieblas y el efecto Venturi para la remoción de masa de agua. Lo que resulta en la reducción promedio de 0,20 g/m³ de HR interior en invierno respecto al módulo referencial, lo que demuestra al sistema como un regulador higrotérmico viable para sectores vulnerables de alta humedad.

Palabras clave
humedad, niebla, ventilación, vivienda en la costa

RESUMO

Em Lima (Peru), as habitações em ambientes com alta umidade relativa enfrentam condições desfavoráveis à habitabilidade, o que favorece a condensação superficial e a deterioração estrutural quando a umidade relativa interna é superior a 65%. Neste contexto, esta pesquisa avalia a eficiência do protótipo de desumidificação passiva DESHUME em um ambiente de alta saturação hídrica: as colinas de Villa María del Triunfo (692 m acima do nível do mar), onde foram registradas temperaturas de 14,04 °C e umidade relativa de 100%. A metodologia quase experimental in situ baseou-se na análise de dados meteorológicos anteriores (2020-2024) e nas características técnicas dos materiais. A validação foi realizada por meio do monitoramento de variáveis higrotérmicas internas e externas durante 72 horas, em módulos nas escalas 1:2 e 1:1, incorporando-se ao projeto a tecnologia de coletores de névoa e o efeito Venturi para a remoção da massa de água. O resultado foi uma redução média de 0,20 g/m³ na umidade relativa do ar interna no inverno em comparação com o módulo de referência, o que demonstra que o sistema é um regulador higrotérmico viável para áreas vulneráveis com alta umidade.

Palavras-chave
umidade, névoa, ventilação, habitação em áreas costeiras

INTRODUCTION

The Metropolitan city of Lima (Peru) is located in the coastal desert of western South America, where the meeting of the Pacific Ocean and the Andes Mountain Range favors the development of the Lomas ecosystem, with fog banks that form along the coast. The presence of fog at 400-1000 m.a.s.l. in this setting is responsible for a high relative humidity (RH) of up to 100% (Moat et al., 2021). During the winter, from June to September, this saturation affects the consolidated urban settlements in these peripheral areas, which expanded by 1,408.32 ha between 2005 and 2017 (Ministry of the Environment [MINAM], 2021). This climatic situation is manifested in the A.H. Ficus del Pedregal, José Carlos Mariátegui Sector, Villa María del Triunfo (VMT), located near the georeferenced boundary as point 10 (N 8659517, E 290903) (MINAM, 2019), where an RH of 100% has been recorded (SENAMHI, n.d. a). By exceeding the recommended standard of 65% relative humidity in a dwelling's occupied spaces (American National Standards Institute [ANSI] / American Society of Heating, Refrigerating and Air-Conditioning Engineers [ASHRAE]. 62.1, 2025), there is a proliferation of mold and bacteria, as well as the degradation of air quality, which represents a health risk for the inhabitants by increasing the prevalence of chronic respiratory conditions (Campos-Vásquez et al., 2025). This environmental problem not only affects the population's habitability due to weather conditions but is also accentuated by the vulnerability of self-builds, evidenced by a predominance of low-durability materials in housing, such as fiber cement roofs or calamine sheets, earth floors, and OSB or triplay walls (Ministry of Housing, Construction and Sanitation, [MVC], n.d.). These are highly hygroscopic materials that tend to absorb excessive moisture from the environment. This unfavorable environment poses an imminent risk to the materials' durability and does not guarantee adequate insulation or hygrothermal comfort (Tejeda Martínez, 2018). Faced with this problem, recent research has proposed strategies for indoor humidity control using passive or hybrid systems, including the integration of innovative architectural components, such as 3D-printed tiles (Posani et al., 2025). Other approaches similarly propose hybrid ventilation systems with energy recovery for dehumidification (Chen et al., 2023). However, these systems require advanced construction layouts, which make their practical implementation in homes difficult. At the same time, as a sustainable alternative, the capture of atmospheric water using fog catcher technology has been widely studied in the literature. Conventional two-dimensional models (fog nets) that use Raschel meshes on slopes have demonstrated high collection efficiency in arid ecosystems (Ismail & Go, 2021; Qadir et al., 2018). Recently, geometric innovations have been explored, including fog-catcher cylinders for greater wind resistance (Kanooni & Kohan, 2024) and vertical-thread fog harps that improve drainage (Shi et al., 2018). However, despite proven advances in their performance, these devices are installed predominantly as autonomous infrastructure outside living spaces. Thus, a gap remains in the literature regarding the direct integration of this technology into the building. Consequently, this research evaluates the regulation of the absolute humidity (AH) expressed in (g/m^3) by means of a passive dehumidification system that integrates the fog catcher's technology and the Venturi effect, applied to a standard housing module located in the study area.

METHODOLOGY

The research adopted an experimental quantitative approach, using a quasi-experimental design and an in situ comparative evaluation method, with a descriptive and comparative scope. The project aims to reduce internal humidity in a house by implementing a passive dehumidification system. First, areas with the highest fog concentration were identified to define the study area. Later, once located, photographic registration forms were used to determine the characteristics of the dwellings. An analysis of meteorological data from the last five years' winter period was also carried out, along with a study of the materials' thermal performance. In this way, ventilation and collection principles were applied, including the Venturi effect, wind collectors, and fog-catcher technology. Also, to determine the range of habitability and evaluate the prototype's impact, hygrothermal comfort parameters were established following the international standard ANSI/ ASHRAE 62.1-2025, which serves as the regulatory instrument for evaluating naturally conditioned spaces. The acceptable limit for indoor relative humidity is set at 65%. Complementarily, the thermal performance of the building envelope was analyzed using the guidelines of the Peruvian Technical Standard EM.110. With this, the modeling was designed in AutoCAD (2D) and SketchUp (3D). Subsequently, the effectiveness of the prototype was evaluated by comparing two 1:2-scale models: one as a reference and the other intervened with the prototype at 1:1 scale. The modules' scale was justified for logistical feasibility and methodological rigor; these proportions allowed manual transfer, field assembly, and improved control during experimentation. On the other hand, the prototype was kept at a 1:1 scale strictly due to the physical and constructive characteristics of the Raschel mesh. Subsequently, digital measuring instruments, such as hygrometers and anemometers, were used to collect CSV files with RH (%), temperature (°C), and wind speed (m/s) data, which affected the indoor conditions of both models. Finally, hygrothermal calculation equations were applied to obtain the AH value (g/m^3) and to determine the prototype's efficiency.

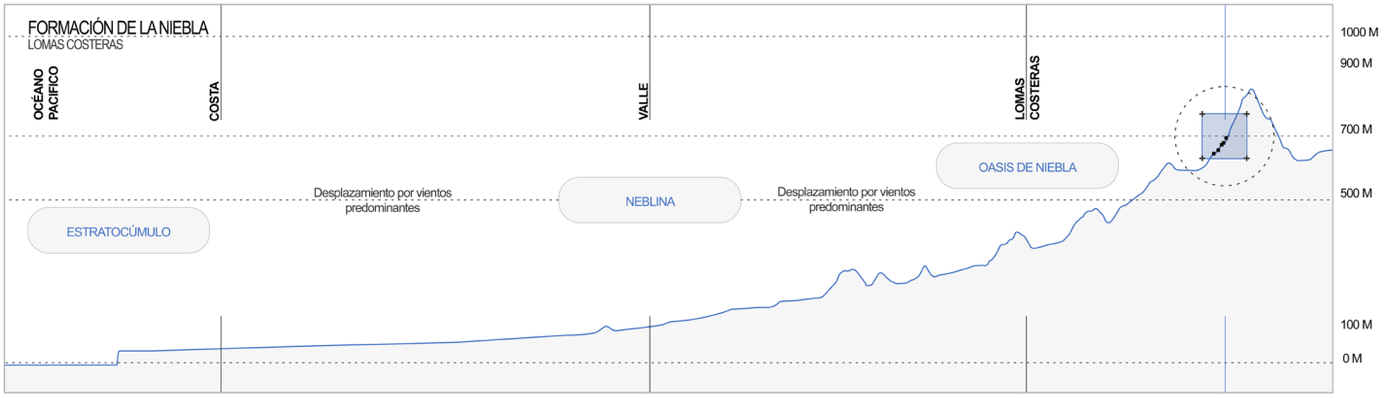


Figure 1. Formation of coastal fog. Source: UNDP (2018).

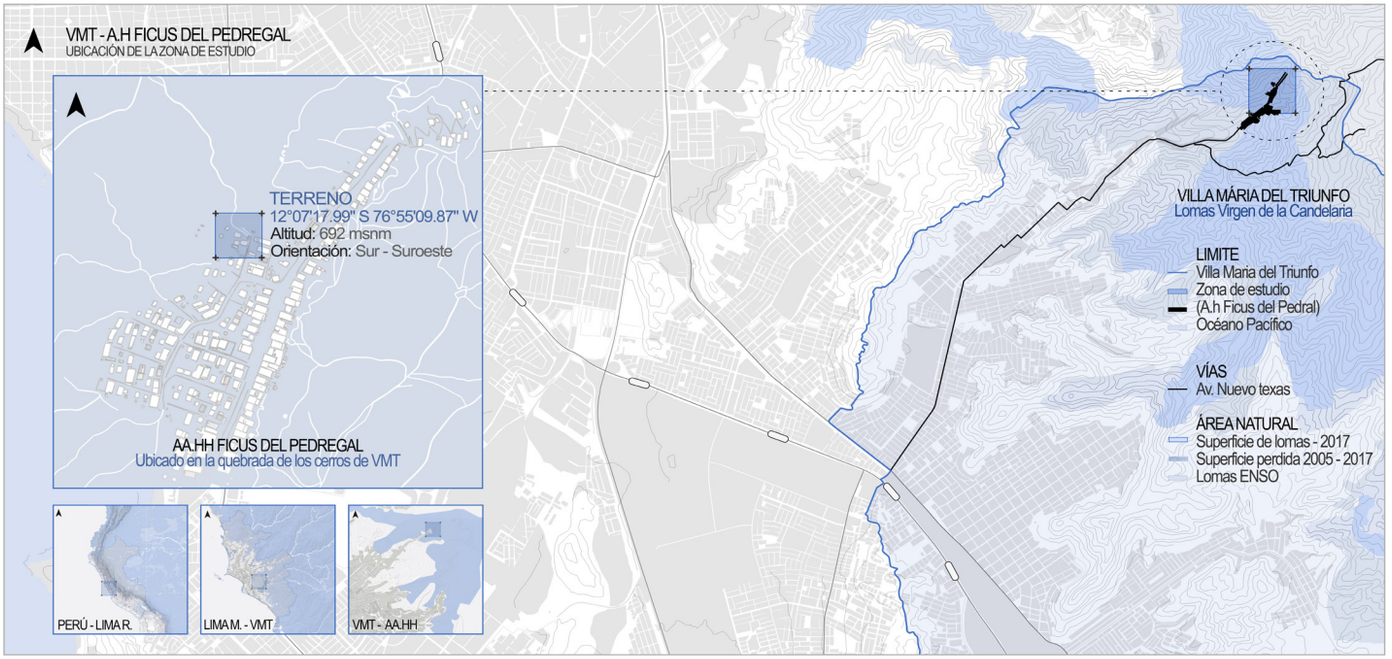


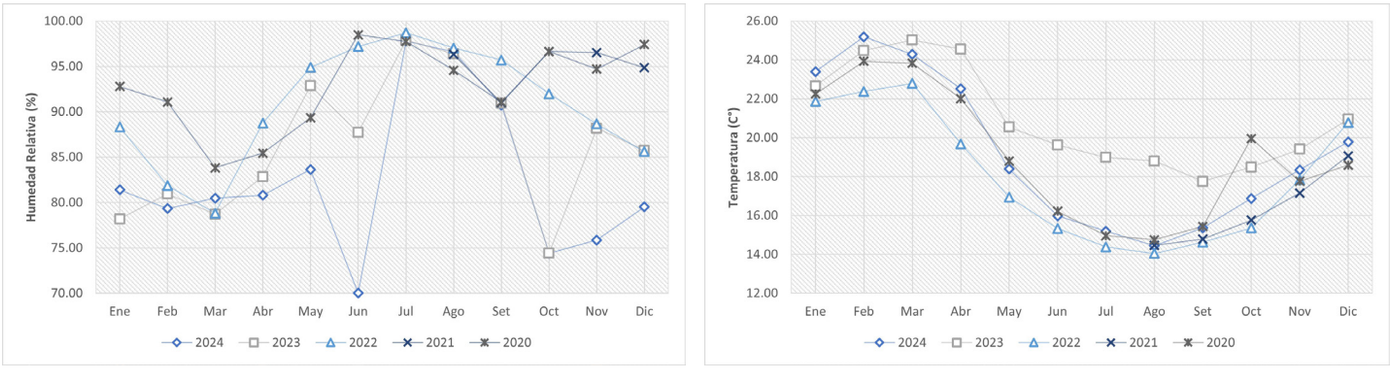
Figure 2. Location of the study area - A.H. Ficus del Pedregal, VMT. Source: Prepared by the authors.

COASTAL FOG FORMATION

The Humboldt Current and the upwelling of cold Pacific waters influence the condensation and formation of coastal fog (United Nations Development Program [UNDP], 2018). When transported by the south and southwest winds towards the foothills of the Andes at altitudes of 400 to 1000 meters above sea level, they create fog banks or oases (Moat et al., 2021) and record RH values of 100% (SENAMHI, n.d, a.) (Figure 1). Humidity, defined as the amount of water vapor in the air, can condense into droplets when the air reaches saturation (Tejeda Martínez, 2018). It is expressed in relative or absolute humidity.

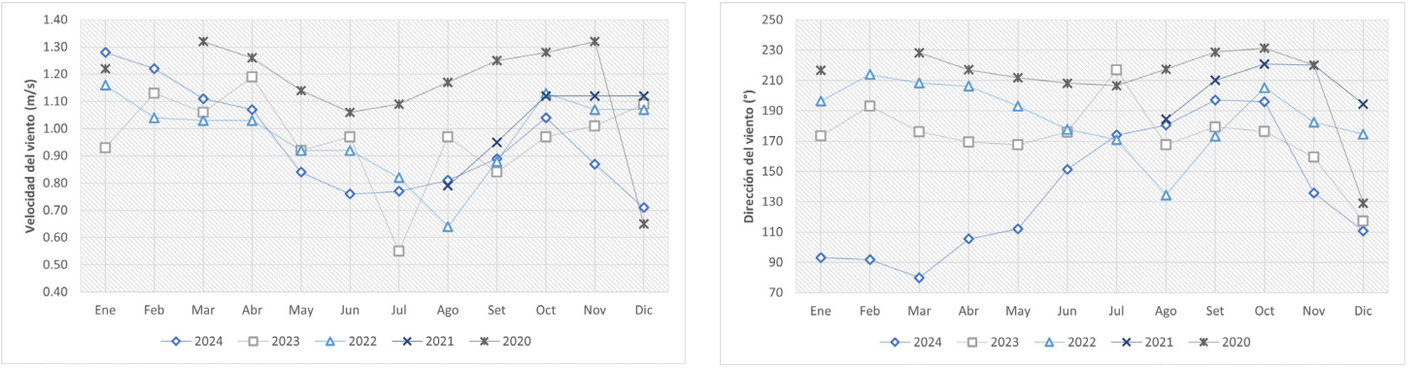
IDENTIFICATION OF THE STUDY AREA

The investigation considered four criteria for the DESHUME project site: 1) Proximity to a coastal hill, 2) Humidity present in the atmosphere, 3) Altitude oscillating from 400 to 1000 meters above sea level, and 4) Orientation perpendicular to the prevailing winds. Therefore, the selected urban area is the A.H. Ficus del Pedregal, José Carlos Mariátegui sector, near the Virgen de la Candelaria Hills, in the district of VMT (MINAM, 2019) (Figure 2). The study area is located at 692 m.a.s.l. (12°07'17.99" S; 76°55'09.87" W), facing the prevailing winds and has fog banks that reach a 100% RH during the winter.



a) b)

Figure 3. (a) Average relative humidity; (b) Average temperature (2020-2024). Source: SENAMHI (n.d. b)



a) b)

Figure 4. (a) Average wind speed; (b) Average wind direction (2020-2024). Source: SENAMHI (n.d.b).

METEOROLOGICAL DATA

To determine the characteristics influencing fog formation and humidity, 5 years of meteorological data (2020-2024) were collected, obtained from the Automatic Meteorological Station of VMT, 112233, located at 292 m.a.s.l., at coordinates 12°9'59" S and 76°55'12" W (SENAMHI, n.d. b). The station performed continuous monitoring of the variables of relative humidity (%), air temperature (°C), wind speed (m/s), and wind direction (°); and the data were recorded with a continuous hourly frequency in CSV files. The records obtained were processed into monthly average values, which were subsequently checked interannually to obtain a final average value.

RELATIVE HUMIDITY AND TEMPERATURE

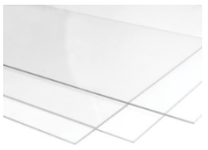
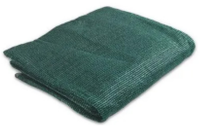
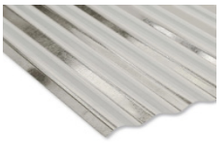
The RH (%) data recorded during the winter of 2020 to 2024 indicate that environmental values exceed the standards, reaching up to 100% (Figure 3a). Also, during the months from June to September, the record of monthly average temperatures for the five years evaluated shows that the lowest temperatures occur in August, at 14.04 °C (Figure 3 b).

WIND SPEED AND DIRECTION

In the winter months of the analyzed period, average speed values showed a progressive increase, reaching a maximum of 5.5 m/s and a minimum of 0.00 m/s, with an average of 0.89 m/s (Figure 4a). The wind direction is measured in degrees relative to true north (0°). In this sense, the predominant direction during the winters of 2020 to 2024 was from the south -southwest, with an average of (≈186.25°) (Figure 4, b).

THERMAL PROPERTIES OF THE MATERIALS

The construction properties of the houses were recorded using photographic record forms. Subsequently, an analysis of the materials' thermal characteristics (Table 1) was carried out to determine their insulating capacity, to consider these conditioning factors in the modules (1:2), and to ensure greater efficiency of the prototype (1:1). For this, the performance (Equation 1) and insulation capacity (Equation 2) were evaluated against the predominant climatic aspects of the study area. The city of Lima was identified in Bioclimatic Zone 1: Coastal Desert. Then, the materials were classified by construction system, and their compliance with the

Properties	Triplay	Acrylic	Raschel Mesh	Metallic calamine
Materials used				
Construction system	Wall	Opening	-	Roof
Dimension (m)	2.44x1.221[1]	1.83x1.221[1]	4.20 x 1.001[1]	3.60x0.801
Thermal Conductivity (λ)	0.14 W/°Cm2[2]	0.200 W/° Cm2[2]	-	0.14 W/°Cm2[2]
Thermal Resistance (R)	0.28 m²°C/W	0.17 m²°C/W	-	0.21 m²°C/W
Thermal Transmittance (U)	3.57 W/m°C	5.88 W/m°C	-	4.76 W/m°C
Moisture Content (%)	5-8	-	-	-
Composition of the Film	Kraft paper+phenolic resin	-	HPPE-UV	Galvanized steel+Zinc
Surface coverage (%)	100	100	50	-
Water vapor permanence (μ)	50	-	-	-
Waterproofing (Approved/ Rejected)	Low	Approved	-	Approved

1 Standard commercial format, 2 Obtained from the EM Technical Standard 110.

Table 1. Technical characteristics of the materials. Source: Prepared by the authors.

maximum permissible thermal transmittance values was evaluated in accordance with the EM.110 Technical Standard (MVCS, 2016).

$$U = 1 / Rt. \quad \text{(Equation 1)}$$

$$Rt = e / \lambda \quad \text{(Equation 2)}$$

Triplay's hygrothermal properties indicate low resistance to vapor entry (μ≈30-50), facilitating the diffusion of moisture into its fibers. This permeability, combined with an RH of more than 65%, creates critical conditions for pathologies such as absorption swelling and fungal colony proliferation. Therefore, this envelope requires a varnish coating to counteract the wooden panel's absorbency. Similarly, metallic calamine, despite its corrosion-resistant zinc coating (90g/m²), has high transmittance and thermal conductivity, allowing heat or cold to pass through without forming a thermal buffer. This shows that the predominant materiality of the houses performs poorly as an insulator in the face of environmental conditions, thereby influencing indoor humidity levels.

CONFIGURATION OF THE PROTOTYPE

Natural or passive ventilation is based on two principles that mobilize the air by natural forces within a room (Saber et al., 2021). One of them is the cross-ventilation generated by the wind (Al-Shamkhee et al., 2022). In the design of passive ventilation systems, the Venturi effect enables air movement without mechanical means (Venturi, 1797). Additionally, Bernoulli's principle reports that the pressure of a fluid decreases as its velocity increases (Suárez et al., 2021). According to this, several studies show that, in order to guarantee the continuity of the air flow, the reduction in the cross-section in a duct (Venturi effect) can accelerate the local wind sufficiently to generate a negative pressure zone that induces the continuous suction of the air (Zhang et al., 2021), maximizing natural ventilation rates (Blocken et al., 2011) (Figure 5, a). This principle was adapted to the design to favor the entry of external air and encourage internal circulation. Thus, the duct of the prototype comprises three successive sections, (i) an inlet section, with a convergence angle of 73° where the air enters at high pressure; (ii) a throat or core section, where the reduction in dimensions concentrates the flow and generating a low pressure zone; and (iii) an outlet section with a divergence angle of 52°, where the duct recovers its dimensions and the flow returns to high pressure conditions (Figure 5, b). The relationship between the angles of convergence and divergence, as well as between the duct's height and width, proved crucial to optimizing the natural movement of air.

The prevailing wind direction determined the prototype's location. Therefore, the fundamentals of the wind catcher were adapted (Figure 6, a) (Ortego Fernández,

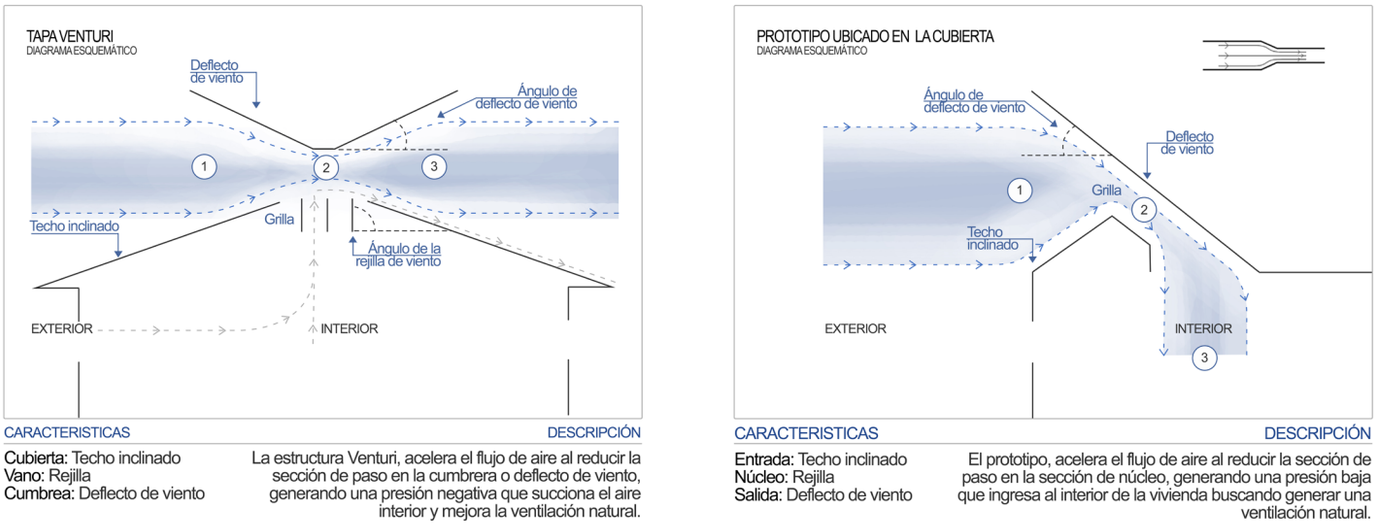


Figure 5. (a) Schematic diagram of the Venturi effect. Source: Zhang et al., 2021; (b) Schematic diagram of the prototype. Source: Prepared by the authors.

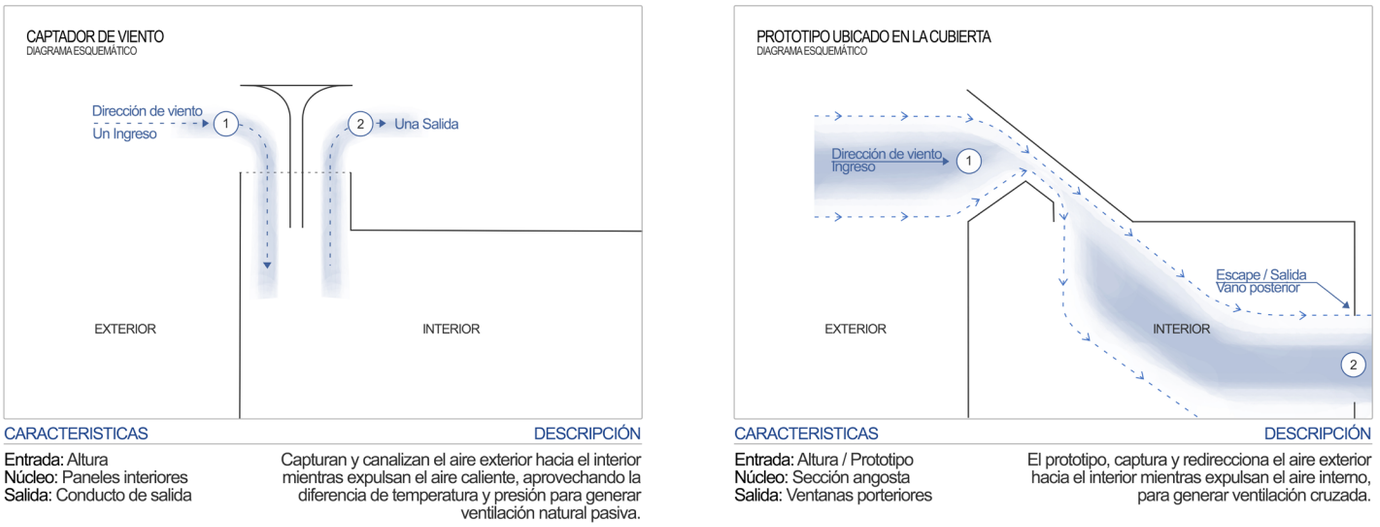


Figure 6. (a) Schematic diagram of wind catcher. Source: Ortego Fernández (2020); (b) Schematic diagram of the prototype. Source: Prepared by the authors.

2020), having a design that seeks to capture and redirect outdoor air currents inside the housing module through a duct that facilitates its entry and distribution. In this way, the configuration of the prototype allows the capture and introduction of external airflow into the house, encouraging internal circulation and cross-ventilation, which promotes the removal of indoor humidity (Figure 6, b).

The design of the prototype not only aims to avoid the accumulation of moisture through ventilation, but also seeks to capture the air coming from the outside, with an RH close to 100%, introducing it with reduced levels, after being mechanically filtered by the meshes, thus obtaining a passive dehumidifying system (Tejeda Martínez, 2018). Therefore, the two-dimensional fog catcher technology is incorporated (Qadir et al., 2018), recognized as an effective passive solution for water harvesting in arid ecosystems and coastal hills. The physical principle is based on the direct interception of fog composed of microscopic water droplets suspended in the air, with diameters ranging from 1 to 30 microns (Márquez Robles, 1993). When the wind pushes this saturated mass against a perpendicularly installed porous surface, the droplets impact the filaments, coalescing and falling by gravity (Ismail & Go, 2021) (Figure 7, a). Thus, the mesh acts as a physical filter that extracts liquid water mass from the airflow before it enters, thereby actively reducing its absolute humidity. The efficiency of this water removal

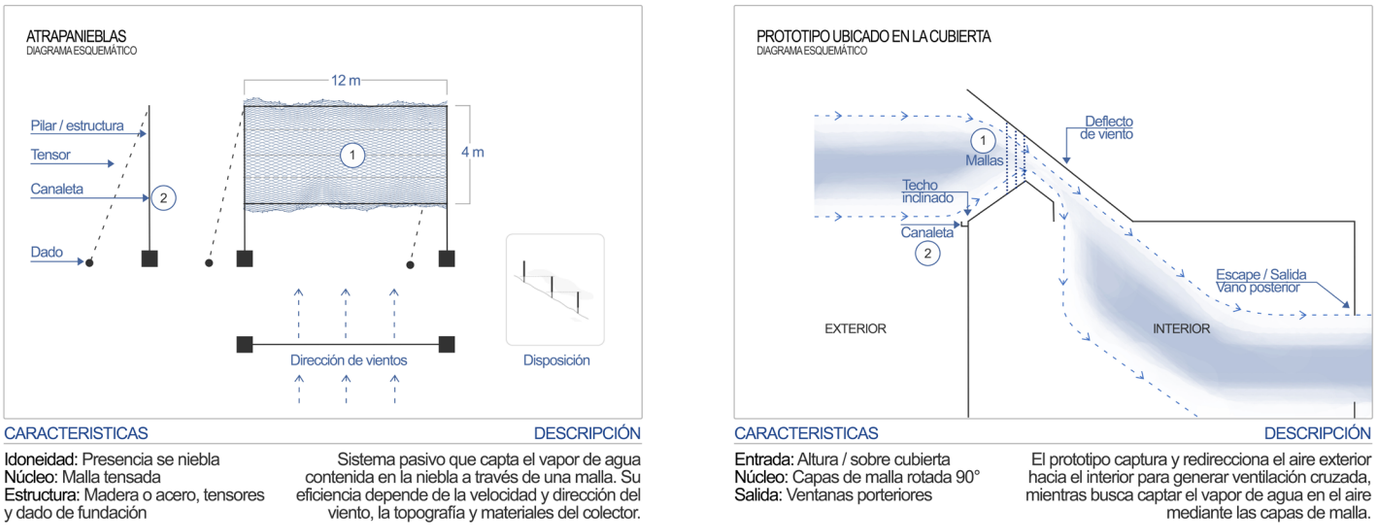


Figure 7. (a) Schematic diagram of the fog catcher. Source: Di Bitonto (2019); (b) Schematic diagram of the prototype. Source: Prepared by the authors.

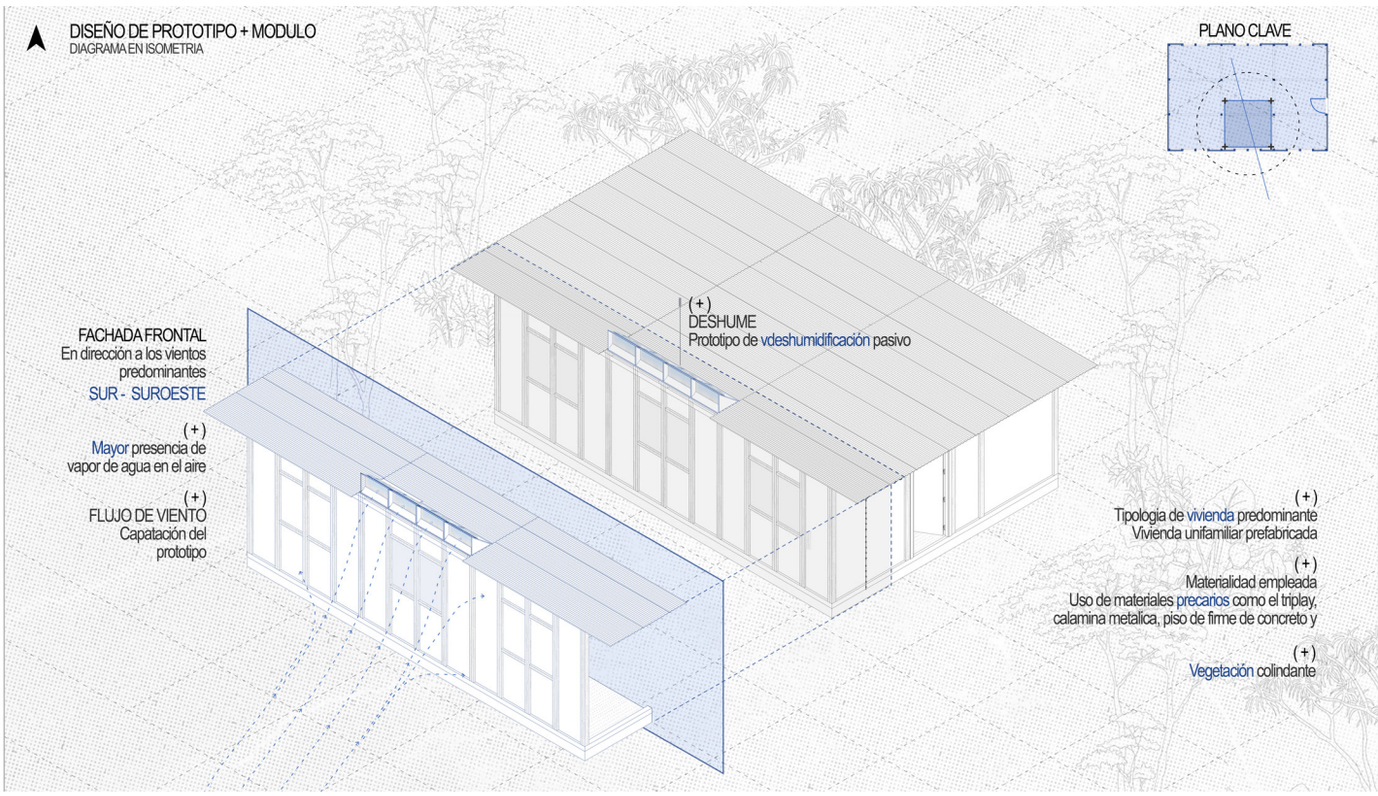


Figure 8. Implementation of a prototype in a dwelling. Source: Prepared by the authors.

is directly proportional to the size of the collecting surface, measured as liters collected per square meter per day (L/m²/day) (Ghiasi, Aslani & Alisoltani, 2025). This makes it possible to capture at least 1 L/m²/day of installed mesh. (Vásquez-Ramírez, Cieza-León & Cieza-León, 2020). In this sense, to maximize airflow impact given the prototype's smaller front opening area (0.24 m²) and dehumidify an interior volume of 1.82 m³, the design compensates for this limitation by increasing the net capture area. The core consists of three layers of polyethylene Raschel mesh in parallel, spaced 4cm apart, and alternating

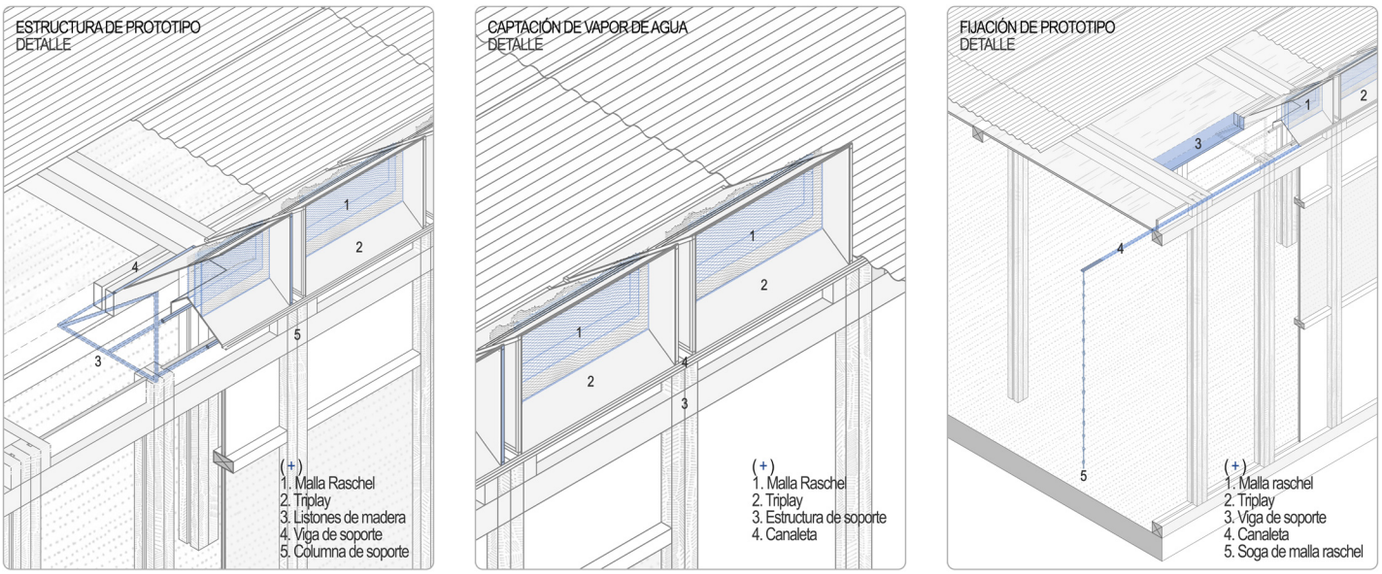


Figure 9. (a) Detail of the installation; (b) Detail of the capture; (c) Detail of the redirection of the collected water. Source: Prepared by the authors.

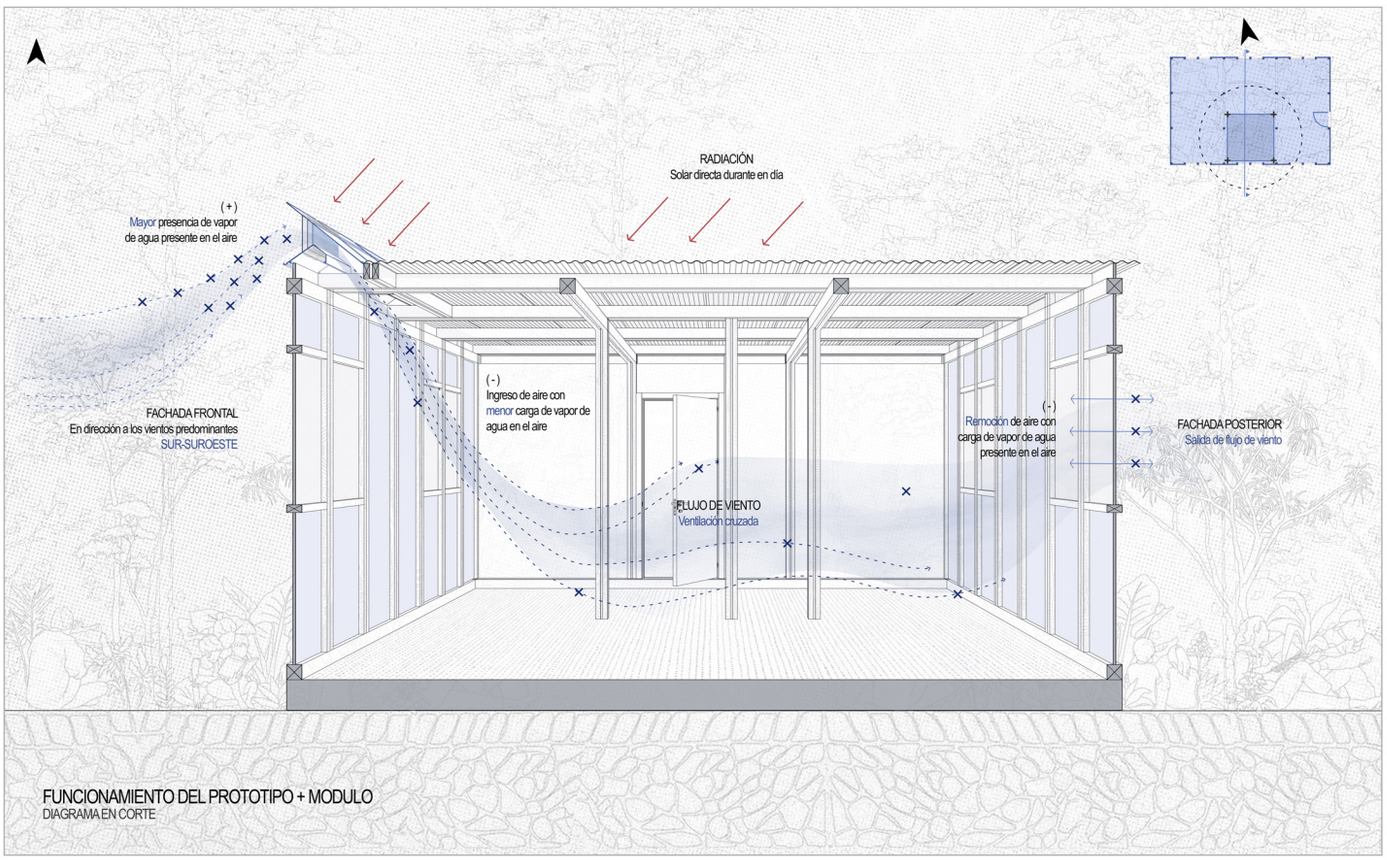


Figure 10. Operation of the DESHUME prototype in a dwelling. Source: Prepared by the authors.

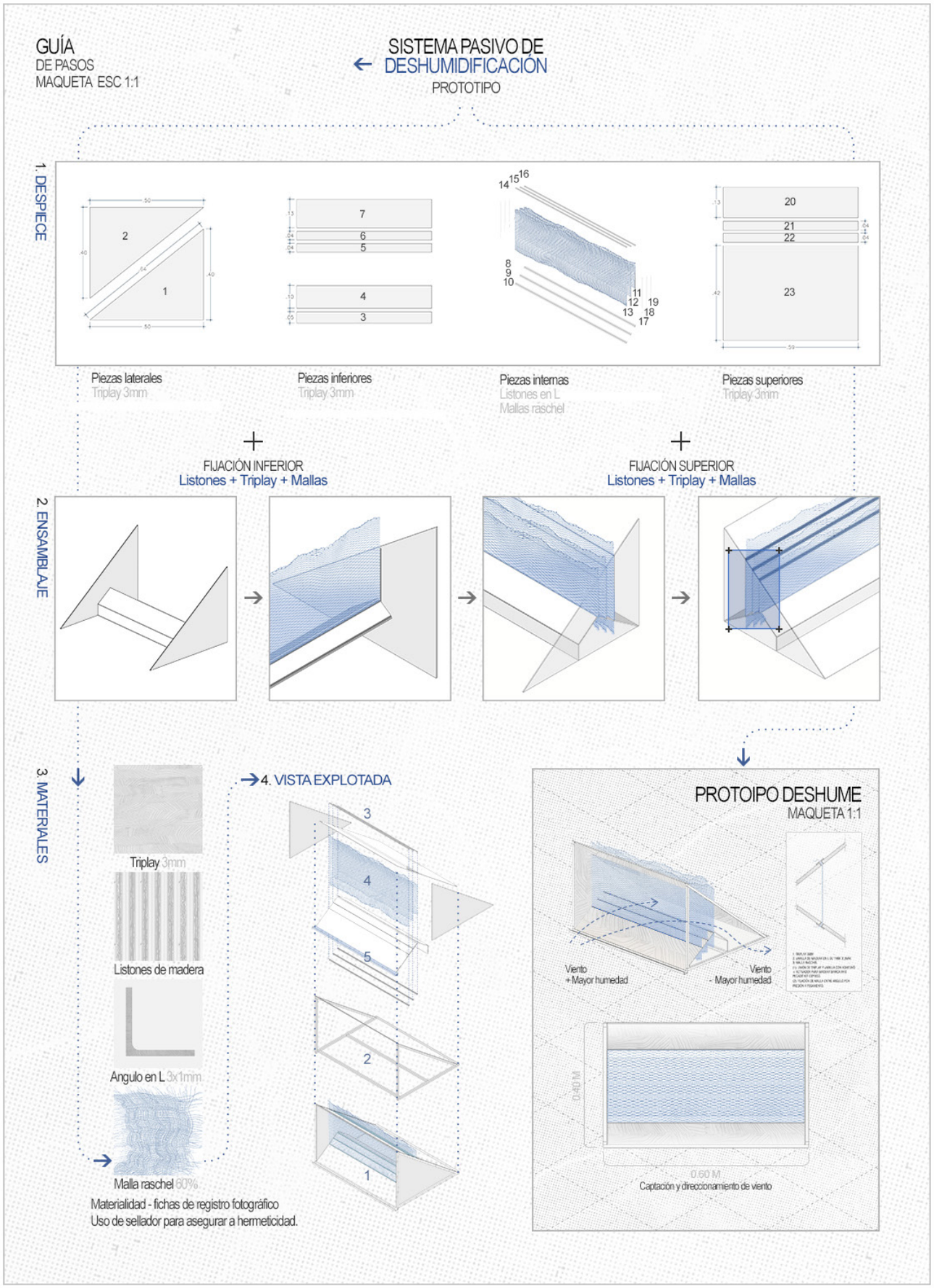


Figure 11. Assembly of the prototype. Source: Prepared by the authors.



Figure 12. Photographic record of the Prototype's assembly. Source: Prepared by the authors.

horizontally and vertically to avoid overlap (Figure 7 b). This configuration densifies the moisture-collecting surface within a reduced area, considering wind orientation, the optimal shade of 50%-60% (Regalado & Ritter, 2016), and reducing its wear from factors such as radiation. Finally, the captured water is redirected by gravity through an external gutter. In this way, fog-catcher technology is used and enhanced to develop a prototype that efficiently integrates wind, surface area, and humidity.

PROTOTYPE + MODULE DESIGN

A 5.50×8.80 m housing module was designed to replicate the characteristics of the study area's typologies (Figure 8). The prototype was installed on the facade, perpendicular to the prevailing winds, on the wooden structures (Figure 9a), which serve as supports to ensure its proper installation and operation. This arrangement allows the three layers of mesh to intercept water vapor in the wind flow (Figure 9, b), redirecting the captured water towards a gutter (Figure 9, c), and, in turn, the pressure generated by the Venturi effect allows the airflow to enter the house. In this way, the prototype facilitates natural ventilation and reduces the accumulation of indoor humidity, ultimately allowing its exit through the rear openings (Figure 10).

ASSEMBLY OF THE PROTOTYPE

The assembly of the prototype at 1:1 scale (Figure 11) involved dismantling its components, taking into account the selected materials and the system's construction logic. An adhesive and activator kit for wood was used in this process, enabling fast and efficient attachment. It was started by joining the side pieces (1) and (2) with the lower ones (3) and (4). Subsequently, the three pairs of lower L-angles (8, 9, and 10) were attached at one end of pieces (4) and (7), and at both ends of pieces (5) and (6). Then, the meshes were placed successively: (11) between (4-5), (12) between (5-6), and (13) between (6-7). The pieces that exert pressure on each mesh were simultaneously adhered to sides (1) and (2), thereby ensuring their attachment. In the next step, the Raschel meshes (11, 12, and 13) were tightened and fixed to the sides (1) and (2) using 3×1mm rods (17, 18, and 19) on both sides, which were pressed between these and the side pieces. Then, the three pairs of upper L-angles (14, 15, and 16) were adhered at the ends of pieces (20) and (23), and at both ends of pieces (21) and (22). Then, the meshes were arranged in sequence: (13) between (20-21), (12) between (21-22), and (11) between (22-23), and secured to sides (1) and (2). Finally, the joints were sealed with Sikaflex-11FC adhesive to ensure the prototype's tightness (Figure 12).

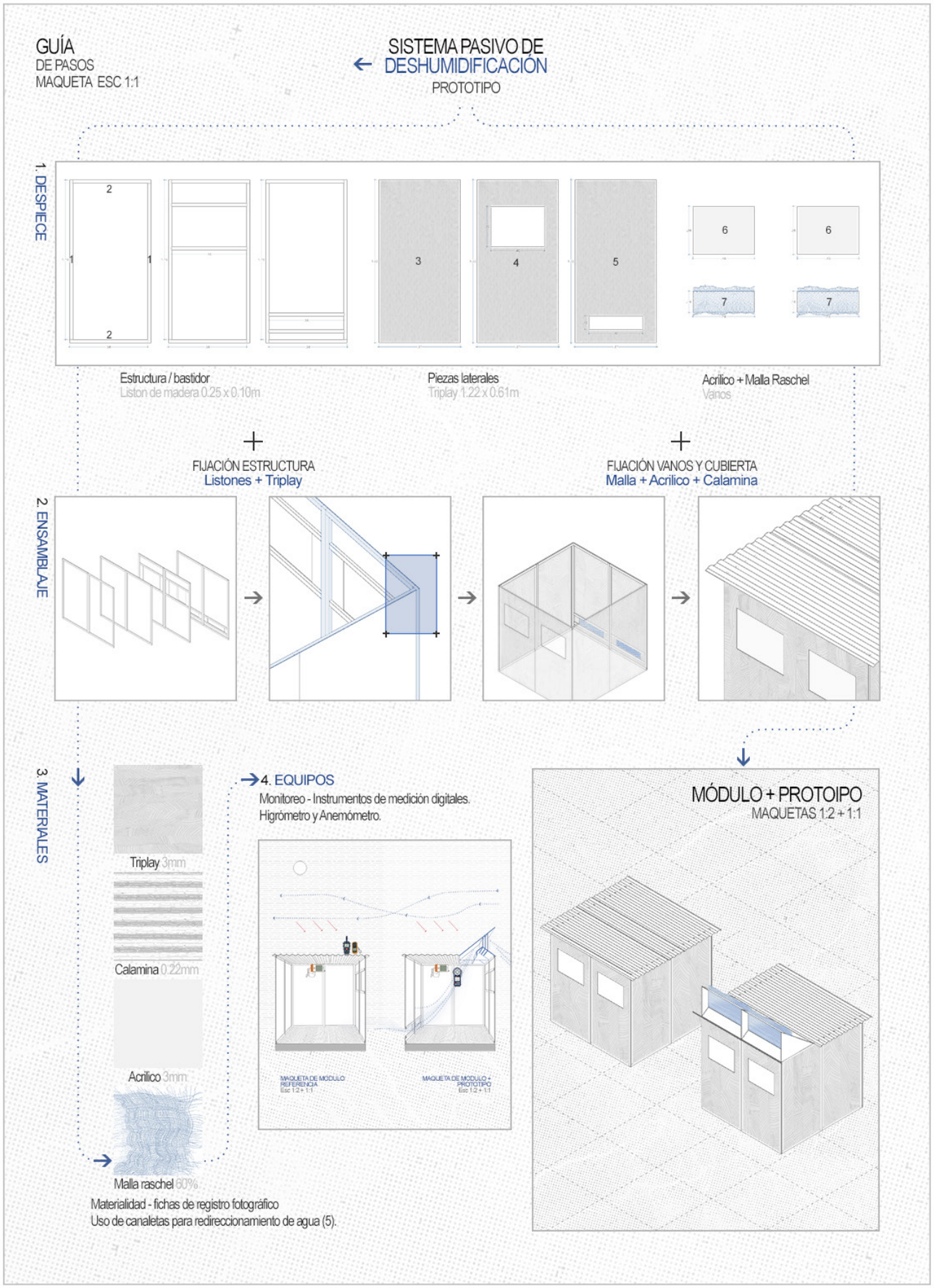


Figure 13. Assembly of the module. Source: Prepared by the authors.



Figure 14. Photographic record of the module's assembly. Source: Prepared by the authors.

ASSEMBLY OF THE MODULE

Subsequently, from a section of the house's front facade, two 1:2-scale models were set up to optimize experimental control in terms of resources, dimensions, and constructability, and to ensure the representativeness of the modules for the study area's climatic conditions. The assembly began with the arrangement of 16 wooden slats (1) and (2), forming 8 frames of 1.22×0.61m, each structured by two slats of both types. Next, 1.22×0.61m (3)(4)(5) Triplay plates were fixed on the 8 frames: two complete pieces formed a side wall. A span of 0.30×0.40m was made on the front wall in each piece (4), and finally, on the back wall, a smaller span of 0.10×0.40m (5) in a single piece. The front spans were covered with 3mm acrylic plates (6), and the back with a layer of Raschel mesh (7). Then, the walls were joined, sealing possible openings with Sikaflex-11FC adhesive to ensure greater tightness. 0.22 mm metal calamine was used for the roof and secured to the structure with nails; the remaining openings were also sealed to prevent leaks. In this way, the assembly of the module and prototype is completed (Figure 13) (Figure 14).

MONITORING AND DATA COLLECTION

During monitoring, the 1:2-scale modules remained unoccupied to control variables such as humidity sources from internal activities. This delimitation made it possible to isolate the performance of the DESHUME system from external climatic conditions and its interaction with the envelope materials, without anthropogenic interference. Likewise, data collection took place after installing the 1:2-scale models onsite, with only one incorporating the 1:1 prototype. Measuring equipment was installed both inside and outside; RH, temperature, and wind speed data were recorded at 15-minute intervals for 3 consecutive days. The temperature and RH were recorded by an Elitech GSP-6 hygrometer inside and a Benetech GT1368 outside. Likewise, the wind speed was recorded with a Wintact WT87B anemometer inside at a height of 1m and 0.50m from the front wall, and with a Benetech GM816 outside. The instruments operated within their respective factory calibration, with very small technical error margins: the inner hygrometer has an accuracy of ±0.5°C and ±3% RH; the outer hygrometer has an accuracy of ±1.5°C and ±5.0% RH; and both anemometers have an operating speed error margin of ±5%. To ensure the representativeness of the hygrothermal conditions, the indoor anemometer was located at 1.00m height, considering comfort and ventilation criteria (Zhai et al., 2015), which determine a range of 1.00m to 1.10m as suitable for evaluating the airflow in the human occupation zone (torso or head

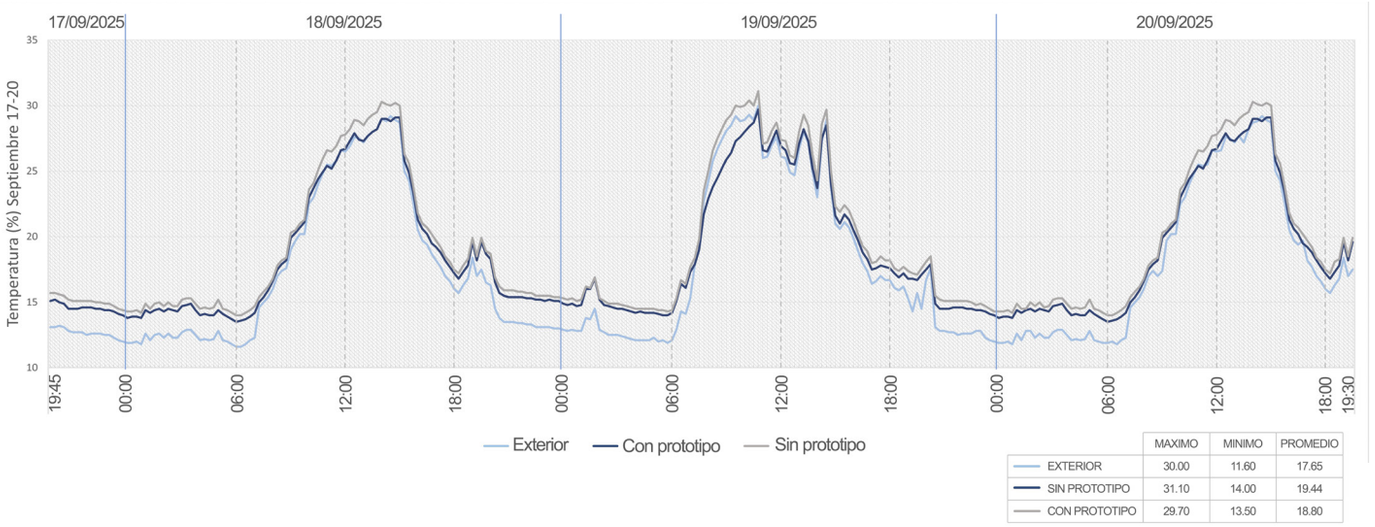


Figure 15. Temperature record - VMT, 2025. Source: Prepared by the authors.

level). Likewise, the instrument was spaced 0.50m from the front wall to avoid measurement bias introduced by thermal transfer and the envelope boundary layer. Finally, the outdoor measurement was performed at a 1.20m SNPT in a clear area to record the unobstructed ambient airflow.

DATA ANALYSIS

Subsequently, a hygrothermal calculation was performed using the Magnus-Tetens approximation (Vaisala, 2013) to convert temperature (°C) and relative humidity (%) into absolute humidity (g/m³). The saturation vapor pressure Pws in hPa was calculated first (Equation 3) and then the actual vapor pressure Pw in hPa (Equation 4).

$$P_{ws}(T) = A \cdot 10^{\frac{m \cdot T}{T+T_n}} \quad (\text{hPa}) \qquad \text{(Equation 3)}$$

$$P_w = P_{ws} \cdot \frac{RH}{100} \quad (\text{en hPa}) \qquad \text{(Equation 4)}$$

Also, to determine the AH (Equation 5), it was required to convert the temperature from °C to °K (Equation 6) and the actual vapor pressure Pw from hPa to Pa (Equation 7), obtaining values in g/m³. This information enabled the comparison of the data collected from the reference module with that from the intervened module and, in turn, validated the effectiveness of the DESHUME system.

$$\boxed{A = C \cdot \frac{P_w}{T}} \quad (\text{g/m}^3) \qquad \text{(Equation 5)}$$

$$T_K = T(^\circ\text{C}) + 273.15 \qquad \text{(Equation 6)}$$

$$1\ \text{hPa} \times 100\ \text{Pa} \qquad \text{(Equation 7)}$$

Then, using the temperature, wind speed, and AH data, comparative tables were prepared for the 3 measurement moments.

RESULTS AND DISCUSSION

The outdoor temperature varied widely between 12°C and 30°C, with an average of 17.7°C. In comparison, the indoor temperature of the intervened module averaged 18.8°C, slightly lower than the reference (19.4°C), indicating a slight thermal damping effect. The nighttime temperatures ranged from 13.5°C to 15.2°C in the prototype and from 14.2°C to 15.7°C in the reference (Figure 15).

When comparing the hygrothermal comfort band (30%-60%) based on the ANSI/ASHRAE 62.1-2025 Standard and the RNE EM.110, the intervals in which indoor environments achieve comfortable conditions are shown (Figure 16). The time spent in the comfort range during the control was 3 days: Outside (13.5 h), Without prototype (19.75 h), and With prototype (18.5 h).

The outdoor AH exceeded the standards, averaging 12g/m³. The module operated with the DESHUME prototype showed a slight reduction to 10.98g/m³; while the reference module indicated 11.18g/m³. The most noticeable variation was observed in the mornings, with 14.41g/m³ for the prototype compared

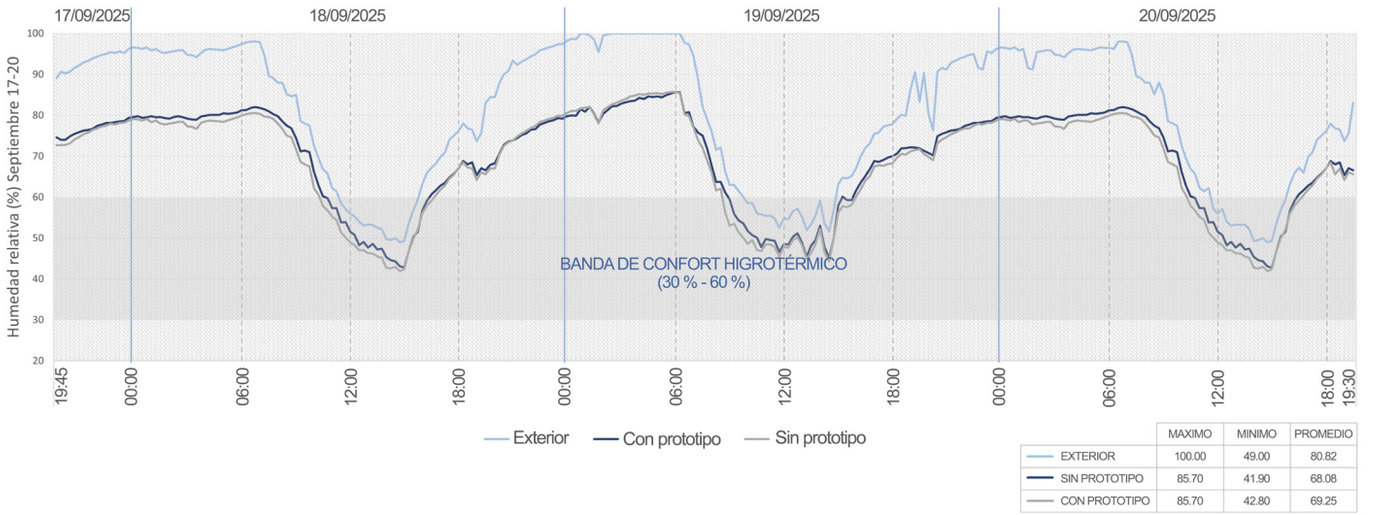


Figure 16. Relative Humidity record - VMT, 2025. Source: Prepared by the authors.

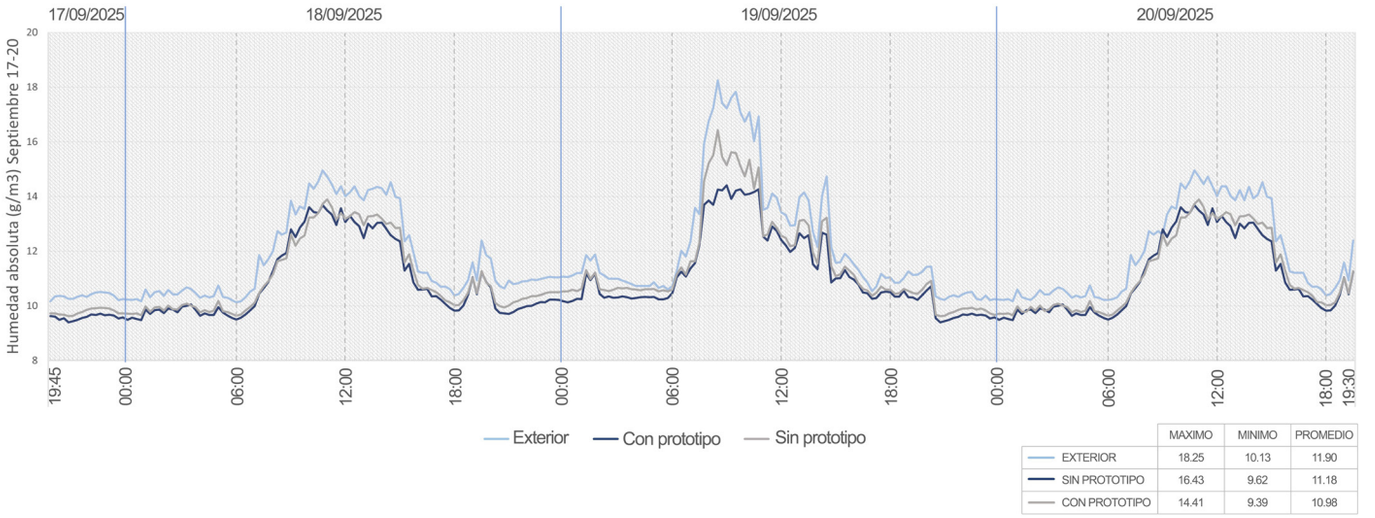


Figure 17. Absolute Humidity record - VMT, 2025. Source: Prepared by the authors.

to 16.43g/m³ for the reference module, indicating a reduction of 2.02g/m³ (Figure 17).

The average outdoor wind speed was 0.44 m/s, with a peak of 2.1 m/s, whereas indoors the anemometer did not record any airflow (Figure 18).

Variations were evident between the variables of absolute humidity (g/m³), wind speed (m/s), and temperature (°C), which reflect internal differences in both modules. The prototype recorded an average of 10.98g/m³ of indoor AH during the study days, which represents a reduction of 0.20g/m³ compared to the reference module (11.18g/m³); they have capture peaks of 2.02g/m³ (12.3%) during the daytime hours and 0.23 g/m³ (2.4%) during the night hours. Although the anemometer did not record measurable indoor wind, these variations indicate that the system functions as a passive regulator of the vapor load by condensation and interception in the Raschel meshes. The decrease in temperature in the prototype module suggests a slight exchange with colder outside air or lower thermal retention. Overall, the prototype demonstrates partial efficiency under weak wind conditions. At this point, its potential as a passive hygrothermal control device through collection stands out, depending on the geometry and the availability of ambient airflow.

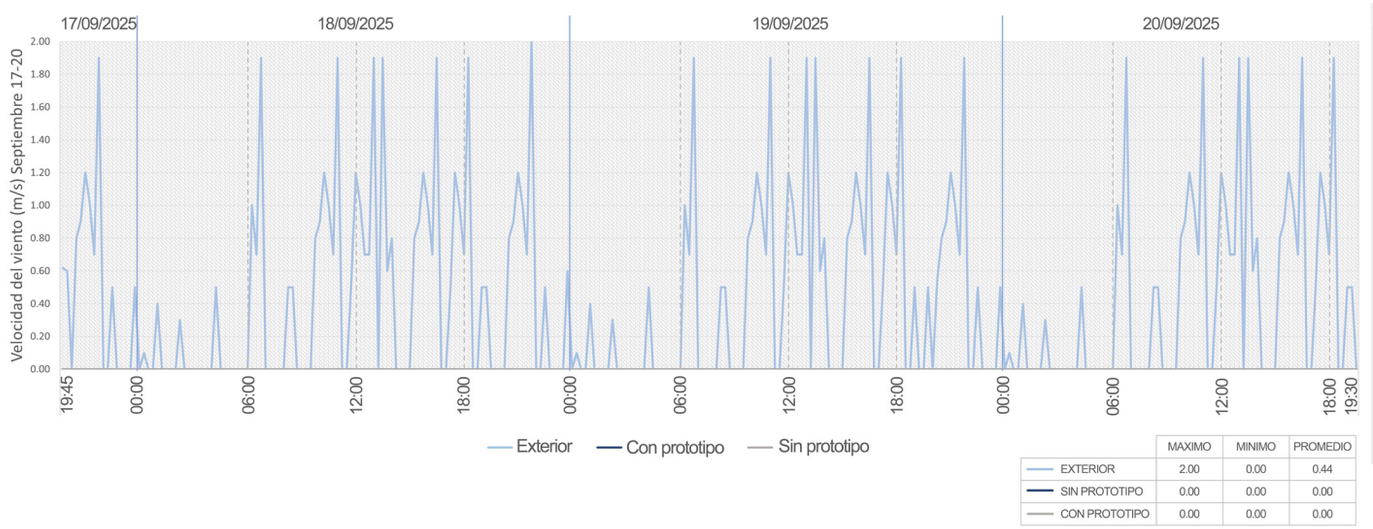


Figure 18. Wind speed record - VMT, 2025. Source: Prepared by the authors.

CONCLUSIONS

The prototype met the main objective of serving as a passive dehumidification strategy, using a modular, easily assembled system conceived for use in homes without requiring major interventions in high-humidity areas. Although the reduction in AH was minimal (1.79%), the prototype demonstrated hygrothermal improvement as a passive system, indicating its potential as a sustainable alternative. Although a slight increase in RH was recorded due to the decrease in indoor temperature, the dehumidification achievement is not invalidated, since a mass of water was removed. An average reduction of 0.20g/m^3 in AH was observed relative to the reference modulus.

The performance of the system is validated by comparing it with the related literature: unlike the reactive storage mechanism of other passive systems that attenuate up to 12% RH at 23°C, in which 2.47g/m^3 of HA is reduced (Zhang, Yoshino & Hasegawa, 2012), DESHUME achieves an active removal of AH (0.20g/m^3) under minimum temperatures and critical saturation conditions (100%RH), by overcoming the dependence on the damping capacity of the construction materials. In addition, when compared with complex solutions, such as the hybrid system (Chen et al., 2023), which reports 5g/m^3 reductions, DESHUME achieves consistent AH removal with a fully passive system, establishing itself as an appropriate strategy for self-construction. However, its performance requires future studies on the mesh's durability under UV exposure and mechanical wind pressure, as well as on the variability of performance with respect to its orientation to prevailing winds.

On the other hand, the Venturi effect did not reduce AH, whereas the moisture retention established by the three layers of mesh predominated. This strategy addressed the reduction in the fog catcher's catchment area and slowed the airflow.

Among the limitations, it can be said that the system's components were not evaluated independently (the geometric sensor without the meshes present), so the specific contribution of the aerodynamic shape versus the mechanical retention of the fabric cannot be broken down. Also, since no Computational Fluid Dynamics (CFD) simulations were performed, it is not possible to accurately estimate the geometry's contribution to the increase in dynamic pressure.

Finally, it is recommended to analyze the relationship between the volume of the 1:2 module (1.82 m^3) and the dimensions of the opening in the 1:1 prototype, whose geometric design allows control of the air pressure and velocity entering the house, as well as the acceleration of the wind's passage. Also, it is suggested to evaluate the behavior of the 1:1 prototype in a real house, for a longer period and in different seasons, using differential pressure sensors or more sensitive anemometers, in addition to considering anthropogenic hygrothermal load factors (breathing and cooking), to evaluate the performance of the system against internal steam sources.

CONTRIBUTION OF AUTHORS CRediT:

Conceptualization, M.N.D.P.; Data Curation, M.N.D.P. and A.L.C.V.P.; Formal analysis, M.N.D.P. and A.L.C.V.P.; Acquisition of financing M.N.D.P. and A.L.C.V.P.; Research, M.N.D.P. and A.L.C.V.P.; Methodology, M.N.D.P. and A.L.C.V.P.; Project management, M.N.D.P. and A.L.C.V.P.; Resources, M.N.D.P. and A.L.C.V.P.; Software. M.N.D.P. and A.L.C.V.P.; Supervision, R.H.V.S.; Validation, M.N.D.P. and A.L.C.V.P.; Visualization, M.N.D.P. and A.L.C.V.P; Writing - original draft, M.N.D.P. and A.L.C.V.P.; Writing - proofreading and editing, M.N.D.P. and A.L.C.V.P.

ACKNOWLEDGMENTS

The authors express their gratitude to the people involved during the experimentation process for their participation, valuable collaboration, and disinterested support in the development of the research. They also extend sincere recognition to the Technological University of Peru for the institutional support provided.

BIBLIOGRAPHIC REFERENCES

Al-Shamkhee, D., Al-Aasam, A. B., Al-Waeli, A. H. A., Abusaibaa, G. Y., & Moria, H. (2022). Passive cooling techniques for ventilation: an updated review. *Renewable Energy and Environmental Sustainability*, *7*(23), 1-16. https://doi.org/10.1051/rees/2022011

American National Standards Institute [ANSI] / American Society of Heating, Refrigerating and Air-Conditioning Engineers [ASHRAE]. (2025). *ANSI/ASHRAE 62.1-2025: Ventilation and Acceptable Indoor Air Quality (Includes ANSI/ASHRAE addenda listed in Appendix Q).* ANISI Webstore. https://webstore.ansi.org/standards/ashrae/ansiashrae622025-2598518?source=blog

Blocken, B., van Hooff, T., Aanen, L., & Bronsema, B. (2011). Computational analysis of the performance of a venturi-shaped roof for natural ventilation: Venturi-effect versus wind-blocking effect. *Computers & Fluids*, *48*(1), 202–213. https://doi.org/10.1016/j.compfluid.2011.04.012

Campos-Vásquez, N., Manturano-Chipana, R. K., & Rabanal-Chávez, E. H. (2025). Causas e Influencia de la humedad en la infraestructura de las edificaciones. *Ciencia y Tecnología*, *24*(2), 27-33. https://doi.org/10.70414/cyt.v24i2.126

Chen, Y., Ozaki, A., Lee, H., Choi, Y., & Arima, Y. (2023). Development of an intelligent envelope system with energy recovery ventilation for passive dehumidification in summer and solar collection in winter. *E3S Web of Conferences*, *396*, 03025. https://doi.org/10.1051/e3sconf/202339603025

Di Bitonto, M. G. (2019). *Oasis productivo: infraestructura de acceso al Parque Pan de Azúcar para la preservación del sector a través de agua de niebla* [Tesis de maestría, Pontificia Universidad Católica de Chile]. Repositorio. https://repositorio.uc.cl/handle/11534/26488

Ghiasi, B., Aslani, Z. H., & Alisoltani, T. (2025). Assessing the feasibility and sustainability of fog water harvesting as an alternative water resource. *Scientific reports*, *15*(1), 19254. https://doi.org/10.1038/s41598-025-03919-3

Ismail, Z., & Go, Y. I. (2021). Fog-to-Water for Water Scarcity in Climate Change Hazards Hotspots: Pilot Study in Southeast Asia. *Global Challenges*, 5(5), 2000036. https://doi.org/10.1002/gch2.202000036

Kanooni, A., & Kohan, M. R. (2024). Fog water harvesting with cylindrical brush. *Scientific Report*s, *14*(1),19679. https://doi.org/10.1038/s41598-024-70637-7

Márquez Robles, J. (1993). Atrapanieblas: una tecnología para la reforestación de las lomas costeras del Perú. *Ingeniería Industrial*, 7(007), 88–98. https://doi.org/10.26439/ing.ind1993.n007.3073

Ministerio del Ambiente [MINAM]. (7 de diciembre de 2019). Decreto Supremo N.° 011-2019-MINAM: Establece el Área de Conservación Regional Sistema de Lomas de Lima. *Diario Oficial del Bicentenario El Peruano. Normas Legales, 5-11*. https://busquedas.elperuano.pe/dispositivo/NL/1834838-3

Ministerio del Ambiente[MINAM]. (15 de agosto de 2021). *Mapa de lomas costeras de Lima Metropolitana*. Sistema Nacional de Información Ambiental [SINIA]. https://sinia.minam.gob.pe/mapas/mapa-lomas-costeras-lima-metropolitana-2021

Moat, J., Orellana-García, A., Tovar, C., Arakaki, M., Arana, C., Cano, A., Faundez, L., Gardner, M., Hechenleitner, P., Hepp, J., Lewis, G., Mamani, J.-M., Miyasiro, M., & Whaley, O. Q. (2021). Seeing through the clouds – Mapping desert fog oasis ecosystems using 20 years of MODIS imagery over Peru and Chile. *International Journal of Applied Earth Observation and Geoinformation*, *103*, 102468. https://doi.org/10.1016/j.jag.2021.102468

Ministerio de Vivienda, Construcción y Saneamiento, [MVCS]. (s.f.). GeoVivienda. Plataforma GIS del Ministerio de Vivienda, Construcción y Saneamiento. https://geo.vivienda.gob.pe/

Norma Técnica EM.110 (2016) [Ministerial Ministerio de Vivienda, Construcción y Saneamiento - MVCS]. Por la cual se establecen los parámetros técnicos de Confort Térmico y Lumínico con Eficiencia Energética. 27 de julio del 2016. https://www.gob.pe/es/i/2619729

Ortego Fernández, I. (2020). Torres de viento. Relectura contemporánea de sistemas energéticos pasivos [Trabajo Fin de Grado, Universidad Politécnica de Madrid]. Repositorio UPM. https://oa.upm.es/57995/

Programa de las Naciones Unidas para el Desarrollo [PNUD]. (16 de mayo de 2018). *Proyecto EbA Lomas: Retos y oportunidades en la conservación de las lomas de Lima Metropolitana*. https://www.undp.org/es/peru/publications/eba-lomas

Posani, M., Voney, V., Odaglia, P., Du, Y., Komkova, A., Brumaud, C., Dillenburger, B., & Habert, G. (2025). Low-carbon indoor humidity regulation via 3D-printed superhygroscopic building components. *Nature Communications*, *16*, 425. https://doi.org/10.1038/s41467-024-54944-1

Qadir, M., Jiménez, G. C., Farnum, R. L., Dodson, L. L., & Smakhtin, V. (2018). Fog water collection: Challenges beyond technology. *Water*, *10*(4), 372. https://doi.org/10.3390/w10040372

Regalado, C. M., & Ritter, A. (2016). The design of an optimal fog water collector: A theoretical analysis. Atmospheric *Research*, *178–179*, 45–54. https://doi.org/10.1016/j.atmosres.2016.03.006

Saber, E. M., Chaer, I., Gillich, A., & Ekpeti, B. G. (2021). Review of intelligent control systems for natural ventilation as passive cooling strategy for UK buildings and similar climatic conditions. *Energies, 14*(15), 4388. https://doi.org/10.3390/en14154388

Servicio Nacional de Meteorología e Hidrología del Perú [SENAMHI]. (s.f. a). *Estaciones meteorológicas.* Datos/ Datos Hidrometeorológicos*.* https://www.senamhi.gob.pe/?&p=estaciones

Servicio Nacional de Meteorología e Hidrología del Perú [SENAMHI]. (s.f. b). *Estadística de la calidad del aire: Estacion 112233.* https://www.senamhi.gob.pe/?p=calidad_del_aire-estadistica&e=112233

Shi, W., Anderson, M. J., Tulkoff, J. B., Kennedy, B. S., & Boreyko, J. B. (2018). Fog harvesting with vertical harps. *ACS Applied Materials & Interfaces*, 10(14), 11979–11986. https://pubs.acs.org/doi/10.1021/acsami.7b17488

Suárez, Á., Dutra, M., Monteiro, M., & Martí, A. C. (2021). El embrollo de Bernoulli: una investigación sobre las concepciones alternativas de los estudiantes en dinámica de fluidos. *Modelling in Science Education and Learning, 14* (2), 17–30. https://doi.org/10.4995/msel.2021.14835

Tejeda Martínez, A. (2018). *La humedad en la atmósfera. Bases físicas, instrumentos y aplicaciones*. Universidad de Colima. http://ww.ucol.mx/publicacionesenlinea/promocion.php?docto=466

Vaisala, O. (2013). Humidity Conversion Formulas*: Calculation formulas for humidity*. (Technical Reference B210973EN-F). https://www.hatchability.com/Vaisala.pdf

Venturi, J. B. (1797). *Recherches expérimentales sur le principe de la communication latérale du mouvement dans les fluides. Houel et Ducros*. Théophile Barrois. https://gallica.bnf.fr/ark:/12148/bpt6k9611865z.textelmage

Vásquez-Ramírez, L., Cieza-León, L., & Cieza-León, D. (2020). Eficiencia de captación de agua con tres tipos de malla atrapanieblas en zonas rurales altoandinas de la sierra norte del Perú. *Revista Ingeniería UC*, 27(3), 319-327. https://servicio.bc.uc.edu.ve/ingenieria/revista/

Zhai, Y., Zhang, Y., Zhang, H., Pasut, W., Arens, E., & Meng, Q. (2015). Human comfort and perceived air quality in warm and humid environments with ceiling fans. *Building and Environment*, 90, 178-185. https://doi.org/10.1016/j.buildenv.2015.04.00

Zhang, H., Yoshino, H., & Hasegawa, K. (2012). Assessing the moisture buffering performance of hygroscopic material by using experimental method. *Building and Environment*, 48, 27-34. https://doi.org/10.1016/j.buildenv.2011.08.012

Zhang, L., Tian, L., Shen, Q., Liu, F., Li, H., Dong, Z., Cheng, J., Liu, H., & Wan, J. (2021). Study on the influence and optimization of the Venturi effect on the natural ventilation of buildings in the Xichang Area. *Energies*, *14*(16), 5053. https://doi.org/10.3390/en14165053

Revista Hábitat Sustentable Vol. 16, N°. 1. ISSN 0719 - 0700 / Págs. 42 - 55
https://doi.org/10.22320/07190700.2026.16.01.03

DESIGN OF AN INDIRECT GREEN FAÇADE SYSTEM TO IMPROVE THERMAL COMFORT IN MULTIFAMILY HOUSING

Recibido 17/12/2025
Aceptado 20/05/2026

DISEÑO DE SISTEMA INDIRECTO DE FACHADA VERDE PARA MEJORAR EL CONFORT TÉRMICO EN VIVIENDAS MULTIFAMILIARES

DESENHO DE SISTEMA INDIRETO DE FACHADA VERDE PARA MELHORAR O CONFORTO TÉRMICO EM HABITAÇÕES MULTIFAMILIARES

Analucia Espinoza-Abarca
Bachiller en Arquitectura
Estudiante, Facultad de Arquitectura
Universidad Tecnológica del Perú
Lima, Perú
https://orcid.org/0009-0007-9240-5433
u20202371@utp.edu.pe

Alis Tasayco-Huanca (Autor de Correspondencia)
Bachiller en Arquitectura
Estudiante, Facultad de Arquitectura
Universidad Tecnológica del Perú
Lima, Perú
https://orcid.org/0009-0001-9807-6294
U20302943@utp.edu.pe

Victor Miranda-Alfaro
Doctor en Ingeniería Ambiental
Docente, Facultad de Ingeniería
Universidad Tecnológica del Perú
Lima, Perú
https://orcid.org/0000-0002-4857-8800
C26968@utp.edu.pe

CC BY SA

ABSTRACT

Unplanned urban growth in Northern Lima has intensified urban heat islands, affecting thermal comfort in self-built multifamily housing. This study evaluates the performance of an indirect green façade system as a passive thermal mitigation strategy in a dwelling located in San Martín de Porres. A quantitative approach with a quasi-experimental design was employed, combining thermal simulation in SIMEDIF 2.0 with in situ measurements using a digital thermo-hygrometer. The results show a reduction in indoor temperature of up to 2 °C in real measurements and up to 3 °C in simulations, as well as a decrease in incident solar radiation on the façade. It is concluded that the system is constructively viable and improves thermal comfort in urban self-built contexts.

Keywords
indirect green façade, thermal comfort, thermal analysis, passive strategies, multifamily housing

RESUMEN

El crecimiento urbano no planificado en Lima Norte ha intensificado las islas de calor urbano, que afectan el confort térmico en viviendas multifamiliares autoconstruidas. Este estudio evalúa el desempeño de un sistema indirecto de fachada verde como estrategia pasiva de mitigación térmica en una vivienda ubicada en San Martín de Porres. Se empleó un enfoque cuantitativo con un diseño cuasiexperimental, que combina la simulación térmica en SIMEDIF 2.0 y mediciones in situ con un termohigrómetro digital. Los resultados muestran una reducción de la temperatura interior de hasta 2 °C en mediciones reales y de hasta 3 °C en simulaciones, además de una disminución de la radiación solar incidente sobre la fachada. Se concluye que el sistema es constructivamente viable y mejora el confort térmico en contextos de autoconstrucción urbana.

Palabras clave
fachada verde indirecta, confort térmico, análisis térmico, estrategias pasivas, viviendas multifamiliares

RESUMO

O crescimento urbano não planejado na região norte de Lima intensificou as ilhas de calor urbanas, afetando o conforto térmico em habitações multifamiliares autoconstruídas. Este estudo avalia o desempenho de um sistema indireto de fachada verde como estratégia passiva de mitigação térmica em uma habitação localizada em San Martín de Porres. Foi empregada uma abordagem quantitativa, com desenho quase experimental, que combina simulação térmica no SIMEDIF 2.0 e medições in situ realizadas com um termohigrômetro digital. Os resultados mostram uma redução da temperatura interna de até 2 °C nas medições reais e de até 3 °C nas simulações, além de uma diminuição da radiação solar incidente sobre a fachada. Conclui-se que o sistema é viável do ponto de vista construtivo e melhora o conforto térmico em contextos de autoconstrução urbana.

Palavras-chave
fachada verde indireta, conforto térmico, análise térmica, estratégias passivas, habitações multifamiliares

INTRODUCTION

Accelerated urban growth and high building density, which raise temperatures in densely urbanized areas due to the reduction of green areas and the predominance of surfaces such as concrete and asphalt, which affect environmental comfort and quality of life, have intensified urban heat islands (UHI) (Faragallah & Ragheb, 2022; Soberón Forsberg & Obregón Párraga, 2016). In Lima, this phenomenon is associated with the progressive replacement of vegetation by buildings and continuous urban growth, factors that favor the accumulation of heat and affect environmental comfort. Thermal differences of up to 3.7 °C have been recorded between districts and are associated with sparse vegetation (Barros & Menacho Casimiro, 2014). In San Martín de Porres, this phenomenon is exacerbated by unplanned urban growth, in which building expansion predominates over the preservation of green areas. The district has only 1.86 m^2 of green space per inhabitant, far below the World Health Organization (WHO) recommendation, leading to heat accumulation and reduced indoor thermal comfort.

Faced with this scenario, passive strategies have become increasingly relevant for improving thermal comfort in homes by reducing heat gain through low-consumption solutions. Among these strategies, vegetation, applied through direct (GF) or indirect (GFS) green facades, attenuates solar radiation, stabilizes the microclimate, and reduces wall and indoor temperatures, decreasing the need for mechanical ventilation (Marchioretto et al., 2023). Similarly, a systematic review of vertical vegetation systems indicates that these systems enhance the thermal performance of buildings through shading, insulation, and evaporative cooling, thereby reducing heat gains and improving indoor comfort (Bustami et al., 2018). While GF is applied directly on the wall and can retain moisture, GFS uses a separate structure that creates a ventilated air chamber, which protects the wall and is more suitable for self-built homes due to its low structural impact (El Menshawy et al., 2022).

On the other hand, several studies have demonstrated the effectiveness of indirect green facade systems as a passive thermal mitigation strategy through experimental and simulation studies. Ramadhan and Mahmoud (2023) report that these facades reduce thermal loads, energy consumption (by up to 75%), and CO_2 emissions (by 45%), while maintaining suitable comfort conditions. Tudiwer and Korjenic (2017) have also shown, through experimental tests, that indirect green walls can lower indoor temperature by up to 5 °C and block about 90% of incident solar radiation. Similarly, Lesjak et al. (2020) conclude, based on experimental measurements and thermal simulations, that indirect green facades are an effective strategy to prevent building overheating by reducing incident solar radiation on the envelope and lowering indoor operating temperatures, thereby improving thermal comfort during the summer.

Suárez et al. (2023) have demonstrated its effectiveness in arid climates by achieving reductions in room temperature of up to 4.4 °C in summer and decreases in the average outdoor temperature of up to 3.9 °C in the warm season. Meanwhile, Gomez et al. (2023), through thermal simulations and orientation-based radiation analysis, demonstrated reductions of up to 74% on east facades, resulting in indoor temperature decreases of between 0.6 °C and 4.5 °C. Finally, Suárez et al. (2020) reported reductions of up to 26.5 °C and 27.4 °C in outdoor surface temperature during the 2019 and 2020 evaluation periods, respectively. In addition, the green-facade wall exhibited a thermal amplitude of nearly 6 °C, significantly lower than that of the facing wall, which ranged from 24 °C to 31 °C.

Although several studies have shown the effectiveness of green facades in reducing indoor temperatures, most have been developed through simulations or in climatic contexts other than Lima's. However, research combining experimental monitoring and thermal simulation has shown that incorporating vegetation into vertical elements is an effective passive strategy to reduce heat gain and improve indoor environmental quality (Domínguez Cicorio et al., 2022). Despite this, there is still little empirical evidence from on-site measurements of the thermal performance of indirect green facade systems in self-built homes in coastal arid climates such as Lima. Consequently, this study seeks to address this gap by evaluating the thermal performance of an indirect green facade system using in situ measurements and thermal simulations.

The research problem lies in the low thermal comfort of self-built homes in San Martín de Porres, due to the absence of passive thermal regulation strategies, limited green areas, and high urban temperatures. These houses, built without technical criteria, have inadequate orientations, poor natural ventilation, and inefficient spatial distribution, which favor the accumulation of heat indoors and affect occupants' well-being. In this context, the following question arises: How does the design of





Figure 1. Study area, SMP, Lima. Source: Google Earth.
Figure 2. Photo of the dwelling. Source: Prepared by the authors.

an indirect green facade system improve thermal comfort in multifamily housing?

The general objective of the study is to design an indirect green facade system that improves thermal comfort in a multifamily home. To do this, the climatic conditions of San Martín de Porres are identified using data from the National Meteorology and Hydrology Service of Peru (SENAMHI), and a lightweight, easy-to-install prototype compatible with self-built homes is developed. Its thermal performance is evaluated through on-site measurements and computer simulations, which compare indoor temperatures before and after its implementation. It is hypothesized that the implementation of a GFS in the house will reduce the indoor temperature by approximately 2-3 °C, due to the decrease in solar radiation and the thermal damping provided by the air chamber and vegetation, as noted by Abdeen and Rafaat (2024) and Suárez et al. (2020) regarding the potential of green facades to improve indoor thermal comfort.

CASE STUDY

The case study is located at coordinates 12.026287° S, 77.082624° W, in the district of San Martín de Porres (SMP), Lima, Peru (Figure 1), and is a self-built multifamily housing unit (Figure 2). The main facade, facing southeast, is exposed to direct solar radiation during the summer, primarily in the morning, which increases the envelope's thermal gains and contributes to higher indoor temperatures. In certain environments, this condition is also associated with operating temperatures above 29 °C.

The building is built with 15-cm-thick hollow-brick load-bearing walls, which limit interventions that would substantially modify the structural layout. This condition limits the feasibility of incorporating certain passive environmental conditioning strategies. The compactness of the floor plan and the small dimensions of the openings also limit the potential for natural ventilation and daylighting, promoting heat accumulation in indoor spaces.

METHODOLOGY

This project adopts a quantitative approach to evaluate the impact of the indirect green facade system by analyzing indoor thermal records and using computer simulations. Its scope is explanatory, as it seeks to identify the causal relationship between the implementation of the indirect green facade system and the reduction in indoor and surface temperatures of the rooms, as well as its effectiveness against solar radiation.

A quasi-experimental design is used, in which surrounding conditions are not manipulated, and the thermal behavior of the rooms is compared with and without the green facade system, allowing analysis of its effects under real conditions. The design is also transversal, since the thermal measurements are carried out over a specific period of time, so the thermal behavior of the rooms is analyzed at a single point in time without longitudinal monitoring.

The study population comprises multifamily dwellings in San Martín de Porres that are exposed to solar radiation. The sample is a second-floor apartment whose orientation allows evaluating the thermal performance of the green facade system. The measurements were taken in the rooms facing said facade, producing detailed data on thermal behavior for the case study.

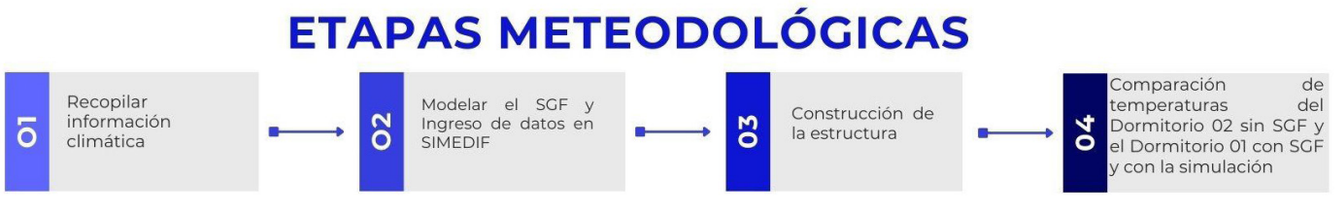


Figure 3. Methodological phases. Source: Prepared by the authors.

YEAR	2024				2025			
Month	FEB	MAR	AUG	SEPT	FEB	MAR	AUG	SEPT
Max. Temperature (°C)	31.9	29	20	21.3	29.5	29.4	20.6	23.2
Humidity	47.43	56.06	67.73	63.93	56.67	51.56	67.9	69.67

Table 1. Monthly temperature in SMP (2024-2025) Source: Prepared by the authors using SENAMHI data (n.d.)

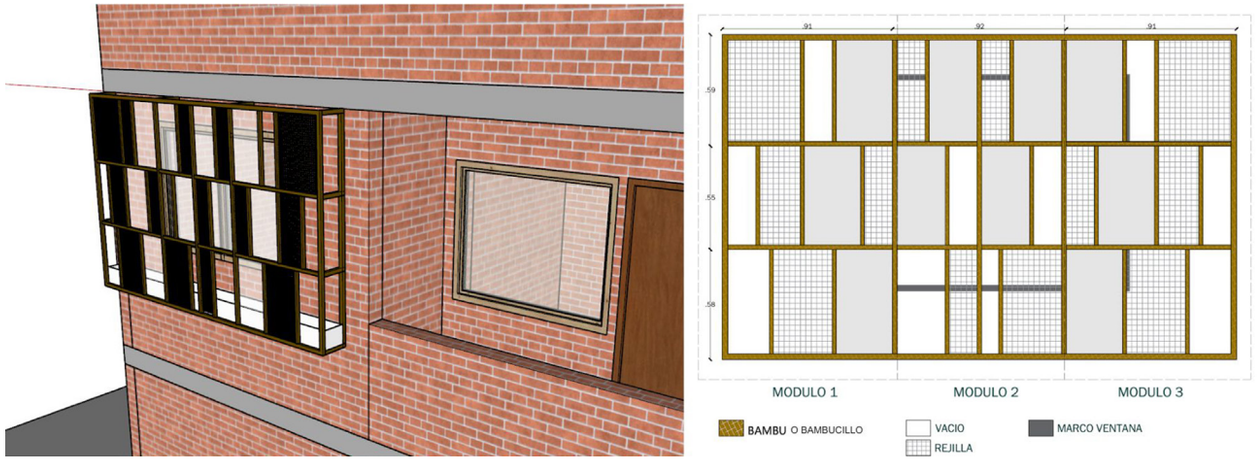


Figure 4. Modeling in SketchUp of the structure and materiality of the dwelling. Source: Prepared by the authors.
Figure 5. GFS structure in AutoCAD. Source: Prepared by the authors.

The techniques used in the research are based on computational models developed primarily in SIMEDIF. This thermal simulation program enables analysis of room thermal behavior based on the materials, climatic conditions, and construction characteristics. AutoCAD and SketchUp were also used, and measurements with a digital indoor thermohygrometer were verified by comparative readings to record the prototype's indoor temperatures.

Below, the methodological stages used in this research are presented, with each phase of the process described from information collection and thermal modeling to data analysis and evaluation of the green facade's impact on thermal comfort (Figure 3).

FIRST PHASE

Climatic data for the district of San Martín de Porres were collected from the records of the National Meteorology and Hydrology Service of Peru [SENAMHI] for the 2024-2025 period, covering maximum temperature, average temperature, and relative humidity in summer and winter.

Table 1 shows monthly temperatures ranging from 20.6 °C to 29.5 °C, with a summer peak of 31.9 °C. The analysis focused on the summer and winter months, the periods with the most extreme values. The months of November, December, February (Summer), and August (Winter) were selected to evaluate the indirect system's performance under these thermal conditions.



Figure 6. Assembly of the bamboo structural system. Source: Prepared by the authors.



Figure 7. Assembly of the structural system of the bambucillo and installation on the wall. Source: Prepared by the authors.

SECOND PHASE

In the second stage, materials were defined, and prototypes of the indirect system were developed. For the structure, bamboo was used for its strength, sustainability, and ease of construction. Two initial prototypes were developed: one made of bamboo, more complex to assemble, and another of fishpole bamboo (bambucillo), which turned out to be lighter and easier to handle. Both were 3D modeled in AutoCAD and SketchUp (Figure 4 and Figure 5). Considering the use of climbing vegetation on support structures, a characteristic configuration of indirect green facade systems, the climbing species Epipremnum aureum, with a growth of LAI ≈ 2.5, Vinca major, Ficus pumila, and Hedera helix, with LAI ≈ 2.5, were also selected due to their resistance to direct solar radiation.

The SIMEDIF software was used for the thermal simulation, where three thermal zones, bedroom 1, bedroom 2, and the living room, were defined, according to the data shown in Table 2. The simulation incorporated the parameters of Table 3, which specify the characteristics of walls and floors, such as

LOCAL	FLOOR AREA m2	VOLUMEN m3
Bedroom 1	10.61	31.09
Living/dining room	9.09	51.024
Bedroom 2	11.21	30.67

Table 2. Characteristics of the thermal zones. Source: Prepared by the authors.

SOLID WALL	SOLAR ABSORPTION	W/m2-K	THICKNESS (m)
Exterior	0.55	8	0.12 y 0.30
Interior	0.15	6	0.12
Floor	0.3	0.01	0.20
Roof	0.4	6	0.20

Table 3. Thermal properties. Source: Prepared by the authors.

conductance, thermal transmittance (U), and thermal inertia. The dimensions of the indirect system (2.5 × 4.5 m) were also input to evaluate its thermal behavior in the model.

For the green facade, the Hedera helix plant was proposed with a leaf length of 0.15m, a stomatal resistance of 160 s/m, and air renewal rates of 23 1/h in summer and 5 1/h in winter.

THIRD PHASE

The objective of this phase was to build the GFS prototype and verify its constructability and integration with vegetation.

In the third stage, two prototypes were built. The first prototype, made of bamboo (2.5 x 1.70 m), required a prior drying process and a complex assembly, with fish-mouth-type cuts, studs, washers, and nuts used to ensure stability (Figure 6). The second prototype, made with 1 1/2" bambucillo, used blade-type tie-downs with a ribbon, which allowed not only to replicate the original design, but also to expand its dimensions to 2.5 × 4.5 m, thanks to its lower weight. Finally, the structure was varnished to improve its durability and resistance to moisture (Figure 7).

FOURTH PHASE

In this phase, the indoor air temperature was compared. For this, the thermal zone 03 was used as a reference room, where the temperature was measured without intervention. Subsequently, a comparison was made with thermal zone 1, in which the indirect green facade system would be installed (Figure 8). This choice is based on the fact that both bedrooms have the same spatial distribution, dimensions, and window-opening size, which minimizes the influence of geometric variables on the results and ensures comparability between the two environments. In addition, the results under these real conditions will be compared with those from the thermal simulation to verify the efficiency of the proposed system.

The measurements were made with a MDL 2140 digital thermohygrometer, with a temperature measurement range of -50 °C to +70 °C and a tolerance of ±1 °C in the range of 0 °C to +40 °C; data were recorded every four hours (8:00, 14:00 and 20:00) during the period from November 1st to December 12th, 2025, selected for representing warm climatic conditions characteristic of the study area.

The sensor was located 1.10 m above floor level and at a minimum distance of 1.0 m from the facade wall; the criteria of the UNE-EN ISO 7726 Standard were followed to represent the occupied area and to avoid interference from surface radiation. During the measurements,

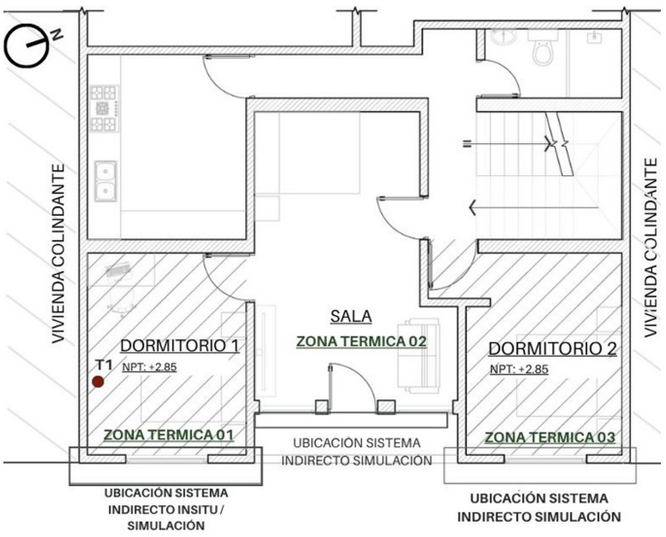


Figure 8. Dwelling's floor plan and location of the thermohygrometer. Source: Prepared by the authors.

the bedroom was kept unoccupied, with the doors and windows closed. No mechanical ventilation was used, and measurements were taken on days without atypical weather, such as rain or strong winds, to ensure comparable conditions before and after the system was installed. Prior to taking the records, the equipment was checked using comparative readings in the same environment to verify data stability.

The data obtained were organized in spreadsheets and analyzed using time profiles, which allowed evaluating the thermal variation generated by the implemented system and comparing the actual thermal behavior of the room with the simulation results.

RESULTS

Two scenarios were considered for the analysis: the base model without intervention and the model with the implementation of the GFS. Both were evaluated using the SIMEDIF program, into which thermal and technical data for walls and windows were input, complemented by real indoor temperature measurements. Finally, the simulation results were compared with those of the in-situ prototype.

BASE MODEL

Figure 9 shows the indoor air temperature forecast in the thermal zones evaluated before the implementation of the green facade for November, December, February, and August. The results show a seasonal increase in indoor temperature from winter to summer, with the most unfavorable thermal conditions in February. In this month, Bedroom 1 recorded the highest maximum temperature (32.5 °C), followed by Bedroom 2 at a

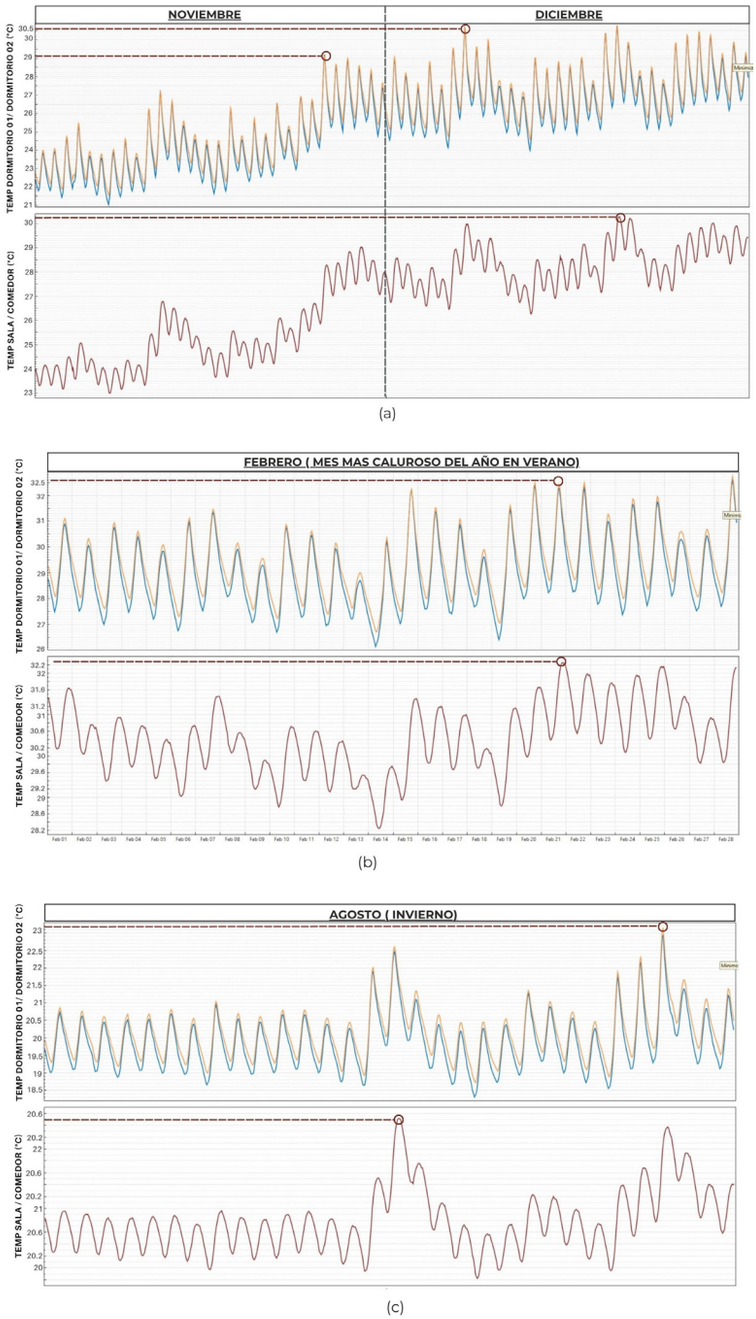


Figure 9. Surface temperature of the thermal zones without the implementation of the GFS in the 4 months analyzed. Source: Prepared by the authors with data from the SIMEDIF.

similar value, while the Living Room reached 32.0 °C. In December, the maximum temperatures ranged from 30.0 to 30.5 °C, while in November they ranged from 28.5 to 29.0 °C. In contrast, during August, a period of lower thermal demand, temperatures dropped to a range of 22.5-23.0 °C.

In comparative terms, the differences between environments were less than 1.0 °C across all months analyzed, indicating a homogeneous indoor thermal response. This behavior suggests that spatial temperature variation is reduced and that the observed overheating is relatively uniform throughout the evaluated dwelling.

Figure 10 presents the hourly distribution of indoor temperature as heat maps, enabling identification of the daily thermal evolution pattern across the four months analyzed. In all cases, the temperature increases progressively from the early morning and reaches values close to 25 °C by noon. However, the period of greatest thermal demand is concentrated

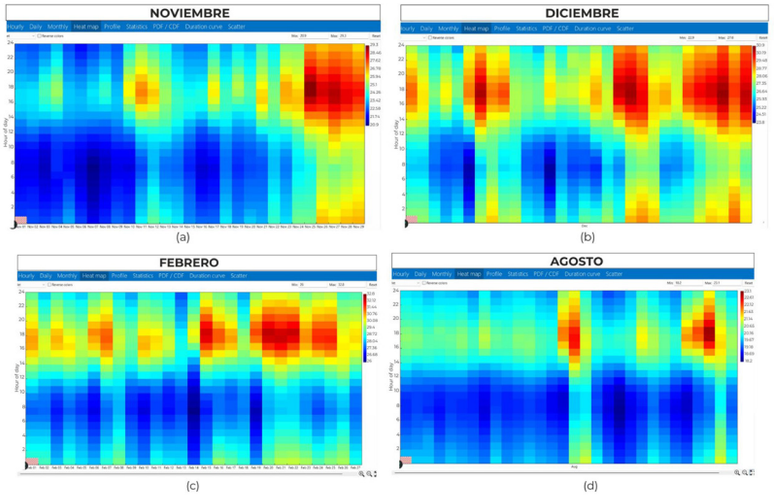


Figure 10. Heat map by time range without GFS. Source: Prepared by the authors with SIMEDIF data.

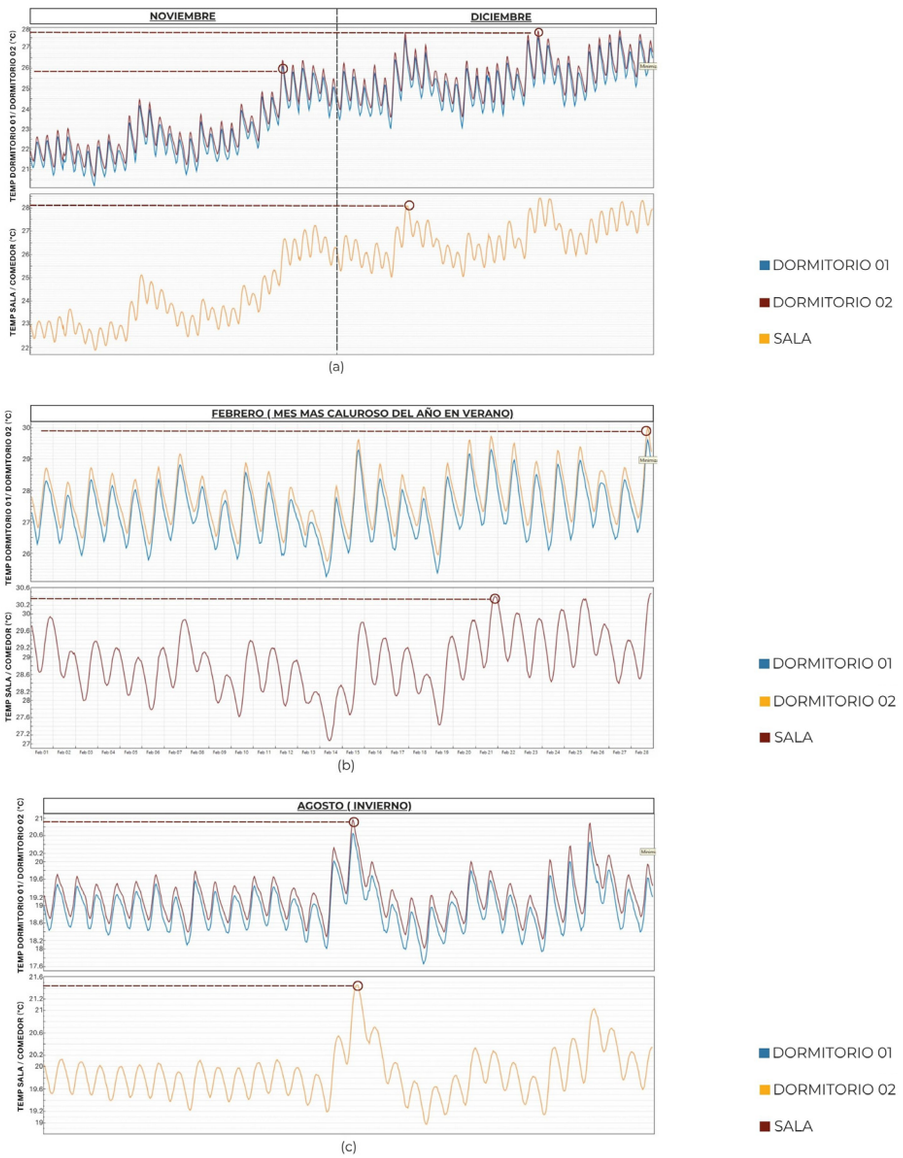


Figure 11. Temperature simulation result with the GFS. Source: Prepared by the authors with data from SIMEDIF.

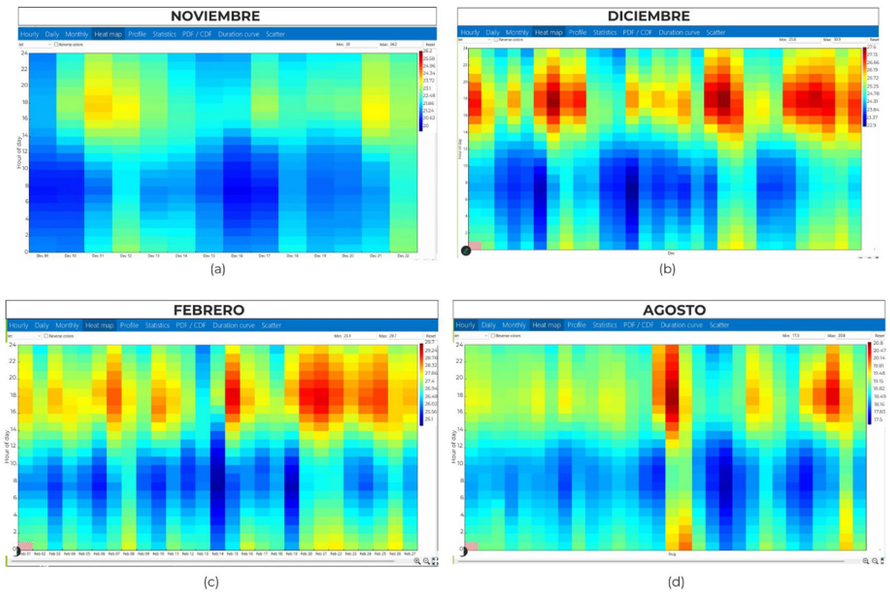


Figure 12. Heat map with time range of the 3 thermal zones with the GFS. Source: Prepared by the authors with data from SIMEDIF.

between 2 pm and 6 pm, during which the three rooms simultaneously reach their maximum values. This behavior confirms the existence of a diurnal thermal delay and identifies this timeframe as the critical period for thermal accumulation inside the dwelling.

MODEL WITH GFS IMPLEMENTATION

Figure 11 shows the indoor thermal behavior after implementing the Green Facade System (GFS) in the evaluated rooms. Compared with the baseline scenario, a reduction in maximum temperatures is observed across all the cases. In Bedroom 2, the maximum values were 21.4 °C in August, 26.0 °C in November, 28.5 °C in December, and 30.0 °C in February, the latter remaining the month of greatest thermal demand. However, even under this condition, the average temperature recorded in February remained around 28 °C, indicating reduced overheating compared to the scenario without GFS.

In Bedrooms 1 and 2, the average temperature in November was approximately 22.8 °C, a decrease of about 2 °C compared to the scenario without intervention. In comparative terms, this decrease was consistent in both rooms, confirming a uniform reduction of the thermal load in long-term spaces.

The analysis of the 24-hour thermal profile indicates that the daily highs remain concentrated between 2 pm and 4 pm, i.e., within the period of highest thermal demand. However, the magnitude of these peaks is lower than in the case without GFS, which evidences a thermal damping effect of the system.

Figure 12 presents the hourly heat maps, showing a progressive decrease in indoor temperature during the night. The average values in this range were approximately 22 °C in November, 26 °C in December, 27 °C in February, and 18 °C in August. Taken together, these results show that implementing the GFS reduces the intensity of daytime overheating and modifies the indoor cooling pattern throughout the daily cycle.

The results from thermal simulations in SIMEDIF and on-site measurements were compared to evaluate the thermal behavior of the Indirect Green Facade System (GFS) in Bedrooms 1 and 2. Table 3 presents the hourly indoor temperature profiles with and without the system's implementation during November and December, for both evaluation methods.

The measurements were carried out under the same time conditions: the first and last three days of each month were analyzed at 2 pm and 8 pm, the periods of maximum daytime thermal load, and the night period of accumulated heat release. In both methods, lower indoor temperatures were recorded in the GFS scenario than in the case without intervention (Tables 4 and 5).

In the *in-situ* measurements, the average indoor temperature difference between the two scenarios was close to 2 °C; maximum reductions of up to 3 °C were observed, with greater differences recorded at night. On the other hand, the SIMEDIF simulation showed decreases of 1-2.5 °C, maintaining similar thermal

DATE	BEDROOM 2 WITHOUT GFS		BEDROOM 1 WITH GFS	
	14:00PM	20:00PM	14:00PM	20:00 PM
01/11/2025	22.8°C	21.5°C	21.2°C	19.4°C
02/11/2025	23.6°C	21.9°C	22. 3°C	20.9°C
03/11/2025	22.5°C	20.9°C	21.5°C	19.2°C
28/11/2025	24.9°C	23.5°C	22.7°C	21.3°C
29/11/2025	24.2°C	22.8°C	22.2°C	21.4°C
30/11/2025	25.3°C	24.8°C	23.4°C	22.8°C
01/12/2025	24.4°C	22.6°C	22,3°C	20.9°C
02/12/2025	24.8°C	23.6°C	23,2°C	22.5°C
03/12/2025	25.5°C	22.9°C	23.5°C	22.9°C

Table 4. Comparison of temperatures with and without GFS, by on-site measurement in November and December. Source: Prepared by the authors.

DATE	BEDROOM 1 WITHOUT GFS SIMEDIF		BEDROOM 1 WITH GFS SIMEDIF	
	14:00PM	20:00PM	14:00PM	20:00 PM
01/11/2025	23.7°C	23.1°C	22.24°C	22.04°C
02/11/2025	23.83°C	22.96°C	22.36°C	21.89°C
03/11/2025	24.12°C	23.49°C	22.34°C	22.06°C
28/11/2025	28.03°C	27.39°C	25.43°C	25.51°C
29/11/2025	27.54°C	26.97°C	25.3°C	25.08°C
30/11/2025	27.14°C	26.32°C	24.89°C	24.63°C
01/12/2025	28.05°C	27.41°C	25.44°C	24.27°C
02/12/2025	27.88°C	26.87°C	25.51°C	25.13°C
03/12/2025	26.65°C	26.33°C	24.69°C	24.59°C

Table 5. Comparison of temperatures with and without green facade system (GFS) in Bedroom 1 using SIMEDIF simulation. Source: Prepared by the authors.

behavior across the evaluated times and slight variations among the analyzed days. The greatest thermal differences were observed in November, mainly in the afternoon.

In general, both methods show a consistent trend towards lower indoor temperatures associated with the incorporation of GFS across all evaluated cases (Tables 4 and 5).

DISCUSSION

The thermal simulation developed in SIMEDIF identified the indirect green facade system's behavior faced with overheating in the analyzed dwelling. In the base scenario, Bedroom 1 exhibited the most critical condition, with maximum temperatures of up to 32.5 °C in February, while incorporating the system resulted in an approximate 3 °C reduction. This performance suggests that the system attenuates the

thermal gain through the vegetation shading and the damping effect of the air chamber, thereby moderating the indoor temperature. This behavior aligns with what Manso and Castro-Gomes (2015) noted: green wall systems improve the microclimate of the envelope by providing shade, complementary insulation, and evaporative cooling generated by vegetation. Perini et al. (2011) also argue that the presence of an air layer between the vegetation cover and the facade can increase the thermal resistance of the envelope and reduce heat transfer to indoor spaces, reinforcing the thermal protection effect observed in the present study.

The *in-situ* measurements confirmed a temperature decrease during the most demanding hours, with reductions of up to 2 °C, consistent with the simulation. This reinforces the robustness of the observed behavior. It aligns with the findings reported by Suárez et al. (2020) on the ability of green facades to reduce heat transfer to the interior. Similarly, Padovan et al. (2022) recorded an average reduction of 4.4 °C in indoor air temperature, with maximum decreases of up to 7.3 °C in rooms protected by an indirect green facade. Susorova et al. (2013) also point out that vegetation reduces the facade's surface temperature and limits heat transfer by conduction into the building, thereby reducing thermal loads in protected spaces. In this framework, the findings support the research hypothesis by showing that green facades can reduce the thermal gain in self-built homes. However, their effectiveness depends on context variables such as incident radiation, orientation, and ventilation. Unlike previous studies conducted in more industrialized systems, this case shows that it is possible to achieve measurable thermal improvements through solutions with low construction complexity and that use locally available materials. This observation is consistent with Perini et al. (2011), who point out that indirect green facade systems can be implemented using different support structures and materials, maintaining thermal benefits on the envelope without necessarily requiring complex or high-tech modular systems.

However, the study's limitations should be considered when interpreting its results. At the methodological level, the evaluation was focused on a small number of rooms, which limits the scope for generalization. At the instrumental level, the analysis was based primarily on air temperature and did not incorporate additional thermal comfort variables, such as relative humidity, air velocity, or radiant temperature. The simulation also used standardized parameters that simplify the urban environment, so there may be differences between the modeled behavior and the system's actual behavior.

From a constructive perspective, the prototype's implementation allowed seeing the relevant differences among the materials used. The use of 3-inch bamboo was limited by weight, making it difficult to use in precarious buildings, whereas 1 1/2-inch bambucillo was more suitable as a lightweight structural alternative. This observation not only has practical implications for the system's viability but also broadens the discussion about the adaptability of green facades in contexts of self-construction and structural constraints.

Taken together, the study demonstrates that the green facade system can improve the thermal performance of low-cost housing through a technically feasible and constructively adaptable passive strategy. Its main contribution lies in providing quantitative evidence on the system's behavior in a humid coastal climate such as that of San Martín de Porres, Lima, where the effectiveness of these solutions has been little explored. Incorporating bambucillo as a lightweight alternative also makes a practical contribution to the design of passive solutions that are replicable in similar urban contexts.

CONCLUSIONS

The evaluation of the indirect green facade system (GFS) showed improved indoor thermal performance compared with the no-intervention scenario. In the base model, the simulations showed indoor temperatures of up to 32.5 °C in February, the warmest month, in E-SE-facing spaces, peaking between 2 pm and 8 pm. After implementing the GFS, maximum temperatures in the living room decreased by up to 7.7%, with similar reductions in the bedrooms and greater thermal stability. This effect was most noticeable during the hours of greatest thermal load (2 pm - 4 pm), as it attenuated the overheating peaks.

The comparison between the thermal simulations and the on-site measurements showed a consistent trend. In the evaluated bedroom, the GFS reduced the indoor temperature by approximately 2 °C under real conditions, while the SIMEDIF simulation indicated a decrease of approximately 3 °C. This difference is due to the model assuming fully developed vegetation cover, whereas in situ, the vegetation was in an intermediate growth stage, attenuating the observed thermal effect.

In the winter months, the system helped maintain more stable indoor temperatures, with values between 20.5 °C and 21.4 °C, avoiding sharp decreases at night, when lows near 18 °C were recorded. This behavior suggests that GFS not only reduces summer overheating but also favors greater seasonal thermal stability.

In this context, the implementation of passive strategies, such as the indirect green facade system, represents an accessible alternative for improving living conditions in self-built high-density urban housing, where technical

and economic limitations make it difficult to incorporate more complex solutions. Its application allows reducing the indoor thermal load and dependence on mechanical air conditioning systems.

Finally, the main contribution of this study is to demonstrate that a green facade system can improve the thermal performance of low-cost self-built homes, providing applied evidence for the development of passive environmental conditioning strategies. The work also expands knowledge of the performance of these systems in humid coastal climates, such as Lima, where their effectiveness is usually reported as more limited than in other climatic contexts, yet quantifiable thermal improvements were identified.

Additionally, the study incorporates bambucillo as a viable alternative for lightweight structures, increasing the system's constructability in homes with structural constraints. Together, these findings provide technical and constructive criteria that can guide the design, adaptation, and implementation of passive solutions in urban environments with similar building and climatic characteristics.

CONTRIBUTION OF AUTHORS CRediT:

Conceptualization, A.E.A. and A.T.H.; Data Curation, A.E.A. and A.T.H.; Formal analysis, A.E.A. and A.T.H.; Acquisition of financing A.E.A. and A.T.H.; Research, A.E.A. and A.T.H.; Methodology, A.E.A., A.T.H. and V.M.A.; Project management; Resources; Software. A.E.A. and A.T.H.; Supervision, V.M.A.; Validation, V.M.A.; Visualization, V.M.A.; Writing - original draft, A.E.A., A.T.H. and V.M.A.; Writing - revision and editing, A.E.A. A.T.H. and V.M.A.

BIBLIOGRAPHIC REFERENCES

Abdeen, N., & Rafaat, T. (2024). Assessing vertical green walls for indoor corridors in educational buildings and its impact outdoor: A field study at the universities of Canada in Egypt. *Results in Engineering,* 21, 101838. https://doi.org/10.1016/j.rineng.2024.101838

Barros, P. P. M., & Menacho Casimiro, E. E. (2014). Modificaciones térmicas en Lima: Análisis de la isla de calor urbana. *Anales Científicos, 75*(1), 90–99. https://doi.org/10.21704/ac.v75i1.952

Bustami, R. A., Belusko, M., Ward, J., & Beecham, S. (2018). Vertical greenery systems: A systematic review of research trends. *Building and Environment, 146*, 226–237. https://doi.org/10.1016/J.BUILDENV.2018.09.045

Domínguez Cicorio, C. E., García Solorzano, L. A., & Ruíz Torres, R. P. (2022). Monitoreo térmico de barrera vertical con vegetación, evaluando el desempeño a través de la experimentación y herramienta de simulación. *Revista de ciencias tecnológicas*, *5*(1), e94. https://recit.uabc.mx/index.php/revista/article/view/94

El Menshawy, A. S., Mohamed, A. F., & Fathy, N. M. (2022). A comparative study on green wall construction systems: Case study of South Valley campus of AASTMT. *Case Studies in Construction Materials, 16*, e00808. https://doi.org/10.1016/j.cscm.2021.e00808

Faragallah, R. N., & Ragheb, R. A. (2022). Evaluation of thermal comfort and urban heat island through cool paving materials using ENVI-Met. *Ain Shams Engineering Journal*, *13*(3), 101609. https://doi.org/10.1016/J.ASEJ.2021.10.004

Gómez, A., Esenarro, D., Martinez, P., Vilchez, S., & Raymundo, V. (2023). Thermal Calculation for the Implementation of Green Walls as Thermal Insulators on the East and West Facades in the Adjacent Areas of the School of Biological Sciences, Ricardo Palma University (URP) at Lima, Peru 2023. *Buildings*, *13*(9). https://doi.org/10.3390/buildings13092301

Lesjak, V., Pajek, L., & Košir, M. (2020). Indirect green façade as an overheating prevention measure. *Gradevinar*, *72*(7), 569–583. https://doi.org/10.14256/JCE.2797.2019

Manso, M., & Castro-Gomes, J. (2015). Green wall systems: A review of their characteristics. *Renewable and Sustainable Energy Reviews*, *41*, 863–871. https://doi.org/10.1016/J.RSER.2014.07.203

Marchioretto, J., Pereira Junior, A. C., Nozawa, I. A., & Fontes, M. S. G. de C. (2023). Fachadas verdes: potencial de sombreamento e atenuação solar da espécie Merremia dissecta. *Encontro Nacional de Conforto no Ambiente Construído*, *17*(1), 1–10. https://doi.org/10.46421/encac.v17i1.3848

Padovan, L. D. G., Fontes, M. S. G. de C., & Barbosa, M. C. (2022). Influência térmica da fachada verde no ambiente interno. *PARC: Pesquisa Em Arquitetura E Construção*, *13*, e022005. https://doi.org/10.20396/parc.v13i00.8661203

Perini, K., Ottelé, M., Haas, E. M., & Raiteri, R. (2011) Greening the building envelope, facade greening and living wall systems. *Open Journal of Ecology*, *1*(1), 1-8. http://www.doi.org/10.4236/oje.2011.11001

Ramadhan, A. M., & Mahmoud, A. H. (2023). Evaluating the efficiency of a living wall façade as a sustainable energy-saving alternative in hot arid regions. *Journal of Engineering and Applied Science, 70*(96), 1–25. https://doi.org/10.1186/s44147-023-00259-9

Servicio Nacional de Meteorología e Hidrología del Perú [SENAMHI]. (s.f.). Ministerio del Ambiente Pronóstico del Tiempo a nivel Nacional. https://www.senamhi.gob.pe/?p=pronostico-meteorologico

Soberón Forsberg, V. S., & Obregón Párraga, E. (2016). Identificación de islas de calor en la ciudad de Lima Metropolitana utilizando imágenes del satélite landsat 5TM. *Anales Científicos*, *77*(1), 34-44. https://doi.org/10.21704/ac.v77i1.475

Suárez, P. A., Cantón, M. A., & Correa, É. (2020). Desempeño térmico de fachadas verdes tradicionales de orientación este en viviendas seriadas emplazadas en climas áridos. *Revista Hábitat Sustentable*, *10*(2), 82–93. https://doi.org/10.22320/07190700.2020.10.02.06

Suárez, P., Cantón, M. A., & Correa, É. (2023). Comportamiento térmico estacional de fachadas verdes conformadas por especies trepadoras perennes en muros másicos orientados al oeste. Estudio de casos en zonas áridas. *Cuaderno Urbano, 35*(35). https://doi.org/10.30972/crn.35356773

Susorova, I., Angulo, M., Bahrami, P., & Brent Stephens. (2013). A model of vegetated exterior facades for evaluation of wall thermal performance. *Building and Environment*, *67*, 1–13. https://doi.org/10.1016/J.BUILDENV.2013.04.027

Tudiwer, D., & Korjenic, A. (2017). The effect of living wall systems on the thermal resistance of the façade. *Energy and Buildings, 135*, 10–19. https://doi.org/10.1016/j.enbuild.2016.11.023

Optimization of the thermal comfort of an eco-friendly house: Open foam modeling of sandwich-type walls with Ichu (Stipa Ichu) insulation
Henry Javier-Ninahuaman, Kenny Montalvo-Morales, Jose Rojas-Guillén, Grimaldo Quispe-Santivañez
Revista Hábitat Sustentable Vol. 16, N°. 1. ISSN 0719 - 0700 / Págs. 56 - 69
https://doi.org/10.22320/07190700.2026.16.01.04

OPTIMIZATION OF THE THERMAL COMFORT OF AN ECO-FRIENDLY HOUSE: OPEN FOAM MODELING OF SANDWICH-TYPE WALLS WITH ICHU (STIPA ICHU) INSULATION

Recibido 03/03/2026
Aceptado 27/05/2026

OPTIMIZACIÓN DEL CONFORT TÉRMICO DE UNA CASA ECOLÓGICA: MODELAMIENTO EN OPENFOAM DE MUROS SANDWICH CON AISLANTE DE ICHU (STIPA ICHU)

OTIMIZAÇÃO DO CONFORTO TÉRMICO DE UMA CASA ECOLÓGICA: MODELAGEM NO OPENFOAM DE PAREDES SANDWICH COM ISOLAMENTO DE ICHU (STIPA ICHU)

Henry Javier-Ninahuaman (Autor de Correspondencia)
Doctor en Ciencias Ambientales y Desarrollo Sostenible
Docente, Facultad de Ingenieria, Escuela Profesional de Ingenieria Agroindustrial
Universidad Tecnológica del Perú
Huancayo, Perú
https://orcid.org/0000-0002-3864-4181
C21259@utp.edu.pe

Jose Rojas-Guillén
Doctor en Ciencias de la Educación
Docente, Departamento de Ingeniería
Universidad Tecnológica del Perú
Huancayo, Perú
https://orcid.org/0009-0002-3210-07622
c27875@utp.edu.pe

Kenny Montalvo-Morales
Magíster en agronegocios
Docente, Facultad de Ingeniería, Escuela Profesional de Ingeniería Agroindustrial
Universidad Nacional Autónoma Altoandina de Tarma
Tarma, Perú
https://orcid.org/0000-0003-4403-4360
kmontalvo@unaat.edu.pe

Grimaldo Quispe-Santivañez
Doctor en Ingeniería
Docente e investigador, Facultad de Ingeniería, Escuela Profesional de Ingeniería Agroindustrial
Universidad Nacional Autónoma Altoandina de Tarma
Tarma, Perú
https://orcid.org/0000-0001-6168-8935
gquispe@unaat.edu.pe

CC BY SA

Revista Hábitat Sustentable Vol. 16, N°. 1. ISSN 0719 - 0700 / Págs. 56 - 69
https://doi.org/10.22320/07190700.2026.16.01.04

ABSTRACT

The use of sustainable materials is an important means of achieving thermal comfort in homes in cold climates. The study performs CFD (computational fluid dynamics) analysis in OpenFOAM of an eco-friendly house to optimize the sandwich-type walls (wood chipboard/ stipa ichu/wood chipboard) using response surface methodology in a complete central design, to achieve thermal comfort in extreme cold environments using the PMV average vote prediction index. The evaluation collected data from an on-site weather station, validated it, simulated it, and predicted its performance at extreme cold ambient temperatures. The results indicate the optimal wall thickness for thermal comfort in the eco-friendly house at external temperatures of -10 °C and -20 °C, and explain the complex effects of external temperature on PMV. The study concludes by providing the optimal minimum dimensions of the sandwich-type wall (wood chipboard/ stipa ichu/wood chipboard) that preserve thermal comfort.

Keywords
thermal insulation, construction materials, computational fluid dynamics, bioclimatism, rural housing

RESUMEN

El uso de materiales sostenibles es una alternativa importante para lograr el confort térmico en viviendas ubicadas en climas fríos. El estudio realiza un análisis por dinámica de fluidos computacional (CFD) en OpenFoam de una casa ecológica, con el fin de optimizar las paredes de tipo sándwich (maderba/ichu/maderba) mediante la metodología de superficie de respuesta en un diseño central completo, para lograr confort térmico en entornos de frío extremo mediante el índice de predicción de voto medio (PMV). La evaluación recogió datos de una estación meteorológica in situ, los validó, simuló y predijo su desempeño a temperaturas ambientales de frío extremo. Los resultados indican el grosor de pared óptimo para el confort térmico en la casa ecológica con temperaturas externas de -10 °C y -20 °C y, además, explican los efectos complejos del comportamiento de la temperatura externa sobre el PMV. EL estudio proporciona las medidas mínimas óptimas de la pared tipo sándwich (maderba/ichu/maderba) que logran preservar el confort térmico.

Palabras clave
aislamiento térmico, materiales de construcción, dinámica de fluidos computacional, bioclimatismo, vivienda rural

RESUMO

O uso de materiais sustentáveis constitui uma alternativa importante para garantir o conforto térmico em residências localizadas em climas frios. O presente estudo realiza uma análise por dinâmica de fluidos computacional (CFD) no programa OpenFoam de uma casa ecológica, com o objetivo de otimizar as paredes do tipo sanduíche (madeira/ichu/madeira) por meio da metodologia de superfície de resposta em um projeto central completo, para alcançar o conforto térmico em ambientes extremamente frios, utilizando o índice de previsão de votação média (PMV). A avaliação coletou dados de uma estação meteorológica in situ, validou-os, simulou-os e previu seu desempenho em condições de temperatura ambiente extremamente baixa. Os resultados indicam a espessura ideal da parede para o conforto térmico na casa ecológica em contextos com temperaturas externas de -10 °C e -20 °C, além de explicar os efeitos complexos do comportamento da temperatura externa sobre o PMV. O estudo fornece as medidas mínimas ideais para paredes do tipo sanduíche capazes de preservar o conforto térmico.

Palavras-chave
isolamento térmico, materiais de construção, dinâmica de fluidos computacional, bioclimatismo, habitação rural

Revista Hábitat Sustentable Vol. 16, N°. 1. ISSN 0719 - 0700 / Págs. 56 - 69
https://doi.org/10.22320/07190700.2026.16.01.04

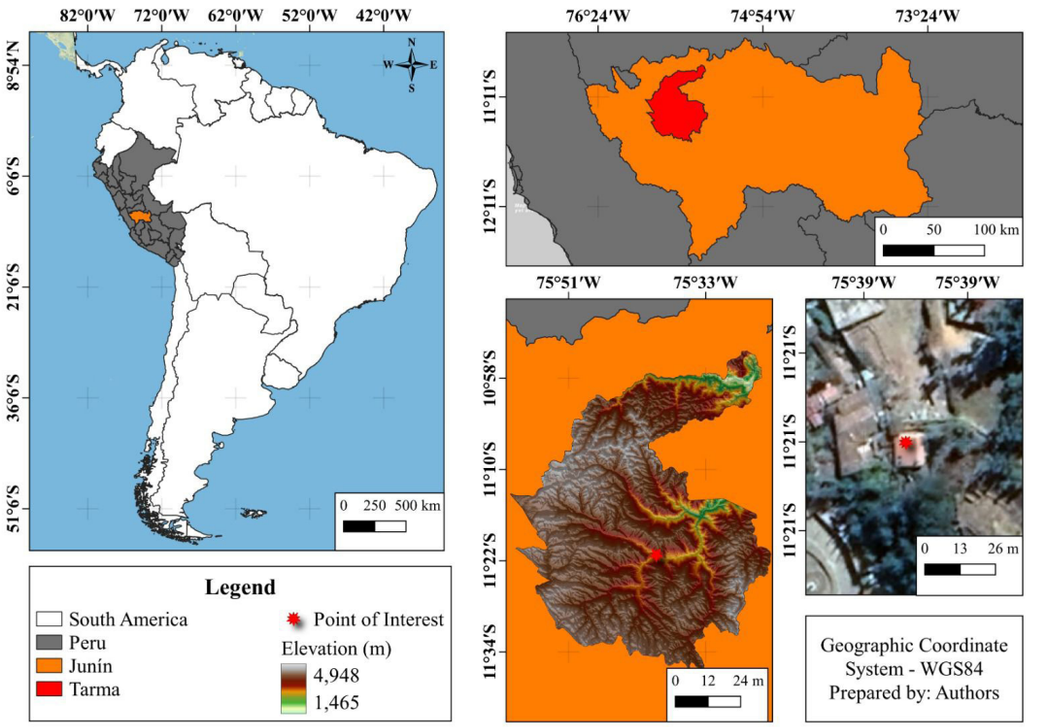


Figure 1. Location of the experimental unit: Eco-friendly house in Muruhuay, Peru. Source: Prepared by the authors.

INTRODUCTION

Thermal comfort is a key factor in ensuring suitable living conditions and reducing energy demand in homes in cold climates, especially in high Andean regions, where temperatures can drop dramatically at night. Conventional homes in these areas often have thermal insulation problems, increasing their reliance on heating sources and leading to elevated heating costs (Marchante González & González Santos, 2020). These energy costs lead to so-called energy poverty, whose effects on the health and economy of the inhabitants are widely documented (Hills, 2012).

Using sustainable, locally sourced materials is an effective means of improving the thermal performance of buildings (Ortiz Caicedo et al., 2023). For instance, the ichu (*Stipa ichu*) can be found in the high-altitude Andean regions of Peru and Bolivia. It is an indigenous grass of the Andes that grows at altitudes above 3500 m.a.s.l. and is a key resource for construction, livestock feed, and soil conservation. The ichu grows in poor soils and in low-humidity conditions, tolerates extreme temperatures, from frost to intense solar radiation, and is resistant to strong winds and precipitation (Charca et al., 2015). Its fibers are light, flexible, and easy to handle; they are hollow, which allows the static air core inside to confer low thermal conductivity, as they act as micro-thermal barriers that reduce heat transfer by conduction, resulting in reduced heat loss in cold climates (Frías et al., 2020; Piñas et al., 2020).

Despite its benefits, the use of ichu in construction still presents challenges, especially regarding optimizing its thickness. The lack of detailed technical studies has limited its application to traditional construction and has failed to provide quantifiable efficiency criteria. Hence, it is necessary to analyze its thermal behavior using advanced tools that evaluate its performance in different configurations. This study proposes optimizing thermal comfort in eco-friendly houses by varying ichu wall thickness through CFD (Computational Fluid Dynamics) simulations (Moreno-Casas et al., 2020).

METHODOLOGY

The research follows a path that starts with on-site measurements (temperature and humidity) before implementing the model and verifying the simulation's accuracy. Validation is then conducted using the average absolute error index between the CFD Model and reality. After that, a statistical design is used to analyze simulation data on external temperature and wall thicknesses to calculate PMV and optimize thermal comfort using the Response Surface Methodology (RSM).

The eco-friendly house used for the thermal comfort

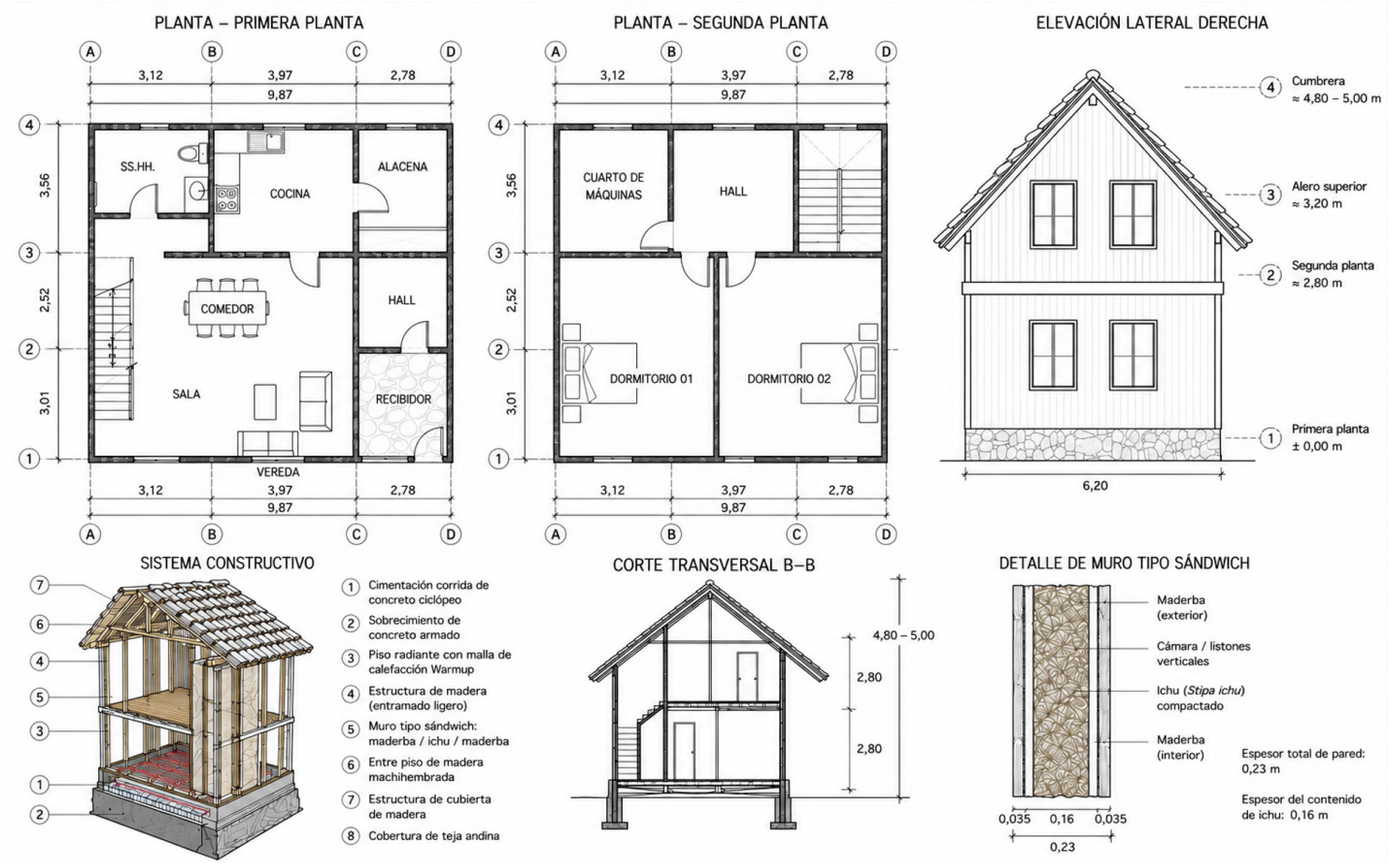


Figure 2. Constructive diagram of the house under study. Source: Prepared by the authors.

analysis and the model's validation is located in the Muruhuay Village Center of Tarma, Peru, at coordinates -11.347435 N, -75.652674 E (Figure 1).

The house under study is a sustainable two-floor construction. The first floor consists of a living-dining room, kitchen, bathroom, hall, and storage room. The second floor has two bedrooms and a machine room. Built with a huayruro wooden structure, it is reinforced with steel supports and has 23-cm-thick sandwich-type walls (chipboard/ichu/chipboard) and doors. The ichu collected was physiologically mature and naturally dried at room temperature, with a moisture content matching the ambient environment (8-12%). The house has a radiant floor heating mesh set on a chip bed. Its roof features an Andean tile ridge, with a triplay ceiling below (President of the UNAT Organizing Committee, 2017). The indoor heat flow dynamics rise during the day and fall at night. The research assumes the house is north-facing, has double-glazed windows, and represents a real house. Figure 2 shows the house's schematics.

The scenarios consisted of performing steady-state simulations representing the most critical cold nighttime conditions, matching the extreme design values for the Andean Highlands during the winter solstice, the period with the lowest temperatures and zero solar radiation. Wall thicknesses from 7.75 cm to 57.2 cm and external temperatures from -27.4 °C to 15 °C were evaluated. Two fixed 15-cm-thick layers of wood were used to maintain constant thermophysical properties, with the ichu core thickness as the variable parameter (ranging from 4.75 cm to 54.2 cm). No other changes were made to the house's structure.

DEVELOPMENT OF A CFD THERMAL COMFORT MODEL IN OPENFOAM

Thermal comfort is the psychological state that reflects one's satisfaction with the thermal environment (Fanger, 1970), and it can be predicted using environmental predictor variables. Meteorological data were collected daily by the meteorological equipment (RK 900 05 RIKA) at 15-minute intervals for 4 months (December 2025 and January, February, and March 2026). The sensors outside the house were placed 3.78 m from the floor, parallel to one of the north-facing windows, and the indoor sensor was

Revista Hábitat Sustentable Vol. 16, N°. 1. ISSN 0719 - 0700 / Págs. 56 - 69
https://doi.org/10.22320/07190700.2026.16.01.04

placed 1.5 m above the floor in the central part of the main hallway on the ground floor. These locations had already been used by Marchante González & González Santos (2020) to assess the effects on people of average height and to evaluate winds and thermal cycles at the study unit's location. The sensors sent data to a wireless data logger, which was then exported to CSV format for processing. From these, representative samples were used to design the CFD model. The data were validated according to the standard metrics to evaluate the difference between CFD and field measurements, using the mean absolute error (MAE) indicator, which was 10.6%, for the sample of 40 *y* observations (y_i, ,,2,3 ..., n) and *40* predictions (Hodson, 2022). After that, the data processing consisted of determining the walls' thermal conductivity index using the house's actual data. Using these data, the simulations were run, including PMV calculations and optimization following the experimental design.

The numerical domain in OpenFOAM was generated using blockMesh, and a control volume was defined to represent the cross-section of the sandwich-type wall. For the minimum resolution for numerical stability, the criteria of Tominaga et al. (2008) were applied; the domain was divided into three functional blocks along the X-axis, corresponding to the physical layout of the house (wood chipboard/ichu/wood chipboard). Each block was discretized at the outset with a base mesh of 10x10x10 cells, ensuring sufficient node density at each stage. Accurate capture of thermal gradients at the interfaces was achieved by selecting a higher level of refinement (1 - Advanced Refinement), which increased resolution in areas with thermal transitions. The calculations were performed using the second-order linear Gauss scheme and an implicit Euler temporal scheme; as a result, the energy equation was monitored, reaching an absolute residual of 10^{-6}, which was sufficient to ensure the stability and validity of the thermal results.

It is necessary to point out that the CFD simulation considered an architectural envelope with high hermeticity. Infiltrations through joints or ventilation grilles were omitted to evaluate the maximum insulation potential of the ichu panel, thereby avoiding interference from losses. In this way, the flows created exclusively obey the density gradients, moving the air from a lower to a higher floor.

NUMERICAL DETAILS OF THE SIMULATION

A structured mesh comprising hexahedral cells and 3 functional blocks (sandwich-type wall layers) was used for the spatial discretization. The numerical schemes included: the Euler time derivative; the Gauss-linear gradients; and the Laplacian via the corrected Gauss-linear (a second-order scheme that corrected for the mesh's non-orthogonality). A linear interpolation (interpolationSchemes), i.e., of the second order, and the gradient on the faces (snGradSchemes) normal to the faces, corrected for non-orthogonality, were used. A tolerance of $1x10^{-6}$ and a RelTol (relative tolerance) of 0 was used in addition to the Convergence criteria (fvSolution), for the temperature (T) solver. The solver iterated until the temperature equation residual was reduced to below 10^{-6} (in absolute value), ensuring numerical stability and physical consistency.

The boundary and initial conditions were determined using the 0/*/T and blockMeshDict files. The former (border section in blockMeshDict) was specified for the atmosphere (patch type) to group the outer faces where the fixed-temperature condition is applied. The specific faces are defined by vertex indices: (0 4 8 0), (3 7 11 7), (0 1 5 4), (2 3 7 6), and (0 1 2 3). These faces define the borders exposed to the outdoor environment. Standard walls were used to group the internal faces between regions and other borders where the thermal insulation conditions are applied. On being the vertices of the specific faces: (8 9 13 12); (9 10 14 13); (10 11 15 14); (4 5 9 8); (5 6 10 9); (6 7 11 10) and (12 13 14 15), these faces represent internal walls and borders not exposed to the environment. Walls in zeroGradient set the boundary conditions for the Temperature (0/*/T files), indicating that there is no normal heat flow to the walls or atmosphere in the outer region of the fixedValue air. As such, the temperature at the atmospheric boundary (outside air) was kept constant. The initial conditions for the outdoor temperature (0/*/T files) were kept constant in the internalField across all regions, in accordance with the research design. The chipboard used has a thermal conductivity of 0.1 W/m·K (manufacturer's data), twice that of the pressed Ichu (0.05 W/m·K), suggesting it allows faster heat transfer. The density and specific heat are the same for both materials, which implies that the amount of energy required to change their temperatures per unit mass is the same. Air has a thermal conductivity (0.026 W/m·K) that is significantly lower than that of solids, which act as insulators by comparison (Atahuachi Layme & Carcausto Quispesayhua, 2018; Cárdenas Cristobal & Espinoza Ramírez, 2024; Mendoza et al., 2021). The thermo-physical properties were determined according to the constant/*/Thermophysical Properties and are shown in Table 1.

Next, the scenario prediction was made, and the data were processed using the free software OpenFOAM v12 for Windows and Salome Version 9.10.0, after being plotted in AutoCAD V25. Thermal comfort was calculated using a standard implementation of the ISO 7730 predicted mean

	Air	Ichu	Chipboard
Density (ρ) kg/m³	1.225	250	250
Conductivity W/m·K	0.026	0.05	0.10
Specific heat (Cp) J/kg.K	1000	1200	1200

Table 1. Thermo-physical properties of the eco-friendly house's materials. Source: Manufacturer data; Atahuachi Layme & Carcausto Quispesayhua (2018); Cárdenas Cristóbal & Espinoza Ramírez (2024).

$$PMV = (0{,}303e^{-0{,}036M} + 0{,}028) * \{(M - W) - 3{,}05 * 10^{-3} * [5733 - 6{,}99(M - V) - p_a] - 0{,}42[(M - V) - 58{,}15] - 1{,}7 * 10^{-5} * M * (5867 - p_a) - 0{,}0014 * M * (34 - t_a) - 3{,}96 * 10^{-8} * f_{cl} * [(t_{cl} + 273)^4 - (\bar{t}_r + 273)^4] - f_{cl} * h_c * (t_{cl} - t_a)\}$$

$$t_{cl} = 35{,}7 - 0{,}028 * (\mathrm{M} - \mathrm{V}) - I_{cl}\{3{,}96 * 10^{-8} * f_{cl}[(t_{cl} + 273)^4 - (\bar{t}_r + 273)^4] - f_{cl} * h_c * (t_{cl} - t_a)\}$$

$$h_{cl} = \begin{Bmatrix} 2{,}38 * |t_{cl} - t_a|^{0{,}25} \; si \; 2{,}38 * |t_{cl} - t_a|^{0{,}25} > 12{,}1\sqrt{v_{ar}} \\ 12{,}1 * \sqrt{v_{ar}} \; si \; 2{,}38 * |t_{cl} - t_a|^{0{,}25} < 12{,}1\sqrt{v_{ar}} \end{Bmatrix}$$

$$f_{cl} = \begin{Bmatrix} 1{,}00 + 1{,}290 * l_{cl} \; si \; l_{cl} \leq 0{,}078 \; \frac{m^2}{w} \\ 1{,}00 + 0{,}645 * l_{cl} \; si \; l_{cl} > 0{,}078 \; \frac{m^2}{w} \end{Bmatrix} \quad \text{(Equation 1)}$$

vote (PMV) formula (Olesen & Parsons, 2002). PMV is the standard used to determine thermal comfort under ASHRAE standards, based on Fanger calculations (Equation 1).

Where: M is the metabolic rate (W/m²); W is the external Work (W/ m²); Icl is the clothing insulation (Clo); fcl is the clothing Surface Area Factor; ta is the air temperature (°C); tr is the mean radiant temperature (°C), var is the air velocity relative to the body (m/s); pa is the partial pressure of water vapor in the air (Gilani, Khan & Pao, 2015).

The small variations were in the indoor temperature and humidity results. The air velocity was kept constant at 0.1 m/s, with a clothing insulation (clo) of 1.0, corresponding to moderate winter clothing. The Average Radiant Temperature (Tmr) was the same as the indoor Temperature, and a Metabolic Activity Level (Met) of 1.0 for a pure sedentary lifestyle was used to reflect the accuracy of the experimentation under the discrete scale of Table 2, where the thermal comfort zones follow the methodology (Fanger, 1970) and ASHRAE standards in Mora & Bean (2018), as the thermal comfort values are divided into three classes based on the PMV (Roelofsen & Jansen, 2024)

The statistical analyses were processed in the Minitab version 20 educational license software, using the DOE Experimental Design and RSM Response Surface of Composed Central Design of 13 treatments (4 negative, 4 positive, and 5 axial

Comfort	PMV
Very cold	-3.0
Pretty cold	-2.0
Somewhat cold	-1.0
Neutral	0
Somewhat hot	+ 1.0
Pretty hot	+ 2.0
Very hot	+ 3.0
Class	PMV intervals
A	-0.2 < PMV<0.2
B	-0.5 < PMV<0.5
C	-0.7 < PMV<0.7

Table 2. Discrete scale and predicted mean vote classes, PMV. Source: Mora & Bean (2018).

points) (Table 3), from which the contour plots, solid meshes, interactions, and optimization were obtained.

The optimal wall width was determined by minimizing the acceptable thermal comfort according to ISO 7730 (Ergonomics of the thermal environment) and by analytically assessing thermal comfort (Fanger, 1970; Olesen & Parsons, 2002) using the PMV. The interval considered comfortable for class C starts at -0.7, because it is only somewhat cold, and extends

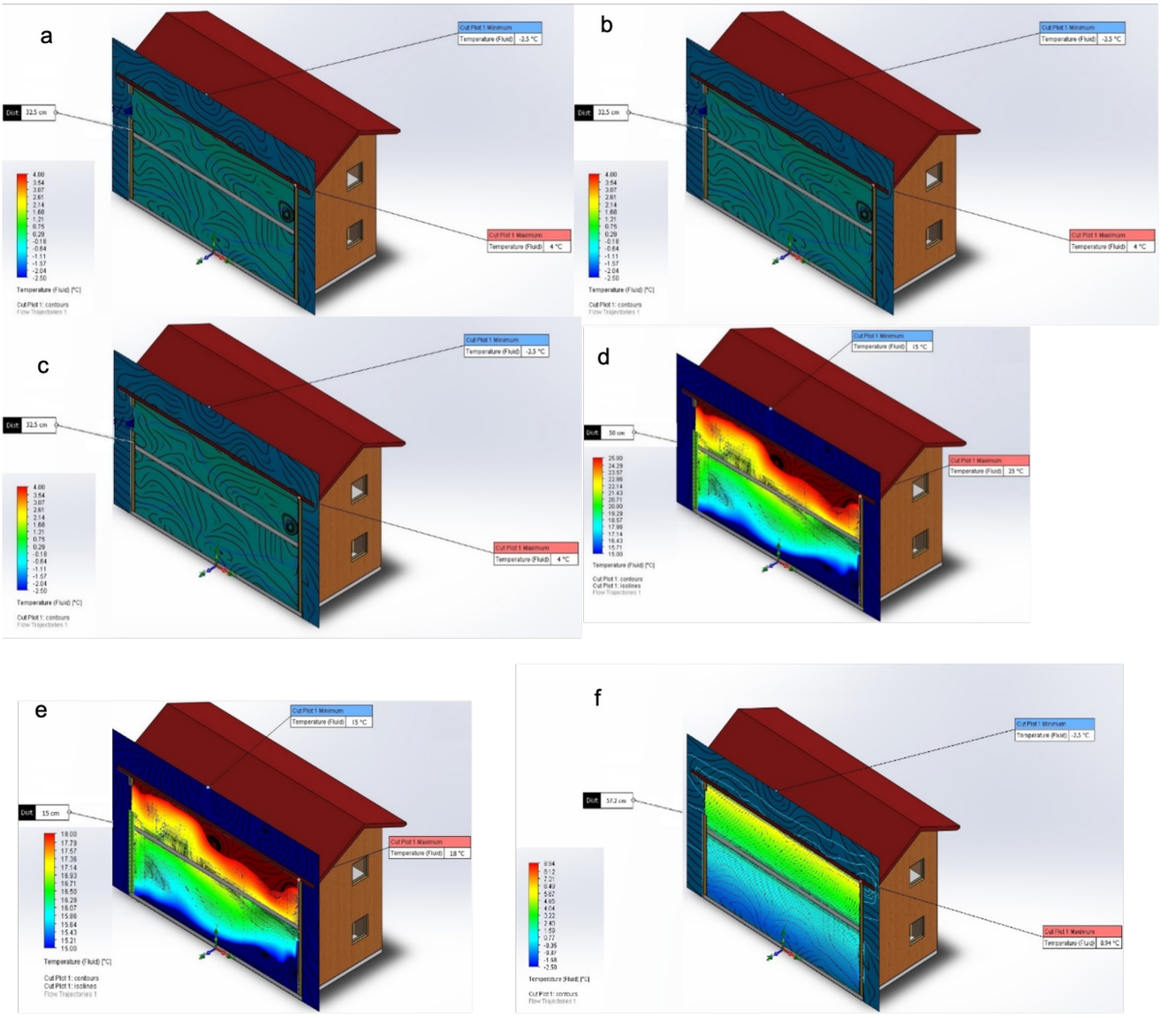


Figure 3. Comparison of the eco-friendly house's CFD simulations using the experimental optimization design, showing the wall thicknesses and outdoor and indoor temperature scales. Part 1. Source: Prepared by the authors.

up to +0.7; the best values are close to 0. Those of class A vary from -0.2 to +0.2, simulated at the extreme temperatures of -10 °C and -20 °C.

RESULTS

CFD SIMULATION

The thermal comfort behavior inside the eco-friendly house is shown graphically. Low temperatures of up to 4 °C are observed throughout the house in Figures 3a, 3b, and 3c when the outdoor temperature is -2.5 °C, and the wall thickness is 32.5 cm. This internal temperature effect increases to 8.94 °C when the wall is 57.2 cm thick, and the wind temperature is higher on the upper floor than on the lower, with greater coldness on the lower floor (Figure 3f).

Outdoor temperatures of 22.24°C and wall thicknesses of 32.5 cm cause overheating inside, reaching up to 28.74°C on the second floor and a minimum of 22.24°C (Figure 4a). At this level, switching to lighter clothing is recommended. By reducing the wall thickness to 7.75 cm at sub-zero temperatures, as shown in Figure 4b, temperatures near 0°C are achieved. At temperatures below -20°C and wall thicknesses between 32.5 cm and 50 cm, thermal discomfort is observed in these cold spots inside. Figure 3c - Figure 3g.

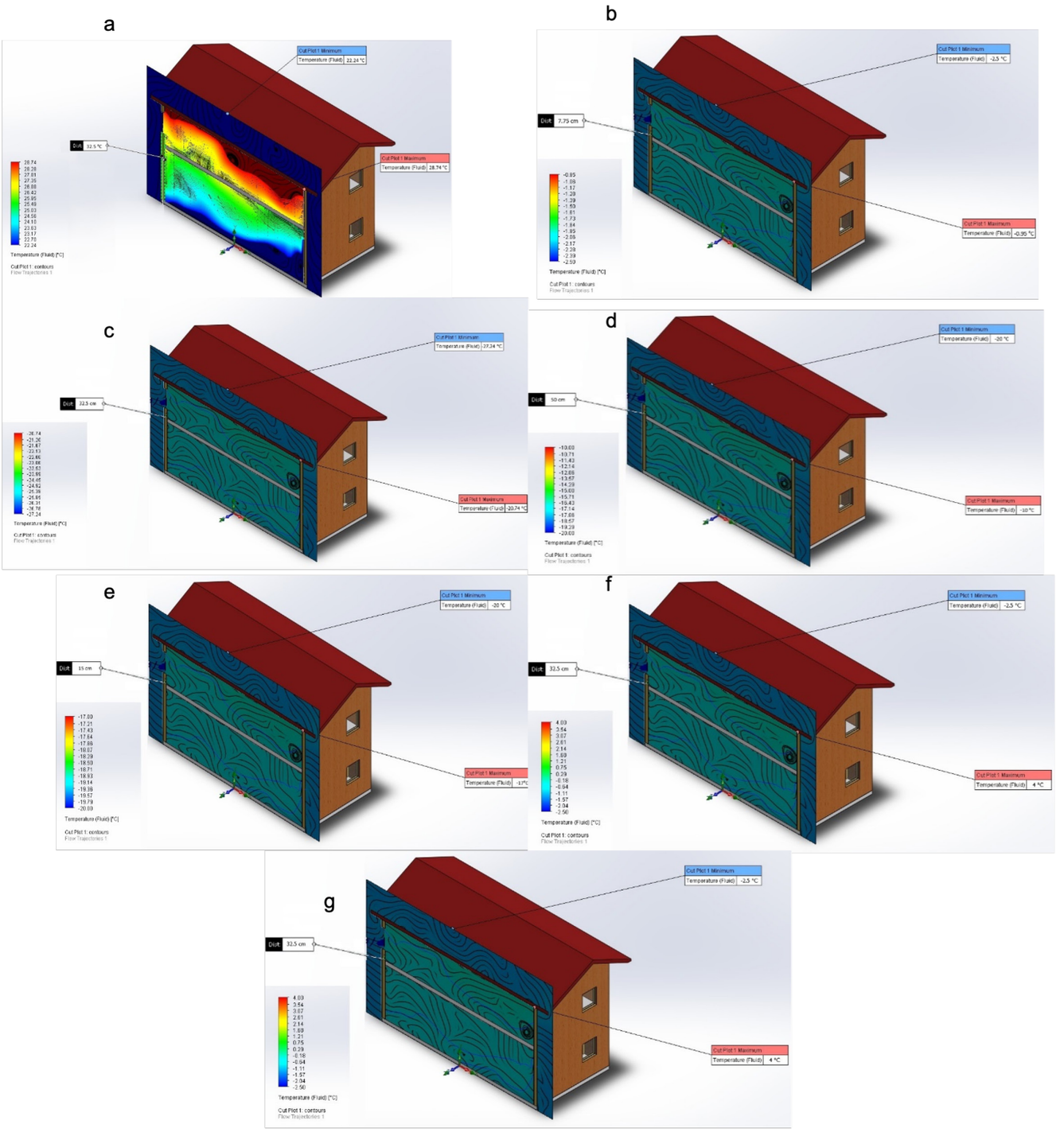


Figure 4. Comparison of the eco-friendly house's CFD simulation, based on the experimental optimization design, showing wall thicknesses and indoor and outdoor temperature scales. Part 2. Source: Prepared by the authors.

Wall thickness has a first-degree effect, and the temperature outside the eco-friendly house has a second-degree effect. This shows that both factors are highly significant (α = 0.05) for thermal comfort inside the house, but with complex effects regarding outdoor temperature, with the PMV index varying counterintuitively at very cold outdoor temperatures (Figure 5a)

The contour diagram (Figure 5c) shows thermal comfort zones even at low temperatures ranging from 0°C to -20°C. This becomes possible by increasing the thickness of the wall containing the ichu. If PMV values between -0.7 and 0.7 are considered comfortable, it is possible to achieve comfort with wall thicknesses above 40 cm, and the ichu can even enhance thermal comfort in temperate climates up to an ambient temperature of 15°C.

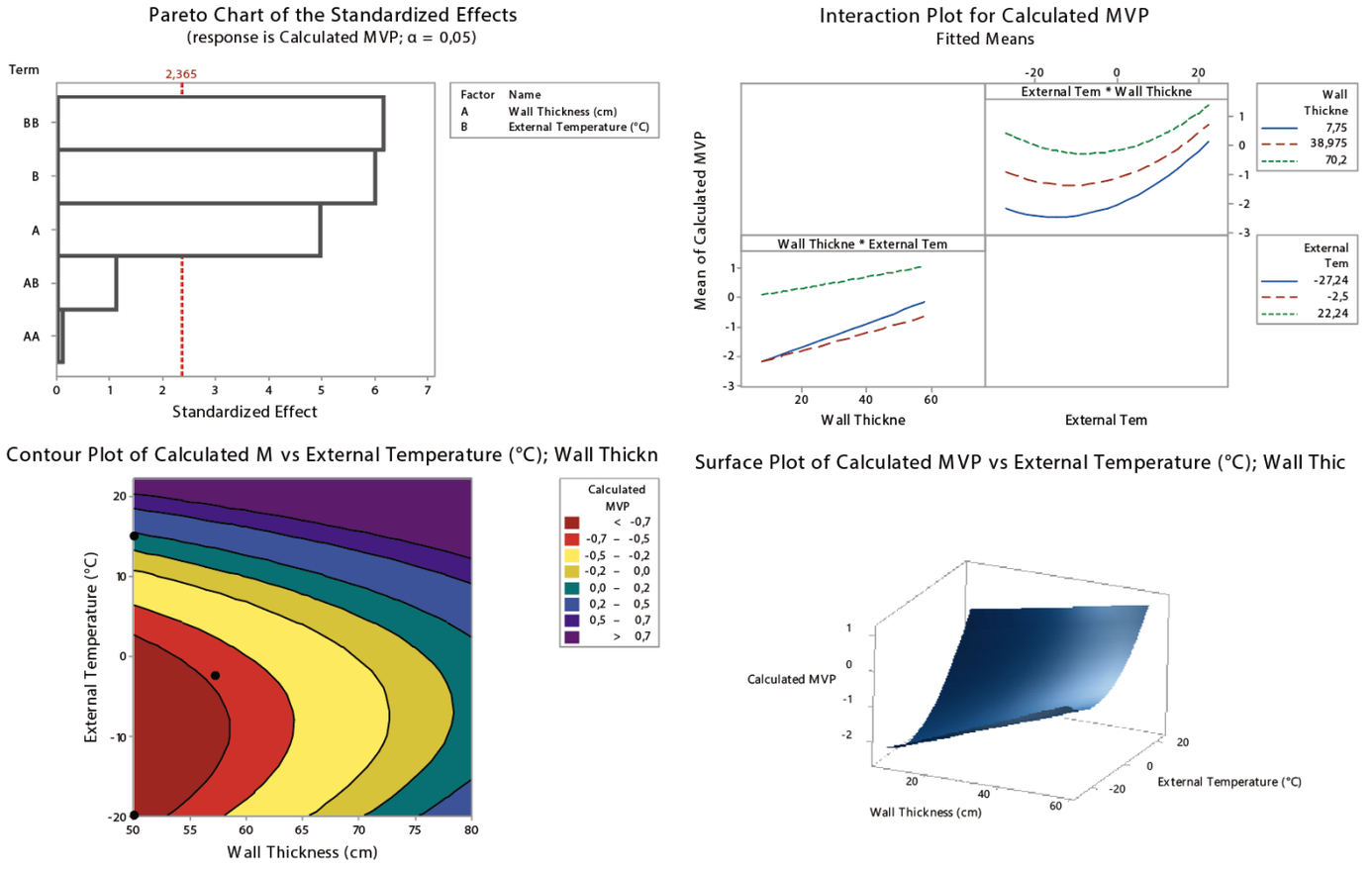


Figure 5. a) Pareto diagram identifies the standardized effects. b) Interaction of PMV means. c) Contour plot showing the spaces of thermal comfort and discomfort. d) 3D graph of thermal comfort in the eco-friendly house. Source: Prepared by the authors.

In Figure 5d, the 3-D response surface graph shows that higher temperatures and thicker wall thicknesses (optimization values) yield higher PMV values, which even exceed the thermal comfort ranges (classes A, B, and C). This value decreases with the wall thickness and when the temperature drops to extreme levels (-20°C). The thermal comfort range of class A is from -0.2 to 0.2, class B from -0.5 to 0.5, and class C from -0.7 to 0.7. It can be seen that thermal comfort can be achieved using PMV with wall thicknesses of 50, 60, and 65 cm for extreme temperatures from -10 °C to -20 °C (Zheng et al., 2021).

Specific calculations were conducted to determine the minimum wall thicknesses at -10 °C for PMV values of 0, -0.7, -0.5, and -0.2. The minimum thickness is 57.20 cm (Figure 6a – Figure 6d), and for temperatures of -20 °C, minimum thicknesses of 57, 53.07, 57.20, and 57.20 were obtained, respectively (Figure 6e – Figure 6h).

THERMAL COMFORT CALCULATION USING THE PREDICTED MEAN VOTE (PMV)

The model was subjected to thermal comfort assessment using PMV, following the experimental design, with wall thickness (cm) and external temperature (°C) as variables for the eco-friendly house. The other external parameters were kept constant. The results are shown in Table 3 as per the response surface design.

DISCUSSION

The wood chipboard's higher thermal conductivity (0.10 W/m·K) indicates that temperature changes propagate through it faster than through Ichu (0.05 W/m·K). The value obtained from the simulation is

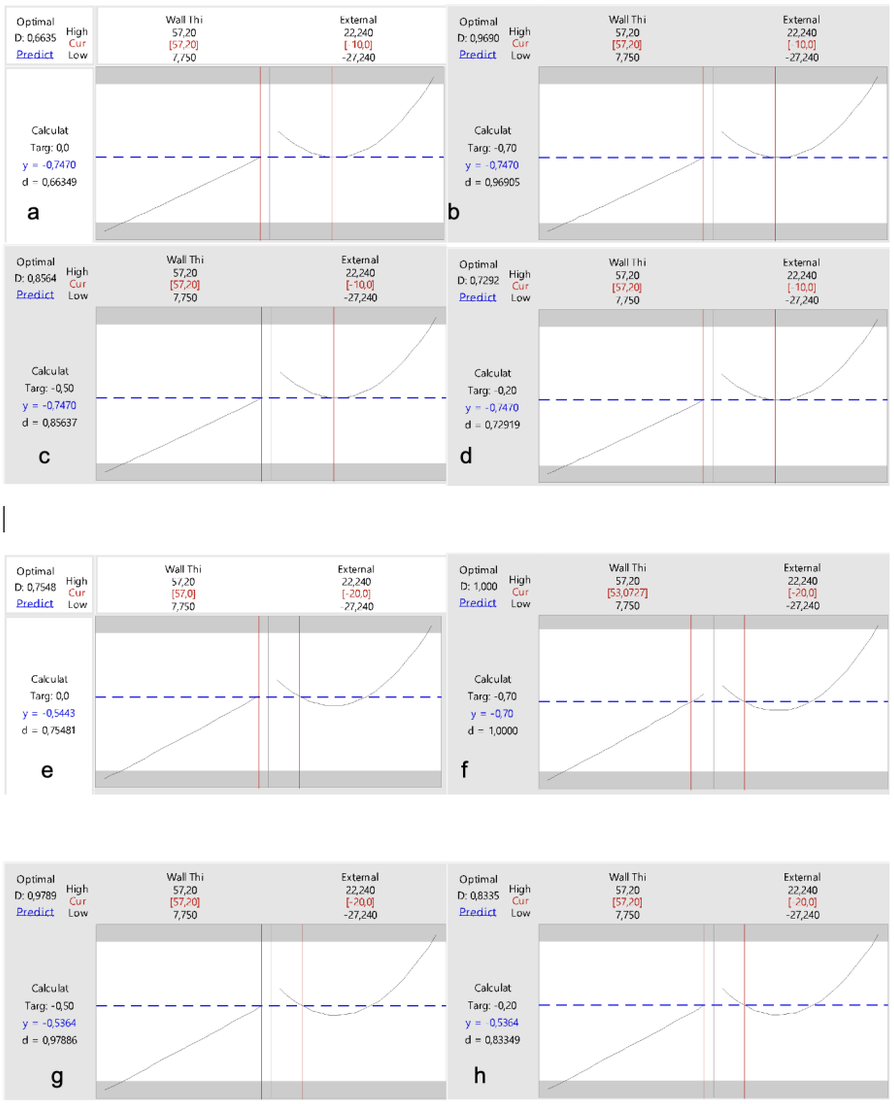


Figure 6. Optimization of wall thickness at extreme temperatures of -20 °C and -10 °C, with prediction and acceptable desirability. Source: Prepared by the authors.

Wall thickness (cm)	Outdoor temperature (°C)	Indoor temperature	PMV Calculation
32.5	-2.5	16	-1.29
32.5	-2.5	15.5	-1.42
32.5	-2.5	15	-1.57
50	15	20	0
15	15	17	-0.99
57.2	-2.5	18	-0.69
32.5	22.24	24	0.89
7.75	-2.5	14	-1.92
32.5	-27.24	16	-1.29
50	-20	18	-0.69
15	-20	13	-2.22
32.5	-2.5	16	-1.35
32.5	-2.5	15	-1.55

Note: The repetitions in Table 3 are the central points of the experimental design and allow measuring the model's variance and clearly reflect the system's sensitivity to thermal inertia. As the house can store heat, the internal temperature and PMV are not static; they exhibit slight fluctuations due to the flow of waste heat produced by the thermal cycle.

Table 3. Optimization design and thermal comfort calculation using the eco-friendly house's predicted mean vote (PMV). Source: Prepared by the authors.

consistent with the findings of Mendoza et al. (2021), who reported values ranging from 0.047 to 0.113 W/m·K. This emphasizes the model's fidelity. Ichu has insulating properties, with a thermal conductivity lower than that of screw wood (0.141 W/m·°C); this property supports the proposed structural model, and it is readily found in the Andean Highlands, where cold temperatures affect the inhabitants (Mendoza et al., 2021). The layout of the eco-friendly house evidences different thermal behaviors. In the house's roof, higher temperatures are recorded in all the simulations, presumably due to the use of tiles (thermal conductivity of 0.476 W/m·K), wood, and chipboard in the ceiling that naturally increase the temperature (Rat et al., 2023; Suleiman et al., 1999). It should also be recalled that hot air always rises through the "chimney effect", explained by the movement caused by the air pressure difference (0.1 m/s) that drives the less dense air upward (Suárez & Molina, 2015).

A main finding is a quadratic relationship between outdoor temperature and PMV. There is an optimal external temperature at which the minimum thermal comfort occurs for a given wall thickness. This nonlinearity is an empirical result arising from the complex interaction between heat-transfer mechanisms (conduction and natural convection within the house) and energy storage in the different components.

The thickness of the wall with ichu is higher than the experimental results of Molina-Fuertes, Horn-Mutschler & Gómez-León (2024), who used 0.4 m glass wool to achieve an indoor thermal amplitude of 17.1 °C, outdoor at 6.4 °C, and adobe walls with 0.40 m solid wood in the form of a shutter placed at night, which achieves values close to thermal comfort. It can be confirmed that using ichu inside the walls to preserve the house's internal heat longer would require slightly more space than other materials currently used. Several thermal comfort zones have been identified even at temperatures below -20°C by thickening the wall with ichu and sandwich-type chipboard; both materials have a relatively low thermal conductivity (0.05 W/m·K and 0.10 W/m·K, respectively). Increasing wall thickness increases Δx in the thermal resistance equation, thereby increasing the wall's thermal resistance and reducing the rate of heat flow from the warm inside to the cold outside (González-Domínguez, Monzón-Verona & García-Alonso, 2019). The indoor temperature remains stable and is affected less by the outdoor temperature at -20°C and -10°C when the wall thickness exceeds 57.20 cm, resulting in better PMV.

The recommended thickness of 57.20 cm satisfies the ISO 7730 standard, and optimal thermal comfort is achieved with a PMV close to 0, with an acceptable class A range generally between -0.2 and +0.2 (Olesen & Parsons, 2002). The calculated wall width to achieve thermal comfort based on the PMV is consistent with the thermal resistance of the wood and the ichu in a sandwich-type arrangement and is economically sustainable (van Niekerk, 2020). So, it is confirmed that these optimized values are an economic inclusion for inhabitants of the cold highlands and extreme temperatures in light of the Sustainable Development Goals (United Nations, 2019).

The validation of the optimized thickness of 57.2 cm is performed by comparing the Total Thermal Resistance (Rt) with conventional materials. Ichu's conductivity (k=0.05 W/m·K) allows a proposed wall with Rt=11.44 m^2.K/W, whereas a standard adobe wall (k=0.80 W/m·K) would require 9.15 m to achieve the same insulation (Piñas et al., 2020). The proposed width of the sandwich-type wall, although it appears thick by urban standards, is efficient and realistic in extreme cold in rural areas, eliminating the need for high-energy active heating systems.

CONCLUSIONS

The chipboard/ichu/chipboard sandwich-type wall is a highly effective technical solution for thermal insulation in extreme cold climates. Using Response Surface Methodology (RSM), it was determined that a critical thickness of 57.2 cm provides Class A thermal comfort in an eco-friendly house at an outdoor temperature of -20 °C.

Wall thickness has a first-degree relationship with PMV, whereas external temperature has a quadratic effect, indicating complex interactions in achieving thermal comfort. Therefore, the loss of comfort increases nonlinearly due to the extreme decrease in outdoor temperature, underscoring the need for insulation thicknesses greater than conventionally needed in high Andean areas to counteract this physical phenomenon.

The computational fluid dynamics confirms thermal stratification in two-floor houses. The air displaced by the internal pressure difference is concentrated on the second floor, suggesting that the architectural design should prioritize sleeping areas on upper floors to take advantage of the heat generated by the sandwich system.

CONTRIBUTION OF AUTHORS CRediT:

Conceptualization, H.J.; Data curation, J.R.; Formal analysis, H.J.; Acquisition of financing, H.J., G.Q.; Research, H.J., K.M.; Methodology, H.J.; Project management, H.J., G.Q.; Resources, J.R.; Software. J.R.; Supervision, H.J.; Validation, K.M., J.R.; Visualization, H.J.; Writing - original draft, H.J.; Writing - revision and editing, H.J., K.M.

ACKNOWLEDGMENTS

The Technological University of Peru is thanked for its Financing of P-2024-SUR-19, through the R&D project competition 2024 UTP Southern Region, under RR N° 0168-2024-R-UTP

GLOSSARY OF TERMS AND ACRONYMS

CFD: Computational Fluid Dynamics. This is a discipline that uses algorithms and numerical methods to solve cases of fluid and heat transfer.

Thermal conductivity (k): The property to conduct heat; its units are W/mK

Spatial discretization: Division of the continuous domain into a finite number of cells.

Euler Scheme: An implicit first-order numerical method for the discretization of temporal derivatives.

Gauss Linear: Second-order discretization based on the Gauss divergence theorem.

Thermal inertia: The ability to maintain the energy received and release it progressively.

Hexahedral Mesh: Mesh composed of six-sided elements (cubes or prisms)

OpenFOAM: Open-source software for solving thermal and fluid simulation problems.

PMV: Predicted mean vote. It is an index that predicts the thermal sensation based on the mean of the votes.

PPD: Predicted percentage of dissatisfied. An index that counts thermally uncomfortable people.

RSM: Response Surface Methodology. Statistical and mathematical techniques for modeling and analyzing responses influenced by variables of interest.

BIBLIOGRAPHIC REFERENCES

Atahuachi Layme, G. M., & Carcausto Quispesayhua, Y. N. (2018). *Aislante termoacústico a base de Stipa Ichu para atenuar el ruido y cambios drásticos de temperatura en viviendas de sectores en expansión urbana de la ciudad de Puno*. [Tesis de maestría, Universidad Nacional del Altiplano]. Repositorio Institucional - UNAP. https://repositorio.unap.edu.pe/handle/20.500.14082/11138

Cárdenas Cristobal, J. M., & Espinoza Ramírez, K. (2024). Utilización de unidades termo-modulares de vivienda para combatir el friaje extremo con materiales oriundos de Tayabamba - La Libertad – 2021 [Tesis de pregrado, Universidad Nacional del Santa]. Repositorio Institucional - UNS. https://alicia.concytec.gob.pe/vufind/Record/UNSR_09f576f8c5882bcc0a5e467258693592/Description#details

Charca, S., Noel, J., Andia, D., Flores, J., Guzman, A., Renteros, C., & Tumialan, J. (2015). Assessment of Ichu fibers as non-expensive thermal insulation system for the Andean regions. *Energy and Buildings*, 108, 55–60. https://doi.org/10.1016/j.enbuild.2015.08.053

Fanger, P. O. (1970). *Thermal comfort: analysis and applications in environmental engineering*. Danish Technical Press.

Frías, M., Caneda-Martínez, L., Sánchez de Rojas, M. I., Tenazoa, C., & Flores, E. (2020). Scientific and technical studies on eco-efficient binary cements produced with thermally activated ichu grass: Behaviour and properties. *Cement and Concrete Composites*, 111, 103613. https://doi.org/10.1016/j.cemconcomp.2020.103613

Gilani, S. I. U. H., Khan, M. H., & Pao, W. (2015). Thermal Comfort Analysis of PMV Model Prediction in Air Conditioned and Naturally Ventilated Buildings. *Energy Procedia*, *75*, 1373–1379. https://doi.org/10.1016/J.EGYPRO.2015.07.218

González-Domínguez, P. I., Monzón-Verona, J. M., & García-Alonso, S. (2019). New Thermal-Conductivity Constitutive Matrix in Fourier's Law for Heat Transfer Using the Cell Method. *Applied Sciences*, *9*(21), 4521. https://doi.org/10.3390/APP9214521

Hills, J. (2012). *Getting the measure of fuel poverty: final report of the Fuel Poverty Review*. CASE report 72. https://sticerd.lse.ac.uk/dps/case/cr/casereport72.pdf

Hodson, T. O. (2022). Root-mean-square error (RMSE) or mean absolute error (MAE): when to use them or not. *Geoscientific Model Development*, *15*(14), 5481–5487. https://doi.org/10.5194/GMD-15-5481-2022

Marchante González, G., & González Santos, A. I. (2020). Evaluación del confort y disconfort térmico. *Ingeniería Electrónica, Automática y Comunicaciones*, *41*(3), 21–40. https://dialnet.unirioja.es/servlet/articulo?codigo=9513886

Mendoza, M. A., Piñas Moya, M. J., Horn Mutschler, M. J., & Gómez León, M. M. M. (2021). Conductividad térmica de compuestos tipo sándwich usados en la industria de la construcción. *TECNIA*, *31*(1), 42–50. https://doi.org/10.21754/tecnia.v21i1.1198

Molina-Fuertes, J. O., Horn-Mutschler, M. J., & Gómez-León, M. M. (2024). Evaluación del comportamiento térmico de un sistema constructivo de pared en zona altoandina utilizando un módulo experimental. *Tecnia*, *34*(2), 53–61. https://doi.org/10.21754/TECNIA.V34I2.2170

Mora, R., & Bean, R. (2018). Thermal Comfort: Designing for People. *Ashrae Journal*, (02), 40-46. https://commons.bcit.ca/besys/files/2018/08/Thermal-Comfort-Design-for-People.pdf

Moreno-Casas, P. A., Scott, F., Delpiano, J,. & Vergara-Fernández, A. (2020). Computational tomography and CFD simulation of a bio filter treating a toluene, formaldehyde and benzo [a] pyrene vapor mixture. *Chemosphere*, *240,* 124924. https://doi.org/10.1016/j.chemosphere.2019.124924

Naciones Unidas. (2019). *Informe de Los Objetivos Del Desarrollo Sostenible 2019*. Naciones Unidas Nueva York https://ods.org.mx/docs/doctos/SDG_Report2019_es.pdf

Olesen, B. W., & Parsons, K. C. (2002). Introduction to thermal comfort standards and to the proposed new version of EN ISO 7730. *Energy and Buildings*, *34*(6), 537–548. https://doi.org/10.1016/S0378-7788(02)00004-X

Ortiz Caicedo, P. L., Gonzales Vega, A. A., Montaño Roldan, V. L., Chica Tambaco, A. J., & Álava Vélez, C. E. (2023). Eficiencia de sistemas de aislamiento térmico. *Ibero-American Journal of Engineering & Technology Studies*, *3*(2), 43–50. https://doi.org/10.56183/IBEROTECS.V3I2.631

Piñas, J. M., Lira, L., Horn, M., Solis, J. L., & Gómez, M. M. (2020). Influence of Stipa ichu on the thermal and mechanical properties of adobe as a biocomposite material. *Journal of Physics: Conference Series*, *1433*(1), 012003. https://doi.org/10.1088/1742-6596/1433/1/012003

Presidente de la Comisión Organizadora de la UNAAT. (24 de enero de 2017). *Año del Buen Servicio al Ciudadano. RESOLUCIÓN DE PRESIDENCIA N° 007-2017-CO-P-UNAAT.* Universidad Nacional Autónoma Altoandina de Terma [https://cdn.www.gob.pe/uploads/document/file/2178617/RESOLUCI%C3%93N%20DE%20PRESIDENCIA%20N%C2%B0%20007-2017-CO-P-UNAAT.pdf

Rat, E., Martínez-Martínez, S., Sánchez-Garrido, J. A., Pérez-Villarejo, L., Garzón, E., & Sánchez-Soto, P. J. (2023). Characterization, thermal and ceramic properties of clays from Alhabia (Almería, Spain). *Ceramics International*, *49*(9), 14814–14825. https://doi.org/10.1016/J.CERAMINT.2022.05.328

Roelofsen, P., & Jansen, K. (2024). Modification in the (NEN-) EN-ISO 7730 Model, with Regard of the Thermal Indoor Climate Assessment in Dutch Offices. *Jounarl of Building Design and Environment*, *2*(2), 35033. https://doi.org/10.37155/2811-0730-0302-15

Suárez, C., & Molina, J. L. (2015). Análisis del efecto chimenea en fachadas ventiladas opacas mediante correlaciones del flujo másico inducido. Aplicación para el dimensionado de anchos de cámara. *Informes de la Construccion*, *67*(538), e087. https://doi.org/10.3989/IC.13.155

Suleiman, B. M., Larfeldt, J., Leckner, B., & Gustavssor, M. (1999). Thermal conductivity and diffusivity of wood. *Wood Science and Technology*, *33*(6), 465–473. https://doi.org/10.1007/S002260050130

Tominaga, Y., Mochida, A., Yoshie, R., Kataoka, H., Nozu, T., Yoshikawa, M., & Shirasawa, T. (2008). AIJ guidelines for practical applications of CFD to pedestrian wind environment around buildings. *Journal of Wind Engineering and Industrial Aerodynamics*, *96*(10–11), 1749–1761. https://doi.org/10.1016/J.JWEIA.2008.02.058

van Niekerk, A. J. (2020). Inclusive Economic Sustainability: SDGs and Global Inequality. *Sustainability 12*(13), 5427. https://doi.org/10.3390/SU12135427

Zheng, Z., Zhang, Y., Mao, Y., Yang, Y., Fu, C., & Fang, Z. (2021). Analysis of SET* and PMV to evaluate thermal comfort in prefab construction site offices: Case study in South China. *Case Studies in Thermal Engineering*, *26*, 101137. https://doi.org/10.1016/J.CSITE.2021.101137

Revista Hábitat Sustentable Vol. 16, N°. 1. ISSN 0719 - 0700 / Págs. 70 - 95
https://doi.org/10.22320/07190700.2026.16.01.05

CHAKIÑAN: RECOVERY OF ANCESTRAL INFRASTRUCTURE AND MANAGEMENT OF THE LIVING TERRITORY IN THE COMMUNITY OF LAS LAGUNAS, SARAGURO, ECUADOR

Recibido 13/02/2026
Aceptado 27/05/2026

CHAKIÑAN: RECUPERACIÓN DE INFRAESTRUCTURA ANCESTRAL Y GESTIÓN DEL TERRITORIO VIVO EN LA COMUNIDAD DE LAS LAGUNAS, SARAGURO, ECUADOR

CHAKIÑAN: RECUPERAÇÃO DE INFRAESTRUTURA ANCESTRAL E GESTÃO DO TERRITÓRIO VIVO NA COMUNIDADE DE LAS LAGUNAS, SARAGURO, EQUADOR

Flor Lozano-Guamán (Autor de Correspondencia)
Magíster en Arquitectura con mención en Construcción Sostenible
Arquitecta, Diseñadora de Interiores SD Arquitectura
Saraguro, Ecuador
https://orcid.org/0009-0001-4417-2512
flor.lozano@ucuenca.edu.ec

Angel Lozano-Guamán
Magíster en Proyectos Arquitectónicos
Arquitecto,
Antropólogo, SD Arquitectura
Saraguro, Ecuador
https://orcid.org/0009-0001-8931-9645
kurylogu@gmail.com

CC BY SA

Revista Hábitat Sustentable Vol. 16, N°. 1. ISSN 0719 - 0700 / Págs. 70 - 95
https://doi.org/10.22320/07190700.2026.16.01.05

ABSTRACT

Indigenous communities in Ecuador, such as Las Lagunas in Saraguro, possess an autonomous organization based on the Ayllu and the Andean worldview. Their system of ancient trails, called chakiñanes, has historically facilitated mobility and connectivity with sacred sites. However, the lack of upkeep and the pressure of motorized urban development threaten their survival. This research analyzes chakiñanes as ancestral infrastructure for sustainable habitat management. Through a multiscalar, mixed approach —integrating participatory mapping, photogrammetry, and the diagnosis of water and spiritual infrastructure—44 ancient trails were identified. The findings reveal that 95% of the community considers these routes vital to their identity, despite their physical fragmentation. It is concluded that revitalizing the chakiñanes through a micro-basin approach and the use of local materials will not only restore pedestrian mobility but also strengthen territorial governance for sustainable habitat and cultural landscape conservation.

Keywords
cultural landscape, pedestrian mobility, ancestral infrastructure, community planning

RESUMEN

Las comunidades indígenas de Ecuador, como Las Lagunas en Saraguro, poseen una organización autónoma basada en el Ayllu y en la cosmovisión andina. Su sistema de caminos antiguos, llamados chakiñanes, ha facilitado históricamente la movilidad y la conexión con sitios sagrados. No obstante, la falta de mantenimiento y la presión del desarrollo urbano motorizado amenazan con su desaparición. Esta investigación analiza los chakiñanes como infraestructura ancestral para la gestión del hábitat sustentable. Mediante un enfoque mixto multiescalar —que integró mapeo participativo, fotogrametría y el diagnóstico de la infraestructura hídrica y espiritual— se identificaron 44 caminos antiguos. Los hallazgos revelan que el 95% de la comunidad considera estos ejes vitales para su identidad, a pesar de su fragmentación física. Se concluye que revitalizar los chakiñanes bajo una lógica de microcuenca y de materiales locales no solo recuperará la movilidad peatonal, sino que también fortalecerá la gobernanza territorial de un hábitat sostenible y la conservación del paisaje cultural.

Palabras clave
paisaje cultural, movilidad peatonal, infraestructura ancestral, planificación comunitaria

RESUMO

As comunidades indígenas do Equador, como a de Las Lagunas, em Saraguro, possuem uma organização autônoma baseada no Ayllu e na cosmovisão andina. Seu sistema de caminhos antigos, chamados chakiñanes, tem facilitado, historicamente, a mobilidade e a conexão com locais sagrados. No entanto, a falta de manutenção e a pressão do desenvolvimento urbano motorizado ameaçam fazê-los desaparecer. Esta investigação analisa os chakiñanes como infraestrutura ancestral para a gestão sustentável do habitat. Por meio de uma abordagem mista e multiescalar — que integrou mapeamento participativo, fotogrametria e o diagnóstico da infraestrutura hídrica e espiritual —, foram identificados 44 caminhos antigos. Os resultados revelam que 95% da comunidade considera esses eixos vitais para sua identidade, apesar de sua fragmentação física. Conclui-se que a revitalização dos chakiñanes, sob uma lógica de microbacia e com o uso de materiais locais, não apenas recuperará a mobilidade dos pedestres, mas também fortalecerá a governança territorial de um habitat sustentável e a conservação da paisagem cultural.

Palavras-chave
paisagem cultural, mobilidade de pedestres, infraestrutura ancestral, planejamento comunitário

Revista Hábitat Sustentable Vol. 16, N°. 1. ISSN 0719 - 0700 / Págs. 70 - 95
https://doi.org/10.22320/07190700.2026.16.01.05

INTRODUCTION

The community landscape of indigenous peoples is constantly transforming and faces the challenge of integrating ancestral knowledge into habitat planning to ensure territorial sustainability. In this scenario, intervention in ancestral areas requires a deep understanding of the logics of historical occupation and the Andean cosmovision, where architecture is conceived as an intrinsic dialogue with the *Pachamama* (Lozano Guamán, 2021). Including this approach allows contrasting the limitations of contemporary construction models, in which the combination of nature and culture constitutes the emerging paradigm for planning and revitalizing territories based on their heritage resources (Pérez Bustamante & Parra Ponce, 2004). Under this approach, it becomes key to recover systems such as *bahareque,* which represent local identity and technique (Lozano Guamán, 2022). One of the fundamental elements of this territorial configuration is the *Chakiñanes*, mobility systems used since pre-Columbian times that take into account not only the complex Andean topography, but also a symbolic structure connecting the social and productive life of the communities.

The study of these ancient roads in America has the *Qhapaq Ñan* (Inca Trail) as its backbone, a physical and spiritual road network that linked the lands of the *Tawantinsuyo*. This monumental infrastructure not only attests to the constructive dominance of the Inca civilization, but also represents the result of a strategic expansion that took advantage of and perfected the pre-existing traces of earlier cultures (Marca Chérrez, 2011). As Guerrero Baca (2017) argues, understanding these ancestral territorial and constructive systems is imperative for the conservation of heritage in Latin America, as they blend the natural landscape with social identity. This system also facilitated efficient territorial control across different altitudinal levels through a dynamic organization of economic, political, and social relations (Ordóñez Suárez, 2019).

In the Ecuadorian context, the *Qhapaq Ñan* profoundly influences the identity of peoples such as the Kichwa Saraguro, in the province of Loja. In this southern area, the route connects archaeological landmarks such as Cerro Carboncillo and Tambo de Villamarca, which descends towards the Paquishapa River, to join settlements such as Ingapirca and Tambo Blanco (Marca Chérrez, 2011). This territorial occupation logic is also reflected in the architecture, morphological configuration, and spatial organization of settlements, where the transition from the vernacular to the modern requires a rigorous typological analysis, under the premise that the inhabited space is the product of an accumulated knowledge that links materiality with identity (Lozano Guamán, 2014).

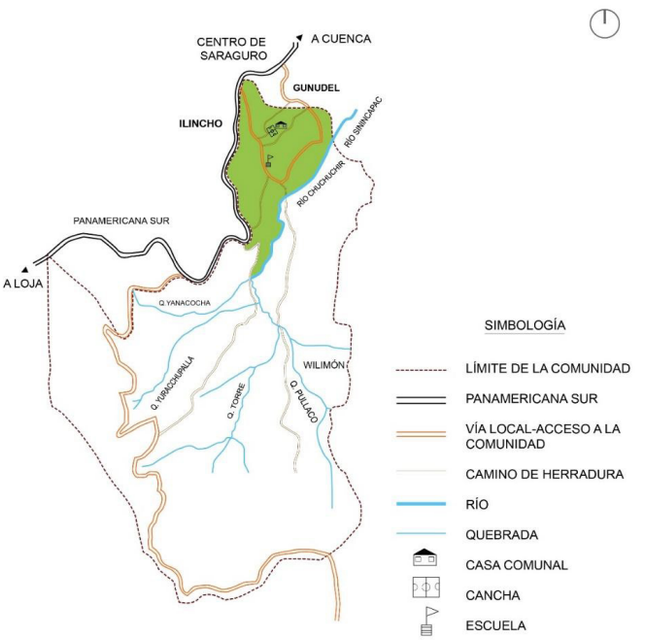


Figure 1. Schematic map of the Las Lagunas community territory. Source: Prepared by the Authors, based on Quizhpe Guamán (2013).

Despite its incalculable historical value and its loss in Andean ritual, a large part of this network in the Saraguro canton lacks preventive conservation plans, even though it is considered a valued element in provincial planning (Dávila Egüez, 2015). This technical shortcoming jeopardizes the survival of the ancestral *Chakiñanes*, which today serve as the last vestige of pre-Columbian connectivity and living memory in the region. To provide a geographical dimension to this phenomenon, a multiscale location and general location map was developed (Figure 1), which allows a cartographic approach from the macro-regional context to the specific section being intervened in. The protection of this fabric becomes ever more urgent when considering that the pressure of motorized urban development on Andean pedestrian infrastructure not only alters local mobility, but also jeopardizes the continuity of cultural landscapes rooted in earthen-built architecture. As noted by Colosi et al. (2025), contemporary transformation dynamics and the lack of connection in territorial planning accelerate the material loss of vernacular heritage environments, forcing the proposal of strategies to rescue local constructional knowledge in the face of urban anthropogenic risk.

THE TERM CHAQUIÑÁN

The term *Chakiñan*, derived from the Kichwa words *chaki* (foot) and *ñan* (way), technically refers to the narrow pedestrian paths that form the basis of local mobility in the Andean world. According to the Ordóñez Suárez road system classification (2019), these roads

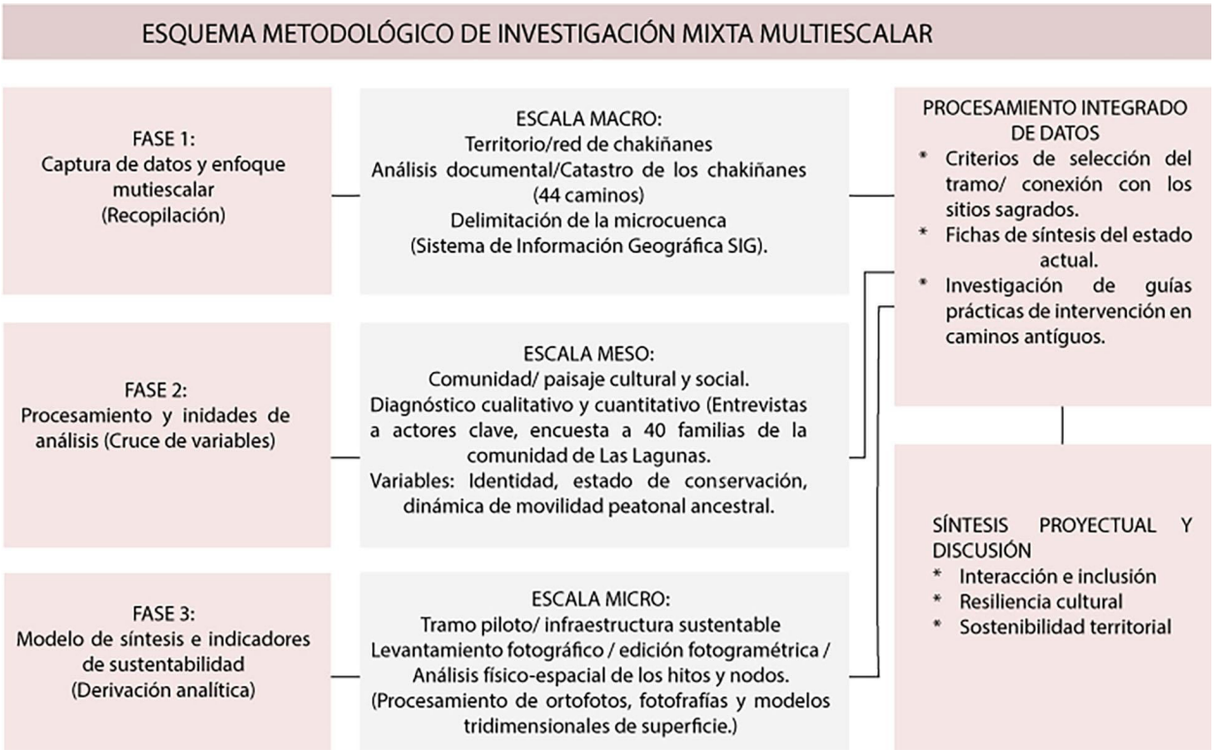


Figure 2. Design methodology. Source: Prepared by the Authors.

are organized by order of importance. The *Qhapaq Ñan* acted as the first-order route that connected the central lines of the four styles of the *Tawantinsuyo*; the *Runa Ñan* functioned as the second-level route destined to connect regions; and finally, the *Chakiñan* was established as the third-level route, whose main role was to link internal areas, the communities, and the *Ayllu*. This capillary network of *Chakiñanes*, albeit narrow, was fundamental for the Inca state vision by serving as the dynamizing axis of social and economic relations at a local scale (Marca Chérrez, 2011), which allows the flow of *mitimaes* (family groups) and the exchange of mass consumer products in geographically complex sectors such as Saraguro (Canziani Amico, 2012).

Based on this, the research raises the following question: How does the recovery of this network of ancient roads, *Chakiñanes*, contribute to the resilience of sustainable habitats and the preservation of symbolic and functional structures in contemporary indigenous communities? The objective is to propose an intervention model that links vernacular techniques with autonomous territorial planning.

METHODOLOGY

This research is conducted using a mixed approach, based on exploratory and descriptive methodologies (Hernández Sampieri & Mendoza Torres, 2018). The methodology follows a multiscale vision that allows understanding the territory as a living system (Figure 2).

MACRO SCALE: TERRITORIAL DELIMITATION AND LIST OF CONNECTIVITY NETWORKS

The macro-scale approach was structured around the geographical boundary and morphometric analysis of the micro-basin, which is home to the community territory of the *Lagunas Chukidel Ayllullacta* in the Saraguro Canton, Loja province, Ecuador, defining it as the fundamental biophysical unit for sustainable habitat planning. In this phase, the implementation and layout logic of the *Chakiñanes* were evaluated in relation to topographic variables and the surface water network. For this, a geospatial database was designed using Geographic Information Systems (GIS), and digital terrain models (MDE, in Spanish) were used as cartographic inputs. This technical procedure aimed to correlate terrain slopes with the sinuosity coefficients of ancestral paths, enabling the examination of energy efficiency and topographic adaptability patterns associated with pedestrian mobility within the community territory.

At the same time, the reconstruction of the historical road fabric was complemented by on-site social mapping and field route validation. This method integrated local collective memory with global positioning (GPS) techniques to georeference a list of

historical road networks and systematically register vernacular toponymy associated with biophysical and family governance landmarks (*Ayllu*). Based on Montaño Huerta's (2017) suggestions regarding the visibility of underlying spatial logics in the planning of intercultural landscapes, the methodological framework treated the original nomenclature as a record of environmental memory. The inclusion of qualitative community perception data alongside the geometric layers of the territory (Quizhpe Guamán, 2013) helped consolidate a unified cartographic matrix. This technical instrument served as the spatial basis for delimiting and justifying the selection of the section under investigation at a higher resolution in subsequent scales, dispensing with conventional urban planning approaches that omit the non-motorized mobility infrastructure of historical origin.

MESO-SCALE: SOCIO-SPATIAL CHARACTERIZATION AND COMMUNITY DYNAMICS OF THE HABITAT

The meso-scale approach was proposed using a mixed-methods research design to correlate the population's socio-spatial perception with the dynamics of use, appropriation, and conservation of the historical pedestrian network. For the qualitative component, the methodological procedure involved designing and administering semi-structured, intergenerational interviews. This instrument aimed to collect information to reconstruct the collective environmental memory and analyze the historical evolution of the habitat in the face of contemporary urban and road transformation processes. The data collection was directed at three women leaders of the community council, selected through intentional non-probability sampling. The inclusion criteria adopted for this group of key informants required: a) generational representativeness and historical permanence in the area; b) knowledge of vernacular toponymy and community social mapping; and c) exercise of roles linked to local governance and territorial decision-making.

On the other hand, the quantitative component was administered via a questionnaire to a sample of 40 heads of household from Las Lagunas. To standardize the survey of the inhabited space, non-probabilistic sampling by quotas was applied, which projects a distribution of response units across the six consolidated sectors that make up the community's morphology: Wabo loma, Lirios, Waile, Takchana, Rarik, and Yarimala. The survey's methodological design operationalized habitability and sustainability variables, focused on measuring the frequencies of use of the *Chakiñanes*, the reasons for pedestrian displacement (access to agricultural plots, grazing, water supply, or mystical connectivity), the typology of material damage to the trails, and the community valuation regarding the protection of the cultural landscape. The qualitative data collected were processed using categorical content analysis, while the quantitative data were tabulated in statistical matrices for subsequent cross-tabulation of spatial variables.

MICRO SCALE: PHYSICAL-SPATIAL ANALYSIS AND PHOTOGRAMMETRIC RECORDING OF THE PILOT SECTION

The microscale approach focused on the morphological recognition of the accesses and intersections connecting the central motorized highway to the *Chakiñanes* network. The methodological procedure combined fieldwork with near-remote sensing techniques and systematic high-resolution photographic recording. For the geometric characterization of the built environment, a terrestrial photogrammetric reconstruction method by sections was applied. This process consisted of sequentially capturing images with longitudinal overlap exceeding 70% to generate two-dimensional orthomosaics and digital surface models. These tools allowed evaluating, with metric precision, the sections of the paths, the materiality of the enclosures, and the configuration of the accesses.

Through this micro-detail documentation, the physical continuity of the pedestrian paths was parameterized to analyze their permeability and accessibility conditions to local water nodes and symbolic infrastructure (springs and sacred landmarks). The monitoring of the graphic pieces included digital rectification and scaling of the samples, which establish a geometric baseline for identifying morphological anomalies, variations in the original road width, and physical obstructions.

PARAMETERIZATION AND TECHNICAL CRITERIA OF THE CONSTRUCTIVE CHARACTERIZATION

For the material characterization and evaluation of the conservation status of the *Chakiñanes*, the methodological procedure was adapted from the standardized technical guidelines for intervention in the Andean Road system. The analytical variables were coded based on two heritage reference instruments: the protocol of the Qhapaq Ñan Project (INPC, 2004), from which the method of physical-environmental diagnosis of pre-Hispanic roads was extracted, and the Guide for training in preventive conservation of archaeological structures in stone and earth (Qhapaq Ñan-Ecuador, 2019), from which the deterioration indicators in lithic masonry were adopted.

The application of both frameworks structured a technical comparison matrix used in microscale field surveys. This instrument standardized the observation along three lines: a) basic road morphology (cuttings, backfill, platforms



Figure 3. Glossary of the Constructive Characteristics of the Royal Inca Trail. Source: Prepared by the Authors, using INPC (2004).

or steps typologies); b) materiality and containment systems (supporting walls or cobblestones); and c) physical vulnerability (erosion by runoff or loss of sections). By operationalizing these manuals as field diagnostic tools, a parametric database of pre-existing elements was consolidated (Figures 18 and 19). This geometric characterization constitutes the essential technical scaffolding for discussing the material findings and for grounding the subsequent consolidation guidelines in the study area (Figures 3 and 4).

RESULTS AND DISCUSSION

CHARACTERIZATION, INVENTORY, AND TOPONYMY OF THE ANCESTRAL NETWORK OF CHAKIÑANES (MACRO SCALE)

The processing of geospatial data, combined with the validation of the community social mapping, resulted in the identification and cataloging of a historical road network comprising 44 active and latent *Chakiñanes* within the territory of Las Lagunas (Figure 5). Far from constituting only isolated linear vestiges, these axes of mobility are structured as a highly integrated green, low-emission infrastructure that responds to the morphological, hydric, and socio-cultural logics specific to the Andean cultural landscape. When systematically classifying these paths (Table 2), a direct correspondence between the vernacular nomenclature and the governance of the living space is observed. The registration of family milestones in 29.5% of the road toponymy corroborates the idea that the historical pedestrian network is inseparable from the residential and kinship structure of the Ayllu, where public space serves as a physical support for collective memory and social cohesion. This functional and symbolic link validates the suggestions of Montaño Huerta (2017) regarding the original toponymy as a living environmental archive, and allows to contrast the contemporary models of conventional urban planning critically; while the latter impose numerical

Revista Hábitat Sustentable Vol. 16, N°. 1. ISSN 0719 - 0700 / Págs. 70 - 95
https://doi.org/10.22320/07190700.2026.16.01.05

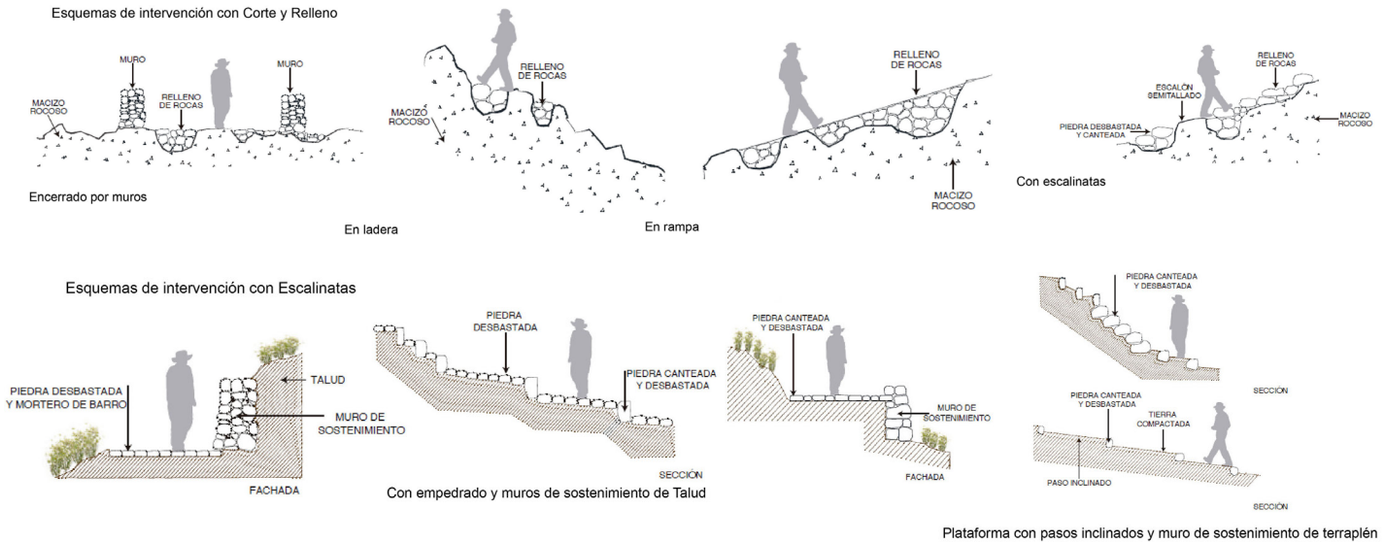


Figure 4. Intervention methods with Cuttings, Backfill, and Steps. Source: Prepared by the Authors based on Qhapaq Ñan-Ecuador (2019).

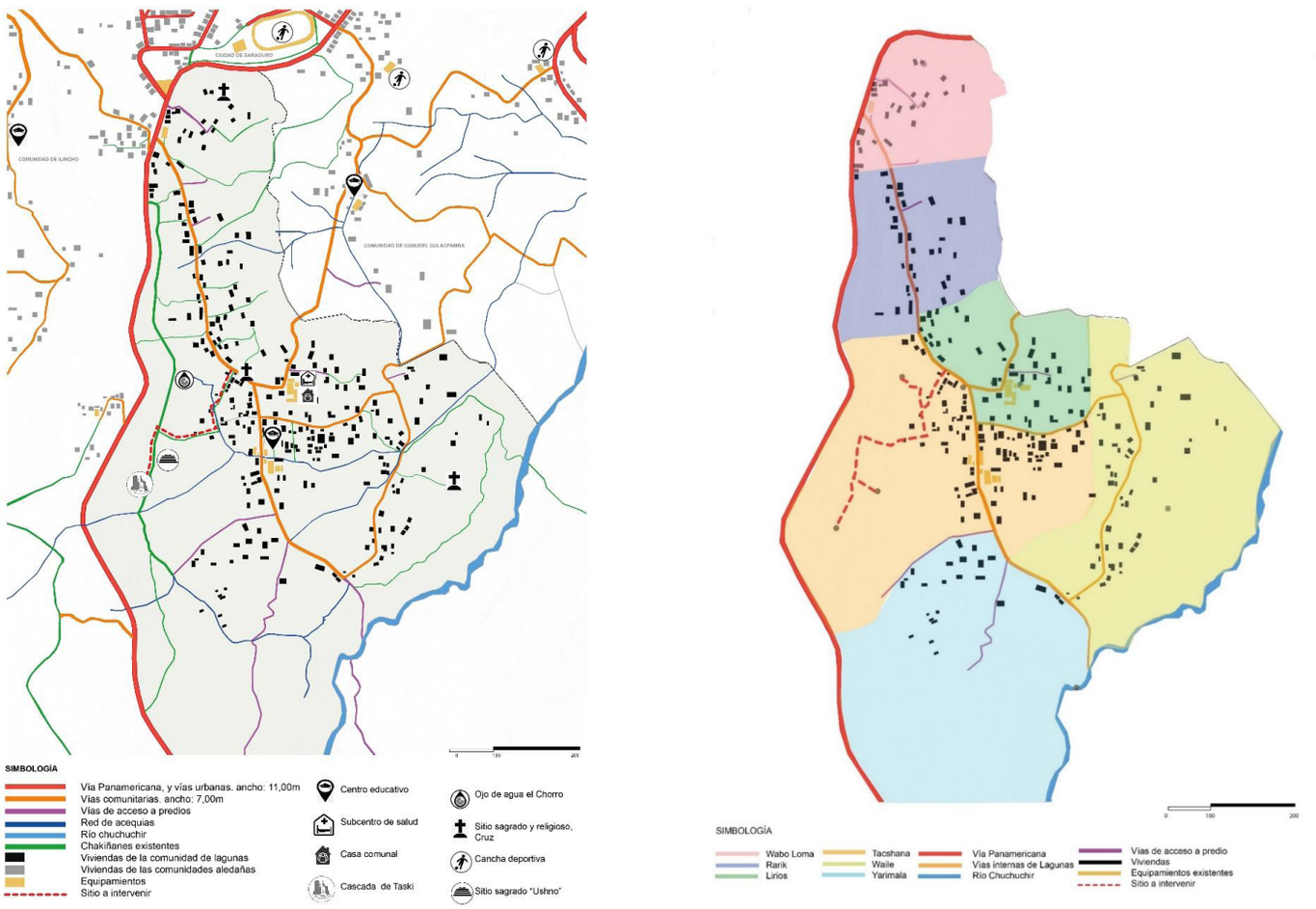


Figure 5. Fragment scale map and sectors of the Las Lagunas community. Source: Lozano Guamán, 2022.

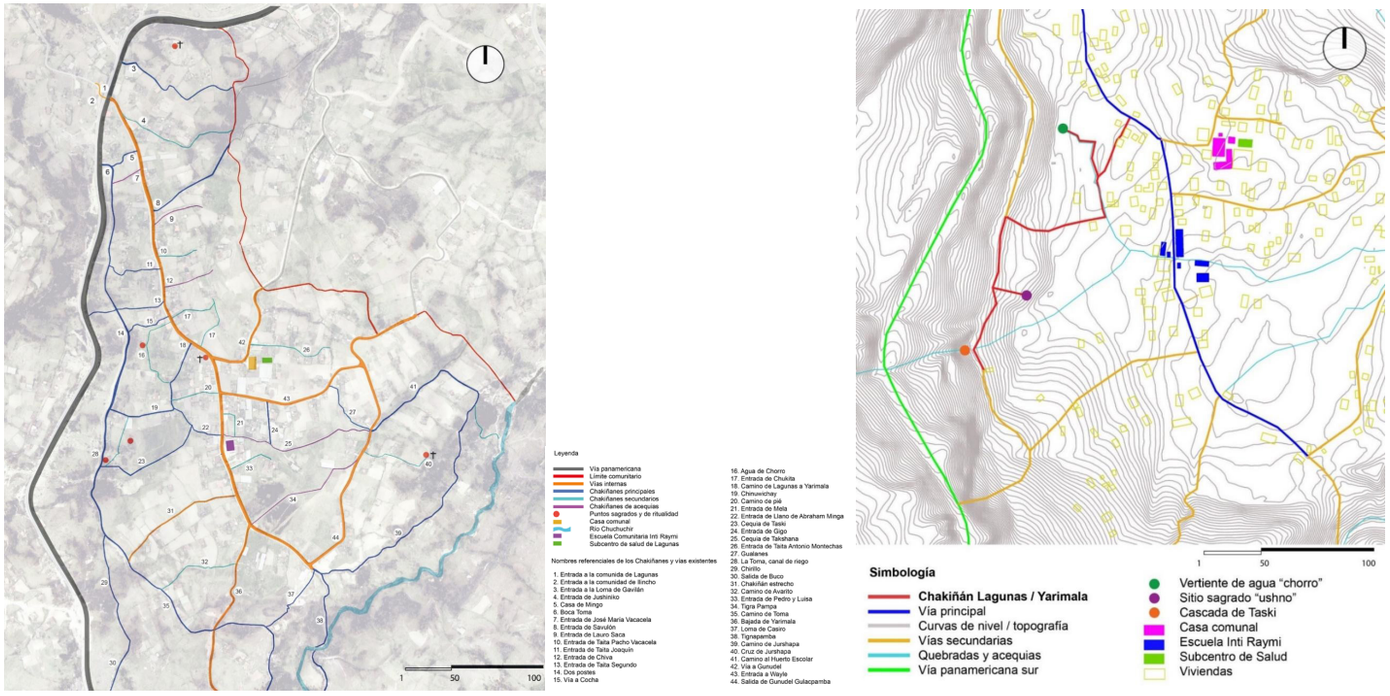


Figure 6. Mapping of the Chakiñanes and irrigation canals of the community of Las Lagunas. Topographic survey. Source: Prepared by the Authors using Google Maps.

Category	Registered Names (according to Mapping and Collective Memory)
Entrances and Sectors (Connectivity)	(1) Entrance to the Lagunas community, (2) Entrance to the Ilincho community, (3) Entrance to the Gavilán Hill, (4) Entrance to Jushiniko, (15) Road to Cocha, (17) Entrance to Chukita, (18) Route from Lagunas to Yarimala, (21) Entrance to Mela, (30) Exit from Buco, (36) Descent from Yarimala, (42) Road to Gunudel, (43) Entrance to Wayle, (44) Exit from Gunudel Gulacpamba.
Family and Personal Milestones (Toponymy)	(5) Mingo's House, (7) Entrance of José María Vacacela, (8) Entrance of Savulón, (9) Entrance of Lauro Saca, (10) Entrance of Taita Pacho Vacacela, (11) Entrance of Taita Joaquín, (12) Entrance of Chiva, (13) Entrand of Taita Segundo, (22) Entrance to Plains of Abraham Minga, (24) Entrance of Gigo, (26) Entrance of Taita Antonio Montechas, (32) Avarito's Road, (33) Entrance of Pedro and Luisa.
Hydrography and Irrigation (Infrastructure)	(6) Inlet, (16) Stream, (23) Taski irrigation canal, (25) Takshana irrigation canal, (28) La Toma irrigation canal, (35) Toma Road.
Physical and Landscape Milestones	(14) Two posts, (19) Chinuwichay, (27) Gualanes, (29) Chirillo, (34) Tigra Pampa, (37) Casiro Hill, (38) Tignapamba, (39) Jurshapa Road, (40) Jurshapa Cross, (41) Road to Huerto Escolar.
Specific Typologies	(20) Footpath, (31) narrow Chakiñán.

Table 1. Identification of the names of the Chakiñanes of the community of Las Lagunas. Source: Prepared by the Authors.

or extraneous nomenclatures that disarticulate the sense of belonging, the *Chakiñanes* network preserves a transgenerational social cartography that guides the autonomous territorial management of the community (Figures 5 and 6).

SOCIO-SPATIAL DYNAMICS AND TRANSFORMATIONS OF THE COMMUNITY HABITAT (MESO SCALE)

The coding of the interviews and the statistical analysis reveal a structural contradiction between the symbolic persistence of the *chakiñánes* and their progressive material degradation in Las Lagunas. Historically, this footpath network operated as an infrastructure of physical connectivity and identity cohesion (Rodríguez Valbuena, 2011). However, the intergenerational testimonies (Table 1) mark a rupture in the 1960s: the opening of motorized roads altered the territorial metabolism, displacing the central pedestrian line and fragmenting the social fabric. This phenomenon aligns with Lozano Guamán, Jaramillo-Benavides, & Lozano-Guamán (2025) in that conventional planning tends to erode community autonomy and toponymy by dismantling self-managed collective spaces (Cerasi & Quaroni, 1990).

Name	Age	Sector	Key Contribution
Rosa Angelita Guamán	84	Lirios	Historical importance of the Chakiñán as the only connection and warning about forgetting their original names.
Rosa Delia Quizhpe	64	Rarik	Vindication of ancestral identity (Chukidel Ayllullacta) and the link between education, values, and language.
Rosa Vicenta Guamán	57	Rarik	Management perspective from the town hall, emphasizing community autonomy and the risk of losing public space.

Table 2. Synthesis of interview responses. Source: Prepared by the Authors.

Question	Variable/Option	Percentage (%)	Numerical results for the 40 respondents (100%)
1. Sector where the respondent community member lives	Rarik	32.50%	The majority sector of origin (13 out of 40 community members).
	Wabo Loma	17.50%	Representative zone linked with Waile (7 out of 40 community members).
	Waile	17.50%	Representative zone linked with Wabo Loma (7 out of 40 community members).
	Yarimala	15.00%	Regular intermediate participation (6 out of 40 community members).
	Takshana	12.50%	Low participation in the diagnosis (5 out of 40 community members).
	Lirios	5.00%	Fewer census records (2 out of 40 community members).
	Total of the Question	100.00%	Exact closure on the sample of 40 community members surveyed.
2. The use that they give to Chakiñanes at present	Transfer of animals	43.80%	43.8% of all uses mentioned (28 mentions).
	Access to crops	23.40%	23.4% of all uses mentioned (15 mentions).
	On the way to another community	17.20%	17.2% of all uses mentioned (11 mentions).
	Access to housing	15.60%	15.6% of all uses mentioned (10 mentions).
	Total of the Questions	100.00%	Based on the 64 accumulated mentions.
3. The frequency with which a chaquiñán is used	Rarely	45.00%	Predominantly sporadic in frequency (18 responses).
	3 to 4 times a week	27.50%	Regular intermediate use for work (11 replies).
	Once, or several times a day	17.50%	Intensive daily road users (7 replies).
	Once a week	10.00%	One-time, recurring, low-frequency use (4 replies).
	Total of the Questions	100.00%	Sample of 40 community members surveyed.
4. Aspects that affect the Chakiñanes at present	Lack of upkeep	41.30%	41.3% of the total mentions (26 mentions).
	Authorities have a lack of interest in the upkeep	34.90%	34.9% of the total mentions (22 mentions).
	Lack of control over misuse by the population	14.30%	14.3% of the total mentions (9 mentions).
	Insecurity when walking	9.50%	9.5% of the total mentions (6 mentions).
	Total of the Questions	100.00%	Based on the 63 responses.

Question	Variable/Option	Percentage (%)	Numerical results for the 40 respondents (100%)
5. Level of collaboration in the case of reconstruction of a chaquiñán	Partial	47.50%	Predisposition conditioned to time or resources (19 replies).
	Total	42.50%	Direct and absolute civic commitment to the work (17 replies).
	Little	7.50%	Severe limitations or low interest in support (3 replies).
	None	2.50%	Refusal or absolute impossibility to join mingas (1 reply).
	Total	100.00%	Sample of 40 community members surveyed.
6. Use that could be given to the Chakiñanes at present (Projection)	Better connection between the community and the...	33.30%	33.3% of the ideas for improvement (24 mentions).
	Create a tourist route throughout the...	29.20%	29.2% of the ideas for improvement (21 mentions).
	Rest spaces	22.20%	22.2% of the ideas for improvement (16 mentions).
	Cycle path	13.90%	13.9% of the ideas for improvement (10 mentions).
	Just keep them passable	1.40%	1.4% of the ideas for improvement (1 mention).
	Total of the Questions	100.00%	Based on the 72 projection-based responses.

Table 3. Matrix of survey questions and answers. Source: Prepared by the Authors.

The quantitative data (Table 3) empirically support this morphological transition. Although there is a consensus on their cultural value, 45.00% of respondents use them "rarely", linking their current use almost exclusively to the shepherding of animals (43.80%) and access to crops (23.40%). Thus, the *Chakiñán* is relegated to a secondary peri-urban role, which alters what Van der Voordt & De Jong (2002) define as the functional balance of the habitat. This physical breakdown has led to conflicts over altered land boundaries, which require the activation of indigenous justice to restore territorial organization (Rodríguez Valbuena, 2011). Although 41.30% attribute the deterioration to a lack of institutional upkeep, the *Ayllu*'s social capital remains latent: 42.50% express a strong willingness to participate in reconstruction *mingas* (community work). In light of these metrics, road rehabilitation aligns with Borja & Muxí (2003) by optimizing autonomous collective space and supporting a sustainable habitat model grounded in low-emission mobility and community landscape management.

MICRO SCALE

The analysis, through photographic registration and photogrammetric editing, of the accesses from the main road network to the internal footpath network shows the physical discontinuities in the ancestral mobility system. The section-level restitutions show that the disturbances are concentrated in the transition zones of the motorized road network. Land privatization and irregularities in perimeter enclosures have reduced the historical useful widths of the paths, transforming traditional meeting nodes into residual corridors. This fragmentation jeopardizes community access to water and productive and spiritually significant infrastructure.

By superimposing physical (accessibility, conservation, and connectivity) and symbolic (cultural landscape landmarks) variables, a strategic pilot section was selected (Figures 7, 8, and 9). The selection criteria considered its multidimensional representativeness: the path connects the Lirios and Yarimala sectors and integrates three nodes of the Andean hydraulic-ceremonial infrastructure: El Chorro (spring), Ushno (ceremonial center), and the Taski Waterfall (ecological-ritual system).

The diagnosis of these components reveals a degree of environmental vulnerability. While El Chorro exhibits stable water quality, though threatened by surface runoff, the Taski Waterfall is severely affected by anthropogenic contamination and reduced flow rate. The functional analysis of the maps, following Van der Voordt & De Jong (2002), showed that this section serves as a transversal connector between topographic ridges and scattered water plains. Thus, the selected *Chakiñán* encapsulates the microbasin's geomorphological complexity and actively connects the territory.

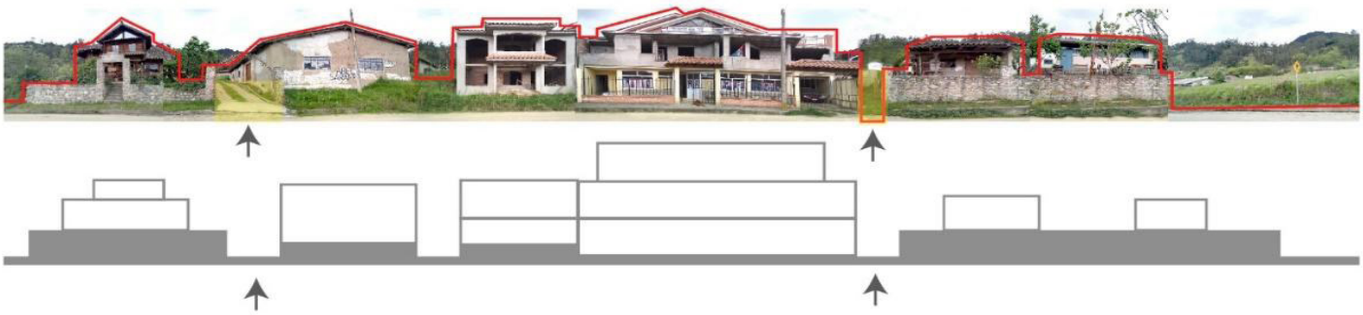


Figure 7. Section 1/9. Photogrammetric analysis from the main road of Las Lagunas. Source: Prepared by the Authors.

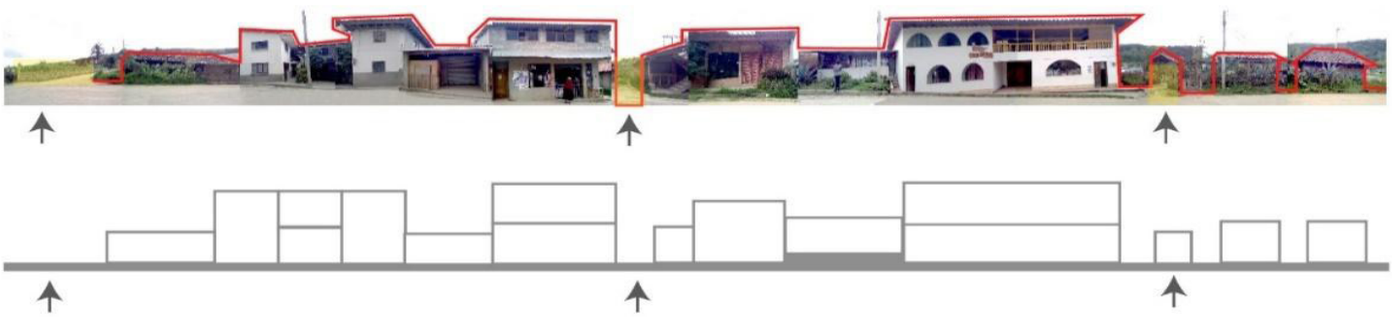


Figure 8. Section 2/9. Photogrammetric analysis from the main road of Las Lagunas. Source: Prepared by the Authors.

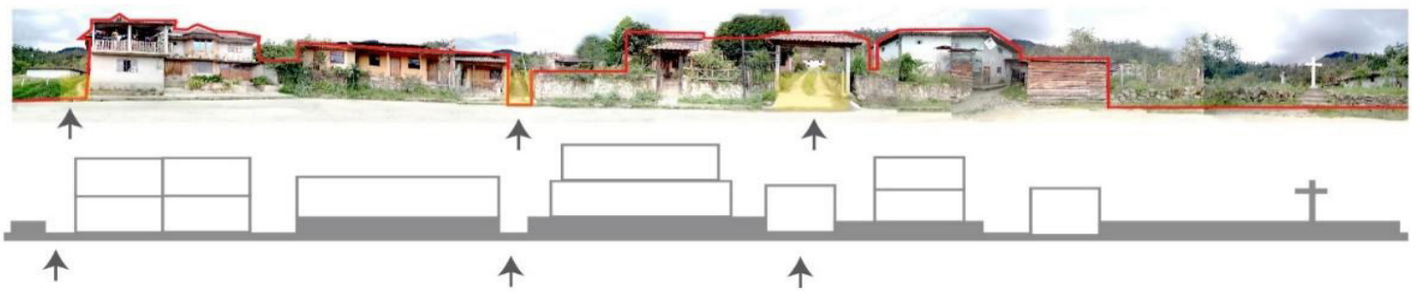


Figure 9. Section 3/9. Photogrammetric analysis of 3 sections. Source: Prepared by the Authors.

INTERVENTION PROPOSAL: SUSTAINABLE HABITAT REVITALIZATION STRATEGIES

Guidelines for Sustainable Design and Multiscale Articulation

The conversion of the empirical and analytical findings to the proposal's approach is instrumentalized through a low-emission infrastructure territorial revitalization model. The pilot project is conceived as a connective system adapted to the dynamics of the living territory of the Las Lagunas community. Based on the problems identified, such as the loss of useful width, ecological degradation, and pedestrian fragmentation, the intervention is guided by four operational dimensions focused on sustainable habitat:

- Morphological Recovery and Spatial Justice: Restoration of original road sections (1.50 m to 3.00 m) to mitigate the physical obstacles detected by photogrammetry and restore the continuity of the communal autonomous pedestrian flow (Lozano Guamán et al., 2025).
- Preventive Conservation of Water Ecosystems: Implementation of non-invasive passive construction techniques in springs and pre-Hispanic structures to prevent material degradation and surface water pollution (Qhapaq Ñan-Ecuador, 2019).

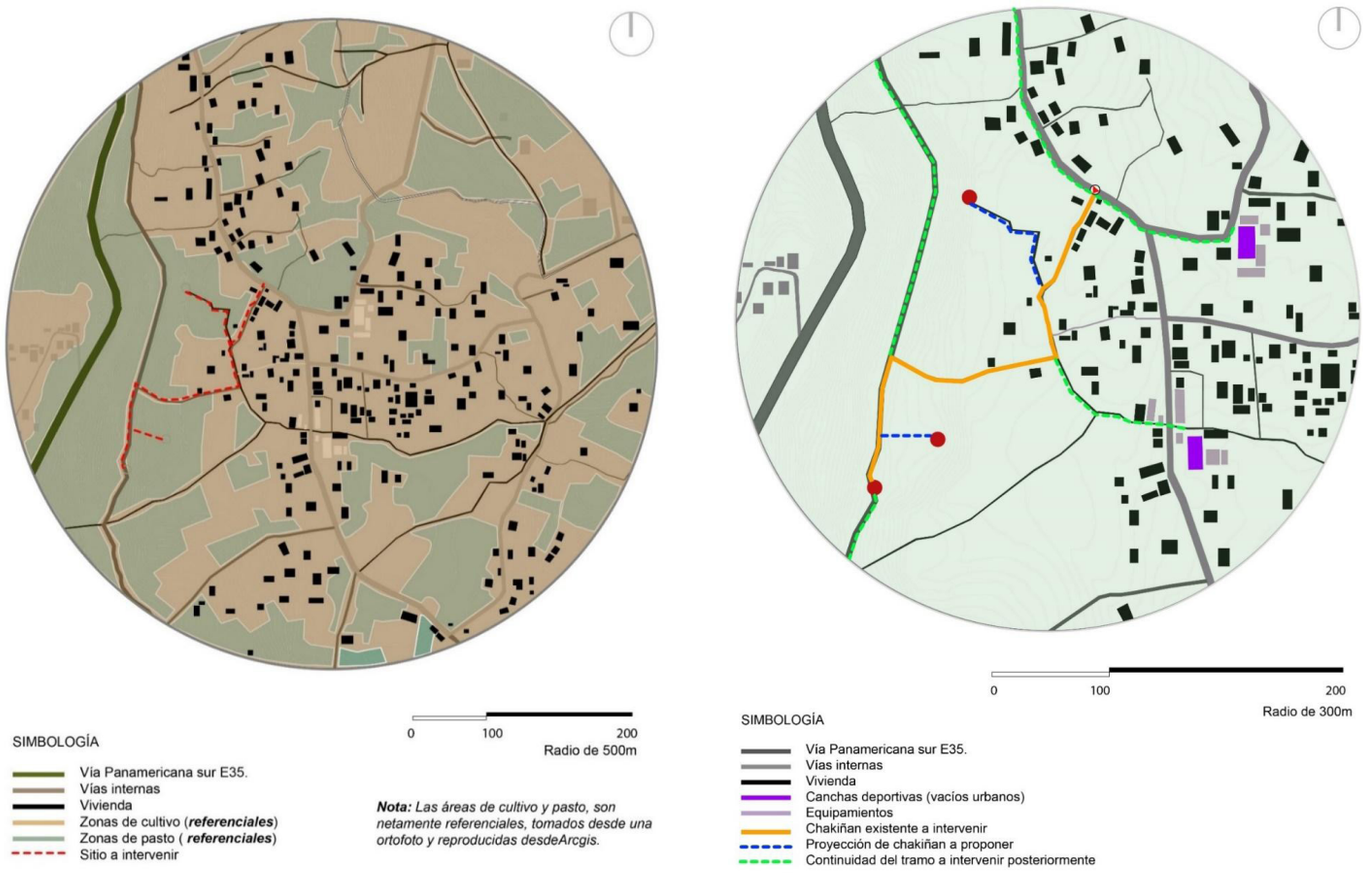


Figure 10. Land Use Maps - connection of community facilities and sacred sites of the chosen section in 500 m and 300 m radii. Source: Prepared by the Authors using Google Maps.

- Inclusion and Topographic Mitigation: Slope stabilization and design of steps, pedestrian ramps, and permeable paths adapted to the Andean relief, which optimizes the safety of mobility on a human scale without altering the natural runoff.
- Landscape Revitalization and Identity Signage: Incorporation of native vegetation to consolidate biological corridors and installation of visual communication devices based on vernacular toponymy (Montaño Huerta, 2017).

Zoning by sections of morpho-landscape intervention

According to the micro diagnosis, the route was subdivided into homogeneous sections to handle boundary and accessibility conflicts.

Road transition section and accesses: They consolidate the entrance from motorized roads through stone-wall edge stabilization and include open irrigation canals to mitigate erosion from rain runoff and watershed runoff (Figure 12).

Immediate connecting sections: Located in areas of high agricultural pressure. They redefine the limits of the *Chakiñan* through living fences featuring endemic flora, ensuring pedestrian flow and the passage of small livestock, which account for 43.80% of the identified productive uses (Figure 10 and Figure 11).

Based on the diagnostic results, a pilot section was selected for its symbolic value and spiritual connectivity. The selection criterion prioritized the path that links the Lirios sector with Yarimala, integrating three nodes of connectivity of the water-spiritual infrastructure and their value within the heritage landscape, such as: *The Chorro* (spring), *The Ushno* (ceremonial center), and the *Taski Waterfall* (Figure 13, Figure 14, Figure 15, Figure16, and Figure 17).

CULTURAL LANDSCAPE ARCHITECTURE: INTERVENTIONS IN SACRED SITES AND SUPPORTING INFRASTRUCTURE (TAMBOS)

The architectural intervention formalizes the articulation between local knowledge, heritage preservation, and sustainable planning through the singularized treatment of three sacred sites (Figure 18), as described in Table 4.

- Revitalization of the Chorro (spring). Technical confinement of the spring through a local stone-

Revista Hábitat Sustentable Vol. 16, N°. 1. ISSN 0719 - 0700 / Págs. 70 - 95
https://doi.org/10.22320/07190700.2026.16.01.05

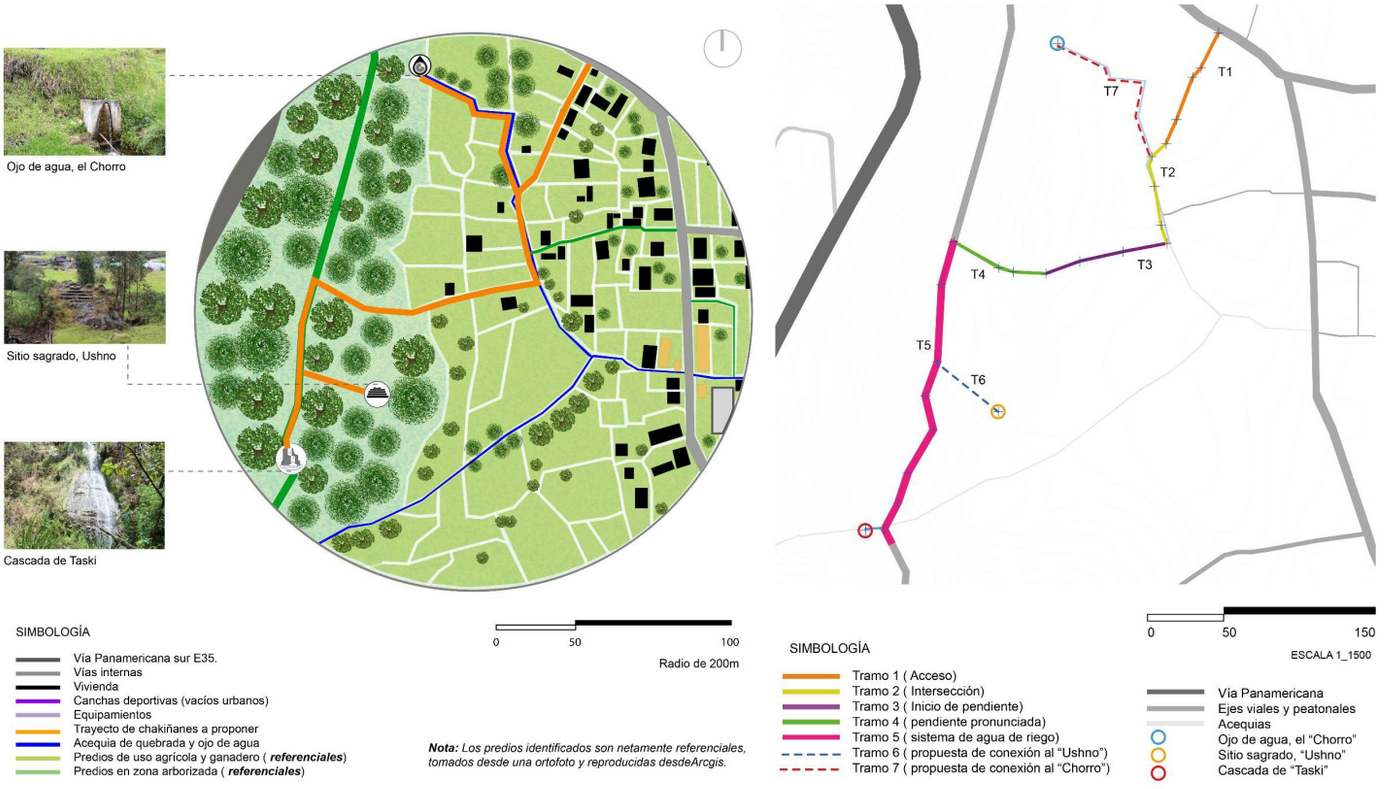


Figure 11. Map within a 200 m radius of the sacred sites to be intervened. Division by sections. Source: Ortofoto, ArcGIS.



Figure 12. Route of the Chakiñán to be intervened. Source: Prepared by the Authors.

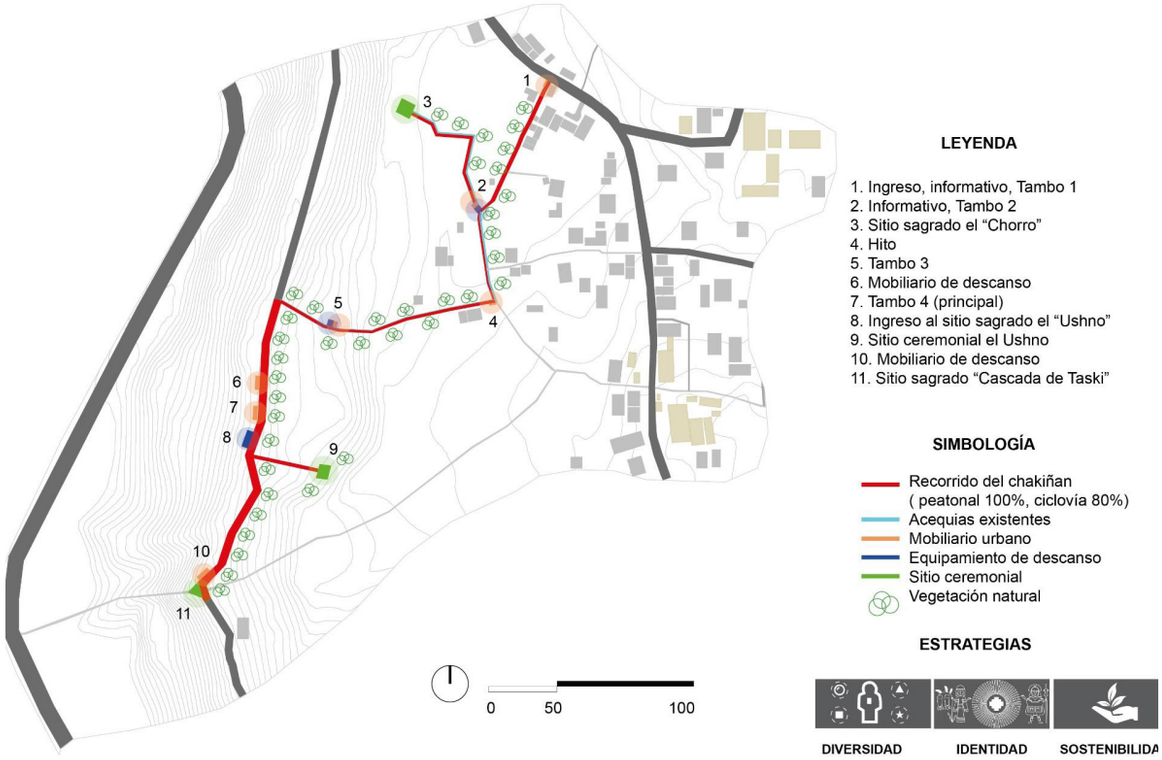


Figure 13. Map of intervention proposal by sections according to their physical characteristics and strategies. Source: Prepared by the Authors.

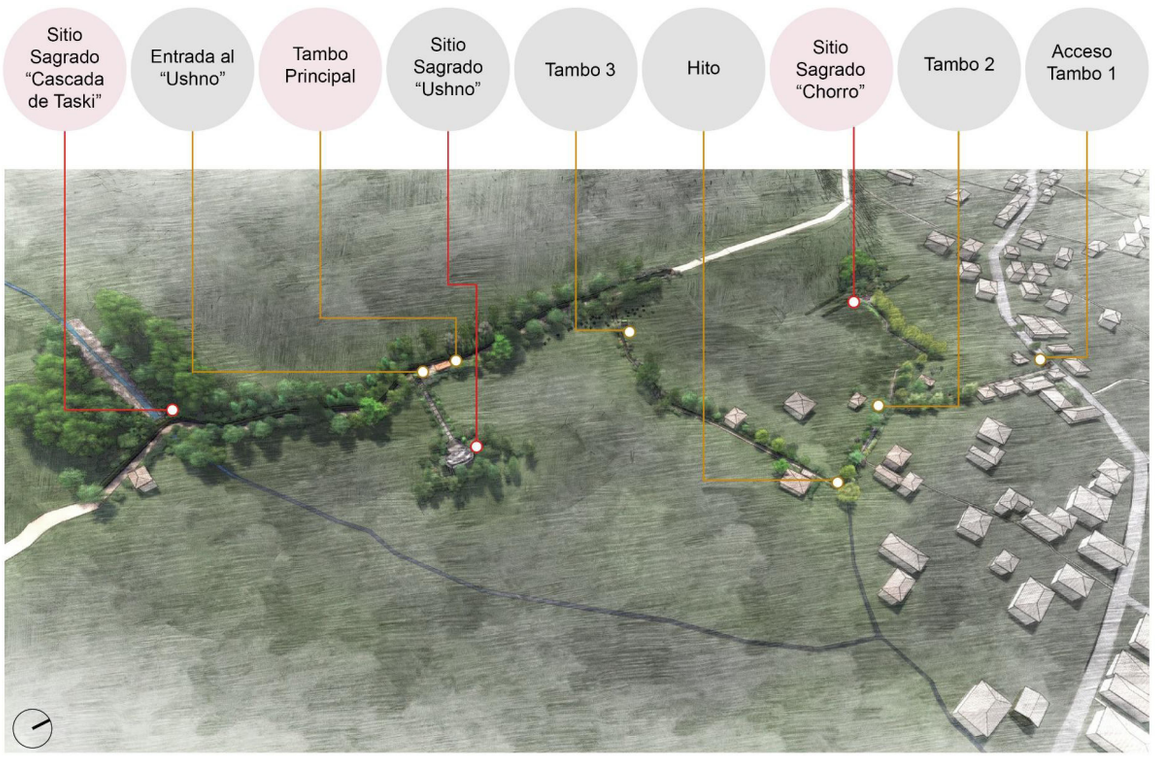


Figure 14. Aerial visualization of the intervention by sections. Source: Prepared by the Authors.

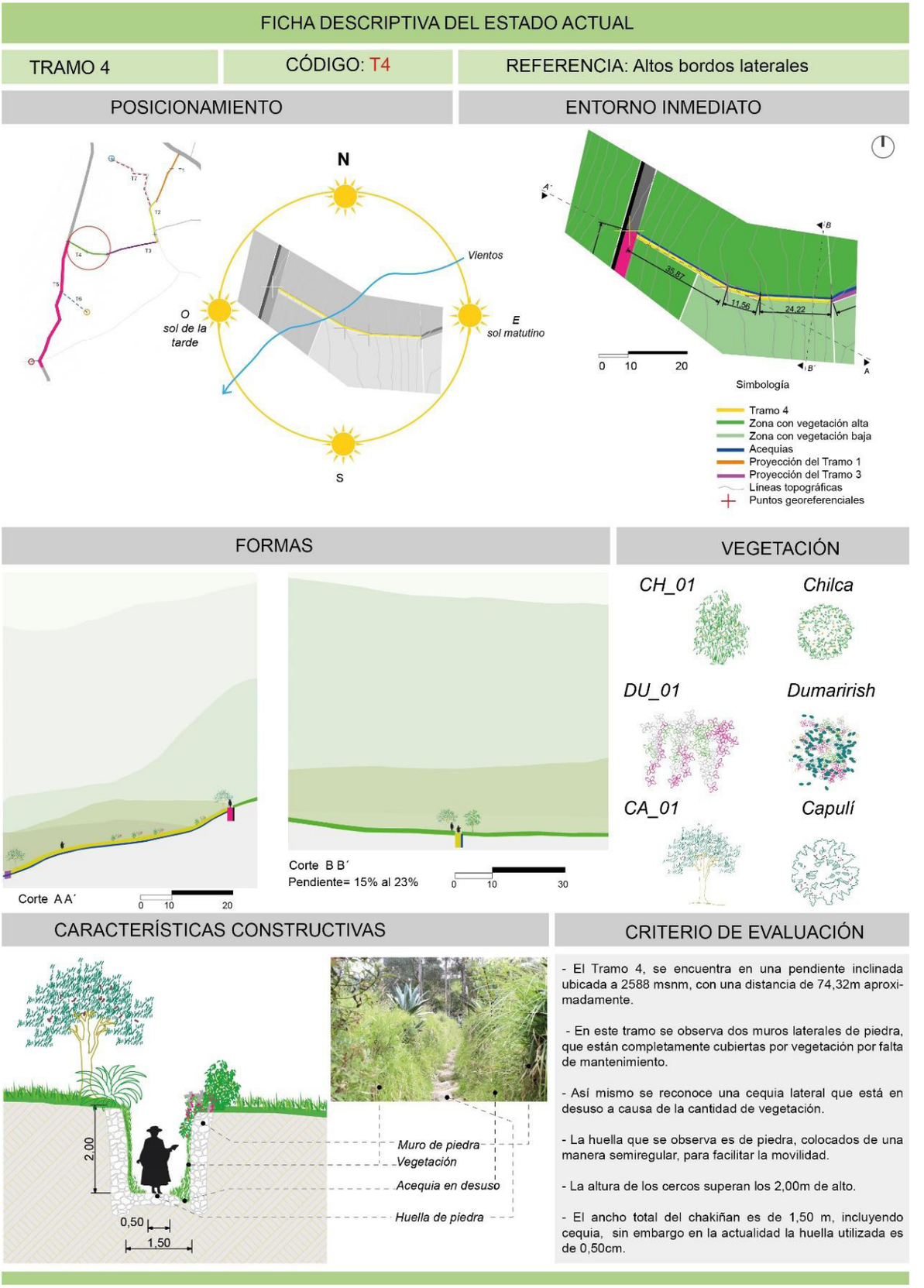


Figure 15. Analysis sheets of the Current State of Section 4. Source: Prepared by the Authors.

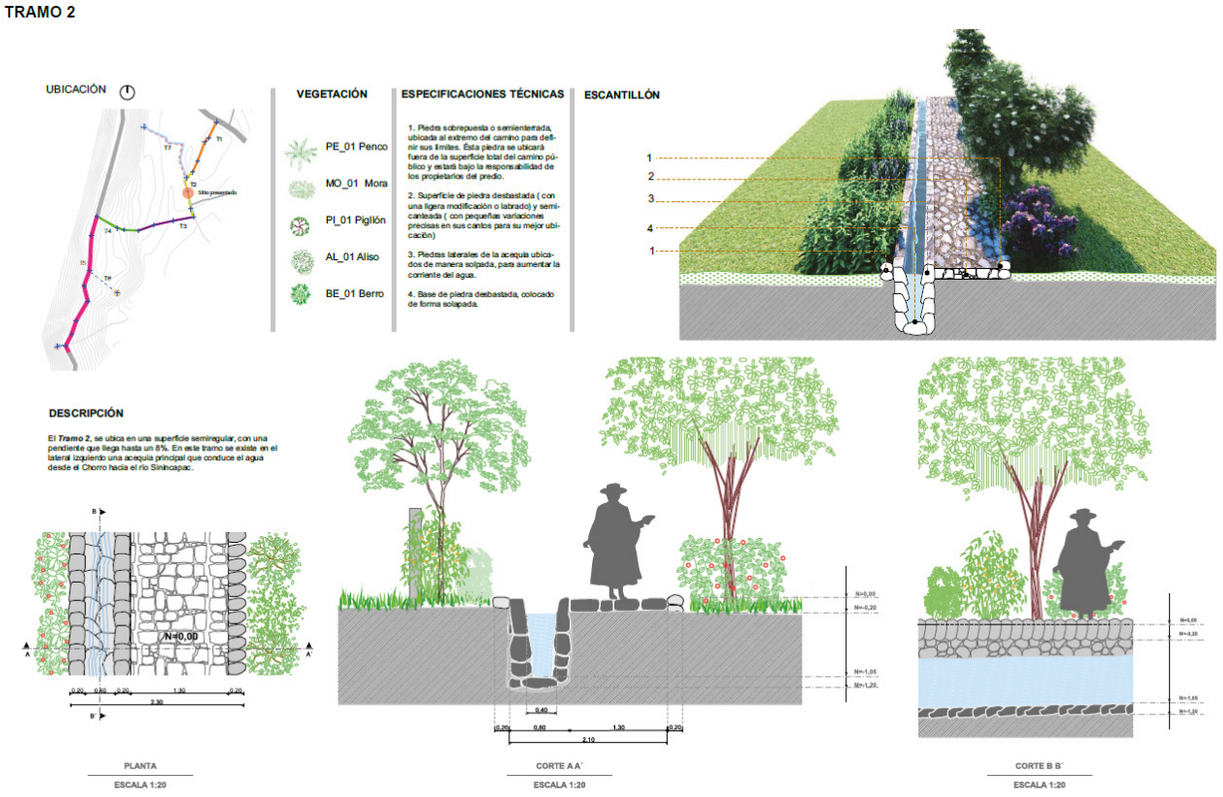


Figure 16. Proposal for an intervention in the Chakiñán Section 2. Source: Prepared by the Authors.

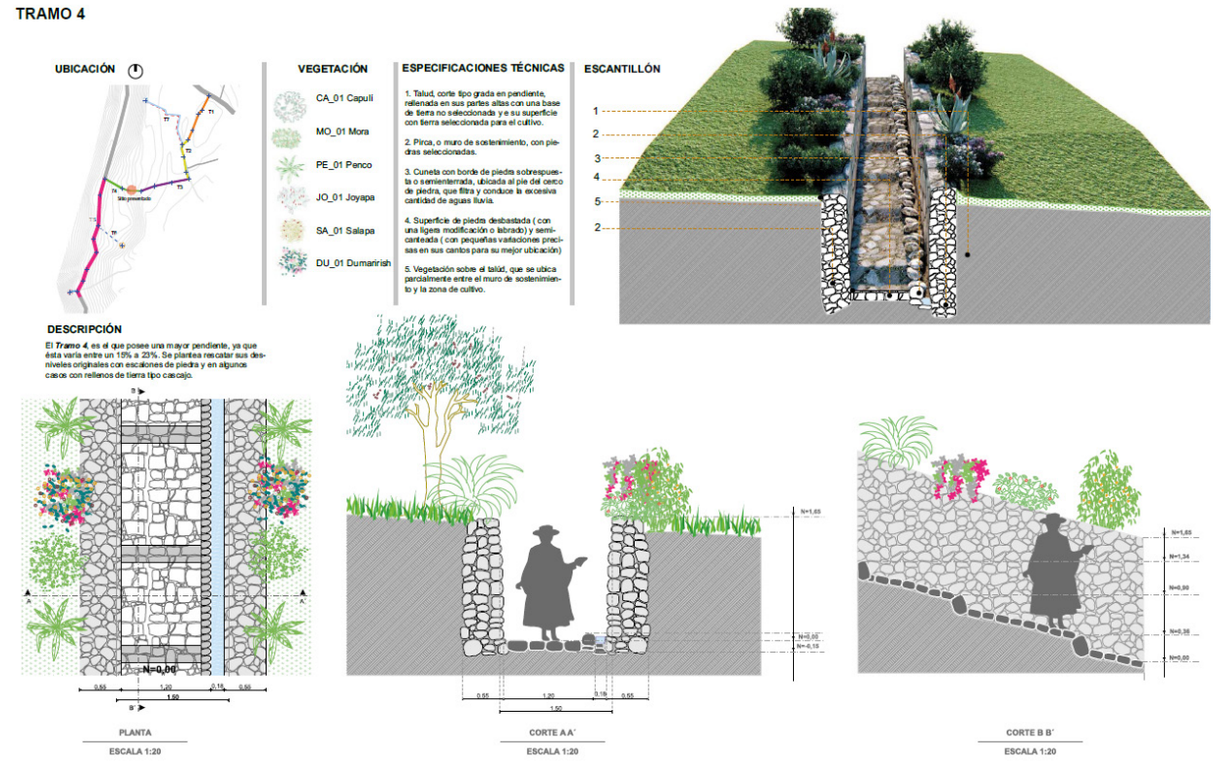


Figure 17. Proposal for intervention in the Chakiñán Section 4. Source: Prepared by the Authors.

Revista Hábitat Sustentable Vol. 16, N°. 1. ISSN 0719 - 0700 / Págs. 70 - 95
https://doi.org/10.22320/07190700.2026.16.01.05

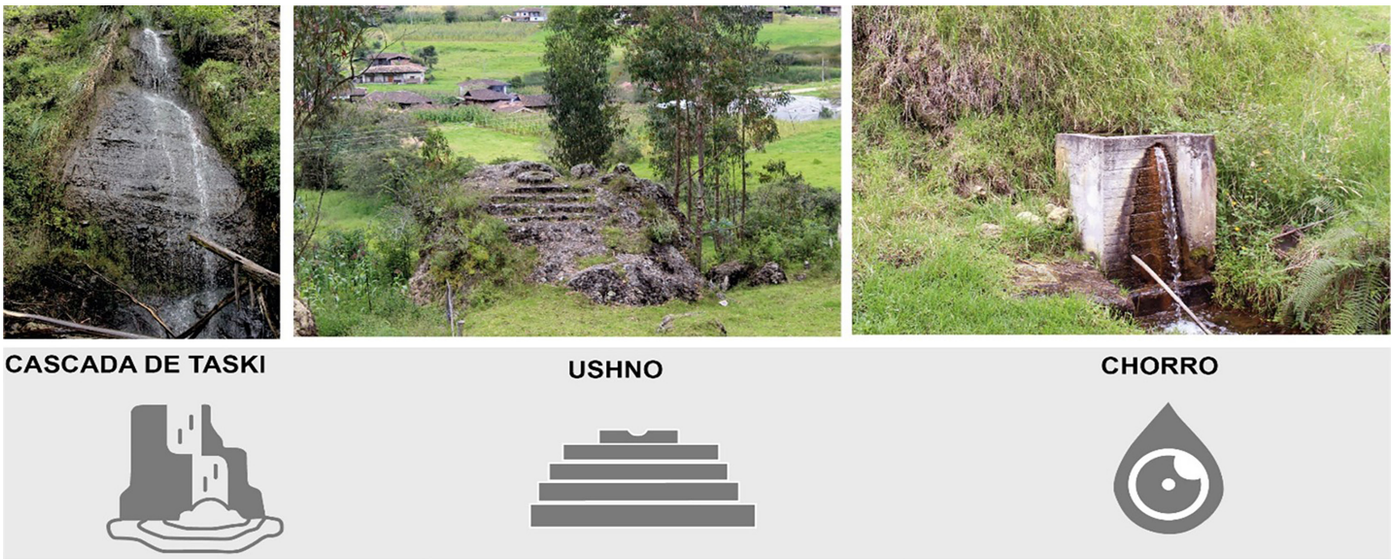


Figure 18. Photograph of the sacred sites to be intervened. Source: Prepared by the Authors.

TASKI WATERFALL	USHNO	CHORRO
Description: Sacred Andean symbol for healing and rituals; it represents the origin of life and the blood of the earth.	Description: Pyramidal structure for ceremonies and astronomical milestones, with water or *chicha* as the protagonists.	Description: An underground spring that historically served as a sacred place for bathing princesses or *ñustas*.
Status: Presents critical contamination and a progressive decrease in its natural flow.	Status: Strategically located near the Inca road network due to the abundance of water sources in the environment.	Status: Good-quality water via natural filtration; requires channeling to prevent overflows and exposure to external agents

Table 4. Characteristics of the sacred sites: El Ushno, El Chorro, and Taski waterfall. Source: Prepared by the Authors.

collection vessel to avoid external pollutants, adding a ceremonial space and, in turn, restoring its role as a community laundry and social-cohesion node under water-efficiency criteria (Figure 19 and Figure 20).

- Consolidation of the Ushno: Removal of invasive vegetation and perimeter delimitation of the archaeoastronomical structure with permeable stone pavements, which highlight the geometry of the platform for its preventive conservation and ceremonial use (Figure 21 and Figure 22).
- Healing of the Taski Waterfall: Implementation of artificial subsurface flow wetlands (phytoremediation) prior to discharge to mitigate critical pollution, complemented with low-impact viewpoints integrated into the topography (Figures 23 and 24).

To support the route and in view of the projected community and tourist use expressed by 29.20% of the respondents, the ancestral typology of the Tambo (resting place) is incorporated. These structures function as shelters, territorial control points, and landscape interpretation pavilions. Its materiality is based on low-emission architecture and circular metabolism, through:

- Load-bearing structure: Local wooden frames and *bahareque* systems (mud, straw, and cane) (Calderón, 1985), which reduce the incorporated carbon footprint and revalue the vernacular technologies of Saraguro (Cevallos Salas, 2003) (Figure 25).
- Passive strategies: Green roofs with native vegetation to optimize thermal insulation and integrate the volume into the landscape environment (Figure 26).
- Ecological sanitation: Composting dry toilet modules in the main pavilion. This solution addresses the lack of sewerage in the micro-basin, prevents aquifer contamination, and closes the nutrient cycle by generating organic fertilizer for local crops (Figures 27 and 28).

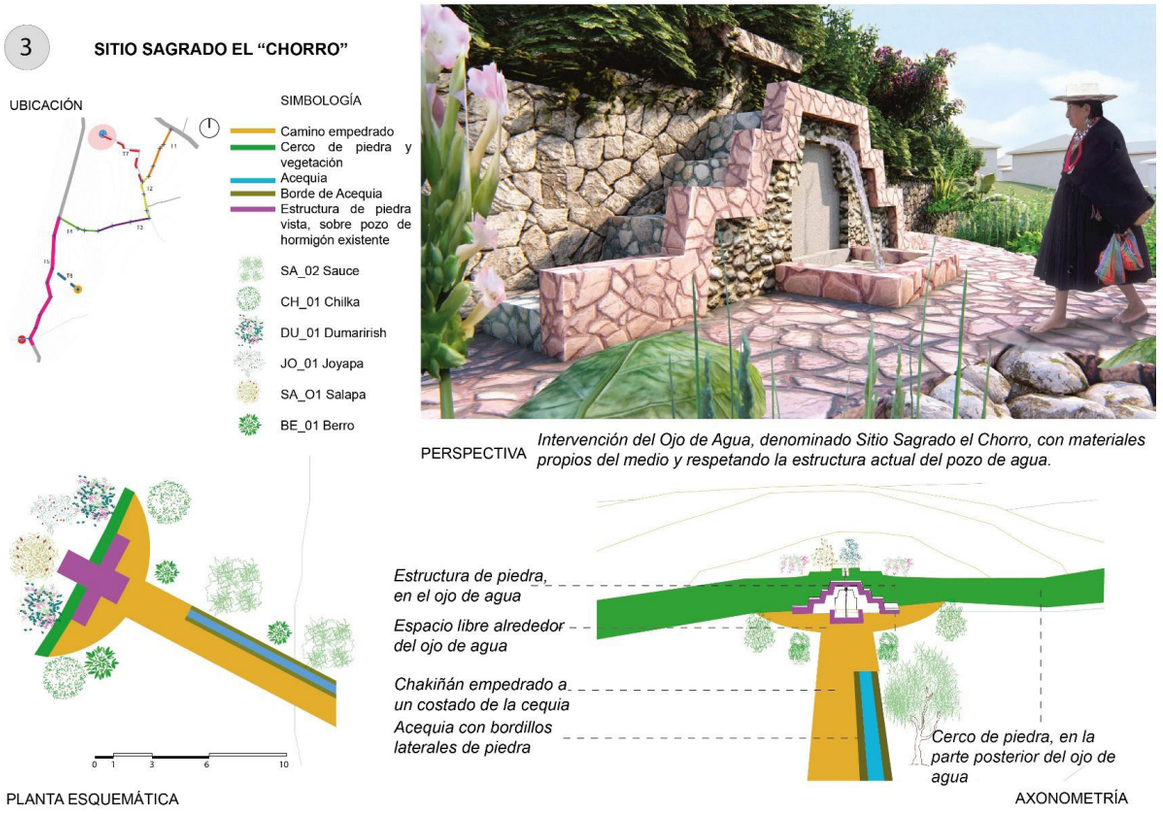


Figure 19. Proposal for the intervention of Section 3. Source: Prepared by the Authors.

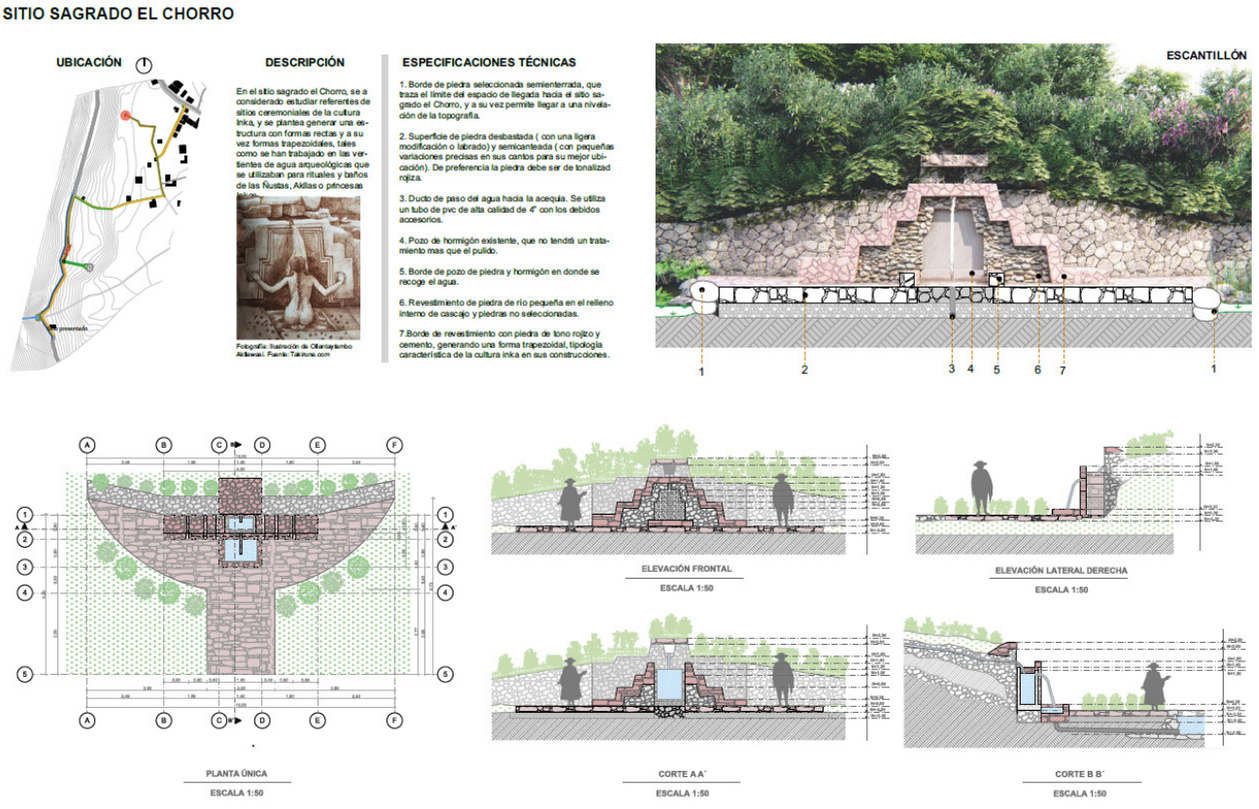


Figure 20. Proposal of intervention in the El Chorro sacred site. Source: Prepared by the Authors.

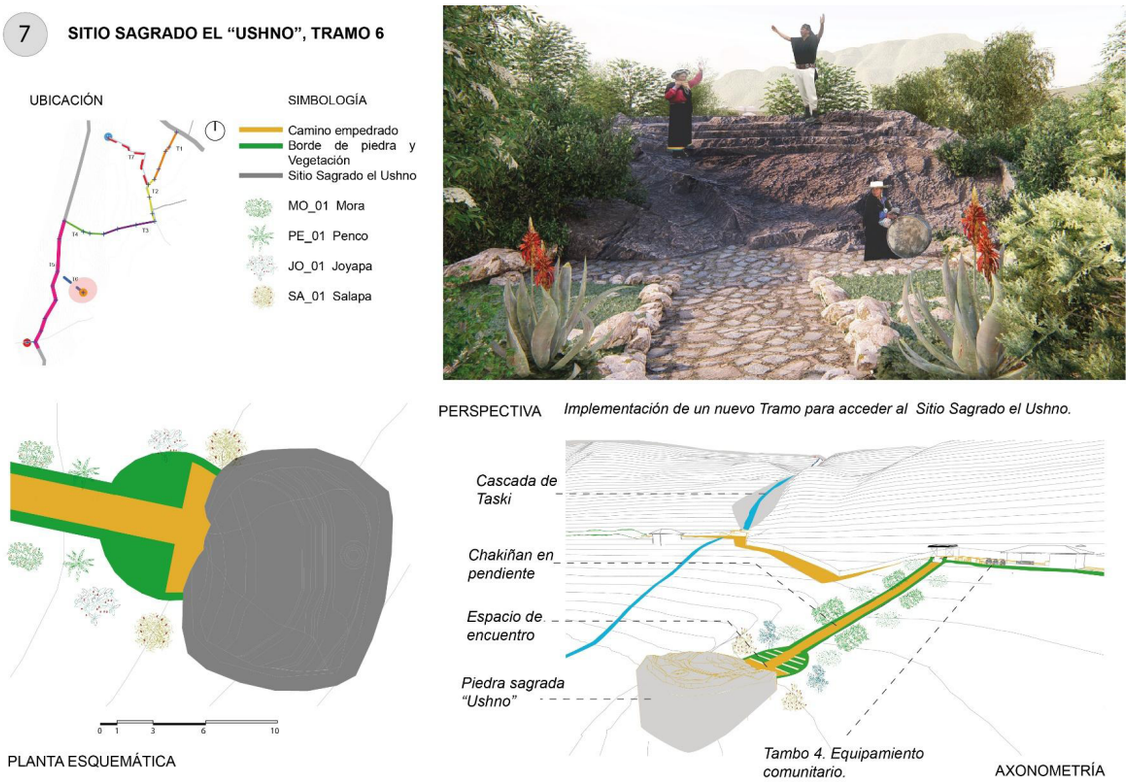


Figure 21. Proposal for Section 7's intervention. Source: Prepared by the Authors.

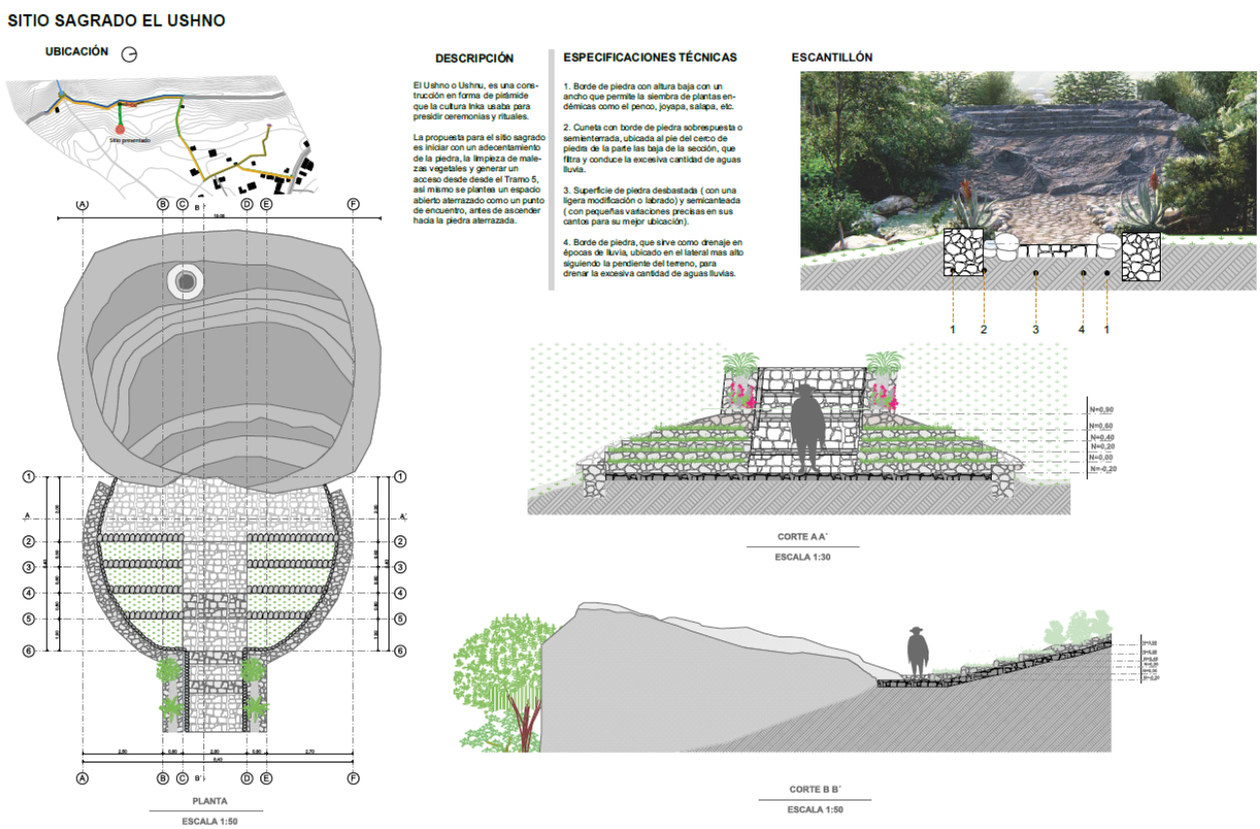


Figure 22. Proposal of intervention in the El Ushno sacred site. Source: Prepared by the Authors.

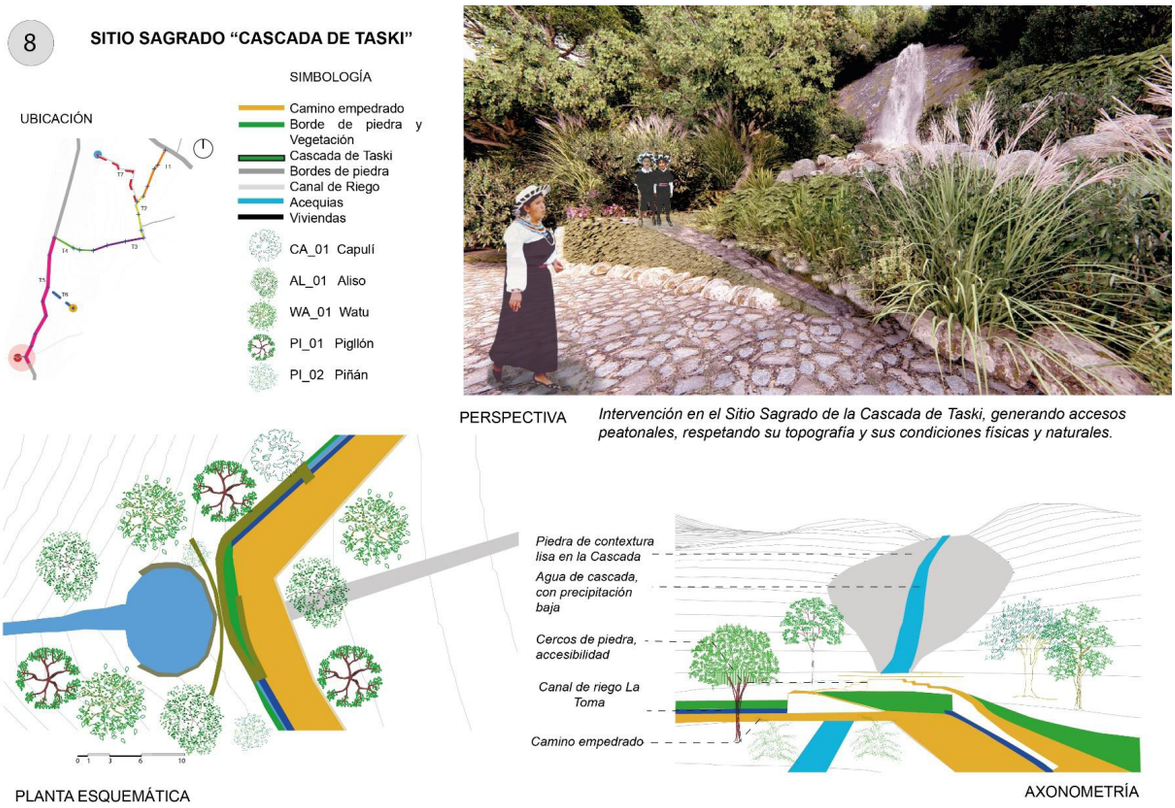


Figure 23. Proposal for Section 8's intervention. Source: Prepared by the Authors.

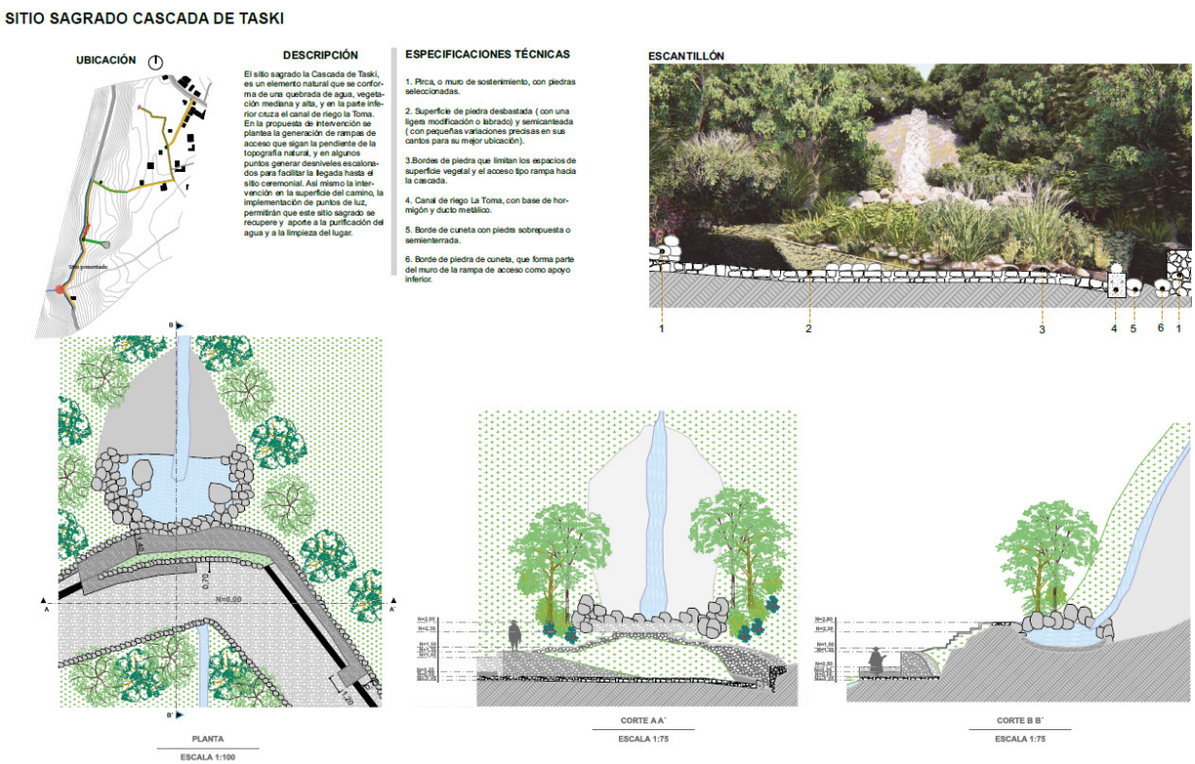


Figure 24. Proposal of intervention in the Taski Waterfall sacred site. Source: Prepared by the Authors.

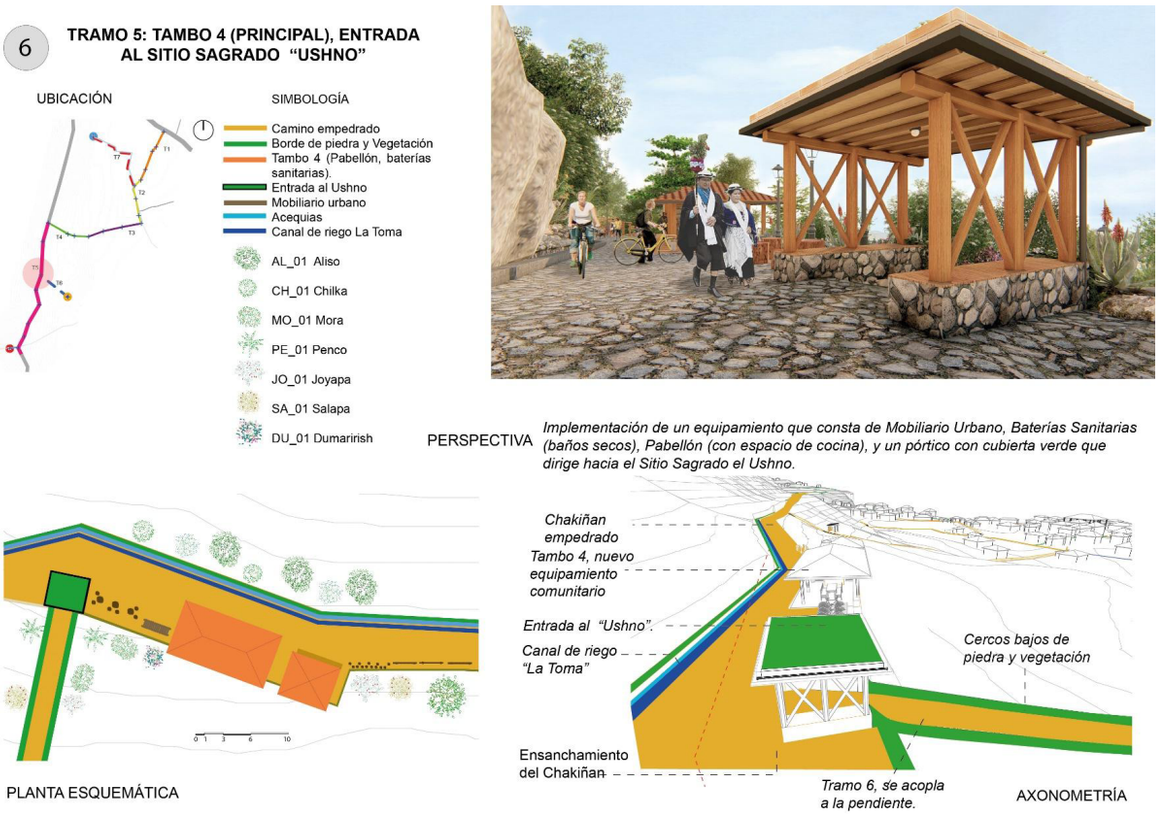


Figure 25. Proposal for the intervention of Section 6. Source: Prepared by the Authors.

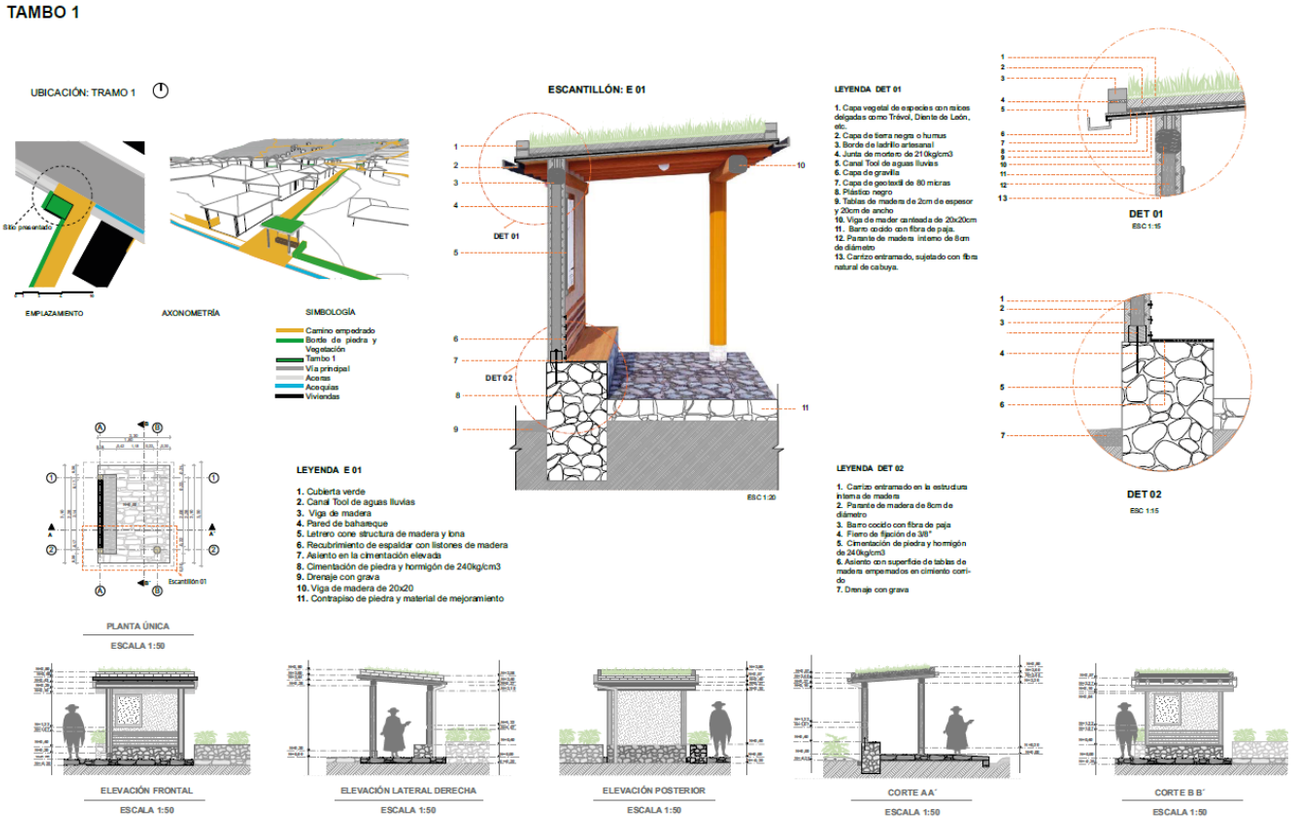


Figure 26. Proposal for Tambo 1: bahareque and green cover. Source: Prepared by the Authors.

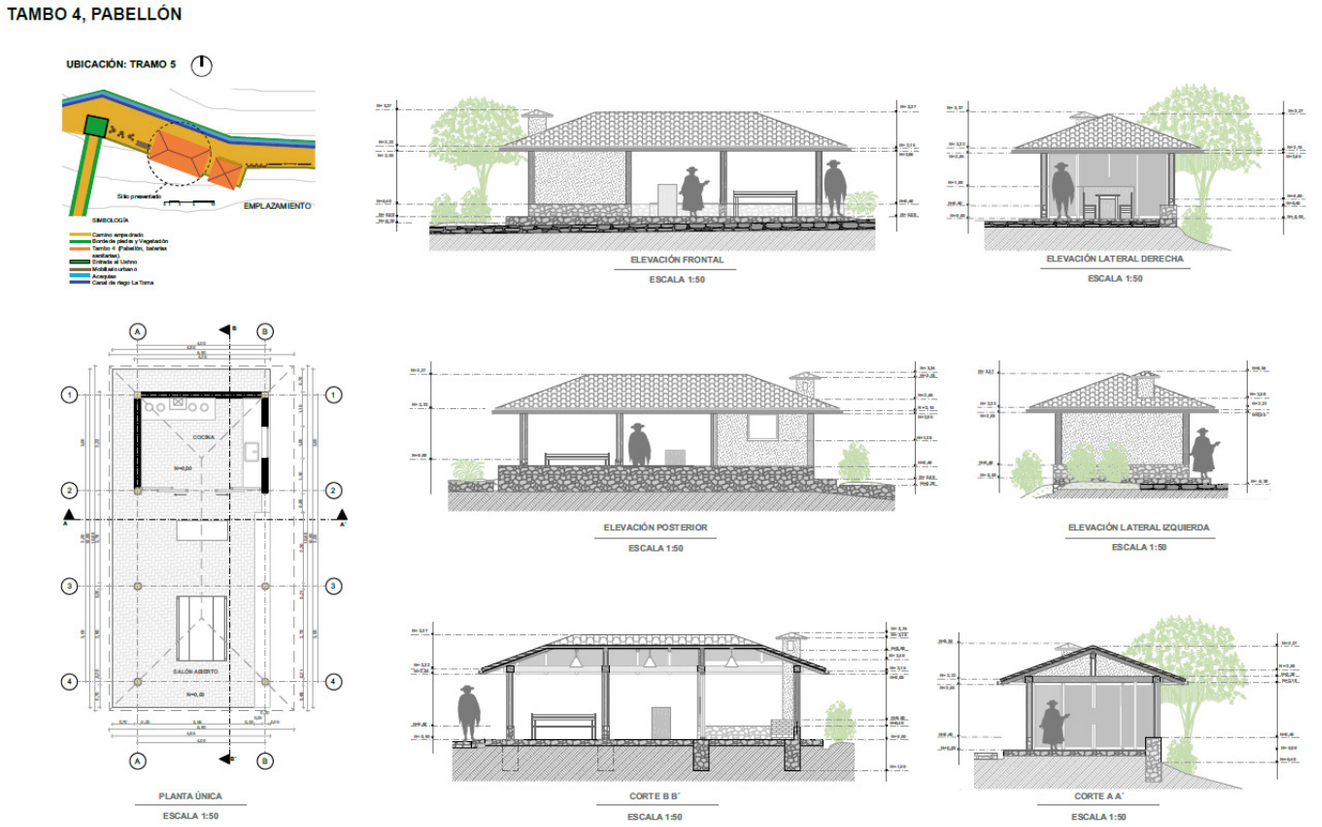


Figure 27. Tambo 4 proposal, main pavilion with the bahareque construction system. Source: Prepared by the Authors.

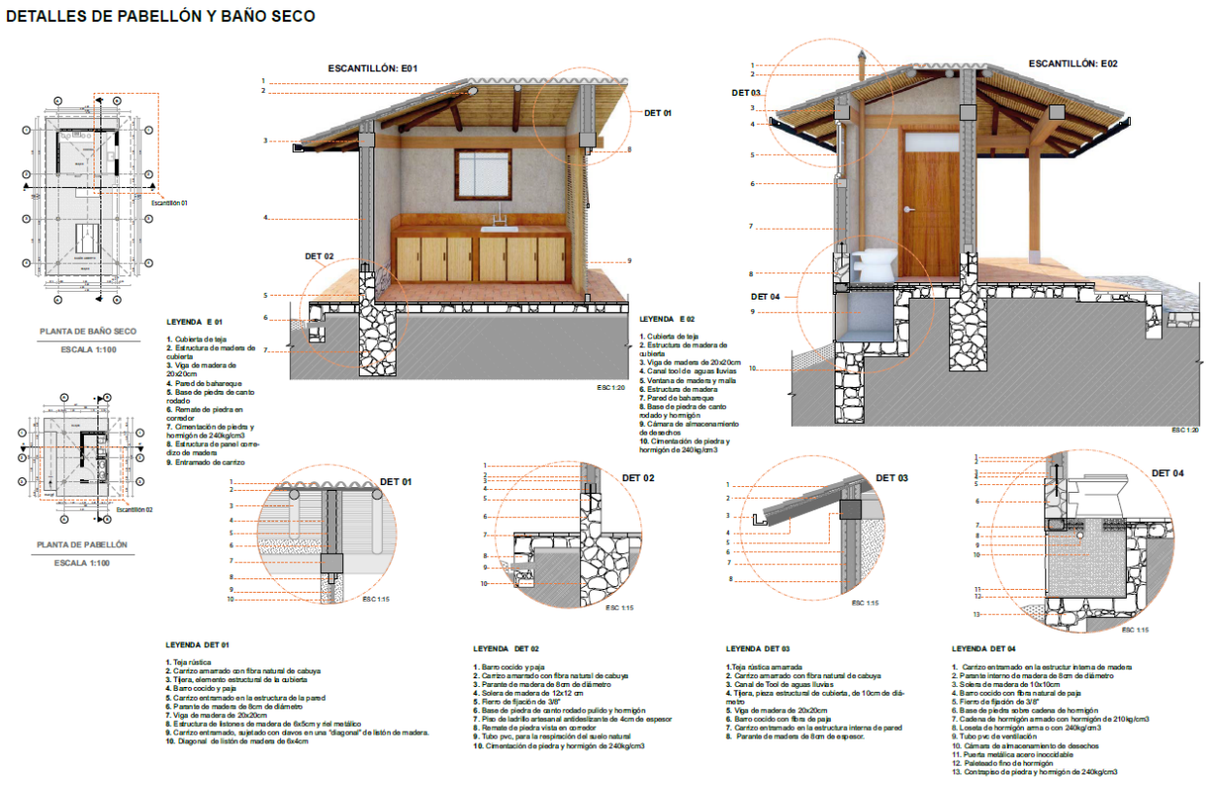


Figure 28. Constructive details of the pavilion and dry toilet. Source: Prepared by the Authors.



A. Tramo 1 del Chakiñán intervenido, con la recuperación del cerco verde lateral.

B. Tramo 7, intervención de espacio peatonal juto a la acequia existente.

C. Intersección del Tramo 1,2 y 7.

D. Intervención del Sitio Sagrado El Chorro.

Figure 29. 3D visualizations. Source: Prepared by the Authors.



E.Tramo 4, intervención en la superficie y la recuperación de los cercos de piedra laterales, acequia y vegetación.

F. Tramo 5. Implementación del Tambo principal, baterías sanitarias, y mobiliario urbano.

G. Implementación de un acceso desde el Tramo 5 hacia el Sitio Sagrado el Ushno.

H. Intersección entre el Tramo 2, Tramo 3 y la continuidad de la acequia que conduce el agua del sitio sagrado el Chorro.

Figure 30. 3D visualizations. Source: Prepared by the Authors.



Figure 31. 3D visualizations. Source: Prepared by the Authors.

DISCUSSION

The contribution of this research to the field of sustainable habitat lies in validating ancestral mobility as a form of green, low-emission infrastructure for climate change mitigation and rural territorial planning. The multiscale and integrated analysis of the *Chakiñanes* network shows that these structures do not operate as isolated linear vestiges, but as dynamic components of an interconnected Andean cultural landscape. This conceptual approach agrees with the multidimensional approaches presented by Novoa Ríos & Hernández García (2026), who argue that the comprehensive rehabilitation of the habitat requires intertwining the technical functionality of the infrastructure with the perceptual and spatial dimensions that communities configure in their daily lives. Faced with contemporary models of peripheral and motorized urban planning that fragment micro-basins, the preservation of permeable pedestrian paths, the collective management of runoff water through ditches, and the use of low environmental impact construction systems — such as the *bahareque* — guarantee ecological coherence and the conservation of territorial heritage in mountain contexts (Guerrero Baca, 2017; Cristancho Barrios, 2024; Gonzalo Sánchez, 2012).

The operational response of the Las Lagunas community to the systematization and cataloging of its road network corroborates the theories of participatory planning aimed at sustainability. The development of self-managed internal regulations demonstrates that community infrastructure has internal governance mechanisms capable of dispensing with centralized state regulatory frameworks for its preventive conservation, provided that the physical space corresponds to the social mapping of the landscape. This dynamic makes visible the concept of emerging heritages proposed by Alegría & Valencia (2024), understood as manifestations and subaltern memories that derive their validity from the daily practices of communities and challenge the monumental and institutional notions of conservation (Figure 29, Figure 30, and Figure 31).

This phenomenon can be seen in the immediate physical appropriation by the local population, as reflected in the initiation of autonomous maintenance tasks and the formulation of collective regulations to protect their trails. As in the community management experiences analyzed by Arango-Marín et al. (2025), these assembly practices configure territorial care networks that mitigate the deficiencies of conventional urbanism, which prioritize the reproduction of community life and the autonomous preservation of sustainable habitat. In this way, the structured territorial design from the operational dimensions of the Andean cosmovision works as a catalyst for heritage awareness (Corrales Blanco, Pineda Iriarte & Salazar Rodríguez, 2021). Likewise, the observed effect of irradiation on neighboring communities suggests that the recovery of the *Chakiñán* activates the Saraguro people's socio-spatial memory. The viability of the proposed model lies in its ability to reactivate the *minga*, consolidating it not only as a collaborative work system, but also as a tool for cultural resistance, the management of the living territory, and the safeguarding of the sustainable landscape (Pacheco Arévalo, 2007; Quizhpe Guamán, 2013).

CONCLUSIONS

The research shows that the *Chakiñanes* system constitutes an active mobility model with low emissions and high social efficiency. The results confirm that the territorial fragmentation caused by motorized urban expansion can be effectively mitigated by applying ancestral construction techniques that combine water resource management with pedestrian traffic. The community work of the *minga* is validated as a technical, operational, and sustainable governance mechanism, capable of ensuring the permanence of the cultural landscape in the face of the pressures of conventional development.

The cartographic and statistical analysis indicates that, despite the morphological transformations initiated in the 1960s by the opening of vehicular roads, 95.00% of the population of Las Lagunas identifies these trails as essential components of their identity and territorial structure. This persistence takes on scientific significance when evaluated at the basin scale. The geometric lines are not isolated, but rather are ecological ribs that connect the microbasin, strategically linking the water recharge points, the ceremonial centers, and the residential areas. This geomorphological logic responds to respecting the topography and to the union of water cycles as an integrating system of space and collective life.

From the perspective of territorial heritage, the *Chakiñan* transcends its original function of physical connectivity to consolidate itself as an ecological corridor and repository of Andean biodiversity, hosting endemic species (joyapa, penco, aliso) and medicinal plants, linking landmarks of high hydric-spiritual significance such as El Chorro, El Ushno, and the Taski Waterfall. Therefore, the proposed technical intervention is not defined as a conventional modernization of the infrastructure, but as a strategy for the reactivation of the social-spatial memory, demonstrating that architectural technique and landscape design can serve as material support for the continuity of the local community and its symbolic logics.

Finally, this study establishes a binding dialogue between vernacular knowledge and academia, translating local knowledge into a universal technical language that bases the validity of traditional systems within the framework of sustainable habitat. For future planning processes in territories of high cultural relevance, three operational guidelines are recommended:

For territorial research: To make planning studies subject to the processes of community life and local praxis, thereby avoiding the museification of identity and promoting its validity as an engine of sustainable development.

For academic training: To reorient the teaching of architecture and urbanism towards interventions grounded in active listening and socio-ecological sensitivity, using graphic representation as a tool for the technical rescue of vernacular systems.

For local management: To use architectural cataloging and social cartography as internal mediation tools to resolve boundary conflicts and consolidate collective legal security, thereby guaranteeing the historical and spatial continuity of the community habitat.

CONTRIBUTION OF AUTHORS CRediT

Conceptualization: F.M.L.G., A.K.K.L.G.; Data Curation: F.M.L.G., A.K.K.L.G.; Formal analysis: F.M.L.G., A.K.K.L.G.; Acquisition of financing: F.M.L.G., A.K.K.L.G.; Research: F.M.L.G., A.K.K.L.G.; Methodology: F.M.L.G., A.K.K.L.G.; Project management: F.M.L.G.; Resources: F.M.L.G.; Software: F.M.L.G.; Supervision: A.K.K.L.G., A.K.K.L.G.; Validation: A.K.K.L.G.; Visualization: F.M.L.G.; Writing - original draft: F.M.L.G.; Writing - revision and editing: A.K.K.L.G.

ACKNOWLEDGMENTS

Comunidad Las Lagunas Chukidel Ayllullacta. SD ARQUITECTURA.

BIBLIOGRAPHIC REFERENCES

Alegría, L., & Valencia, M. (Eds.). (2024). *Patrimonios emergentes en Chile contemporáneo*. Colección Cultural y Patrimonio (Vol.7). Servicio Nacional del Patrimonio Cultural – Subdirección de Investigación. https://www.investigacion.patrimoniocultural.gob.cl/sites/www.investigacion.patrimoniocultural.gob.cl/files/2025-07/libro_patrimonios_emergentes_vf_baja.pdf#page=141

Arango-Marín, M., Cardona-González, M., Mejía-Amézquita, V., & Zapata-Arango, L. F. (2025). Voces que resguardan al territorio de Riosucio (Caldas). Prácticas comunitarias como redes de cuidado. *Bitácora Urbano Territorial*, 35(1), 77-88. https://revistas.unal.edu.co/index.php/bitacora/article/view/117304/94953

Borja, J., & Muxi, Z. (2003). *El espacio público, ciudad y ciudadanía*. Editorial Electa.

Calderón, A. (1985). *Saraguro huasi: La casa en la "tierra del maíz"*. Banco Central del Ecuador.

Canziani Amico, J. (2012). *Ciudad y territorio en los Andes: Contribuciones a la historia del urbanismo prehispánico*. Pontificia Universidad Católica del Perú. https://doi.org/10.18800/9786124146022

Cerasi, M., & Quaroni, L. (1990). *El espacio colectivo de la ciudad: construcción y disolución del sistema público en la arquitectura de la ciudad moderna* (1a ed.). Oikos-Tau.

Cevallos Salas, P. (2003). El bahareque en zonas sísmicas. En J. A. Cordero, E. J. Martínez, y C. Martins Neves (Eds.), *Técnicas mixtas de construcción con tierra* (pp. 37-48). Proterra. https://redproterra.org/wp-content/uploads/2020/06/3_PP-T%C3%A9cnicas-Mixtas_2003.pdf

Colosi, F., Bacigalupo, C., De Meo, A., Kobata Alva, S. A., Orazis, R., Rojas Vasquez, G. E., & León Trujillo, F. J. (2025). Chan Chan (Perú), la ciudad de tierra. La amenaza al paisaje cultural de un sitio Patrimonio Mundial. *ACE: Architecture, City and Environment*, 20(58), 12658. https://doi.org/10.5821/ace.20.58.12658

Corrales Blanco, J. C., Pineda Iriarte, A. P., & Salazar Rodríguez, C. C. (2021). Revalorización de la arquitectura vernácula. Módulo de vivienda para una comunidad asháninka de Alto Kamonashiarii. *Limaq, 7*(007), 175–200. https://doi.org/10.26439/limaq2021.n007.5185

Cristancho Barrios, K. J. (2024). *Análisis del comportamiento de muros en bahareque de tierra ante cargas horizontales* [Tesis de Magíster, Pontificia Universidad Javeriana]. Centro de recursos para el Aprendizaje y la Investigación. https://doi.org/10.71618/pe8z-e834

Dávila Egüez, R. (2015). *Plan de Desarrollo y Ordenamiento Territorial de la Provincia de Loja 2015-2025*. Prefectura de Loja. https://prefecturaloja.gob.ec/documentos/lotaip/GPL/2017/Enero/Documentos/PDOT_PROV_LOJA.pdf

Gonzalo Sánchez, V. (2012). *Morteros de barro estabilizados con fibras de paja, esparto y sisal para su uso como revestimientos* [Tesis de maestría, Universidad Politécnica de Madrid]. Repositorio Institucional Universidad Politécnica de Madrid. https://oa.upm.es/14429/

Guerrero Baca, L. F. (2017). *Pasado y porvenir de la construcción con bahareque. Gremium, 4*(8), 69-80. https://doi.org/10.56039/rgn08a07

Hernández Sampieri, R., & Mendoza Torres, C. P. (2018). *Metodología de la investigación: las rutas cuantitativa, cualitativa y mixta*. McGRAW-HILL INTERAMERICANA EDITORES. http://www.biblioteca.cij.gob.mx/archivos/materiales_de_consulta/drogas_de_abuso/articulos/sampierilasrutas.pdf

INPC - Instituto Nacional de Patrimonio Cultural. (2014). Guía de identificación y registro del Qhapaq Ñan. Perú. https://qhapaqnan.cultura.pe/sites/default/files/mi/archivo/rcq.pdf

Lozano Guamán, A. K. (2014). *Análisis de la arquitectura tradicional en el cantón Saraguro, como base para una propuesta de diseño contemporáneo* [Tesis de Pregrado no publicada]. Universidad Central del Ecuador.

Lozano Guamán, A. K. K. (2021). Los valores formales de la arquitectura tradicional del pueblo Saraguro, pertinentes al movimiento moderno. Estudio tipológico de la arquitectura tradicional en la comunidad Lagunas, parroquia Saraguro [Tesis de Maestría, Universidad de Cuenca]. Repositorio Institucional UCUENCA. http://dspace.ucuenca.edu.ec/handle/123456789/37454

Lozano Guamán, F. M. (2022). Recuperación de los caminos antiguos "chakiñanes" y sitios sagrados de la comunidad las lagunas del cantón Saraguro, provincia de Loja. [Tesis de Pregrado, Universidad Internacional del Ecuador]. Repositorio Digital UIDE. https://repositorio.uide.edu.ec/handle/37000/4964

Lozano Guamán, F. M., Jaramillo-Benavides, A., & Lozano-Guamán, K. K. (2025). Revitalización del Bahareque ancestral del pueblo Kichwa Saraguro, Ecuador: conservación, adaptación y difusión del patrimonio constructivo. *Revista Hábitat Sustentable*, *15*(1), 116-133. https://doi.org/10.22320/07190700.2025.15.01.09

Marca Chérrez, R. V. (2011). El Qhapaq Ñan a su paso por el cerro de Shuñin en el cantón Oña. [Tesis de Pregrado, Universidad de Cuenca]. Repositorio Institucional UCUENCA. http://dspace.ucuenca.edu.ec/handle/123456789/1979

Montaño Huerta, M. D. (2017). Paisajes interculturales. Análisis, diagnóstico y planificación para la Ordenación de un Territorio. El caso de Cotogchoa. [Tesis de Maestría, Universidad de Cuenca]. Repositorio Institucional UCUENCA https://dspace.ucuenca.edu.ec/items/9b36eecc-96db-4ed2-abe3-9c0dc4b2a64d

Novoa Rios, I. N., & Hernández García, J. (2026). Más que agua, análisis multidimensional del paisaje fluvial: hacia una rehabilitación integral en Fusagasugá, Colombia. *Bitácora Urbano Territorial*, *36*(1), 175-190. https://doi.org/10.15446/bitacora.v36n1.120120

Ordóñez Suárez, R. I. (2019). Plan de conservación preventiva para el tramo del Qhapac Ñan - Camino del Inca, comprendido entre Migüir y Paredones de Molleturo [Tesis de Maestría, Universidad de Cuenca]. Repositorio Institucional UCUENCA. https://dspace.ucuenca.edu.ec/items/e4b46612-b2c7-4201-b293-79c1f5c3a1b3

Pacheco Arévalo, A. C. (2007). Etnias aborígenes y globalización, estudio de caso de la comunidad de Saraguro-Loja. [Tesis de Pregrado, Universidad del Azuay]. Repositorio Institucional. http://dspace.uazuay.edu.ec/handle/datos/962

Pérez Bustamante, L., & Parra Ponce, C. (2004). Paisajes culturales: El parque patrimonial como instrumento de revalorización y revitalización del territorio. *Theoria*, 13(1), 9-24. https://www.ubiobio.cl/theoria/v/v13/1.pdf

Qhapaq Ñan-Ecuador. (2019). *Guía para la capacitación en conservación preventiva de estructuras arqueológicas en piedra y tierra Qhapaq Ñan, sistema vial Andino*. Secretaría Técnica del Qhapaq Ñan - Ecuador / Secretaría Técnica del Qhapaq Ñan - Argentina. https://www.patrimoniocultural.gob.ec/wp-content/uploads/2020/07/Guia_conservacion_estructuras_arqueologicas_qhapaq_nan.pdf

Quizhpe Guamán, L. A. (2013). La organización comunitaria una alternativa para los pueblos andinos: caso la comunidad Lagunas, cantón Saraguro, provincia de Loja [Tesis de Pregrado, Universidad de Cuenca]. Repositorio Institucional Universidad de Cuenca. https://dspace-test.ucuenca.edu.ec/handle/123456789/3727

Rodríguez Valbuena, D. (2011). Territorio y territorialidad. Nueva categoría de análisis y desarrollo didáctico de la Geografía. *Revista Uni-Pluriversidad, 10*(3), 90-100. https://revistas.udea.edu.co/index.php/unip/article/view/9582

Van Der Voordt, D. J. M., & De Jong, T. M. (Eds.). (2002). *Ways to study and research: urban, architectural and technical design*. Delft University Press.

Sociospatial assessment of energy poverty and its gender dimension in vulnerable areas of Granada, Spain
Susana Clavijo-Núñez, Antonio Aguilar-Aguilera, María De-la-Hoz-Torres, Antonio Serrano-Jiménez, David Bienvenido-Huertas
Revista Hábitat Sustentable Vol. 16, N°. 1. ISSN 0719 - 0700 / Págs. 96 - 107
https://doi.org/10.22320/07190700.2026.16.01.06

SOCIOSPATIAL ASSESSMENT OF ENERGY POVERTY AND ITS GENDER DIMENSION IN VULNERABLE AREAS OF GRANADA, SPAIN

Recibido 13/02/2026
Aceptado 27/05/2026

EVALUACIÓN SOCIOESPACIAL DE LA POBREZA ENERGÉTICA Y SU DIMENSIÓN DE GÉNERO EN ÁREAS VULNERABLES DE GRANADA, ESPAÑA

AVALIAÇÃO SOCIOESPACIAL DA POBREZA ENERGÉTICA E SUA DIMENSÃO DE GÊNERO EM ÁREAS VULNERÁVEIS DE GRANADA, ESPANHA

Susana Clavijo-Núñez (Autor de Correspondencia)
Doctora en Arquitectura Investigadora postdoctoral,
Departamento de Ingeniería Agraria y del Medio Natural,
Universidad de La Laguna
San Cristóbal de La Laguna, España
https://orcid.org/0000-0002-8969-754X
sclavijo@ull.edu.es

Antonio Aguilar-Aguilera
Doctor en Ingeniería Civil Investigador postdoctoral,
Departamento Construcciones Arquitectónicas,
Universidad de Granada
Granada, España
https://orcid.org/0000-0001-5045-8560
antojes@ugr.es

María De-la-Hoz-Torres
Doctora en Ingeniería Civil
Profesora Permanente Laboral,
Departamento de Expresión Gráfica Arquitectónica y en la Ingeniería
Universidad de Granada
Granada, España
https://orcid.org/0000-0003-1657-1572
mlhoz@ugr.es

Antonio Serrano-Jiménez
Doctor en Arquitectura
Profesor Permanente Laboral, Departamento Construcciones Arquitectónicas
Universidad de Granada
Granada, España
https://orcid.org/0000-0002-8585-857X
serranojimenez@ugr.es

David Bienvenido-Huertas
Doctor en Arquitectura
Profesor Titular, Departamento Construcciones Arquitectónicas
Universidad de Granada
Granada, España
https://orcid.org/0000-0003-0716-8589
dbienvenido@ugr.es

CC BY SA

Revista Hábitat Sustentable Vol. 16, N°. 1. ISSN 0719 - 0700 / Págs. 96 - 107
https://doi.org/10.22320/07190700.2026.16.01.06

ABSTRACT

Although energy poverty is a widely addressed issue, significant knowledge gaps persist regarding how it disproportionately affects women. This study analyses energy vulnerability and the gender dimension from a socio-spatial perspective, using the city of Granada as a case study. The methodology draws on publicly available census-level data to combine energy and gender indicators and examine their prevalence in areas categorized as vulnerable. The findings reveal a relationship between vulnerable areas, low-income levels, and energy-inefficient buildings. Older women living alone, female-led households, and foreign-born women are identified as at-risk groups, all presenting significantly reduced income levels. The study concludes that there is a need to redefine vulnerable areas, promote energy retrofitting, and incorporate a gender perspective to design comprehensive public policies that contribute to a fair energy transition.

Keywords
energy, women, residential areas

RESUMEN

A pesar de que la pobreza energética es un problema ampliamente abordado, aún persisten lagunas de conocimiento sobre cómo afecta de manera diferenciada a las mujeres. El estudio analiza la vulnerabilidad energética y la dimensión de género desde una perspectiva socioespacial, tomando como caso de estudio la ciudad de Granada. La metodología emplea datos públicos a escala censal para combinar indicadores energéticos y de género y analizar su prevalencia en áreas categorizadas como vulnerables. Los resultados evidencian una relación entre áreas vulnerables, bajos ingresos y construcciones energéticamente ineficientes. Se identifican como grupos de riesgo las mujeres mayores en hogares unipersonales, los hogares encabezados por mujeres y las mujeres extranjeras, que presentan ingresos significativamente reducidos. Se concluye que es necesario redefinir las áreas vulnerables, promover la rehabilitación energética e integrar el enfoque de género, a fin de diseñar políticas públicas integrales que contribuyan a una transición energética justa.

Palabras clave
energía, mujeres, áreas residenciales

RESUMO

Embora a pobreza energética seja uma questão amplamente abordada, ainda persistem lacunas de conhecimento sobre como ela afeta as mulheres de forma diferenciada. Este estudo analisa a vulnerabilidade energética e a dimensão de gênero sob uma perspectiva socioespacial, tomando como caso de estudo a cidade de Granada. A metodologia utiliza dados públicos em escala censitária para combinar indicadores energéticos e de gênero, com o intuito de analisar sua prevalência em áreas classificadas como vulneráveis. Os resultados evidenciam uma relação entre áreas vulneráveis, baixa renda e edifícios energeticamente ineficientes. São identificados como grupos de risco as mulheres idosas em domicílios unipessoais, os domicílios chefiados por mulheres e as mulheres estrangeiras com rendimentos significativamente reduzidos. Conclui-se que é necessário redefinir as áreas vulneráveis, promover a reabilitação energética e integrar a perspectiva de gênero, com o objetivo de elaborar políticas públicas integrais que contribuam para uma transição energética justa.

Palavras-chave
energia, mulheres, áreas residenciais

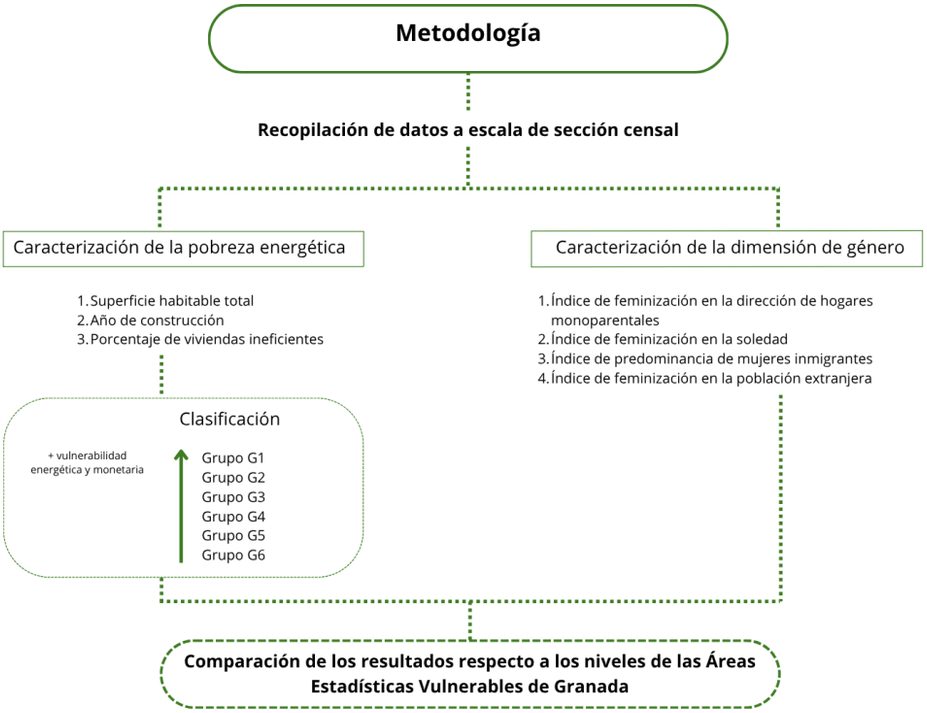


Figure 1. Outline of the applied methodology. Source: Prepared by the Authors.

INTRODUCTION

Energy poverty (EP), a multidimensional problem located at "the intersection between household incomes, energy costs and the energy efficiency of the housing stock" (Faiella & Lavecchia, 2021), is linked to other dimensions of poverty and inequality, such as the gender gap. At the same time, the academic review of the feminization of energy poverty, although relevant, is lacking (Longhurst & Hargreaves, 2019). From a gender perspective, women continue to take on more of the tasks of caring for and maintaining the home. As a result, they have historically been the most affected by the lack of secure access to basic services, while also facing the burden of household responsibilities and difficulties paying energy bills (McDowell, 1999).

A key problem is the lack of data on the gender dimension in EP (Clancy, 2016). It was initially analyzed from technical aspects such as consumption and thermal perception (Cecelski, 2004), and subsequently in terms of its comprehensive impact on EP (Clancy et al., 2017). Currently, there are still limitations due to the lack of disaggregated data (Bradshaw, Chant & Linneker, 2017), as well as conceptualizations and prejudices about the feminization of EP (Listo, 2018). It is also evident that an intersectional approach is needed, in which factors such as gender, age, or social class are intertwined, generating both privileges and disadvantages (Viveros Vigoya, 2016).

In Europe and Spain, more than half of single-parent households are at risk of poverty or social exclusion, especially those supported by women, who earn 18.6% less than men and have a higher unemployment rate (Alguacil Denche, Llano Ortiz & Sanz Angulo, 2024; Technical Secretariat of European Anti-Poverty Network [EAPN-EN], 2024). Andalusia has one of the highest incidence rates of EP in Spain (Romero Mora, Barrella & Centeno Hernáez, 2024), due to the combination of low wages, increased climatic severity, and a poor built environment (Castaño-Rosa, Solís-Guzmán & Marrero, 2020). Granada is one of the most affected cities, with documented structural problems, such as the continuous power cuts in the northern neighborhoods (Ramirez, 2023), a strong energy demand due to severe weather conditions (Bienvenido-Huertas et al., 2020), and poor energy performance in social housing from the point of view of adaptive comfort (Calama-González et al., 2024). However, the literature lacks studies that integrate the gender dimension from an intersectional approach in the analysis of EP in Granada.

It is necessary to incorporate this dimension through a socio-spatial approach, which examines the susceptibility of spatial environments (e.g., neighborhoods) to risks arising from specific dynamics. Using this analysis in social problems allows consideration of temporal factors and different input variables (Panda, 2017). In the case of EP, this approach allows detecting its unpredictability, as it can

vary with household characteristics and social inequalities within the same area (Pérez-Fargallo et al., 2026).

The general aim of the article is to determine the relationship between energy poverty and the gender dimension at the census scale in vulnerable areas in Granada. The findings, which incorporate an intersectional gender approach, enable analysis of the influence of the feminization of energy poverty in Granada and will serve as a basis for developing public policies that effectively advance a fair transition.

METHODOLOGY

The proposed methodology combines a quantitative analysis of energy and gender variables in Granada, as detailed in the phases shown in Figure 1.

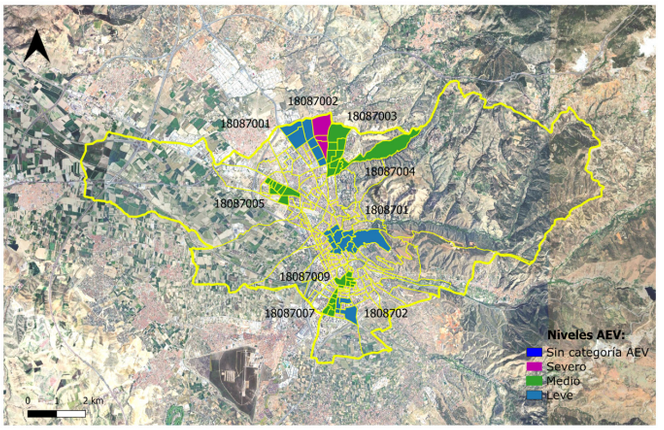
CASE STUDY

The city of Granada (Spain) was selected as the study area, and vulnerable statistical areas (VSAs) from the Vulnerable Neighborhoods Catalog were included (Ministry of Transport, Mobility and Urban Agenda, 2021). The characterization of the VSAs allows the classification of the census sections into five levels (not vulnerable, mild, medium, severe, and critical) based on three indicators: unemployed population, population without studies, and housing in poor condition.

Granada has mild, medium, and severe VSA levels (Figure 2). In the case of mild, 3 VCAs are detected, with the Almanjáyar neighborhood standing out as one of the areas with the most reported cases of energy poverty in the city. The medium level has the majority of the city's VCAs (6 in total). They cover the neighborhoods of Cartuja, La Chana, Monteverde-Caserío de Montijo, Zaidín chico, and Zaidín-Vergeles. Finally, the La Paz-Rey Badis area has the most severe VCAs.

MATERIALS

Firstly, technical and socio-economic public data on the real estate stock were collected from sources that



Código	Nivel de vulnerabilidad	Nº viviendas	Superficie (Ha)	Nº secciones censales
1808701	Leve	10615	135,95	12
1808702	Leve	2810	37,07	5
18087001	Leve	4065	106,69	5
18087003	Medio	-	77,81	5
18087005	Medio	5610	48,49	9
18087004	Medio	2860	121,66	4
18087007	Medio	3775	25,09	6
18087009	Medio	3900	26,75	8
18087002	Severo	1.555	64,20	4

Figure 2. Location of the vulnerable statistical areas of Granada. Source: Prepared by the Authors.

provided disaggregated information (Table 1). In the databases of the National Institute of Statistics [INE] for 2021 and 2023, the disaggregated resolution was at the census section level, whereas for the energy certificates it was at the housing scale and was grouped into the corresponding sections to unify the unit of analysis. The data have been collected for 180 census sections of the city of Granada.

The energy certificates database underwent fine-tuning, including eliminating duplicate records, excluding certificates with empty fields, and discarding records with errors in the survey reference. After this process, the database comprised 27,484 residential energy certificates, with coverage by census section calculated as the ratio of available certificates to the total number of housing units (Table 2).

Survey/database	Year	Spatial scale	Reference
Household Income Distribution Atlas	2023	Census section	(INE, 2025)
Population and housing census	2021	Census section	(INE, 2023)
Andalusia energy certificates registry	2025	Housing	(Junta de Andalucía, 2025)

Table 1. Databases of socio-economic and technical character of the built environment used in the study. Source: Prepared by the Authors.

Mean (%)	Median (%)	Q1 (%)	Q3 (%)	Min. (%)	Max. (%)
16.3%	13.7%	8.8%	19.3%	2.5%	65.3%

Table 2. Coverage of energy efficiency certificates in Granada. Source: Prepared by the Authors.

CHARACTERIZATION OF ENERGY POVERTY

An analysis was carried out using three energy indicators of the dwelling, selected according to the methodology of Aguilar, Guerrero-Rivera and de la Hoz-Torres (2025), and obtained from the available databases of building energy certificates. No additional indicators were incorporated because energy data sources were not available at the census level. The indicators used were total living area, year of construction, and the percentage of inefficient housing (Equation 1).

$$ID_i = \frac{D_{i,E} + D_{i,F} + D_{i,G}}{D_i} \cdot 100 \quad [\%] \qquad \text{(Equation 1)}$$

Where ID_i is the percentage of inefficient housing; $D_{i,E}$ is the number of homes with an E label; $D_{i,F}$ is the number of homes with an F label; $D_{i,G}$ homes with a G-label; and D_i the total number of homes tagged.

These energy indicators were complemented by the EP indicator, based on the socio-spatial adaptation of the 2M indicator, which has been used in a variety of studies in the scientific literature (Antepara et al., 2020; Sánchez-Guevara Sanchez et al., 2020a). As these investigations indicate (Equation 2), given that the average energy expenditure in Spain is approximately 5%, a threshold of 10% is considered.

$$EPR = \frac{EC}{DI} \cdot 100 \quad [\%] \qquad \text{(Equation 2)}$$

Where EPR is the rate of EP; EC is the annual cost or expenditure of energy consumption obtained through energy certificates (€); and DI is the average annual net income of the dwelling (€).

The energy cost was calculated by breaking down the costs of the different energy vectors used by the dwelling: electricity, natural gas, liquefied petroleum gas (LPG), and biomass (Equation 3), based on the consumption data included in the energy certificate.

$$EC = ECC + NGCC + LPGCC + BCC \quad [€] \qquad \text{(Equation 3)}$$

Where ECC is the annual cost of the dwelling's electricity consumption (€); NGCC is the annual cost of natural gas consumption (€); LPGCC is the annual cost of LPG consumption (€); and BCC is the dwelling's annual cost of biomass consumption (€).

The cost of electricity consumption was calculated based on a series of considerations regarding the typical characteristics of Spain (Equation 4). In this sense, the Voluntary Price for the Small Consumer (PVPC, in Spanish) tariff was considered, without time discrimination (Royal Decree 216, 2014).

$$ECC = 1{,}21 \cdot \left(((C_e \cdot P_e) + CP) \cdot (1 + ElT) + RM\right) \quad [€] \text{ (Equation 4)}$$

Where C_e it is the energy consumption obtained from the dwelling's energy certificate (kWh); P_e is the price of the PVPC electricity tariff (€/kWh); CP is the cost of the contracted power (€); ElT is the electricity tax; and RM is the rental of the meter (€). The values associated with the tariffs were obtained from the average PVPC values for 2025. Regarding power, a 4.6 kW contract was considered, representative of the average contracted power in the country (ENDESA, 2025).

As for natural gas, billing under the last-resort tariff (TUR, in Spanish) was considered. The formulation used would be Equation 5:

$$NGCC = 1{,}21 \cdot ((C_{NG} \cdot P_{NG}) \cdot (1 + T) + FC + RM) \quad [€] \text{ (Equation 5)}$$

Where C_{NG} is the natural gas consumption (kWh); P_{NG} is the price of the variable term of natural gas (€/kWh); T is the tax on hydrocarbons; FC is the fixed-term price of natural gas (€); and RM is the rental of the meter (€). Finally, the costs of LPG and biomass were obtained using Equation 6 and Equation 7.

$$LPGCC = C_{LPG} \cdot P_{LPG} \quad [€] \qquad \text{(Equation 6)}$$

$$BCC = C_B \cdot P_B \quad [€] \qquad \text{(Equation 7)}$$

Where C_{LPG} is the LPG consumption (kWh); P_{LPG} is the price of propane (€/kWh); C_B is the biomass consumption (kWh); and P_B is the biomass price (€/kWh).

ENERGY POVERTY CLASSIFICATION

Once the EP results were available, the census sections were classified into different levels, following the methodologies proposed in previous studies of the Community of Madrid (Sanz-Fernández et al., 2016; Sánchez-Guevara Sánchez, Sanz Fernández & Núñez Peiró, 2020b). The methodology consists of the two-dimensional location of households when comparing the income variables (DI) and energy expenditure (EC).

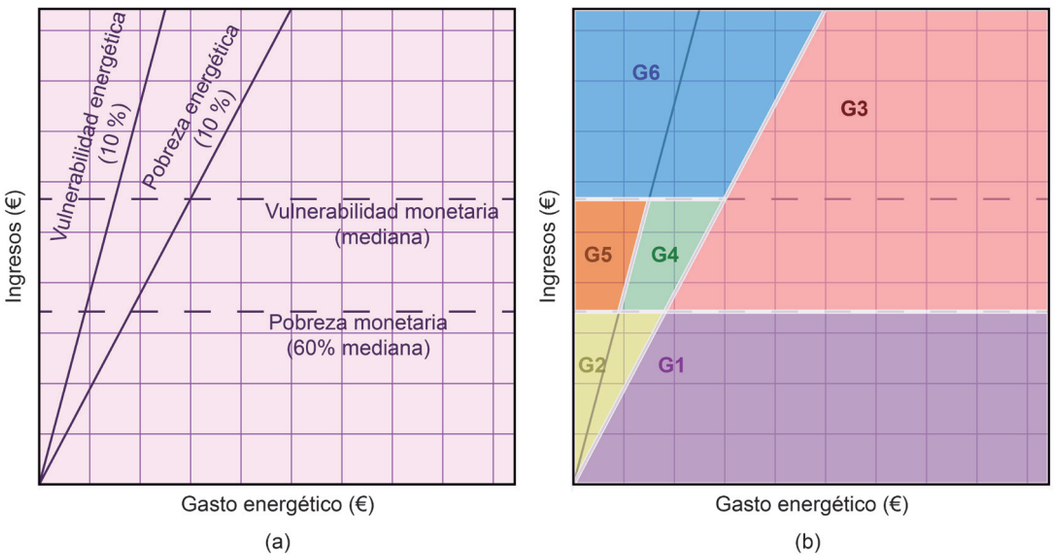


Figure 3. Classification of households: (a) thresholds and (b) groups. Source: Prepared by the Authors based on the methodology of Ana Sanz-Fernández (Sanz-Fernández et al., 2016) and Carmen Sánchez-Guevara Sánchez (Sánchez-Guevara Sánchez et al., 2020b).

This approach includes some lines-thresholds, which led to six different groups (Figure 3):

- Group G1: Census tracts with households suffering from both monetary poverty (60% of median income) and EP (10% of energy expenditure compared to income).
- Group G2: Census tracts suffering from monetary poverty.
- Group G3: Census tracts that suffer from EP, but not monetary poverty (they would be in monetary vulnerability, median income).
- Group G4: Census tracts with households in the energy vulnerability (5% of energy expenditure) and monetary vulnerability category.
- Group G5: Census tracts in the monetary vulnerability category.
- Group G6: Census tracts without energy or monetary vulnerability.

CHARACTERIZATION OF THE FEMINIZATION OF ENERGY POVERTY

To analyze the feminization of energy poverty, four partial gender indicators were used based on disaggregated data from the INE and on the limitation of applying existing feminization indices in the literature (Capetillo-Ordaz et al., 2024). The partial indicators considered were: feminization index in the leadership of single-parent households (FHH_i); index of feminization in loneliness (FL_i); predominance index of immigrant women ($PFoW_i$) and index of feminization in the foreign population (FFo_i).

The reflects the predominance of single-parent households (Equation 8). This indicator is key, as women earn lower wages, receive lower pensions, and experience higher unemployment rates, which structurally reduces their disposable income for energy bills.

$$FHH_i = \frac{H_{i,w<65} + H_{i,w>65}}{H_i} \cdot 100 \quad [\%] \qquad \text{(Equation 8)}$$

Where $H_{i,w<65}$ is the total number of households headed by women under the age of 65; $H_{i,w>65}$ is the total number of households headed by women over the age of 65; and H_i is the total number of households.

The feminization in the loneliness index (FL_i) reflects the situation of women over the age of 65 who live alone and whose income depends on their pension. The calculation of this index was based on a comparison with respect to households composed of older men (Equation 9).

$$FL_i = \frac{H_{i,w,l>65}}{H_{i,m,l>65} + 1} \cdot 100 \quad [\%] \qquad \text{(Equation 9)}$$

Where $H_{i,w,l>65}$ is the total number of households headed by women over the age of 65 living alone; and $H_{i,m,l>65}$ is the total number of households headed by men aged 65 and older living alone.

The predominance index of immigrant women $PFoW_i$ was included to explore the relationship between immigration and gender inequalities in EP (Equation 10), as they often face socio-economic disadvantages, such as lower-paid jobs or higher unemployment rates.

$$PFoW_i = \frac{W_{i,Fo}}{W_{i,Fo} + W_{i,Sp}} \cdot 100 \quad [\%] \qquad \text{(Equation 10)}$$

Where $W_{i,Fo}$ is the number of women born outside Spain who are residents in the area of analysis; and $W_{i,Sp}$ is the number of women born in Spain in the area of analysis.

Finally, FFo_i reflects the gender composition of immigrant communities and can be used to identify groups of foreign women who might be disproportionately exposed to EP due to socio-economic disadvantages (Equation 11).

$$FFo_i = \frac{W_{i,Fo}}{M_{i,Fo} + 1} \cdot 100 \quad [\%] \qquad \text{(Equation 11)}$$

Where $M_{i,Fo}$ is the number of men born outside Spain.

Finally, the Moran Index is applied to the analyzed variables to examine the spatial autocorrelation of these indicators across sections. Values close to 1 show strong positive spatial clustering, values close to 0 indicate a random distribution, and values close to -1 indicate high spatial dispersion. The statistical significance is evaluated using a pseudo-p-value obtained from 999 random permutations.

RESULTS AND DISCUSSION

The analysis began with an evaluation of the energy indicators and their relationship to the VCAs of Granada; areas that were not classified as VCAs were also considered. As shown in Figure 4, there are clear coincidences among VCAs on some energy indicators, such as year of construction, living area, and annual energy expenditure, with a lower interquartile range in the higher-risk VCAs due to their smaller spatial size. The average construction year for these areas was 1974. The analysis of inefficient housing reveals a clear relationship between VCA severity and housing efficiency. The highest-risk VCA (11% of the vulnerable territory) shows a percentage close to 100% in all sections. For the other VCAs and risk-free zones, the percentages of inefficient housing are similar. Since there is a correlation between energy efficiency and living space (larger homes consume more energy), analyzing the EPR indicator is well-suited to the final evaluation of the EP risk. The 10% threshold for the 2M indicator was considered; 28% of the sections without VCA cataloging were in EP, a percentage that progressively increases with risk: 53% in VCA 1, 75% in VCA 2, and 100% in VCA 3.

The analysis continued with the risk groups of the methodology of Sánchez-Guevara Sánchez et al. (2020b). As shown in Figure 5, in the severe category of VCAs, 100% of the census units were in G1, more extreme cases of energy and monetary poverty. Both in the lower-risk VCAs and in areas without VCA cataloging, census sections were observed within the G1. Although this implies a lack of correlation between VCA cataloging and the risk of EP, the associated percentage values for records in the G1 were dependent on the level of VCA: 0.8% in areas without VCA, 20% at the mild level, and 25% at the medium level. Thus, a relationship was again detected between VCA levels and the risk of EP. In the remaining groups, certain associations were observed between VCA and the predominant group. In this sense, the G3 group predominated in the mild and medium levels (Figure 5). These cases are characterized by low-to-middle income and a lack of energy efficiency in housing. G6 (zero energy and monetary risk) predominated in areas without VCA cataloging, mainly due to higher income levels than in vulnerable areas. However, even in areas without VCA cataloging, EP cases are registered, with percentage values as high as 27.6%. Figure 6 shows the spatial distribution of the sections in each group: G2 and G5 are more uniform, while the other categories group the census sections with greater coherence in their classification as VCAs.

The relationship between residential inefficiency, low income, and EP had already been documented in both Madrid (Sanz Fernández et al., 2016) and Barcelona (Delgado, 2018). The cases of EP in areas without VCA cataloging highlight the importance of using a combination of indicators.

It should be noted that most of the houses predate the basic regulation of 1979, which established the need to implement insulation solutions in building envelopes. However, this relationship may vary due to possible subsequent retrofits. In general, the percentage of sustainable, highly efficient homes in Granada is low, underscoring the need to adopt energy retrofit strategies. Regarding the relationship between energy efficiency and living space, evaluating only the consumption variable could lead to misleading conclusions, since the most severe VCAs had the lowest consumption values due to the smaller area of their housing.

These cases of EP are linked to housing energy inefficiency and low incomes in these VCAs. Although the VCA definition criteria did not originally consider EP criteria, their interrelation with economic and efficiency problems leads to a greater predominance of EP in the most vulnerable areas, including some without VCA cataloging, which may reflect the need to reclassify some census units.

Once the EP was characterized, the gender dimension was evaluated. In Figure 7, some similarity is observed across all zones, except in the severe category. The indicators of feminization

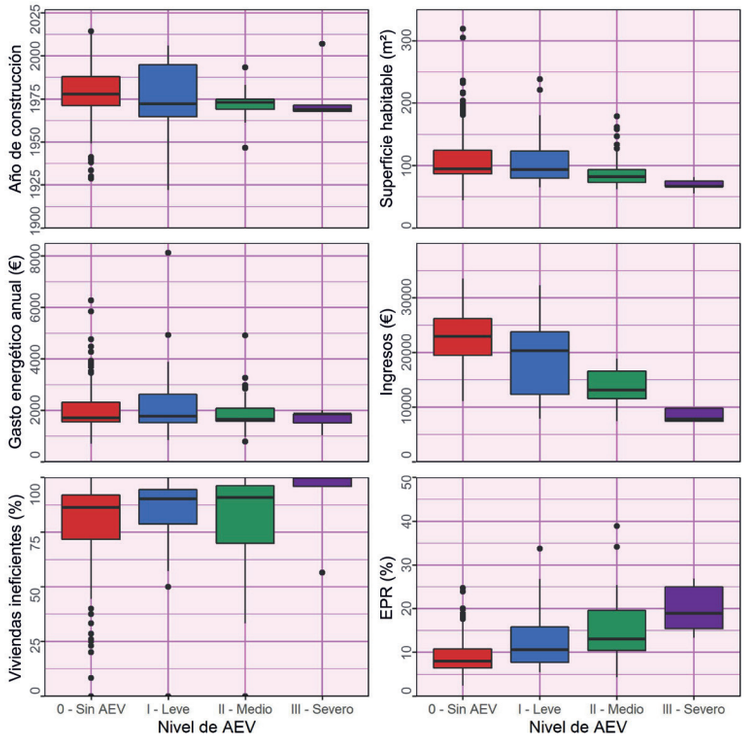


Figure 4. Box diagrams of the results obtained in the energy indicators. Source: Prepared by the Authors.

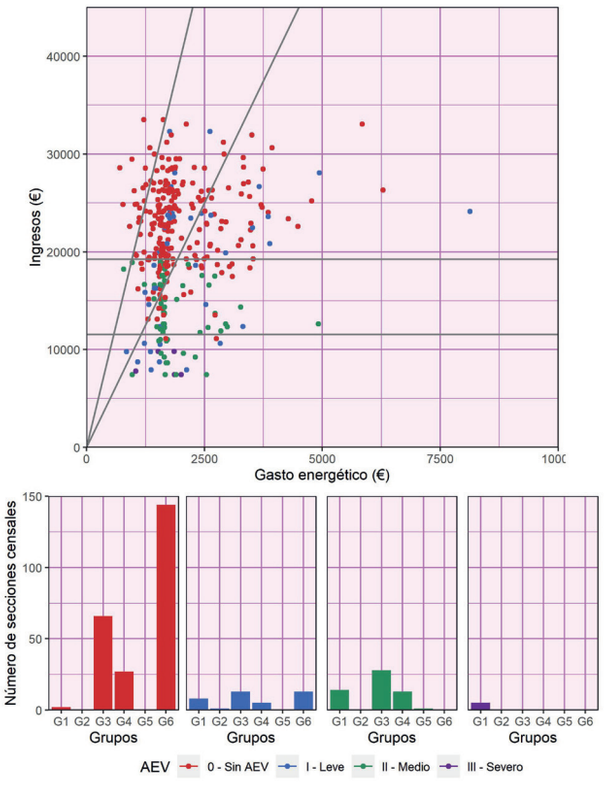


Figure 5. Location of households by energy poverty risk group, as classified by the VCA. Source: Prepared by the Authors.

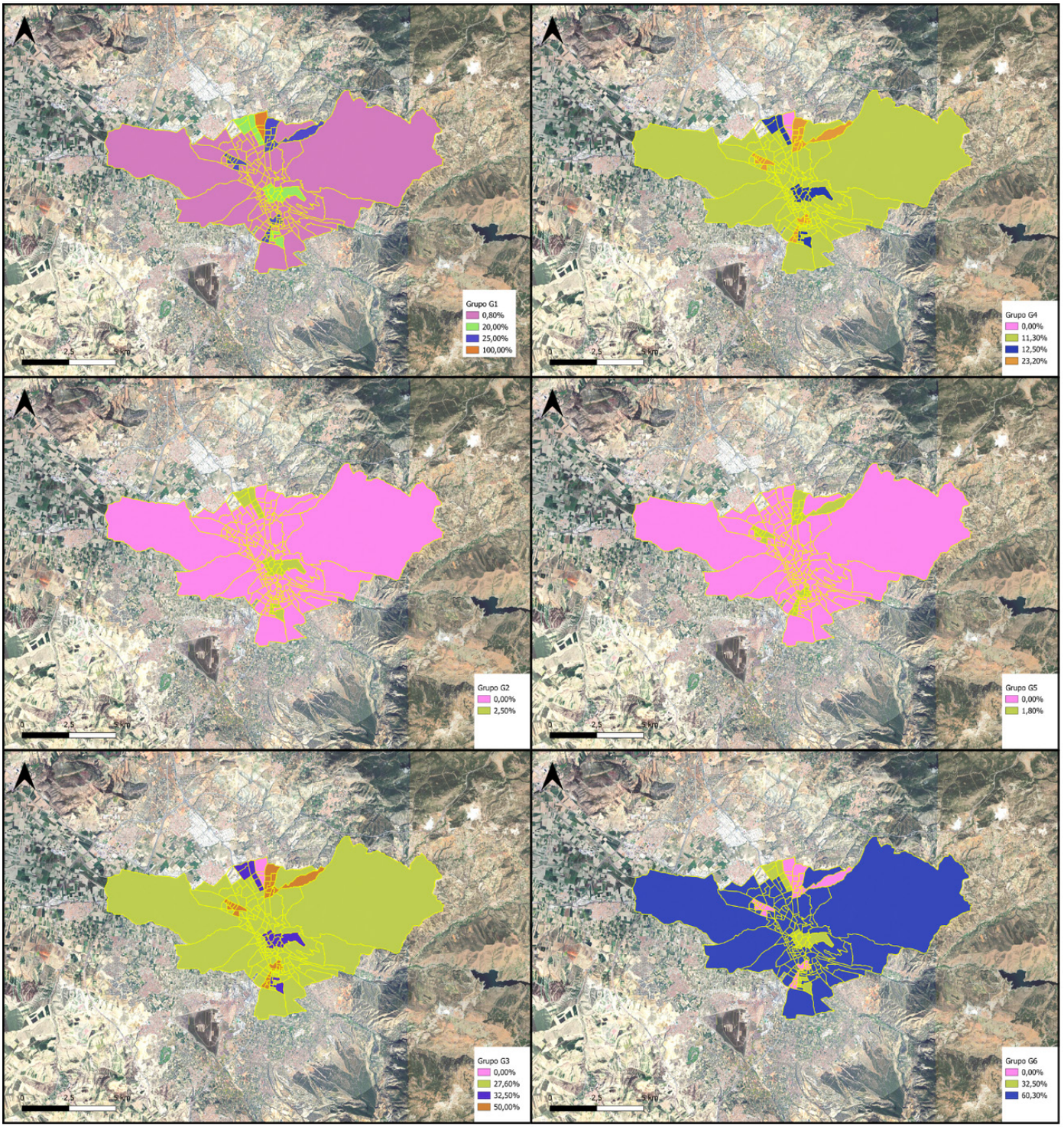


Figure 6. Spatial distribution of EP groups. Source: Prepared by the Authors.

in household management (FHH_i), feminization in solitude (FL_i) and foreign population ($PFoW_i$) and (FFo_i) were lower in the census tracts of La Paz-Rey Badis. The feminization index of loneliness shows values exceeding 100% in male-headed households. The feminization rate of the foreign population also exceeds 100% in the vast majority of cases. Single-parent households are also predominant in the region.

The lower concentration of gender indicators in La Paz-Rey Badis may be associated with the limited extension of VCA 3 in Granada, resulting in a concentration of

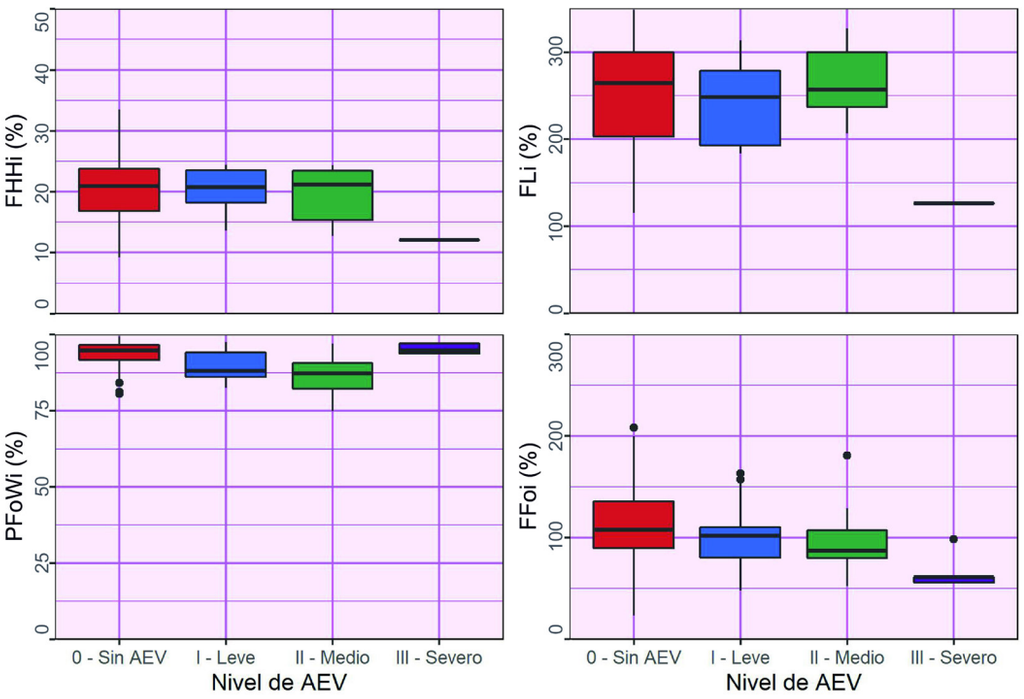


Figure 7. Box diagrams of the gender indicators, classified according to the VCA. Source: Prepared by the Authors.

results. On the other hand, there is a high proportion of vulnerable households headed by single older women, which could be explained by the fact that economic sustenance is usually pensions (which are lower than for men). In the same vein, single-parent households can lead to new EP situations if their incomes align with the usual trends in the business sector.

Regarding the spatial autocorrelation analysis, most indicators show moderate-to-high spatial clustering, with weak clustering in some cases, and are statistically significant in all cases. For example, the year of construction shows a Moran I of 0.455 (p-value=0.001), and the living area shows a Moran I of 0.468 (p-value=0.001), which reflects the residential segregation characteristic of cities. The index of feminization of the foreign population presents a weak positive autocorrelation (I=0.113; p-value=0.005), a consequence of a more dispersed distribution in the territory.

The results show the need to complement official tools for defining vulnerable areas by incorporating energy and gender criteria, to represent the most vulnerable urban areas on which it is a priority to act. Among the study's limitations are the lack of individual-level data, the absence of actual consumption measurements, and the reliance on estimated average tariffs. Future research should incorporate more gender variables to expand the analysis of the feminization of EP.

CONCLUSIONS

Although the city of Granada has been identified as having a high energy vulnerability, the interrelationships between the levels of vulnerable statistical areas, officially recognized in the city of Granada, and their energy-social reality had not been analyzed until now. As reflected in the results, there is a relationship between high levels of VCAs and energy poverty across different dimensions. The main cause of this relationship is low family income (a socio-economic factor), since the city's built environment is characterized by very poor energy performance. In this sense, even in areas that do not have a risk of VCA, significant percentages of cases of energy poverty appear. This raises a binomial in the course of the strategies: on the one hand, the need to redefine the methodology for cataloging VCAs if it is intended to serve as a reference for identifying the areas most at risk of energy poverty in the city. On the other hand, the commitment to energy rehabilitation aims to address one of the factors that drive the proliferation of energy poverty: the inefficiency of city housing. This is especially relevant in the city, since a large share of the city's census sections are not in monetary poverty (except for the cases indicated in the results section).

Similarly, the results have highlighted a possible association between the gender dimension and the city's energy poverty. In this sense, dimensions such as the feminization of loneliness and the foreign population being the majority in the city are usually associated with a lower level of income for families. As

a result of this study, it is expected that these findings will provide a starting point for integrating gender studies into cases of energy poverty, both in Granada and in other cities. Expanding the scale of analysis and incorporating disaggregated data at other levels will allow for the establishment of more robust correlations regarding the implications of energy poverty and gender.

CONTRIBUTION OF AUTHORS CRediT

Conceptualization, D.B.H.; Data Curation, A.A.A. and M.D.H.T.; Formal analysis, S.C.N. and A.S.J.; Acquisition of D.B.H. funding; Research, D.B.H., S.C.N. and A.S.J.; Methodology, A.A.A. and M.D.H.T.; Project Management, D.B.H.; Resources, D.B.H., S.C.N. and A.S.J.; Software, A.A.A. and M.D.H.T.; Supervision, D.B.H. and S.C.N.; Validation, S.C.N.; Visualization, A.S.J.; Writing - original draft, D.B.H. and S.C.N.; Writing - proofreading and editing, A.A.A., M.D.H.T. and A.S.J.

ACKNOWLEDGMENTS

This research was funded by the Ministry of Equality and the Women's Institute of the Government of Spain within the framework of the project 31-01-ID25 entitled "Gender perspective in energy poverty in Spain. Holistic analysis from the urban environment of Spanish cities". It is also part of the INV-INC300 2025 project "Characterization of the feminization of energy poverty in the built environment of the metropolitan area of Granada" funded through the University of Granada.

BIBLIOGRAPHIC REFERENCES

Aguilar, A. J., Guerrero-Rivera, M. F., & de la Hoz-Torres, M. L. (2025). Identifying urban energy-vulnerable areas: a machine learning approach. *Journal of Building Engineering*, *109*, 113047. https://doi.org/10.1016/j.jobe.2025.113047

Alguacil Denche, A., Llano Ortiz, J. C., & Sanz Angulo, A. (2024a). *14º informe. El Estado de la Pobreza. Seguimiento de los indicadores de la Agenda UE 2030 (2015-2023)*. European Anti-Poverty Network [EAPN]. https://www.eapn.es/publicaciones/566/xiv-informe-sobre-el-estado-de-la-pobreza-seguimiento-de-los-indicadores-de-la-agenda-ue-2030-informe-estatal

Antepara, I., Papada, L., Gouveia, J. P., Katsoulakos, N., & Kaliampakos, D. (2020). Improving energy poverty measurement in southern European regions through equivalization of modeled energy costs. *Sustainability,12*(14), 5721. https://doi.org/10.3390/su12145721

Bienvenido-Huertas, D., Rubio-Bellido, C., Farinha, F., Oliveira, M. J., & Pérez-Ordóñez, J. L. (2020). Evaluating the potential of adaptive comfort approach using historic data to reduce energy consumption in buildings in southern Spain. *Building and Environment*, *185, 107313*. https://doi.org/10.1016/j.buildenv.2020.107313

Bradshaw, S., Chant, S., & Linneker, B. (2017). Gender and poverty: what we know, don't know, and need to know for Agenda 2030. *Gender, Place & Culture*, *24*(12), 1667–1688. https://doi.org/10.1080/0966369X.2017.1395821

Calama-González, C. M., Escandón, R., Suárez, R., Alonso, A., & León-Rodríguez, Á. L. (2024). Household energy vulnerability evaluation in southern Spain through parametric energy simulation models and socio-economic data. *Sustainable Cities and Society*, *103*, 105276. https://doi.org/10.1016/j.scs.2024.105276

Capetillo-Ordaz, N. B., Martín-Consuegra, F., Alonso, C., Terés-Zubiaga, J., & Koutra, S. (2024). Inclusivity in urban energy transitions: A methodological approach for mapping gendered energy vulnerability. *Energy Research and Social Science*, *109*, 103426. https://doi.org/10.1016/j.erss.2024.103426

Castaño-Rosa, R., Solís-Guzmán, J., & Marrero, M. (2020). Energy poverty goes south? Understanding the costs of energy poverty with the index of vulnerable homes in Spain. *Energy Research and Social Science*, *60*, 101325. https://doi.org/10.1016/j.erss.2019.101325

Cecelski, E. (2004). *Re-thinking gender and energy: Old and new directions*. ENERGIA/EASE Discussion Paper. https://assets.publishing.service.gov.uk/media/57a08ccded915d3cfd001612/R8346-ConceptRev.pdf

Clancy, J. S. (2016). *In the light of what we know: Gender and energy transformations*. University of Twente.

Clancy, J. S., Daskalova, V. I., Feenstra, M. H., Franceschelli, N., & Sanz, M. (2017). *Gender perspective on access to energy in the EU*. Publications Office of the European Union.

Delgado, L. (Coord.). (2018). *Radiografies de la situació del dret a l'habitatge, la pobresa energètica i el seu impacte en la salut a Barcelon*. Dilogic S.L. https://www.aspb.cat/wp-content/uploads/2018/05/Informe1-Radiografies-DretHabitatge-PobresaEnergetica-Salut-Barcelona.pdf

Endesa. (01 de diciembre de 2025). *¿Qué potencia necesitan los electrodomésticos de tu casa? Guía práctica con ejemplo y tabla*. Endesa S.A. https://www.endesa.com/es/blog/blog-de-endesa/luz/que-potencia-electrica-necesitas

Faiella, I., & Lavecchia, L. (2021). Energy poverty. How can you fight it, if you can't measure it? *Energy and Buildings*, *233*, 110692. https://doi.org/10.1016/j.enbuild.2020.110692

Instituto Nacional de Estadística [INE]. (30 de junio de 2023). *Censo de Población y Viviendas - 2021*. INE base. https://www.ine.es/dyngs/INEbase/operacion.htm?c=Estadistica_C&cid=1254736177108&menu=ultiDatos&idp=1254735572981

Instituto Nacional de Estadística [INE]. (21 de octubre de 2025). *Atlas de Distribución de Renta de los Hogares. Año 2023*. INE base. https://www.ine.es/dyngs/INEbase/operacion.htm?c=Estadistica_C&cid=1254736177088&menu=ultiDatos&idp=1254735976608

Junta de Andalucía. (01 de junio de 2025). *Registro de certificados energéticos de Andalucía*. Datos.gob.es. Gobierno de España - Ministerio para la Transformación Digital y de la Función Pública https://datos.gob.es/es/catalogo/a01002820-registro-de-certificados-energeticos-de-andalucia

Listo, R. (2018). Gender myths in energy poverty literature: A Critical Discourse Analysis. *Energy Research and Social Science*, *38*, 9–18. https://doi.org/10.1016/j.erss.2018.01.010

Longhurst, N., & Hargreaves, T. (2019). Emotions and fuel poverty: The lived experience of social housing tenants in the United Kingdom. *Energy Research and Social Science*, *56*, 101207. https://doi.org/10.1016/j.erss.2019.05.017

McDowell, L. (1999). *Gender, identity and place: Understanding feminist geographies*. University of Minnesota Press.

Ministerio de Transportes Movilidad y Agenda Urbana. (2021). *Catálogo de Barrios Vulnerables de España 2011*. Ministerio de Transportes, Movilidad y Agenda Urbana / Universidad Politécnica de Madrid. https://cdn.mitma.gob.es/portal-web-drupal/vivienda/barrios_vunerables/bbvv_2011_01_andalucia.pdf

Panda, A. (2017). Climate change, drought and vulnerability. In S. Iradaya Rajan & R.B. Bhagat (Eds.), *Climate Change, Vulnerability and Migration*. Routledge India. https://doi.org/10.4324/9781315147741-10

Pérez-Fargallo, A., Clavijo-Núñez, S., Rubio-Bellido, C., Bienvenido-Huertas, D., & Serrano-Jiménez, A. (2026). Defining socio-climate-energy zones based on photovoltaic potential to support new standards for eliminating energy poverty in Chile. *Journal of Cleaner Production*, 554, 148127. https://doi.org/10.1016/j.jclepro.2026.148127

Ramírez, M. J. (14 de enero de 2023). *Granada, tercera capital andaluza que más padece la pobreza energética*. GranadaDigital. https://www.granadadigital.es/granada-pobreza-energetica-tercera-capital-andaluza/

Real Decreto 216 de 2014 [Ministerio de Industria Energía y Turismo]. Por el que se establece la metodología de cálculo de los precios voluntarios para el pequeño consumidor de energía eléctrica y su régimen jurídico de contratación. 28 de marzo de 2014. BOE, (77). https://www.boe.es/buscar/act.php?id=BOE-A-2014-3376

Romero Mora, J. C., Barrella, R., & Centeno Hernáez, E. (2024). *Informe de Indicadores de Pobreza Energética en España 2023*. Cátedra de Energía y Pobreza. Escuela Técnica Superior de Ingeniería [ICAI] – Universidad Pontificia Comillas. https://www.iit.comillas.edu/documentacion/informetecnico/IIT-24-303I/Informe_de_Indicadores_de_pobreza_energ%C3%A9tica_en_Espa%C3%B1a_2023.pdf

Sánchez-Guevara Sánchez, C., Sanz Fernández, A., Núñez Peiró, M., & Gómez Muñoz, G. (2020a). Energy poverty in Madrid: Data exploitation at the city and district level. *Energy Policy*, *144*, 111653. https://doi.org/10.1016/j.enpol.2020.111653

Sánchez-Guevara Sánchez, C., Sanz Fernández, A., & Núñez Peiró, M. (2020b). Feminisation of energy poverty in the city of Madrid. *Energy and Buildings*, *223*, 110157. https://doi.org/10.1016/j.enbuild.2020.110157

Sanz Fernández, A., Gómez Muñoz, G., Sánchez-Guevara Sánchez, C., & Núñez Peiró, M. (2016). *Estudio técnico sobre pobreza energética en la ciudad de Madrid*. Ayuntamiento de Madrid. https://www.madrid.es/UnidadesDescentralizadas/Consumo/NuevaWeb/pobreza%20energ%C3%A9tica/Copy%20of%20Estudio%20Pobreza%20energ%C3%A9tica%204%20febrero%202017.pdf

Secretaría Técnica de European Anti-Poverty Network [EAPN-ES]. (Coodr.). (2024). *Informe Poverty Watch 2024*. European Anti-Poverty Network - España [EAPN-ES]. https://www.eapn.es/ARCHIVO/documentos/documentos/1734609856_informe_poverty_watch_eapn2024.pdf

Viveros Vigoya, M. (2016). Interseccionalidad: Una Aproximación Situada a La Dominación. *Debate Feminista*, *52*, 1–17. https://doi.org/10.1016/j.df.2016.09.005

Recibido 13/02/2026
Aceptado 27/05/2026

ANÁLISIS PARAMÉTRICO VALIDADO MEDIANTE MEDICIONES EN TERRENO DEL CONFORT TÉRMICO EXTERIOR EN ESTACIONAMIENTOS EN TIRUCHIRAPPALLI, INDIA

FIELD-VALIDATED PARAMETRIC ANALYSIS OF OUTDOOR THERMAL COMFORT IN PARKING ENVIRONMENTS IN TIRUCHIRAPPALLI, INDIA

ANÁLISE PARAMÉTRICA VALIDADA EM CAMPO DO CONFORTO TÉRMICO EXTERNO EM AMBIENTES DE ESTACIONAMENTO EM TIRUCHIRAPPALLI, ÍNDIA

Amalan-Sigmund Kaushik-S (Autor de Correspondencia)
Master's in Architecture
Assistant Professor, Department of Architecture
National Institute of Technology Tiruchirappalli
Tiruchirappalli, India
https://orcid.org/0000-0003-3260-4485
kaushik@nitt.edu

Gopalakrishnan Padmanaban
Ph.D. in Architecture
Assistant Professor, Department of Architecture
National Institute of Technology Tiruchirappalli
Tiruchirappalli, India
https://orcid.org/0000-0002-4762-4430
gopal@nitt.edu

Subbaiyan Gnanasambandam
Ph.D. in Architecture
Professor, Department of Architecture
National Institute of Technology Tiruchirappalli
Tiruchirappalli, India
https://orcid.org/0000-0003-4406-034X
subbaiah@nitt.edu

CC BY SA

RESUMEN

La rápida urbanización en ciudades de clima cálido-húmedo ha intensificado el estrés térmico en los estacionamientos con superficies impermeables. Este estudio evalúa la influencia combinada del albedo superficial, del Índice de Reflectancia Solar (SRI, por su sigla en inglés) de la cubierta, de la cobertura vegetal y de la orientación sobre el confort térmico exterior en Tiruchirappalli, India, mediante mediciones en terreno y simulaciones microclimáticas. Este tipo de mediciones, realizadas en tres tipologías de estacionamiento, se utilizaron para validar simulaciones con ENVI-met (R^2 = 0.931 para MRT). Una matriz paramétrica generó treinta y dos iteraciones de diseño en cuatro orientaciones. Los resultados indican que la temperatura radiante media es el principal factor del disconfort térmico. El aumento del albedo superficial y del SRI de la cubierta no redujo de forma consistente el UTCI debido a los efectos de la radiación reflejada. En contraste, una cobertura vegetal del 60 % redujo significativamente el estrés térmico máximo en todas las orientaciones. La orientación este–oeste intensificó la acumulación de calor por la tarde, mientras que la orientación noroeste–sudeste moderó el estrés térmico máximo. La configuración óptima del albedo de 0,2, SRI de 30 y vegetación al 60% en la orientación noroeste-sureste produjo el UTCI medio más bajo (32,49 °C).

Palabras clave
confort térmico exterior, índice universal de clima térmico (UTCI), albedo superficial

ABSTRACT

Rapid urbanization in warm–humid cities has intensified thermal stress in impervious parking environments. This study evaluates the combined influence of surface albedo, roof Solar Reflectance Index (SRI), vegetation cover, and orientation on outdoor thermal comfort in Tiruchirappalli, India, using field measurements and microclimate simulations. Field measurements from three parking typologies were used to validate ENVI-met simulations (R^2 = 0.931 for MRT). A parametric matrix generated thirty-two design iterations across four orientations. Results indicate that mean radiant temperature is the dominant driver of thermal discomfort. Increasing surface albedo and roof SRI alone did not consistently reduce UTCI due to reflected radiation effects. In contrast, 60% vegetation cover significantly reduced peak thermal stress across all orientations. East–West alignment intensified afternoon heat accumulation, whereas Northwest–Southeast orientation moderated peak stress. The optimal configuration of albedo 0.2, SRI 30, and 60% vegetation under NW–SE orientation produced the lowest mean UTCI (32.49 °C).

Keywords
outdoor thermal comfort, universal thermal climate index (UTCI), surface albedo

RESUMO

A rápida urbanização em cidades de clima quente e úmido tem intensificado o estresse térmico em ambientes de estacionamento impermeáveis. Este estudo avalia a influência combinada do albedo de superfície, do Índice de Refletância Solar (SRI, do inglês Solar Reflectance Index) da cobertura, da cobertura vegetal e da orientação sobre o conforto térmico externo em Tiruchirappalli, Índia, por meio de medições em campo e simulações microclimáticas. Medições de campo em três tipologias de estacionamento foram utilizadas para validar as simulações no ENVI-met (R^2 = 0,931 para a TRM). Uma matriz paramétrica gerou trinta e duas iterações de projeto distribuídas em quatro orientações. Os resultados indicam que a temperatura radiante média é o principal fator determinante do desconforto térmico. O aumento isolado do albedo de superfície e do SRI da cobertura não reduziu de forma consistente o UTCI, devido aos efeitos da radiação refletida. Em contrapartida, uma cobertura vegetal de 60% reduziu significativamente o pico de estresse térmico em todas as orientações. O alinhamento leste–oeste intensificou o acúmulo de calor no período da tarde, ao passo que a orientação noroeste–sudeste atenuou o pico de estresse. A configuração ideal de albedo de 0,2, SRI de 30 e 60% de cobertura vegetal, com orientação noroeste-sudeste, resultou no menor UTCI médio (32,49 °C).

Palavras-chave
conforto térmico externo, índice climático térmico universal (UTCI), albedo de superfície

INTRODUCCIÓN

La rápida urbanización ha intensificado el efecto de isla de calor urbana (ICU) al reemplazar la tierra con vegetación por materiales impermeables, elevando las temperaturas de la superficie terrestre (TST) en ciudades de rápido crecimiento como Tiruchirappalli (Calhoun et al., 2024; Deepthi et al., 2024). La magnitud de la ICU está fuertemente determinada por la morfología urbana y las características de la superficie, incluidas la reflectividad, la densidad y la distribución de la vegetación (Huang et al., 2025). Entre las tipologías impermeables horizontales, los estacionamientos constituyen una infraestructura térmicamente crítica, pero poco examinada (Sen, Fernández y Roesler, 2020). La expansión de la propiedad de vehículos privados en contextos residenciales e institucionales ha aumentado sustancialmente la extensión de las áreas de estacionamiento pavimentadas, exacerbando la acumulación localizada de calor y la incomodidad al aire libre (Lin, Song y Qin, 2021; Patel y Kaushik, 2023).

Los climas cálidos y húmedos plantean distintos desafíos térmicos. La humedad elevada restringe el enfriamiento por evaporación, lo que agrava el estrés fisiológico incluso con una variación moderada de la temperatura del aire (Ta). En tales entornos, la temperatura radiante media (TRM) suele dominar la percepción térmica exterior. Las superficies abiertas de asfalto, concreto y adoquines absorben y almacenan la radiación solar, lo que aumenta la temperatura de la superficie y la reradiación de onda larga (Sen et al., 2020). Los materiales de bajo albedo intensifican la acumulación de calor (Ghenai et al., 2023), mientras que la sombra limitada expone a los peatones a una radiación solar directa sostenida. En consecuencia, las áreas de estacionamiento a menudo superan los umbrales de confort térmico durante las horas pico del verano.

Las estrategias de mitigación basadas en materiales, en particular la mejora del albedo de la superficie y los techos reflectantes, han sido ampliamente investigadas. El aumento del albedo del pavimento reduce la absorción solar (Ghenai et al., 2023) y se han propuesto estacionamientos reflectantes como estrategias de mitigación de la ICU a microescala (Sen et al., 2020). Sin embargo, un albedo más alto puede aumentar la radiación de onda corta reflejada a nivel peatonal, elevando la TRM y compensando las posibles ganancias de confort (Taleghani, 2018; Ghoniem, Fahmy y Kamel, 2025). De manera similar, los sistemas de techado con valores altos del Índice de Reflectancia Solar (IRS) reducen el calentamiento de la superficie y contribuyen a una mitigación más amplia de la ICU (Nutakki et al., 2023; Jandaghian, Lacasse y Guar, 2025). Sin embargo, en tipologías de estacionamientos semicubiertos, la radiación reflejada puede redistribuir la carga térmica en lugar de eliminarla, particularmente en espacios que carecen de vegetación y de un flujo de aire efectivo.

La vegetación demuestra consistentemente un potencial de enfriamiento superior al de los materiales reflectantes. Convertir áreas de estacionamiento pavimentadas en espacios cubiertos por árboles reduce significativamente el estrés térmico (Parison et al., 2023). Los árboles reducen la TRM mediante la sombra y la evapotranspiración, mientras moderan la Ta (Rodríguez et al., 2025; Wei, Cheng y Lin, 2025). Estrategias más amplias de ecologización urbana han demostrado un enfriamiento nocturno y una mayor estabilidad térmica (Calhoun et al., 2024) y la infraestructura verde mejora el confort térmico en contextos climáticos (Gidey y Mhangara, 2025; Silva Nascimento et al., 2025). La estructura de la vegetación, incluida la densidad y la configuración de la copa de los árboles, influye aún más en los resultados de comodidad de los peatones (He y Reith, 2023; Pattnaik, Rahman y Pauleit , 2025). De hecho, los análisis comparativos indican que la plantación de árboles puede superar a los pavimentos de bajo albedo en la optimización del confort estival (Zhang et al., 2025).

La orientación espacial introduce un parámetro adicional, aunque menos integrado. La alineación urbana influye en la interceptación solar, la dinámica de las sombras y la distribución del flujo de aire (Abdelwahab, Fekry y Hamed, 2025; Huang et al., 2025). Ciertas orientaciones prolongan la exposición de la tarde e intensifican la acumulación radiante, mientras que las configuraciones oblicuas pueden moderar el estrés máximo (Rachidi et al., 2026). Estudios en contextos indios confirman que la orientación afecta significativamente la ganancia de calor solar y el rendimiento microclimático (Kaushik S. y Amraotkar, 2026; Peter y Kaushik, 2024; Pachauri y Kaushik S., 2025). Sin embargo, los efectos combinados de la orientación, la reflectividad de la superficie y la densidad de la vegetación en las tipologías de estacionamiento aún no se han cuantificado lo suficiente.

La evaluación del confort térmico en exteriores se basa en índices que integran parámetros meteorológicos y radiativos. El Índice Universal de Clima Térmico (UTCI, en inglés), la Temperatura Fisiológica Equivalente (TE) y el Índice de Calor (IC) se emplean ampliamente para evaluar el estrés térmico en los peatones (Silva Nascimento et al., 2025; Peter y Kaushik, 2024). Los índices de confort térmico en exteriores, como UTCI y TE, incorporan la TRM y, por lo tanto, son particularmente adecuados para evaluar las condiciones térmicas de los peatones en entornos exteriores altamente radiactivos. Por el contrario, el IC considera principalmente la temperatura del aire y la humedad relativa y no tiene en cuenta explícitamente el intercambio radiativo ni los efectos del viento. El UTCI fue seleccionado en este estudio debido a su amplia aplicación en la investigación del clima urbano al aire libre y a su idoneidad para evaluar las condiciones térmicas dinámicas en exteriores de ambientes cálidos y húmedos (Wang et al., 2020; Kafy, Alsulamy y Alsaleh, 2026). Dado que el estudio se realizó en un clima tropical cálido-húmedo, los valores de UTCI se interpretaron utilizando la escala calibrada de clima cálido-húmedo propuesta en la literatura reciente, en la que 21,8–30,9 °C corresponde a la ausencia de estrés térmico y 30,9–39,0 °C a estrés térmico moderado (Chen, Fang y Hwang, 2025). Estudios recientes en climas tropicales también han combinado la validación ENVI-met con mediciones de campo y evaluaciones del confort térmico de los peatones para evaluar la efectividad de las estrategias integradas de mitigación bioclimática en ambientes al aire libre (Austin, Solano y Chen Austin, 2025).

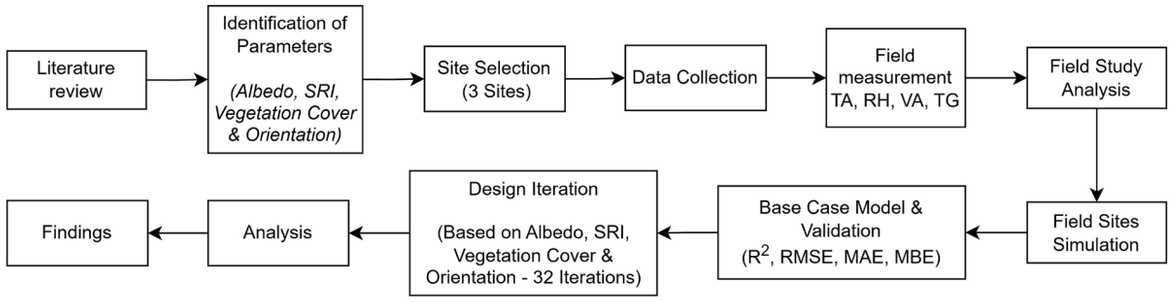


Figura 1. Metodología. Fuente: Preparado por los autores.

A pesar de la extensa investigación independiente sobre albedo, techos fríos, vegetación y orientación, los análisis integrados y validados en terreno que combinan estos parámetros en entornos de estacionamiento cálidos y húmedos siguen siendo limitados. La mayoría de los estudios se centran en intervenciones aisladas o en climas cálidos, áridos y templados, donde los equilibrios evaporativos y radiativos difieren sustancialmente. Esta brecha restringe el desarrollo de pautas de diseño que respondan al clima y puede conducir a soluciones muy simplistas basadas en la reflectividad, que aumentan inadvertidamente la exposición radiante de los peatones.

Este estudio aborda esta deficiencia mediante una investigación combinada basada en mediciones de campo y en simulación en Tiruchirappalli, India. Se instrumentaron tres tipologías representativas de estacionamiento en condiciones pico de verano y se utilizaron los datos para validar simulaciones en ENVI-met (R^2 de hasta 0,931 para MRT). Posteriormente, una matriz paramétrica estructurada evaluó treinta y dos iteraciones de diseño en cuatro orientaciones, variando sistemáticamente el albedo de la superficie, el IRS del techo y la cobertura vegetal. Al integrar el manejo radiativo, la densidad de la copa de los árboles y la alineación solar dentro de un marco cálido-húmedo validado, esta investigación avanza en la comprensión de la dinámica térmica a nivel peatonal en entornos de estacionamiento y propone una estrategia de optimización sensible a la orientación para un diseño tropical sensible al clima.

Aunque estudios previos han examinado la vegetación, los pavimentos reflectantes, los techos fríos y la orientación de forma independiente, pocas investigaciones han cuantificado su interacción combinada en entornos de estacionamiento, en condiciones climáticas cálidas y húmedas, mediante simulaciones validadas en terreno. La literatura existente generalmente evalúa estas medidas de mitigación de forma aislada, lo que limita el desarrollo de una guía de diseño práctica para entornos urbanos reales donde la vegetación puede verse limitada por el espacio, el mantenimiento o la disponibilidad de agua. Este estudio aborda esta brecha al identificar cómo la orientación modifica el rendimiento térmico de la reflectividad de la superficie y de la cubierta de la copa de los árboles, y al establecer una jerarquía de estrategias de mitigación para los microclimas de estacionamiento.

En consecuencia, este estudio tiene como objetivo no solo cuantificar la influencia individual y combinada del albedo de la superficie, el IRS del techo, la cubierta vegetal y la orientación espacial en el confort térmico exterior a nivel peatonal en entornos de estacionamiento, sino también identificar la efectividad relativa y la jerarquía de interacción de estas variables de diseño en condiciones climáticas cálidas y húmedas. Otro objetivo es traducir los resultados de la simulación en un marco práctico de apoyo a la toma de decisiones para contextos en los que la vegetación es limitada o inviable.

Sobre la base de estudios previos de confort térmico urbano, la investigación plantea la hipótesis de que: (1) la cubierta vegetal ejerce una influencia más fuerte en el confort térmico de los peatones que las propiedades de los materiales reflectantes; (2) el aumento del albedo de la superficie y el iRS del techo puede no mejorar proporcionalmente el UTCI debido a la mayor radiación reflejada de onda corta y la TRM elevada; (3) las orientaciones diagonales, como noroeste–sureste, reducen el estrés térmico máximo de manera más efectiva que la alineación este–oeste en condiciones solares tropicales y; (4) la efectividad térmica de las estrategias de mitigación reflectante depende de la orientación y el contexto de la vegetación, lo que indica que el albedo y el IRS del techo no pueden evaluarse independientemente de la geometría solar y las condiciones de la copa de los árboles.

METODOLOGÍA

Este estudio adoptó un marco computacional empírico integrado para evaluar el confort térmico al aire libre en entornos de estacionamiento urbano en condiciones climáticas cálidas y húmedas. El enfoque metodológico combinó mediciones microclimáticas de campo, simulaciones numéricas tridimensionales con ENVI-met v5.7.2, validación estadística de los resultados simulados y evaluación paramétrica sistemática de las variables de diseño. El flujo de trabajo secuencial, desde la caracterización del sitio hasta el análisis de optimización, se ilustra en la Figura 1.

Sitio	Orientación	Superficie del suelo (albedo)	Condición del techo (SRI)	Vegetación-en el sitio	Vegetación-contexto (N/S/E/O)
S01	330°–150° (N–S)	Camino de entrada: adoquines (0,25) Estacionamiento: adoquines (0,25)	Camino de entrada: descubierto. Estacionamiento: lámina GI azul (SRI 24)	3 árboles; altura del tronco 4-5 m; copa escasa	N: 4-5 neem (diámetro 1,5-2,5 m) S: 3 neem (diámetro 2-3 m) + arbustos + pasto E: 1 tronco grande y grueso (diámetro 2 m) + 1 árbol corto y denso (diámetro 4-5 m) O: 2 árboles de tronco mediano (diámetro 3-4 m; densidad media)
S02	0°–180° (N–S)	Camino de entrada: adoquines (0,25) Estacionamiento: PCC (0,30)	Camino de entrada: descubierto Estacionamiento: lámina de metal revestida de verde (SRI 31)	Nulo	N: 1 densidad media (diámetro 4-5 m) + 4 densidad baja pequeña (diámetro ~1 m) S: sin vegetación E: sin vegetación O: 3 árboles de tronco mediano (diámetro 2-3 m; densidad media)
S03	0°–180° (N–S)	Camino de entrada: adoquines (0,25) Estacionamiento: adoquines (0,25)	Camino de entrada: parcialmente sombreado por árboles Estacionamiento: completamente bajo la sombra de los árboles	7 Árboles neem; densidad baja-media; tronco largo; sin arbustos; LAD: 3,5; LAI: 0,4 m²/m³	N: 2 neem (diámetro 4-5 m; densidad media; tronco largo) + edificio de 1 piso S: 2 neem (diámetro 4-5 m; densidad media) E: 2 neem (diámetro 4-5 m; densidad media) + banco (1 piso) O: 2 neem (diámetro 4-5 m; densidad media) Nota: los ángulos del tronco varían; ramificación escasa

Tabla 1. Características del Sitio 01 (S01), Sitio 02 (S02) y Sitio 03 (S03). Fuente: Preparado por los autores.

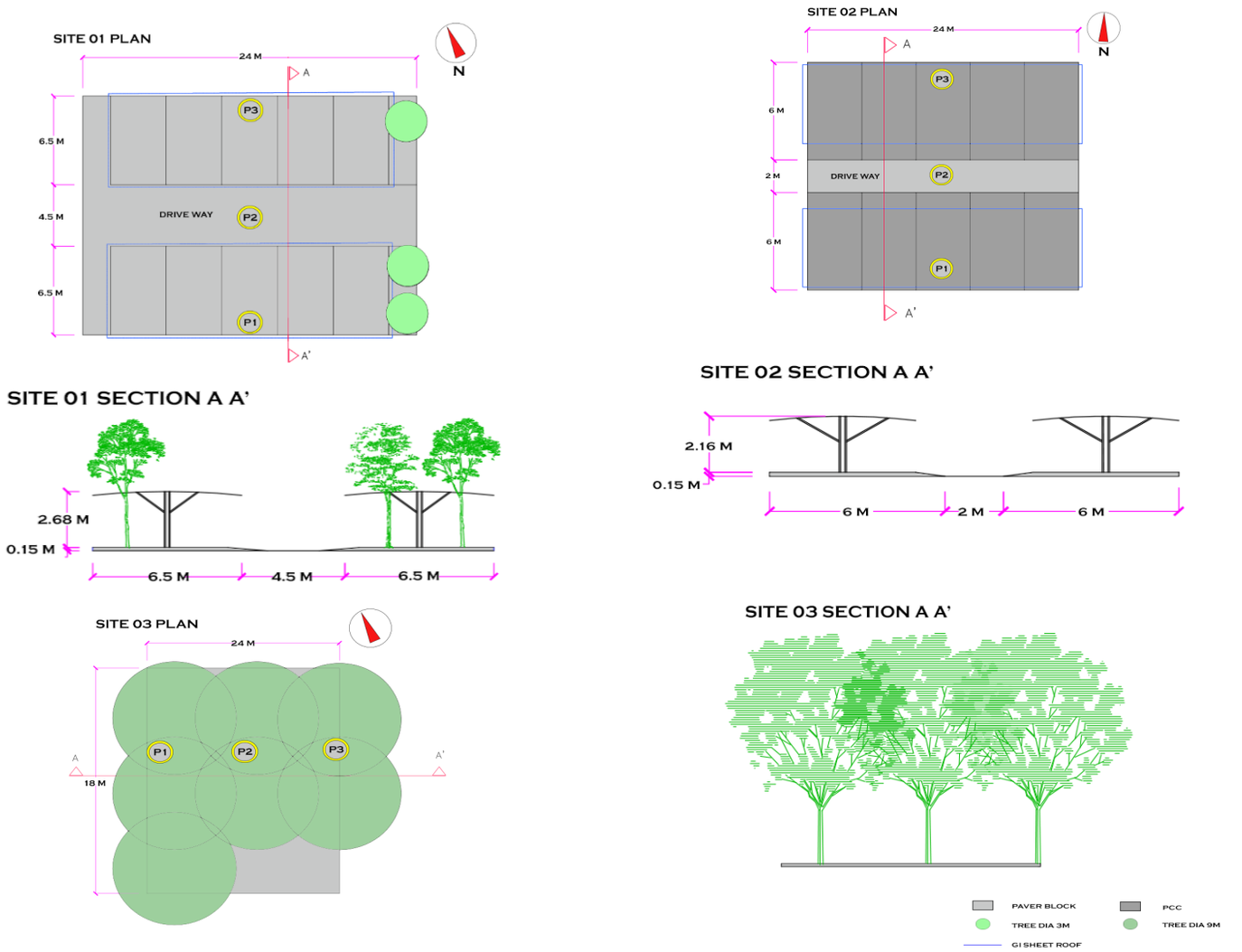


Figura 2. Ilustración de los Sitios 01, 02 y 03. Fuente: Preparado por los autores.

Parámetros	Unidades	Instrumento	Precisión	Imagen
Ta	oC	DeltaOHM_ HD32,3	1/3 DIN	
HR	%		±1,5% (0…90%RH) / ±2% (90…100%RH) @T=15…35°C (lectura de 1,5 + 1,5%) % @ T = rango restante	
Tg	oC		Clase 1/3 DIN	
Va	m/s		± 0,2 m/s (0,1÷1 m/s) ± 0,3 m/s (1÷5 m/s)	

Tabla 2. Parámetros e instrumentos utilizados en mediciones de campo. Fuente: Preparado por los autores.

El estudio se llevó a cabo en Tiruchirappalli (10,79°N), Tamil Nadu, India, una ciudad de nivel 2 de rápida urbanización caracterizada por una alta intensidad de radiación solar, humedad elevada y estrés térmico persistente en verano (Kaushik S. y Amraotkar , 2026; Pachauri y Kaushik S., 2025). Se seleccionaron tres tipologías representativas de estacionamiento para capturar la variación en los materiales de la superficie, las condiciones del techo, la presencia de vegetación y la orientación espacial. El sitio 01 (S01) comprende una configuración semicubierta con techo de metal galvanizado azul (SRI 24) y piso de adoquines (albedo 0.25). El sitio 02 (S02) incorpora techos de metal con revestimiento verde (SRI 31) y superficies mixtas de adoquines y PCC (albedo 0.25–0.30). El sitio 03 (S03) representa una tipología abierta, sombreada predominantemente por árboles maduros de neem (Azadirachta indica), sin techo artificial. Los diseños espaciales y las características seccionales se ilustran en la Figura 2, mientras que los atributos físicos detallados se presentan en la Tabla 1.

Las mediciones en terreno se realizaron el 28 de mayo de 2025, día que se identificó como el más caluroso de la región según los datos meteorológicos decenales. El día seleccionado se caracterizó por una alta intensidad de radiación solar, condiciones de cielo despejado predominantes y temperaturas ambientales elevadas, propias de la exposición extrema al calor del verano en Tiruchirappalli. Por lo tanto, la campaña de medición tenía como objetivo evaluar el estrés térmico a nivel de peatones en condiciones climáticas cálidas y húmedas máximas. Si bien el enfoque seleccionado de días extremos permite evaluar las condiciones de estrés térmico máximo relevantes para el diseño de estacionamientos sensibles al clima, investigaciones adicionales sobre varios días y varias estaciones mejorarían aún más la generalización a climas más amplios. Los datos se registraron durante tres períodos representativos de exposición peatonal: mañana (MAÑ), 9:45-10:45; tarde (TAR), 12:45-13:45; y noche (NOC), 16:45-17:45. En cada sitio, se establecieron tres puntos de medición para representar las zonas expuestas y sombreadas/cubiertas. Todas las mediciones se tomaron a 1,5 m sobre el nivel del suelo para reflejar la exposición térmica de los peatones. La TRM se calculó a partir de las mediciones de temperatura global (Tg), siguiendo los procedimientos de la ISO 7726 para entornos térmicos al aire libre. Las mediciones se obtuvieron con un termómetro de globo negro estándar, con emisividad de 0,95 y un diámetro de 150 mm. El cálculo de MRT incorporó Tg, la temperatura del aire (Ta) y la velocidad del viento (Va) para considerar los efectos de la transferencia de calor por convección en condiciones exteriores (Ecuación 1). Los valores estimados de TRM están sujetos a incertidumbre asociada a la variabilidad en la medición de la temperatura global, la temperatura del aire y la velocidad del viento en condiciones de campo al aire libre. Todos los instrumentos se verificaron en terreno antes de las mediciones para garantizar la consistencia operativa en condiciones de verano al aire libre y cumplían con la norma ISO 7726. Las especificaciones de medición, las unidades y los rangos de precisión se resumen en la Tabla 2.

$$MRT = \left((T_g + 273.15)^4 + \left(\frac{1.10 \times 10^8 \times V_a^{0.6}}{\varepsilon \times D^{0.4}} \right) \times (T_g - T_a) \right)^{0.25} - 273.15$$

(Ecuación 1)

Donde:
Tg es la temperatura del globo (°C)
Ta es la temperatura del aire (°C)
Va es la velocidad del viento (m/s)
E es la emisividad del globo
D es el diámetro del globo (m).

Las simulaciones microclimáticas se realizaron utilizando ENVI-met v5.7.2, un modelo tridimensional no hidrostático capaz de resolver la transferencia radiativa, la dinámica del flujo de aire, los procesos de vegetación y las interacciones superficie–atmósfera a resolución microescala. El dominio computacional replicó la tipología de estacionamiento con una extensión horizontal de 24 m × 22 m. Se aplicó una resolución de cuadrícula de 2 m × 2 m en las direcciones horizontales, con una resolución vertical básica de 0,1 m para capturar gradientes cercanos al suelo relevantes para la comodidad de los peatones. Las simulaciones se realizaron en los mismos intervalos de tiempo que las observaciones de campo. Las variables de salida se extrajeron mediante la herramienta de posprocesamiento Leonardo.

Parámetro	Especificación
Software	ENVI-met v5.7.2
Fecha de simulación	28 de mayo de 2025
Resolución de cuadrícula	2 m (X), 2 m (Y), 0,1 m (Z)
Tamaño del dominio	24 m × 22 m
Métricas de evaluación	Ta; HR; Va; TRM; UTCI
Modelo de vegetación	Neem (Azadirachta indica); Altura: 9 m; Diámetro de la copa: 9 m; IAF: 3,5
Variables de diseño	Albedo: 0,2, 0,4, 0,6 SRI: 30, 60, 90 Cubierta vegetal: 0%, 20%, 40%, 60%
Períodos de simulación	Mañana (09:00-10:00); Tarde (13:00-14:00); Noche (16:00-17:00)
Iteraciones	32 escenarios de simulación

Tabla 3. Entradas y supuestos del modelo. Fuente: Preparado por los autores.

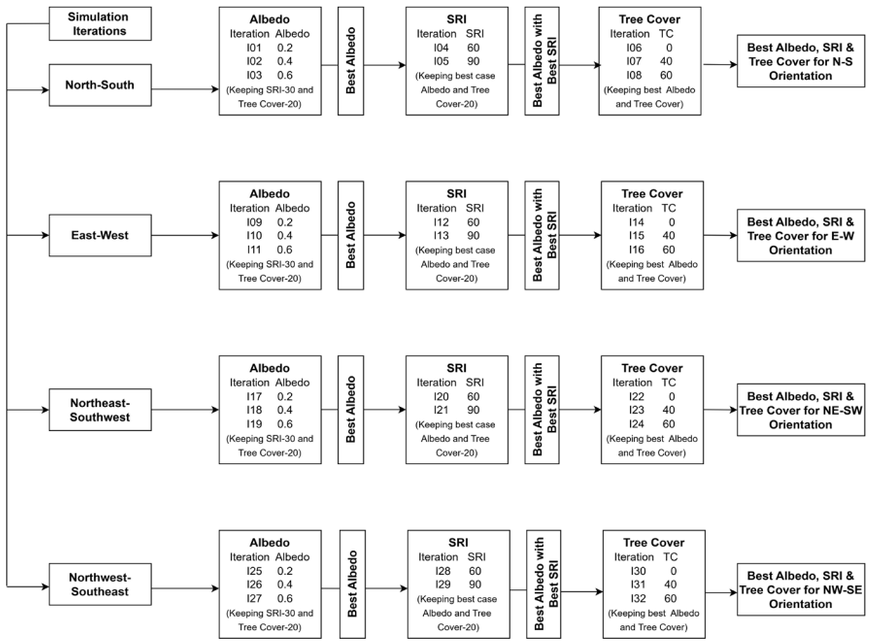


Figura 3. Iteraciones de diseño paramétrico. Fuente: Preparado por los autores.

Las simulaciones ENVI-met se inicializaron con las condiciones meteorológicas correspondientes al período de medición en terreno. La temperatura atmosférica inicial, la humedad relativa y las condiciones del viento se tomaron de observaciones de campo y de datos meteorológicos regionales del 28 de mayo de 2025. Las simulaciones se realizaron de forma continua durante 24 horas, desde las 22:00 del 27 de mayo de 2025 hasta las 22:00 del 28 de mayo de 2025, para estabilizar los procesos de intercambio de energía superficie–atmósfera antes del análisis diurno. La velocidad del viento a una altura de 10 m sobre el suelo se especificó en función de las condiciones medidas en el sitio, con una dirección predominante del viento de sur–suroeste. Se adoptaron condiciones de contorno de cielo despejado para representar el evento de calor extremo de verano investigado en este estudio. Las entradas y suposiciones del modelo se resumen en la Tabla 3. ENVI-met resuelve el intercambio radiativo directo, difuso y reflejado mediante algoritmos integrados de transferencia radiativa. Este estudio se centró principalmente en las respuestas de TRM y UTCI, en lugar de en la descomposición de los componentes individuales del flujo radiativo. El dominio computacional se desarrolló para representar el microclima de estacionamiento inmediato y los elementos contextuales circundantes que influyen en las condiciones térmicas a nivel peatonal. Si bien el tamaño del dominio seleccionado permitió un análisis detallado a microescala con una demanda computacional manejable, los posibles efectos de borde asociados a los dominios de simulación localizados se reconocen como una limitación del estudio.

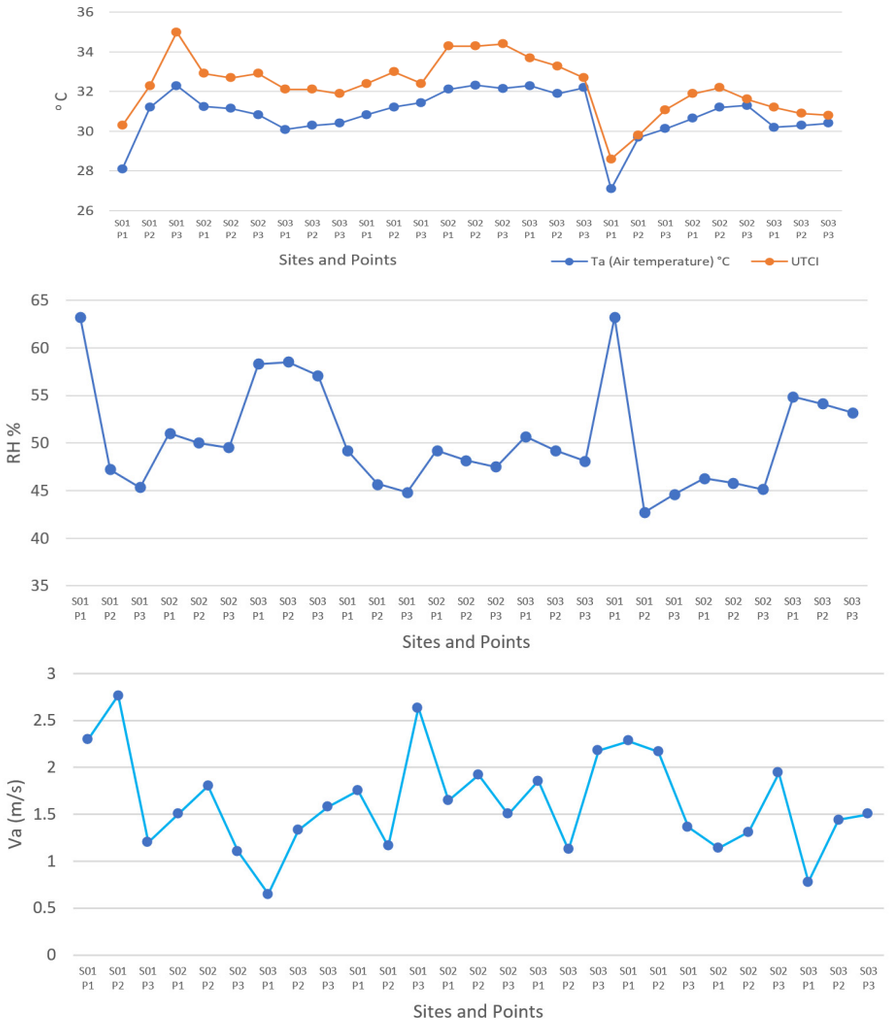


Figura 4. Datos de medición de campo de las series temporales de Ta, UTCI, HR y Va para S01, S02 y S03. Fuente: Preparado por los autores.

La validación del modelo se realizó comparando directamente los valores simulados y los medidos en idénticas condiciones espaciales y temporales. La confiabilidad predictiva se evaluó mediante el coeficiente de determinación (R^2), error cuadrático medio (RMSE, en inglés), error absoluto medio (MAE, en inglés) y error de sesgo medio (MBE, en inglés). Estos indicadores cuantifican la fuerza explicativa, la precisión de la dispersión y la desviación sistemática. Las estadísticas de validación se presentan en la Tabla 4. El fuerte acuerdo entre la Ta medida y la simulada y la TRM confirmó la idoneidad del modelo ENVI-met para la evaluación paramétrica posterior.

Luego de la validación, se desarrolló una matriz paramétrica estructurada para evaluar la influencia combinada del albedo de la superficie, el IRS del techo, la cobertura vegetal y la orientación espacial. Los valores de albedo superficial de 0,2, 0,4 y 0,6 representaron pavimentos de baja, media y alta reflectividad. Los valores del IRS del techo de 30, 60 y 90 simularon niveles variables de rendimiento reflectante. Los escenarios de vegetación modelaron Azadirachta indica con una altura de 9 m, un diámetro de copa de 9 m y un índice de área foliar (IAF) de 3,5 para representar las condiciones maduras de la copa de los árboles. La cobertura vegetal varió entre 0%, 20%, 40% y 60% a lo largo del perímetro del sitio para evaluar los efectos del sombreado y de la evapotranspiración.

La evaluación paramétrica siguió un enfoque matricial escalonado. Para cada orientación, norte–sur, este–oeste, noreste–suroeste y noroeste–sureste, se modeló primero una configuración de base que reflejaba la práctica local prevalente (albedo 0,2, SRI 30, 20% de vegetación). Posteriormente, se varió el albedo, manteniendo constantes el IRS y la vegetación, para determinar la reflectividad superficial óptima. Utilizando el valor de albedo identificado, se varió el IRS del techo y, posteriormente, se realizaron modificaciones sistemáticas en la cubierta vegetal. Este enfoque estructurado resultó en ocho iteraciones por orientación, produciendo un total de treinta y dos escenarios de simulación (I01-I32). Este diseño

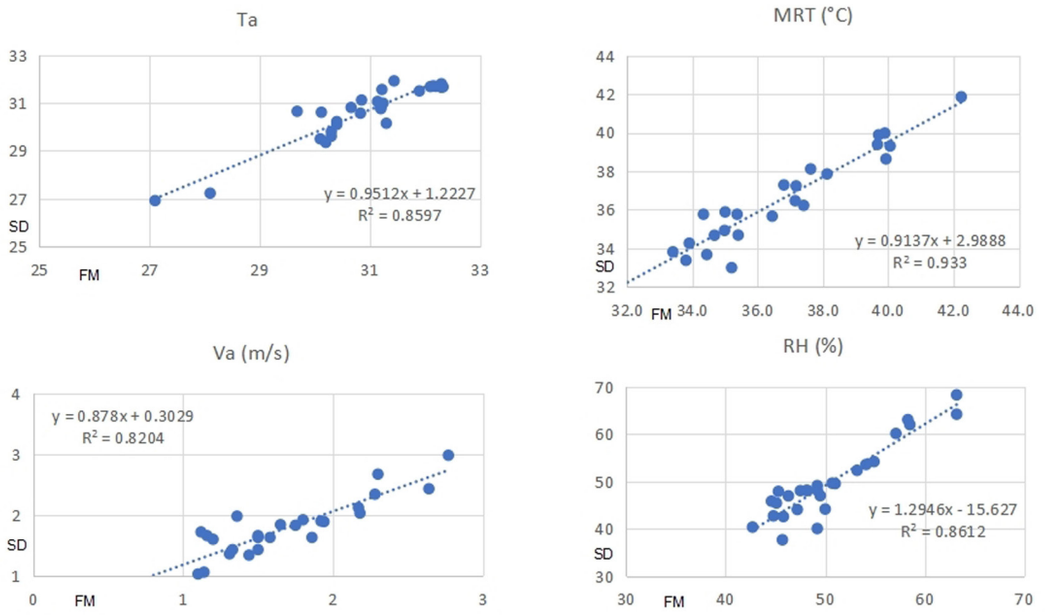


Figura 5. Validación de los datos de medición de campo (FM) y de simulación (SD). Fuente: Preparado por los autores.

Variable	R²	RMSE	MAE	MBE
Ta	0,795	0,55 °C	0,48 °C	-0,28 °C
HR	0,624	3,37 %	2,42 %	−0,76 %
Va	0,776	0,25 m/s	0,18 m/s	+0,10 m/s
MRT	0,931	0,77 °C	0,59 °C	−0,13 °C

Tabla 4. Estadísticas de validación que comparan variables medidas en terreno y de simulación. Fuente: Preparado por los autores.

basado en matrices permitió evaluar tanto los efectos de los parámetros individuales como sus interacciones bajo diferentes alineaciones solares (Figura 3). El rendimiento térmico en todos los escenarios se evaluó principalmente mediante el UTCI, con apoyo de los análisis de Ta y de TRM. El marco comparativo permitió identificar configuraciones optimizadas para reducir el estrés térmico de los peatones en entornos de estacionamiento tropicales.

RESULTADOS Y ANÁLISIS

ANÁLISIS DE MEDICIÓN DE CAMPO

Las mediciones en terreno evidenciaron una variación diurna pronunciada en las tres tipologías de estacionamiento (Figura 4). Todos los sitios registraron una escalada térmica progresiva de la mañana a la tarde, con un pico de estrés entre las 12:45 y las 13:45, seguido de una recuperación parcial por la noche. Sin embargo, la magnitud y la persistencia del estrés térmico variaron sistemáticamente en función de las características de la superficie, la configuración del techo y la presencia de vegetación.

Los sitios S01 y S02, ambos con techos de láminas metálicas con IRS de 24 y 31, de bajo a moderado, registraron TRM y UTCI elevados durante las horas pico. A pesar de la sombra parcial, los valores de UTCI de la tarde superaron los 33-34 °C en áreas semicubiertas y fueron más altos en las zonas expuestas del camino de entrada. El efecto combinado del pavimento de bajo albedo y la reradiación de los techos metálicos calentados intensificó la carga radiante. Las velocidades del viento bajo los cobertizos se redujeron, lo que limitó la disipación convectiva y amplificó aún más la acumulación térmica.

Por el contrario, el sitio S03, completamente sombreado por una copa de neem maduro y sin techo artificial, mostró una TRM consistentemente más baja durante las horas pico, a pesar de una temperatura del aire comparable. Por otro lado, el Sitio S03, completamente sombreado por una copa de neem maduro y sin techo artificial, mostró una TRM

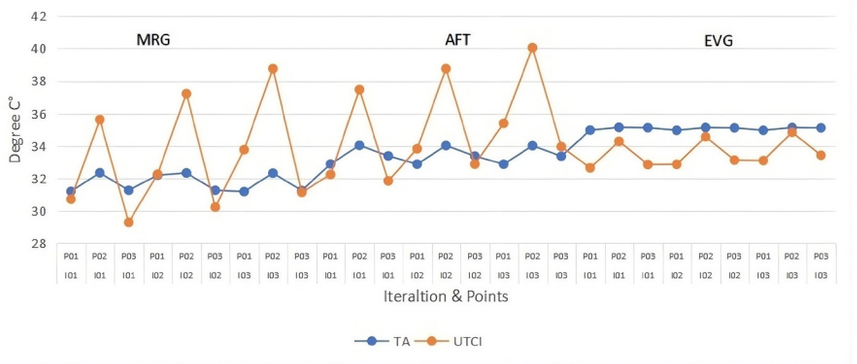


Figura 6. Datos de series temporales de Ta y UTCI para I01, I02, I03. Fuente: Preparado por los autores.

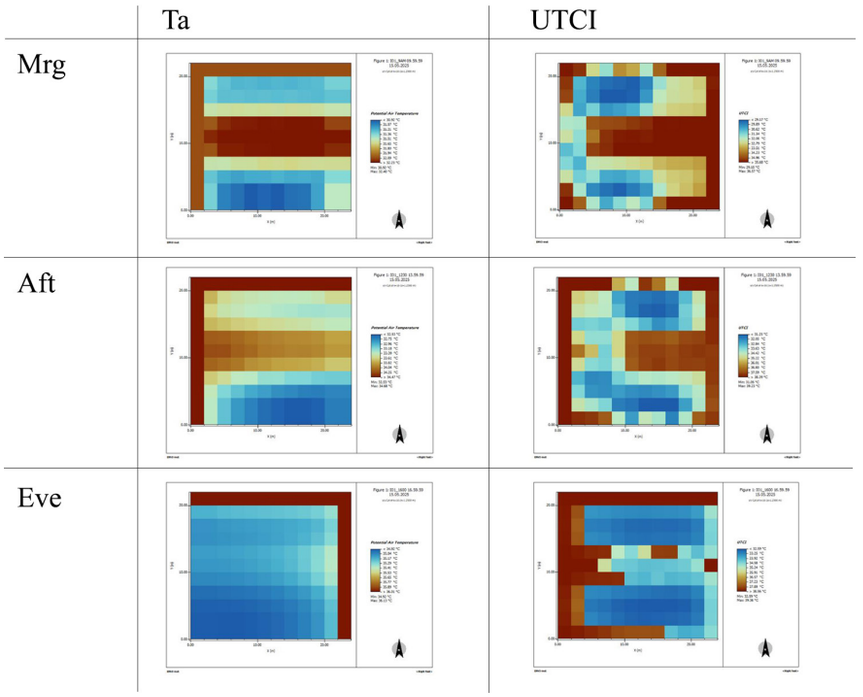


Figura 7. Mapa Ta y UTCI de I01. Fuente: Preparado por los autores utilizando Envi-met v5.7. 2.

consistentemente más baja durante las horas pico, a pesar de una temperatura del aire comparable. Además, el S03 mostró una recuperación nocturna más rápida, lo que indica un menor almacenamiento térmico y una estabilización microclimática mejorada por la evapotranspiración. Estas observaciones en terreno establecen la TRM como el diferenciador dominante entre las tipologías y proporcionan una base empírica para el análisis posterior basado en simulaciones.

ANÁLISIS DE CORRELACIÓN

El análisis de correlación de Pearson confirma el papel dominante de la exposición radiativa. La Ta ($r = 0.894$, $p < 0.001$) y la TRM ($r = 0.668$, $p < 0.001$) mostraron fuertes asociaciones positivas con el UTCI, mientras que la velocidad del viento mostró una correlación débil y no estadísticamente significativa. Los hallazgos refuerzan la conclusión de que en entornos de estacionamiento cálidos y húmedos, el intercambio de calor radiante ejerce una mayor influencia sobre el estrés de los peatones que los mecanismos convectivos.

VALIDACIÓN DEL MODELO

La validación del modelo se realizó comparando los parámetros simulados con los medidos en campo y con ENVI-met, en condiciones temporales y espaciales idénticas (Figura 5). Los resultados de la validación demuestran una concordancia aceptable ($R^2 = 0,931$; RMSE = 0,77 °C) entre los parámetros térmicos medidos y simulados en las condiciones climáticas investigadas, lo que indica que el modelo ENVI-met es adecuado para la evaluación paramétrica comparativa de los microclimas de estacionamiento (Tabla 4). La Ta también

mostró un rendimiento robusto (R^2 = 0,795; RMSE = 0,55 °C). La velocidad del viento logró correlación satisfactoria (R^2 = 0,776), mientras que la humedad relativa presentó concordancia moderada, pero aceptable (R^2 = 0,624). Los valores medios de error de sesgo para Ta y TRM se mantuvieron dentro de ±1 °C, lo que indica una desviación sistemática mínima. En general, las estadísticas de validación confirman que el marco ENVI-met captura de manera confiable la dinámica microclimática y resulta adecuado para la evaluación paramétrica del confort térmico al aire libre en tipologías de estacionamiento.

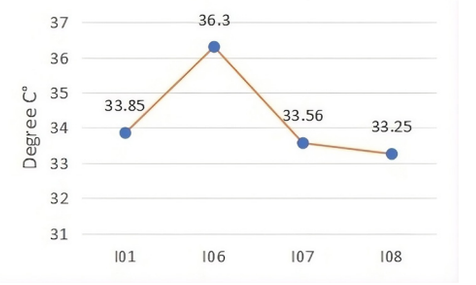


Figura 8. Promedio de UTCI a lo largo del tiempo para I01, I06. I07 y I08. Fuente: Preparado por los autores.

RESULTADOS DE SIMULACIÓN PARAMÉTRICA

Orientación norte-sur

Bajo la alineación norte-sur, las simulaciones revelan una sensibilidad distinta a la densidad de la vegetación, con respuestas comparativamente limitadas a las variaciones en el albedo y IRS (Figura 6). A lo largo de las iteraciones, el UTCI alcanzó su punto máximo en el punto del camino de entrada expuesto (P2), confirmando la exposición solar directa como el principal impulsor del estrés. La recuperación vespertina permaneció incompleta en escenarios de vegetación baja (Figura 7).

El aumento del albedo superficial de 0,2 a 0,6 no se tradujo en reducciones proporcionales del UTCI. En las zonas expuestas, el albedo más alto incrementó marginalmente el pico de UTCI, lo que indica una mayor reflexión de onda corta y una TRM elevada. De manera similar, aumentar el IRS del techo de 30 a 90 produjo una mejora insignificante a nivel de los peatones, lo que sugiere que las ganancias reflectantes se compensaron con la redistribución radiativa.

Por el contrario, la vegetación ejerció una mitigación sustancial. Como se muestra en la Figura 8, aumentar la cobertura de la copa del 0% al 60% redujo de forma consistente el UTCI promedio en todos los períodos de tiempo, con la mayor reducción durante el pico de la tarde. El sombreado redujo significativamente la TRM y limitó la acumulación de calor. Bajo esta orientación, la vegetación dominó claramente sobre la reflectividad del material como principal determinante del confort térmico.

Orientación este-oeste

La configuración este-oeste registró los valores máximos de UTCI entre las orientaciones (Figura 9). La escalada de la tarde fue más pronunciada que en la alineación norte–sur, lo que refleja una exposición solar prolongada a lo largo del eje del estacionamiento. Los ajustes de albedo e IRS produjeron una mitigación mínima en esta configuración. La orientación intensificó tanto la radiación directa como la reflejada, lo que redujo la efectividad de las estrategias basadas en la reflectividad. Aunque la vegetación contribuyó a un enfriamiento medible, su impacto fue moderado por la incidencia solar sostenida durante las horas pico. La alineación este-oeste, por lo tanto, mostró la mayor susceptibilidad a la acumulación térmica del mediodía, en particular en las zonas expuestas.

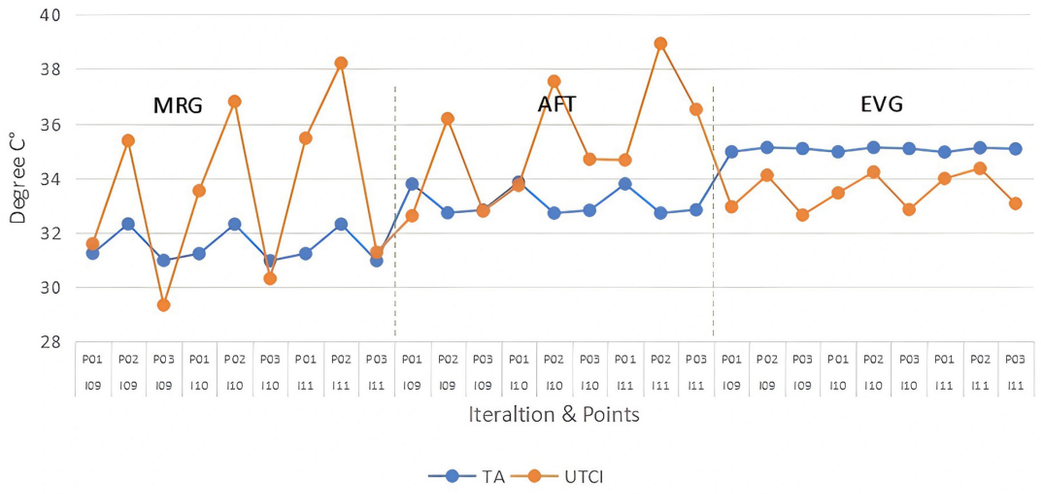


Figura 9. Datos de series temporales para Ta y UTCI para I09, I10 e I11. Fuente: Preparado por los autores.

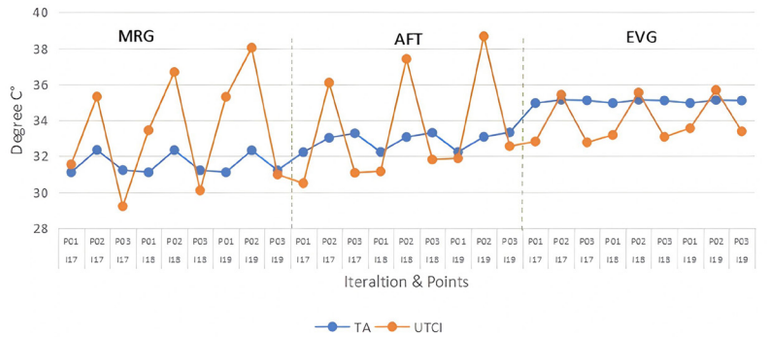


Figura 10. Datos de series temporales para Ta y UTCI para I17, I18 e I19. Fuente: Preparado por los autores.

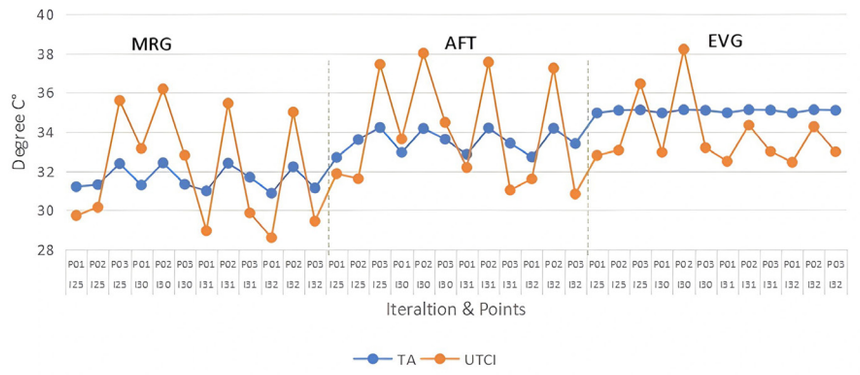


Figura 11. Datos de series temporales para Ta y UTCI para I25, I30, I31 e I32. Fuente: Preparado por los autores.

Orientación noreste-suroeste

La orientación noreste–suroeste (NE–SO) mostró una variación diurna moderada respecto de la alineación este–oeste (Figura 10). El pico de UTCI en P2 permaneció más bajo que bajo la configuración ortogonal este-oeste, lo que indica una menor duración de la incidencia solar directa.

Como en otras orientaciones, los ajustes de albedo e IRS produjeron cambios limitados en el UTCI a nivel peatonal. Sin embargo, la vegetación redujo de manera constante los valores máximos, especialmente en las zonas semiexpuestas. La alineación solar oblicua redujo la acumulación de radiación y, al combinarse con la sombra de la copa, produjo condiciones de la tarde más equilibradas. Esta orientación presentó un estrés máximo moderado y una recuperación nocturna comparable.

Orientación noroeste-sureste

La orientación noroeste–sureste (NO–SE) presentó el pico de UTCI más bajo entre las alineaciones probadas (Figura 11). La trayectoria solar angular redujo la exposición directa prolongada en P2, limitando el aumento de la TRM durante las horas pico. Las modificaciones materiales nuevamente produjeron diferencias marginales. Sin embargo, la integración de la vegetación se tradujo en una reducción sustancial del UTCI promedio (Figura 12). El escenario de la copa del 60% exhibió la tensión máxima más baja en todas las orientaciones. El sombreado redujo la carga radiativa y mejoró la estabilidad microclimática tanto en las zonas cubiertas como en las semiexpuestas. Esta orientación, cuando se combinó con una alta densidad de vegetación, exhibió el desempeño térmico más favorable.

ANÁLISIS COMPARATIVO DE ORIENTACIÓN CRUZADA

El análisis comparativo revela diferencias sistemáticas en la respuesta térmica máxima (Figura 13). Aunque las diferentes configuraciones de estacionamiento produjeron reducciones medibles en el UTCI, la mayoría de los escenarios permanecieron dentro de la categoría calibrada de estrés térmico moderado. En consecuencia, los resultados se interpretan en términos de mejora térmica relativa en lugar de una transición térmica categórica. La alineación este-oeste produjo el UTCI de la tarde más alto, mientras que la alineación NO-SE alcanzó consistentemente los valores máximos más bajos en condiciones de vegetación equivalentes. Las orientaciones norte-sur y NE-SO mostraron un desempeño intermedio.

Las condiciones matutinas fueron similares en todas las orientaciones, lo que indica que la alineación influye principalmente en la acumulación radiativa del mediodía en lugar del estado térmico inicial. Las diferencias se intensificaron durante la intensidad solar máxima, cuando la orientación geométrica gobernaba directamente la

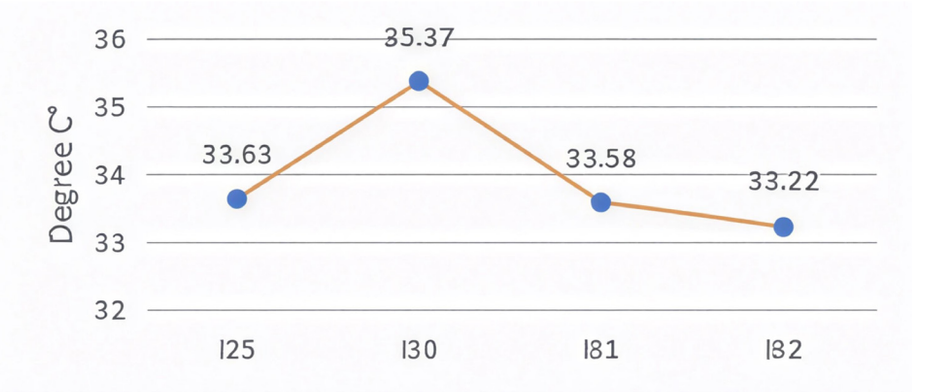


Figura 12. Promedio de UTCI para I25, I30, I31 e I32. Fuente: Preparado por los autores.

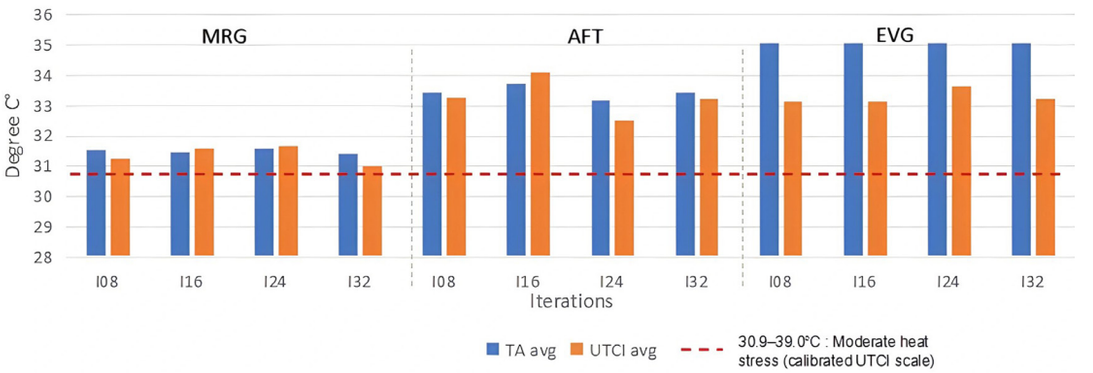


Figura 13. Comparación de series temporales de Ta y UTCI para las iteraciones de mejor rendimiento (I08, I16, I24, I32) . Fuente: Preparado por los autores.

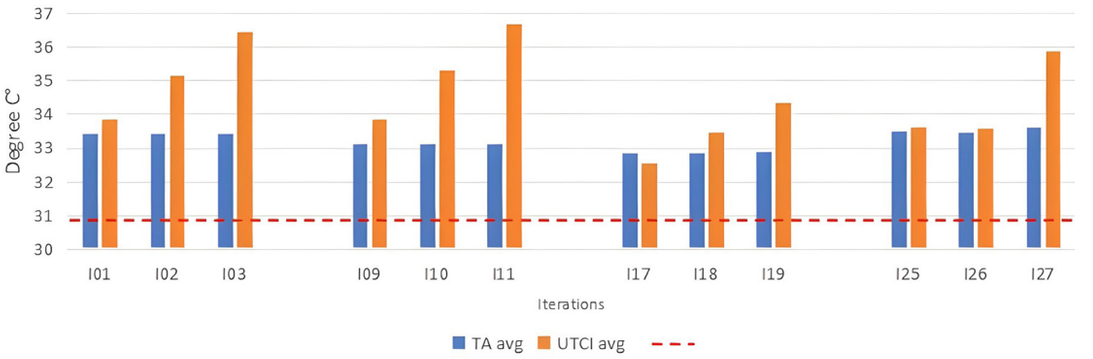


Figura 14. Comparación por la tarde de Ta y UTCI a través de iteraciones con valores variables de albedo superficial. Fuente: Preparado por los autores.

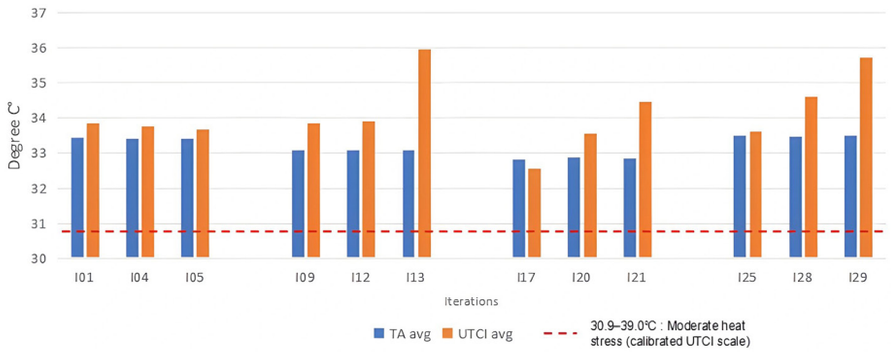


Figura 15. Comparación por la tarde de Ta y UTCI en iteraciones con valores variables de IRS de techo. Fuente: Preparado por los autores.

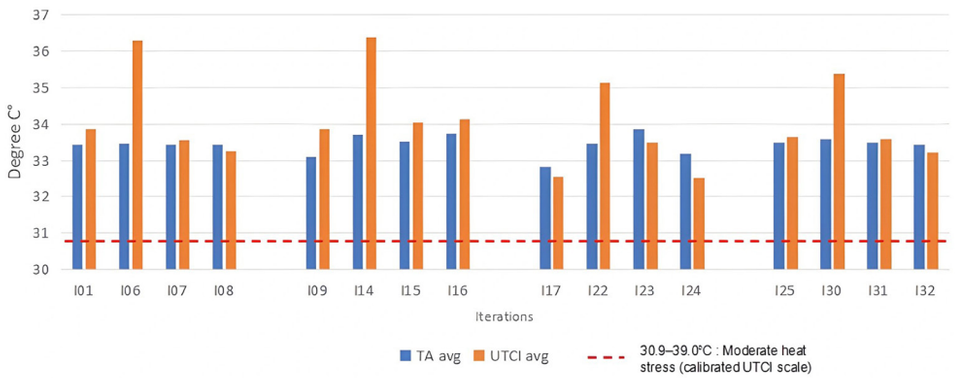


Figura 16. Comparación por la tarde de Ta y UTCI a través de iteraciones con cobertura arbórea variable. Fuente: Preparado por los autores.

duración y el ángulo de la radiación incidente en las superficies expuestas.

Las alineaciones diagonales, particularmente NO–SE, redujeron la acumulación de picos de manera más efectiva que las configuraciones ortogonales este-oeste, lo que demuestra la interacción entre la geometría solar y la exposición de la superficie.

EFECTOS ESPECÍFICOS DE PARÁMETROS

Albedo de superficie

La comparación de la tarde indica que aumentar el albedo de 0,2 a 0,6 no redujo consistentemente el UTCI (Figura 14). En las zonas expuestas, la mayor reflectividad elevó marginalmente el UTCI debido al aumento de la reflexión de onda corta y de TRM. Los efectos se amplificaron en orientaciones ortogonales con incidencia solar sostenida.

Índice de reflectancia solar del techo (SRI)

El aumento de IRS de 30 a 90 produjo un enfriamiento limitado a nivel peatonal (Figura 15). Aunque las superficies del techo experimentaron un calentamiento reducido, la radiación reflejada bajo las áreas semicubiertas redistribuyó la energía radiante hacia los ocupantes, limitando el beneficio general.

Cubierta vegetal

La vegetación demostró el efecto de mitigación más fuerte (Figura 16). El aumento de la copa del 0% al 60% redujo consistentemente el UTCI en todas las orientaciones, con reducciones máximas durante el estrés de la tarde. El sombreado disminuyó significativamente la TRM y suprimió la acumulación radiante, lo que establece la vegetación como el parámetro dominante que influye en el confort térmico.

EFECTOS DE INTERACCIÓN ENTRE ORIENTACIÓN, VEGETACIÓN Y MATERIALES REFLECTANTES

Los resultados muestran que la respuesta térmica del albedo superficial y del IRS del techo no es uniforme en todo el dominio de estudio, pero está fuertemente moderada por la orientación y la densidad de la vegetación. En condiciones de baja vegetación, los aumentos del albedo produjeron respuestas UTCI limitadas o adversas, ya que la radiación de onda corta reflejada aumentó la carga radiante a nivel de los peatones. Por el contrario, cuando

Condición urbana	Prioridad de diseño principal	Implicación térmica esperada
Vegetación factible	60% cubierta de copa + orientación NO-SE	Estrés térmico peatonal más bajo
Vegetación parcialmente factible	Copa moderada + albedo bajo + SRI moderado	Mitigación equilibrada con TRM reducida
Vegetación no factible	Optimización de la orientación + reflectividad controlada	La orientación se convierte en la estrategia pasiva dominante
Contexto de modernización	Sombreado primero, reflectividad en segundo lugar	Evitar depender únicamente de materiales reflectantes
Contexto limitado por el presupuesto	Orientación y sombreado selectivo	Mayor beneficio que las actualizaciones solo de material

Tabla 5. Jerarquía de diseño para entornos de estacionamiento bajo diferentes restricciones urbanas. Fuente: Preparado por los autores.

aumentó la cobertura vegetal, el impacto negativo de la radiación reflejada se redujo debido a la sombra y a una TRM menor. La orientación también modificó la magnitud de estas respuestas: la alineación este-oeste amplificó la acumulación radiativa de la tarde, mientras que la alineación NO-SE moderó la exposición máxima. Estos hallazgos indican que el rendimiento térmico del estacionamiento se debe a la interacción entre los materiales radiativos, la configuración de la copa y la geometría solar, en lugar de a una sola variable de diseño aislada.

La Tabla 5 representa una contribución clave de este estudio al traducir el análisis paramétrico validado en terreno en una jerarquía de diseño operacional para entornos de estacionamiento en climas cálidos y húmedos. El marco demuestra que la efectividad térmica de las estrategias de mitigación no es universal, sino que depende en gran medida de la interacción de la disponibilidad de vegetación, la orientación y las propiedades reflectantes de la superficie. Si bien la vegetación mostró de manera consistente la mayor reducción de la exposición al calor de los peatones, los resultados revelan que la orientación se convierte en el determinante pasivo dominante del diseño cuando la integración de la copa está restringida. Además, los beneficios limitados y dependientes del contexto de los pavimentos de alto albedo y los techos reflectantes sugieren que las intervenciones basadas en materiales deben implementarse junto con estrategias de diseño espacial y paisajístico, en lugar de sustituirlas. En consecuencia, el marco propuesto va más allá de la evaluación aislada de parámetros y proporciona una herramienta de apoyo a la toma de decisiones que vincula el desempeño microclimático con restricciones realistas de diseño urbano, facilitando así decisiones de planificación y modernización más efectivas que respondan al clima.

ANÁLISIS ESTADÍSTICO

Se realizó un análisis estadístico sobre el conjunto de datos completo (n = 288) para cuantificar la relación entre los parámetros ambientales y el confort térmico exterior. El análisis de correlación de Pearson reveló una fuerte asociación positiva entre TRM y UTCI ($r = 0,653$, $p < 0,001$), lo que confirma el papel dominante del intercambio de calor radiativo en la influencia del estrés térmico peatonal. La Ta demostró una correlación positiva moderada ($r = 0,358$, $p < 0,001$), mientras que la humedad relativa mostró una correlación negativa ($r = -0,432$, $p < 0,001$), lo que indica una moderación parcial del UTCI en condiciones simuladas. La velocidad del viento mostró una correlación débil y estadísticamente insignificante, lo que sugiere una influencia convectiva limitada en la configuración de estacionamiento.

Se desarrolló un modelo de regresión lineal múltiple para predecir el UTCI en función de la temperatura del aire, la TRM, la humedad relativa y la velocidad del viento. El modelo de regresión demostró una fuerte capacidad explicativa dentro del conjunto de datos investigado ($R^2 = 0,87$, $p < 0,001$) y se utilizó para evaluar la influencia relativa de las variables ambientales en UTCI bajo las condiciones climáticas investigadas. La relación predictiva derivada (Ecuación 2) se expresa como:

$$UTCI = -2,658 + 0,841(Ta) + 0,229(TRM) - 0,003(HR) - 0,614\ (Viento) \quad \text{(Ecuación 2)}$$

Los coeficientes de regresión estandarizados indican que la TRM ejerce la mayor influencia sobre el UTCI entre las variables ambientales evaluadas, lo que confirma la exposición radiativa como el principal contribuyente al estrés térmico peatonal. Los resultados indican, además, que la cubierta vegetal y la orientación influyen principalmente en el confort al aire libre al modular la TRM y la exposición solar. El factor de inflación de varianza (VIF < 5) indica la ausencia de multicolinealidad. Estos resultados refuerzan la carga radiativa como el mecanismo gobernante del estrés térmico.

RÁNKING DE OPTIMIZACIÓN

La evaluación de las treinta y dos iteraciones evidencia una clara estratificación del desempeño (Figura 17). La alta densidad de vegetación se asoció de manera consistente con un UTCI medio más bajo en todas las orientaciones. La iteración I32 (NO–SE; albedo 0,2; IRS 30; 60% de vegetación) logró el UTCI medio más bajo (32,49 °C), lo que refleja la interacción sinérgica entre el sombreado de la copa y la alineación solar favorable. Por el contrario, la

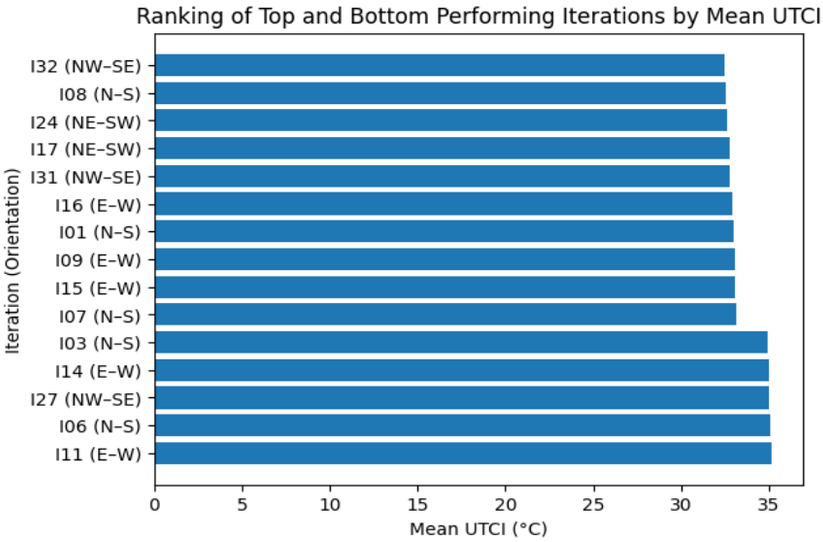


Figura 17. Iteraciones de realización superior e inferior basadas en UTCI medio. Fuente: Preparado por los autores.

vegetación mínima bajo la alineación este–oeste (I11) registró el UTCI medio más alto (35,16 °C). El patrón de clasificación identifica inequívocamente la integración y la orientación de la vegetación como determinantes dominantes del rendimiento térmico, mientras que los ajustes de reflectividad, por sí solos, produjeron una mejora limitada.

DISCUSIÓN

Los hallazgos confirman que la TRM es el principal impulsor del confort térmico al aire libre en entornos de estacionamiento, de acuerdo con estudios que enfatizan la primacía del intercambio radiativo en el estrés térmico de los peatones (Taleghani, 2018). El aumento del albedo de la superficie no mejoró de manera consistente el confort, ya que una mayor reflectividad aumentó la exposición radiante de los peatones, un fenómeno previamente reportado en el que un aumento del albedo de 0,2 a 0,6 elevó los índices de TRM y el estrés térmico (Ghoniem et al., 2025). Aunque los pavimentos reflectantes reducen las temperaturas superficiales, su efectividad depende del sombreado y el contexto espacial (Taleghani, 2018).

De manera similar, los valores más altos de IRS en el techo produjeron un enfriamiento limitado a escala peatonal. Si bien los materiales fríos pueden reducir las temperaturas superficiales y mitigar la ICU (Jandaghian et al., 2025), su impacto en el confort depende de la geometría circundante y de las condiciones de exposición. En tipologías de estacionamientos semicubiertos, la radiación reflejada puede redistribuir la carga térmica en lugar de eliminarla.

La vegetación demostró el efecto de enfriamiento más sustancial, corroborando la evidencia de que la sombra de los árboles reduce el estrés térmico de manera más efectiva que la modificación del albedo (Zhang et al., 2025). Las reducciones observadas con una mayor cobertura de la copa se alinean con el enfriamiento documentado mediante el sombreado y la evapotranspiración (He y Reith, 2023). La influencia de la densidad y estructura de la vegetación en el confort de los peatones respalda aún más estos hallazgos (Pattnaik et al., 2025).

La orientación dio forma a la magnitud y al momento del estrés térmico, con una alineación este–oeste que intensifica la exposición en la tarde, de acuerdo con la investigación que vincula la morfología urbana y la penetración solar con el confort de los peatones (Rachidi et al., 2026). Por lo tanto, las estrategias integradas que combinan vegetación, materiales reflectantes y una planificación sensible a la orientación constituyen la vía más efectiva para mejorar el confort térmico en entornos de estacionamiento cálidos y húmedos.

Al usar la escala UTCI calibrada, los entornos de estacionamiento investigados presentaron predominantemente condiciones de estrés térmico moderado. Dentro de este rango, el aumento de la cobertura vegetal y la orientación favorable redujeron la exposición térmica de los peatones de manera más efectiva que las modificaciones a los materiales reflectantes solos, al limitar la exposición solar directa y reducir la TRM. El análisis de regresión y las comparaciones paramétricas indican, además, que la influencia térmica del albedo, la reflectividad del techo, la vegetación y la orientación están fuertemente interconectadas a través de su impacto conjunto sobre las condiciones radiativas de los peatones.

Más allá de reafirmar los beneficios refrescantes de la vegetación, este estudio revela que la efectividad térmica de los materiales reflectantes depende en gran medida de

la orientación y el contexto de la copa. Si bien un mayor albedo y un IRS en el techo redujeron la absorción de calor en la superficie, no mejoraron consistentemente el confort térmico de los peatones debido al aumento de la exposición radiativa. En condiciones de vegetación restringida, la orientación surgió como un determinante más influyente del confort térmico que la reflectividad del material. Estos hallazgos subrayan la necesidad de estrategias integradas de mitigación y establecen una jerarquía de intervenciones de diseño para entornos de estacionamiento en climas cálidos y húmedos.

LIMITACIONES DEL ESTUDIO E INVESTIGACIONES FUTURAS

Este estudio fue diseñado para evaluar el desempeño térmico del estacionamiento en condiciones representativas de verano pico en un clima cálido-húmedo. En consecuencia, la validación del modelo se centró en un día extremo de verano, por lo que es posible que no capture completamente la variabilidad estacional. Además, se estimó la TRM utilizando la formulación de temperatura global ISO 7726, y se evaluó el confort térmico utilizando UTCI como índice de evaluación primario. Si bien estas opciones metodológicas no afectan la evaluación comparativa de los escenarios de diseño investigados, los estudios futuros deberían incorporar observaciones multiestacionales, análisis de la incertidumbre de los parámetros térmicos derivados, índices de confort alternativos y encuestas de percepción térmica basadas en los ocupantes para mejorar aún más la generalización de los hallazgos.

CONCLUSIÓN

Este estudio investigó la influencia combinada del albedo de la superficie, el IRS del techo, la cubierta vegetal y la orientación sobre el confort térmico a nivel peatonal en entornos de estacionamiento cálidos y húmedos. A través de mediciones en terreno y simulaciones validadas en ENVI-met, los resultados demuestran que la TRM es el determinante dominante del estrés térmico exterior, superando las modificaciones aisladas de la temperatura del aire.

Las estrategias basadas en la reflectividad, por sí solas, resultaron insuficientes. El aumento del albedo de la superficie y el IRS del techo redujeron la absorción de calor del material, pero no redujeron consistentemente el UTCI debido a la radiación reflejada y los efectos de redistribución radiativa. En contraste, la vegetación surgió como la estrategia de mitigación más efectiva. El aumento de la cobertura de la copa al 60% redujo consistentemente el estrés térmico máximo en todas las orientaciones al reducir la TRM a través del sombreado y la evapotranspiración.

La orientación mediaba aun más la acumulación térmica: la alineación este-oeste intensificaba la exposición por la tarde, mientras que la configuración NO-SE moderaba el estrés máximo. El desempeño óptimo se logró mediante la integración combinada de albedo bajo (0,2), SRI moderado (30), cobertura vegetal del 60% y alineación diagonal. Estos hallazgos subrayan que el diseño de estacionamientos que responda al clima de las ciudades tropicales debe priorizar el manejo radiativo mediante la integración de la copa y una planificación sensible a la orientación, en lugar de depender únicamente de materiales reflectantes. Si bien los hallazgos brindan información importante sobre el confort térmico en las condiciones pico de verano, estudios futuros que incorporen períodos de monitoreo prolongados y evaluaciones de la percepción térmica basadas en los ocupantes fortalecerían aún más la generalización a condiciones climáticas más amplias.

Más allá de confirmar los beneficios térmicos de la vegetación, este estudio establece una jerarquía validada en el campo de estrategias de mitigación para entornos de estacionamiento en climas cálidos y húmedos. Los resultados demuestran que la efectividad térmica de los materiales reflectantes no es universal, sino que depende de la orientación y el contexto de la vegetación. Esto proporciona un marco de apoyo para la toma de decisiones en el diseño de estacionamientos sensibles al clima, particularmente en entornos urbanos donde no es posible introducir vegetación extensa.

CONTRIBUCIÓN DEL AUTOR CRediT

Conceptualización: A.S.K.S., P.G.; Curación de Datos: A.S.K.S.; Análisis Formal: A.S.K.S., P.G.; Adquisición de Financiación: P.G., G.S.; Investigación: A.S.K.S.; Methodología: A.S.K.S., P.G.; Administración del Proyecto: P.G., G.S.; Recursos: P.G., G.S.; Software: A.S.K.S.; Supervisión: P.G., G.S.; Validación: A.S.K.S., P.G., G.S.; Visualización: A.S.K.S.; Escritura – Borrador Original: A.S.K.S.; Escritura – Revisión y Edción: P.G., G.S.; Escritura – Revisión y Edición: ASKS, P.G., G.S.

AGRADECIMIENTOS

Los autores declaran que no se recibió financiamiento para esta investigación.

REFERENCIAS BIBLIOGRÁFICAS

Abdelwahab, R. A., Fekry, A. A., & Hamed, R.E.-D. (2025). The effective landscape design parameters with high reflective hardscapes: guidelines for optimizing human thermal comfort in outdoor spaces by design -a case on hot arid climate weather. *Computational Urban Science, 5*,28. https://doi.org/10.1007/s43762-025-00186-w

Austin, D., Solano, T., & Chen Austin, M. (2025). Synergistic Effects of Bioclimatic Strategies on Microclimate Improvement: A Numerical–

Experimental Study at University Campus Scale. *Sustainability, 17*(19), 8867. https://doi.org/10.3390/su17198867

Calhoun, Z.D., Willard, F., Ge, C., Rodriguez, C., Bergin, M., & Carlson, D. (2024). Estimating the effects of vegetation and increased albedo on the urban heat island effect with spatial causal inference. *Scientific Reports, 14*, 540. https://doi.org/10.1038/s41598-023-50981-w

Chen, W.-A., Fang, P.-L., & Hwang, R.-L. (2025). Calibrating the UTCI scale for hot and humid climates through comprehensive year-round field surveys to improve the adaptability. *Urban Climate, 59*, 102267. https://doi.org/10.1016/j.uclim.2024.102267

Deepthi, S., Sudalaimani, K., Radhakrishnan, S. P., & Radhakrishnan, S. (2024). Evaluating urban heat island to achieve sustainable development goals: A case study of Tiruchirappalli city, India. *Sustainable Cities and Society, 116*, 105865. https://doi.org/10.1016/j.scs.2024.105865

Ghenai, C., Rejeb, O., Sinclair, T., Almarzouqi, N., Alhanaee, N., & Rossi, F. (2023). Evaluation and thermal performance of cool pavement under desert weather conditions: Surface albedo enhancement and carbon emissions offset. *Case Studies in Construction Materials, 18,* e01940. https://doi.org/10.1016/j.cscm.2023.e01940

Ghoniem, M., Fahmy, A., & Kamel, T. M. (2025). Evaluating urban surface materials: Albedo optimization and shading for pedestrian thermal comfort in hot-arid environments. *Civil Engineering and Architecture, 13*(6), 4331–4352. https://doi.org/10.13189/cea.2025.130616

Gidey, E., & Mhangara, P. (2025). Improving spatial modeling framework to assess the impact of vegetation cover, water content, and surface temperature on urban heat island effects in Johannesburg, South Africa. *Discover Environment*, 3(1), 74. https://doi.org/10.1007/s44274-025-00264-0

He, Q., & Reith, A. (2023). A study on the impact of green infrastructure on microclimate and thermal comfort. *Pollack Periodica, 18*(1), 42–48. https://doi.org/10.1556/606.2022.00668

Huang, C., Liu, K., Ma, T., Xue, H., Wang. P., & Li, L. (2025). Analysis of the impact mechanisms and driving factors of urban spatial morphology on urban heat islands. *Scientific Reports, 15*, 18589. https://doi.org/10.1038/s41598-025-04025-0

Jandaghian, Z., Lacasse, M., & Gaur, A. (2025). Solar Reflectance Index of Building Envelope Materials: A Comparative Review of North American and European Standards and Long-Term Performance. *Buildings, 15*(6), 888. https://doi.org/10.3390/buildings15060888

Kafy, A. A., Alsulamy, S., & Alsaleh, A. M. (2026). Escalating heat hazard risk in arid urban environments: A two-decade assessment of thermal stress patterns and health risks using UTCI and WBGT indices in Riyadh, Saudi Arabia. *Natural Hazards, 122*, 156. https://doi.org/10.1007/s11069-025-07930-9

Kaushik S., A. S., & Amraotkar, S. (2026). Analyzing the effects of orientation, window size and position on solar heat gain for four Indian cities. *Science, Engineering and Health Studies, 20*, 26040001. https://doi.org/10.69598/sehs.20.26040001

Lin, P., Song, D., & Qin, H. (2021). Impact of parking and greening design strategies on summertime outdoor thermal condition in old mid-rise residential estates. *Urban Forestry & Urban Greening, 63*, 127200. https://doi.org/10.1016/j.ufug.2021.127200

Nutakki, T.U.K., Kazim, W.U., Alamara, K., Salameh, T., & Abdelkareem, M.A. (2023). Experimental Investigation on Aging and Energy Savings Evaluation of High Solar Reflective Index (SRI) Paints: A Case Study on Residential Households in the GCC Region. *Buildings,13*(2), 419. https://doi.org/10.3390/buildings13020419

Pachauri, R., & Kaushik S., A. S. (2025). A comparative evaluation of the effectiveness of glazed and open balconies in low-rise residences in moderate climates via field measurements and simulations. *Science, Engineering and Health Studies, 19*, 25040004. https://doi.org/10.69598/sehs.19.25040004

Parison, S., Chaumont, M., Kounkou-Arnaud, R., Long, F., Bernik, A., Da Silva, M., & Hendel M. (2023). The effects of greening a parking lot as a heat mitigation strategy on outdoor thermal stress using fixed and mobile measurements: case-study project "tertiary forest." *Sustainable Cities and Society, 98*,104818. https://doi.org/10.1016/j.scs.2023.104818

Patel, P., & Kaushik, A. S. (2023). The impact of microclimate on energy performance of office buildings within urban contexts located in a composite climate, the city of Indore. *IOP Conference Series: Earth and Environmental Science, 1210*, 012007. https://doi.org/10.1088/1755-1315/1210/1/012007

Pattnaik, N., Rahman, M. A., & Pauleit, S. (2025). Urban vegetation structure and composition influence pedestrian thermal comfort in public spaces: A case study in Munich. *Urban Forestry & Urban Greening, 114*, 129162. https://doi.org/10.1016/j.ufug.2025.129162

Peter, A., & Kaushik, S. A. S. (2024). A study on the impact of courtyard vegetation on its thermal comfort performance in an educational building of warm and humid climates. *Science, Engineering and Health Studies, 18,* 24040011. https://doi.org/10.69598/sehs.18.24040011

Rachidi, A., Mounir, S. H., Sghir, S., & Lebaut, S. (2026). Urban albedo interventions reshape thermal comfort: A multiscale analysis of heat island, comfort, and energy effects in semi-arid Marrakesh. *Sustainable Cities and Society, 136,* 107090. https://doi.org/10.1016/j.scs.2025.107090

Rodriguez, A., Wood, S., Carmeliet, J., Kubilay, A., & Derome, D. (2025). Local impact of trees on thermal comfort of pedestrians in streets. *Urban Climate, 61,* 102417. https://doi.org/10.1016/j.uclim.2025.102417

Sen, S., Fernandez, J.P.R.M.-R., & Roesler, J. (2020). Reflective Parking Lots for Microscale Urban Heat Island Mitigation. *Transportation Research Record: Journal of the Transportation Research Board, 2674*(8). 663–71. https://doi.org/10.1177/0361198120919401

Silva Nascimento, A. D., Silva, L.V.A.D., Lisboa, M.A.N., Oliveira Silva, A.D., Rodrigues Ferreira, M.F., Silva, S.C.F.D., Melo, M.J.V.D., Silva, A.C.V.D., & Júnior, J. T. C. (2025). How do visitors perceive the urban greenery microclimate in the city's only green space? A case study in Brazilian semi-arid. *Environmental Development, 56,* 101244. https://doi.org/10.1016/j.envdev.2025.101244

Taleghani, M. (2018). The impact of increasing urban surface albedo on outdoor summer thermal comfort within a university campus. *Urban Climate, 24,* 175–184. https://doi.org/10.1016/j.uclim.2018.03.001

Wei, Y.-Y., Cheng, C.Y., & Lin, T.-P. (2025). The influence of trees shade level on human thermal comfort and the development of applied assessment tools. *Landscape and Urban Planning, 263*, 105436. https://doi.org/10.1016/j.landurbplan.2025.105436

Wang, C., Zhan, W., Liu, Z., Li, J., Li, L., Fu, P., Huang, F., Lai, J., Chen, J., Hong, F., & Jiang, S. (2020). Satellite-based mapping of the Universal Thermal Climate Index over the Yangtze River Delta urban agglomeration. *Journal of Cleaner Production, 277*, 123830. https://doi.org/10.1016/j.jclepro.2020.123830

Zhang, T., Fu, X., Qi, F., Shen, Y., Xu, P., Tao, Y., Liu, T., & Song, Y. (2025). Optimizing pedestrian thermal comfort in urban street canyons for summer and winter: Tree planting or low-albedo pavements? *Sustainable Cities and Society, 120*, 106143. https://doi.org/10.1016/j.scs.2025.106143

Revista Hábitat Sustentable Vol. 16, N°. 1. ISSN 0719 - 0700 / Págs. 126 - 141
https://doi.org/10.22320/07190700.2026.16.01.08

PROTECCIÓN DE LA FACHADA DE VIDRIO: ESTRATEGIAS DE MEMBRANAS TEXTILES PARA EL DISEÑO EN ETAPAS TEMPRANAS PARA LA EFICIENCIA ENERGÉTICA DE EDIFICIOS DE OFICINAS EN CLIMAS CÁLIDOS Y HÚMEDOS

Recibido 28/01/2026
Aceptado 27/06/2026

SHADING THE GLASS FAÇADE: TEXTILE MEMBRANE STRATEGIES FOR EARLY-STAGE DESIGN FOR OFFICE BUILDING ENERGY-EFFICIENCY IN HOT–HUMID CLIMATES

SOMBREAMENTO DE FACHADAS DE VIDRO: ESTRATÉGIAS COM MEMBRANAS TÊXTEIS PARA O PROJETO INICIAL DE EFICIÊNCIA ENERGÉTICA EM EDIFÍCIOS DE ESCRITÓRIOS EM CLIMAS QUENTES E ÚMIDOS

Chandrasekaran Chockalingam (Autor de Correspondencia)
Ph.D. in Fully Glazed Building Facades
Professor, School of Architecture and Planning
Vellore Institute of Technology
Vellore, India
https://orcid.org/0000-0003-4215-0202
chandrasekaran.c@vit.ac.in

Madhu Mathi Anbu
Ph.D. in Building Thermal Performance
Professor, Higher academic grade, School of Architecture and Planning
Vellore Institute of Technology
Vellore, India
https://orcid.org/0000-0002-7478-1183
madhumathi.a@vit.ac.in

Mase Noguchi
Ph.D. in Architecture and Sustainable built environment
Associate Professor, Faculty of Architecture, Building and Planning
The University of Melbourne
Melbourne, Australia
https://orcid.org/0000-0003-1437-5455
masa.noguchi@unimelb.edu.au

CC BY SA

Revista Hábitat Sustentable Vol. 16, N°. 1. ISSN 0719 - 0700 / Págs. 126 - 141
https://doi.org/10.22320/07190700.2026.16.01.08

RESUMEN

En el clima cálido y húmedo de la India, la prevalencia de edificios de oficinas de varios pisos totalmente acristalados (FGM, por sus siglas en inglés) conduce a un mayor consumo energético, principalmente debido a la ganancia de calor solar a través de sus extensas superficies de vidrio. Aunque el sombreado exterior es una solución reconocida, los diseñadores a menudo carecen de claridad sobre qué tipo de sistema de sombreado y, en particular, qué material ofrece el mejor rendimiento en las etapas críticas del diseño inicial. Este estudio emplea un marco comparativo basado en simulaciones para evaluar la integración de membranas textiles sostenibles en tres configuraciones de sombreado distintas: pantalla solar fija, estructura fija tipo diagrid y sombreado dinámico. Utilizando un modelo representativo de un edificio de oficinas totalmente acristalado y de varios pisos ubicado en Chennai, la investigación empleó Autodesk Revit para el modelado, eQuest para el análisis energético y Dynamo para la configuración paramétrica, con el fin de realizar un análisis multiobjetivo. Los procedimientos incluyeron la cuantificación de las cargas anuales de enfriamiento para evaluar el rendimiento térmico, la medición de la iluminancia útil de luz diurna (UDI, por su sigla en inglés) para evaluar el confort visual, y el análisis del costo inicial de inversión de los dispositivos de sombreado integrados para determinar el período de retorno económico de cada sistema en comparación con un caso base sin sombreado. El análisis comparativo demuestra el potencial de un ahorro energético considerable en todas las opciones. Sin embargo, los resultados revelaron diferencias marcadas y tendencias contradictorias entre el rendimiento térmico y visual. En particular, la pantalla solar fija se mostró como la solución más eficaz, al equilibrar la reducción de la demanda energética con la viabilidad económica. El estudio concluye que las simulaciones orientadas por materiales son esenciales en la fase inicial del diseño para permitir la toma de decisiones bien fundamentadas que alineen la sostenibilidad con el rendimiento del edificio.

Palabras clave
ahorro energético, fachada totalmente acristalada, sombreado con membrana textil, sombreado dinámico, luz diurna, cálido y húmedo

ABSTRACT

In India's hot and humid climate, the prevalence of fully glazed multi-story (FGM) office structures results in higher energy use, primarily due to solar heat ingress through their extensive glass surfaces. While external shading is a well-known solution, designers often lack clarity on which shading type and, specifically, which material performs best during the critical early design stages. This study employs a simulation-based comparative framework to evaluate the integration of sustainable textile membranes across three distinct shading configurations: fixed solar screen, fixed diagrid, and dynamic shading. Using a representative, fully glazed, multi-storied office building model located in Chennai, the research employed Autodesk Revit for modeling, E-Quest for energy analysis, and Dynamo for parametric setup to conduct a multi-objective analysis. The procedures involved quantifying annual cooling loads to assess thermal performance, measuring Useful Daylight Illuminance (UDI) to evaluate visual comfort, and performing an Initial investment cost of the integrated shading devices to determine the economic payback period for each system compared to a non-shaded base case. Comparative analysis demonstrates the potential for considerable energy savings across all options. However, findings revealed pronounced disparities and contradictory trends between thermal and visual performance. Notably, the fixed solar screen emerged as the most effective solution, balancing energy reduction with economic viability. The study concludes that material-driven simulations are essential in the early design phase to enable well-informed choices that align sustainability with building performance.

Keywords
energy saving, fully glazed façade, textile membrane shading, dynamic shading, day lighting, hot and humid

RESUMO

No clima quente e úmido da Índia, a prevalência de edifícios de escritórios de múltiplos pavimentos totalmente envidraçados (FGM, do inglês fully glazed multi-storey) acarreta um maior consumo de energia, sobretudo devido ao ganho de calor solar por meio de suas extensas superfícies de vidro. Embora o sombreamento externo seja uma solução amplamente conhecida, os projetistas frequentemente carecem de clareza quanto ao tipo de sombreamento e, especificamente, ao material com melhor desempenho nas fases iniciais de projeto, que são críticas. Este estudo emprega uma estrutura comparativa baseada em simulação para avaliar a incorporação de membranas têxteis sustentáveis em três configurações distintas de sombreamento: tela de proteção solar fixa, malha diagonal (diagrid) fixa e sombreamento dinâmico. A partir de um modelo representativo de um edifício de escritórios de múltiplos pavimentos totalmente envidraçado localizado em Chennai, a pesquisa utilizou o Autodesk Revit para a modelagem, o eQuest para a análise energética e o Dynamo para a configuração paramétrica, conduzindo uma análise multiobjetivo. Os procedimentos envolveram a quantificação das cargas anuais de resfriamento para avaliar o desempenho térmico, a medição da Iluminância Útil de Luz Natural (UDI, do inglês Useful Daylight Illuminance) para avaliar o conforto visual e o levantamento do custo de investimento inicial dos dispositivos de sombreamento incorporados, a fim de determinar o período de retorno econômico de cada sistema em comparação com um caso base sem sombreamento. A análise comparativa demonstra o potencial de economias de energia consideráveis em todas as alternativas. Contudo, os resultados revelaram disparidades acentuadas e tendências contraditórias entre os desempenhos térmicos e visuais. Destaca-se que a tela de proteção solar fixa mostrou-se a solução mais eficaz, equilibrando a redução do consumo de energia com a viabilidade econômica. O estudo conclui que simulações orientadas pelo material são essenciais na fase inicial de projeto para viabilizar escolhas bem fundamentadas que conciliem sustentabilidade e desempenho da edificação.

Palavras-chave
economia de energia, fachada totalmente envidraçada, sombreamento por membrana têxtil, sombreamento dinâmico, iluminação natural, ambiente quente e úmido

Revista Hábitat Sustentable Vol. 16, N°. 1. ISSN 0719 - 0700 / Págs. 126 - 141
https://doi.org/10.22320/07190700.2026.16.01.08

LISTA DE ABREVIATURAS

AES: Ahorro anual de energía por m² de área de piso de oficina para enfriamiento de espacios
ASE: Exposición anual al sol
API: Interfaz de programación de aplicaciones.
BIM: Modelo de información de construcción
DOE-2: Software del Departamento de Energía de EE.UU. para uso energético.
ECBC 17: Código de Construcción de Conservación de Energía, Versión 2017
EEM: Medidas de eficiencia energética en E-Quest.
ESD: Dispositivo de sombreado exterior
FGM: Completamente acristalado de varios pisos.
GRIHA V19: Calificación ecológica para la evaluación integrada del hábitat, versión 2019
HVAC: Calefacción, ventilación y enfriamiento
IIC: Costo de inversión inicial por metro cuadrado del área de la oficina
TI: Tecnología de la información
LEED: Liderazgo en energía y diseño ambiental
P & C: Métodos de recorte de polígonos
PTFE: Politetrafluoroetileno
PES: Hilos de poliéster
PVC: Cloruro de polivinilo
SCL: Carga de enfriamiento del espacio
SHGC: Coeficiente de ganancia de calor solar.
TNEB: Junta de Electricidad de Tamil Nadu.
UDI: Iluminancia útil de la luz del día
USD: Dólar estadounidense
VLT: Transmitancia visual de la luz
WWR: Relación ventana-pared

INTRODUCCIÓN

Los edificios comerciales con exteriores completamente acristalados maximizan la luz natural y la estética contemporánea, pero consumen más del doble de energía que sus contrapartes internacionales en India debido a la falta de capacidad de respuesta climática (Consejo de Defensa de Recursos Naturales [NRDC] y Colegio de Personal Administrativo de India [ASCI], 2014). En el clima cálido y húmedo de Chennai (13.0827 N, 80.2707 E), las temperaturas diurnas requieren aire acondicionado constante durante todo el año. Implementar un sombreado exterior efectivo basado en la orientación puede reducir significativamente las cargas de enfriamiento en estas fachadas altamente acristaladas (Chi et al., 2018), lo que demuestra que es mucho más eficiente que el uso de persianas internas (Arumugam y Ramalingam, 2024). Fundamentalmente, el 80% del rendimiento energético a lo largo del ciclo de vida de un edificio se determina en la etapa inicial de diseño, por lo que la integración temprana de datos específicos del acristalamiento y del sombreado del material resulta vital (Hwang y Chen, 2022; Bhatia et al., 2024). Entre las alternativas, las membranas textiles arquitectónicas permiten geometrías estructuralmente viables, rentables y complejas de forma libre. Protegen a las estructuras de la radiación UV y del clima más severo (São João, Carvalho y Fangueiro, 2016) mientras que su ligereza, transparencia y alta reflectividad solar minimizan la absorción de calor solar (Tian et al ., 2020).

En las regiones tropicales, la protección solar adaptativa equilibra la eficiencia visual y térmica en todas las estaciones. El diseño de estos sistemas inteligentes y dinámicos requiere una ingeniería interdisciplinaria compleja (Al-Masrani y Al-Obaidi, 2019), como lo ejemplifican las torres Al-Bahar de Abu Dhabi, que utilizan paraguas plegables de tela de PTFE translúcida, inspirados en la mashrabiya tradicional. Sin embargo, el conocimiento actual sobre las membranas textiles para fachadas sigue fragmentado, con aplicaciones concentradas en Oriente Medio y rara vez implementadas en los trópicos. Este estudio busca cerrar esa brecha comparando una pantalla solar, un diagrid y un sistema de sombreado dinámico, todos con la membrana textil más reciente, para determinar la mayor eficiencia energética, el confort visual óptimo y la inversión inicial más rentable para estructuras de oficinas de varios pisos completamente acristaladas en Chennai.

MEMBRANAS TEXTILES PARA PROTECCIÓN SOLAR DE FACHADAS

Los materiales de membrana son cada vez más populares por su atractivo estético y su uso práctico como envolventes ultraligeras o como revestimiento de fachadas en remodelaciones de edificios (Al-Masrani y Al-Obaidi, 2019). Estas membranas ofrecen eficiencia ambiental, diseño orgánico, alta adaptabilidad, semitransparencia, instalación rápida y mantenimiento mínimo. Fabricados mediante el recubrimiento de estructuras fibrosas sintéticas de alto rendimiento con nuevos polímeros, estos compuestos exhiben durabilidad, hidrofobicidad, resistencia a la llama y a la radiación UV, así como una capacidad de carga y una resistencia al desgarro excepcionales (Nurazzi et al., 2021).

Comúnmente utilizados para la protección solar y las envolventes arquitectónicas, estos diversos diseños de malla mantienen la visibilidad bidireccional y crean efectos artísticos en las estructuras de vidrio (Procaccini et al., 2024). Por lo general, consisten en hilos de poliéster (PES) recubiertos con cloruro de polivinilo (PVC) o en hebras de fibra de vidrio recubiertas con politetrafluoroetileno (PTFE) o con silicona. Disponibles en varios tonos, resistencias e impresiones personalizables, estas pantallas de tela proporcionan un aislamiento térmico rentable y de alto rendimiento (Comitti et al., 2024). Las membranas de vidrio/PTFE son las más duraderas; a menudo duran más de 30 años debido a su resistencia a la intemperie (Wang et al., 2022), mientras que las membranas de PVC son menos resistentes y duran entre 10 y 15 años con alta exposición a los rayos UV (São João, Carvalho, & Fangueiro, 2016). La investigación en curso cuenta con el apoyo de TensiNet (s. f.) y de la iniciativa COST Action TU 1303 (Mollaert et al., 2017).

Serge Ferrari desarrolló Frontside View 381 (Serge Ferrari Group, n. d. b), una membrana reciclable de hilo de PSA recubierta con PVC. Se ha utilizado para la estética y el control del clima en renovaciones como la del Hotel Oasis y en la modernización del edificio Westraven de 2008 en Utrecht. Ligeras y translúcidas, estas membranas están integradas en fachadas cinéticas para responder dinámicamente a la altitud del sol. Aunque está disponible en la India, se utiliza principalmente por motivos estéticos más que por eficiencia energética. Sin embargo, en climas más cálidos, Frontside View 381 reduce significativamente la ganancia de calor solar y el consumo de energía (Ciampi et al., 2022).

Este estudio utiliza Frontside View 381 de Serge Ferrari para sistemas de sombreado fijos y dinámicos. La literatura existente

confirma que el sombreado dinámico no se ha evaluado frente a sistemas fijos (como aletas diagrid y pantallas) en climas cálidos y húmedos. Además, aunque los materiales de sombreado exterior afectan significativamente el rendimiento de las fachadas altamente acristaladas, existen datos limitados sobre cómo el sombreado dinámico, el diagrid o las pantallas influyen en el rendimiento energético y en la luz diurna de los edificios acristalados en climas cálidos y húmedos como el de Chennai.

METODOLOGÍA

Este estudio emplea un flujo de trabajo paramétrico basado en simulación para evaluar los sistemas de sombreado externos de un edificio de oficinas de varios pisos, completamente acristalado (MGF), en el clima cálido y húmedo de Chennai. La metodología integra análisis de energía, simulación de luz diurna y modelado computacional en un entorno digital unificado para una evaluación comparativa.

- Desarrollo del modelo base

Un edificio de oficinas representativo, completamente acristalado, se modeló en Autodesk Revit según las tipologías típicas de oficinas contemporáneas (placas de piso estándar, proporciones de acristalamiento, horarios de ocupación y propiedades de los materiales). El edificio sin sombrear sirve como caso base de referencia. Los datos de EnergyPlus Weather (EPW) de Chennai se integraron para simular con precisión los niveles locales de radiación solar, temperatura y humedad.

- Modelado de sistemas de sombreado

Se aplicaron tres tipologías de sombreado externo a la geometría de la fachada base:

  - Aletas diagrid (miembros estructurales angulados)
  - Sistema de pantalla solar (membranas textiles perforadas paralelas a la fachada)
  - Sistema de sombreado dinámico (paneles cinéticos móviles con relaciones de apertura ajustables)

Para aislar los efectos de la geometría y el comportamiento operativo, los tres sistemas utilizaron la misma membrana textil de Serge Ferrari, Frontside View 381.

- Control paramétrico mediante Dynamo

Las configuraciones de sombreado dinámico se desarrollaron de forma paramétrica en Revit mediante Dynamo (s. f.). Los comandos personalizados calcularon vectores solares en función de la orientación de la fachada, la fecha y la hora, lo que permitió a los paneles cinéticos ajustar dinámicamente sus relaciones de apertura en respuesta a la exposición solar en tiempo real.

- Simulación de energía

El rendimiento térmico se analizó con E-Quest. El modelo Revit se exportó y calibró con parámetros operativos idénticos (configuraciones de HVAC, horarios de ocupación, cargas de iluminación y características de acristalamiento). El consumo anual de energía de enfriamiento de cada sistema se comparó con el caso base para calcular el porcentaje de reducción de la demanda de refrigeración.

- Análisis de luz diurna

El confort visual y la disponibilidad de luz diurna en interiores se evaluaron mediante Autodesk Insight, midiendo específicamente la iluminancia diurna útil (UDI). Este paso aseguró que minimizar la ganancia de calor solar no comprometiera inadvertidamente la penetración necesaria de la luz diurna en interiores.

- Evaluación económica y marco comparativo

Se estimaron los costos de inversión iniciales (fabricación, materiales e instalación) para cada sistema. Luego, se calcularon los períodos de recuperación de la inversión utilizando los ahorros anuales simulados en costos de energía para evaluar la viabilidad financiera a largo plazo. Para garantizar una comparación justa, todas las simulaciones utilizaron condiciones de contorno y períodos de análisis idénticos, aislando la geometría y el comportamiento del sistema como variables principales de rendimiento.

En general, la metodología combina el modelado paramétrico, la simulación de rendimiento y el análisis económico para ofrecer una evaluación integral de las estrategias de sombreado. La integración de herramientas como Revit, Dynamo, E-Quest e Insight permite un flujo de trabajo replicable y escalable para optimizar el diseño en la etapa inicial de la arquitectura sensible al clima. El diagrama de flujo de la metodología general se muestra en la Figura 1.

CONTEXTO DE LA INVESTIGACIÓN

CONTEXTO CLIMÁTICO DE CHENNAI, INDIA

Chennai, situada a 13.0827° de latitud norte y 80.2707° de longitud este, tiene un clima cálido y húmedo. La posición de la ciudad en el ecuador térmico y en la costa evita fluctuaciones estacionales drásticas de la temperatura. El período más cálido se extiende desde finales de mayo hasta principios de junio, con temperaturas máximas que oscilan entre 37 °C y 41 °C. Enero es la época más fresca, con temperaturas que oscilan entre 19 °C y 25 °C.

La membrana de sombreado de muestras seleccionada

Front View 381-3109, fabricada por Serge Ferrari Group (n. d. a), es una tela de poliéster recubierta de PVC de primera calidad con una estructura abierta que se pretensiona durante el recubrimiento (SA Industries BEC, 2014). La Tabla 1 presenta un resumen de las especificaciones técnicas del fabricante. Los datos disponibles sobre transmisión y reflexión se basan en mediciones realizadas a incidencia normal, sin considerar ángulos distintos de la normal.

Herramientas de simulación

Este estudio utiliza herramientas de simulación rápidas y sencillas en la fase inicial de diseño para identificar la solución de sombreado óptima. El flujo de trabajo emplea E-quest

Revista Hábitat Sustentable Vol. 16, N°. 1. ISSN 0719 - 0700 / Págs. 126 - 141
https://doi.org/10.22320/07190700.2026.16.01.08

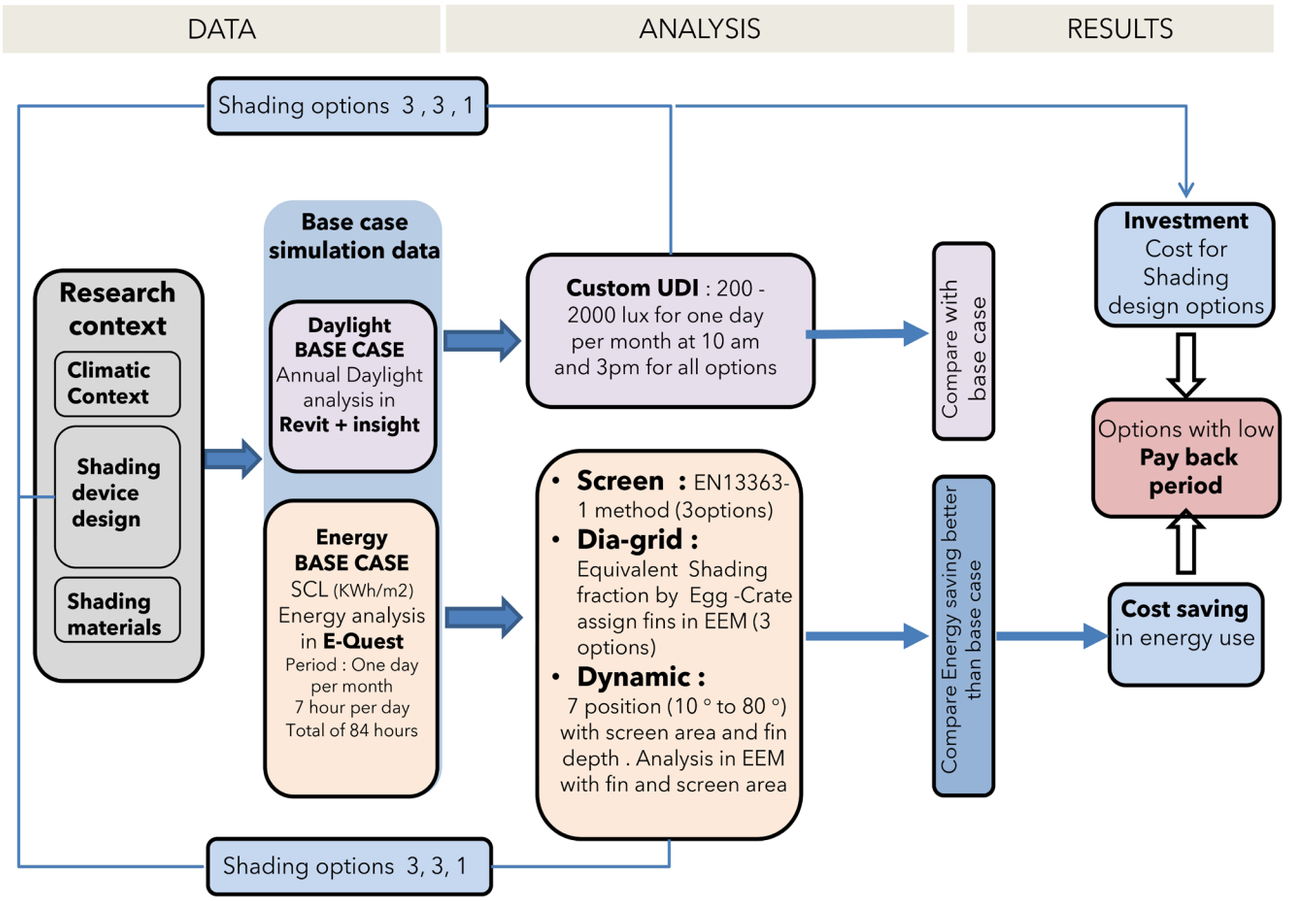


Figura 1. Diagrama de flujo de la metodología. Fuente: Preparación por los autores.

Propiedad material	Valor/especificaciones	Imagen de la aplicación	Imagen de la muestra
Color	Amarillo ceniza-381-3109		
Material	Poliéster recubierto de PVC		
Hilados	1100 Dtex PET HT		
Peso	600 gramos/m2		
Grosor	1,1 milímetros		
Resistencia a la tracción (envoltura/ trama)	330/330 daN/5cm		
Resistencia al desgarro (envoltura/ trama)	65/65 daN/5cm		
Resistencia a la temperatura	- 30 a 70		
Retardancia de llama	Euroclass B-s2, do/EN 13501-1		
Transmisión térmica (Ts) %	29		
Reflexión térmica (Rs) %	36		
Absorción térmica (As) %	35		
Transmisión visual (Tv) %	29		

Tabla 1. Especificación técnica de Front View 381-3109. Fuente: Serge Ferrari Group, (n.d.b).

para el modelado de energía, junto con Revit + Dynamo para la geometría de construcción, el análisis de iluminación y los cálculos de ángulos de sombra e incidencia.

- *E-Quest:* Derivado de DOE-2, este software orientado al usuario proporciona características térmicas dinámicas por hora para analizar la transferencia de calor en la envolvente del edificio y ofrece resultados de nivel profesional con una entrada mínima (Barozzi et al., 2016). Incorpora medidas de eficiencia energética (EME) como subsimulación del modelo base. Este estudio utiliza el asistente de diseño detallado para calcular la carga de enfriamiento del espacio (SCL) y la energía de enfriamiento horaria y anual (kWh) extraída del serpentín de enfriamiento, lo que representa un uso energético importante en climas cálidos como el de Chennai.
- *Revit + Insight:* Revit define la geometría del edificio, mientras que Insight actúa como un complemento integrado para simular la luz del día en función de la geometría, los espacios, la ubicación y los componentes definidos.
- *Dynamo:* Dynamo, una aplicación de programación visual en Revit, utiliza un método computacional basado en nodos para codificar el flujo de trabajo de diseño. En este estudio, la geometría del dispositivo de sombreado se importa a Dynamo para calcular la fracción de sombreado (porcentaje del panel acristalado sombreado) en momentos y orientaciones específicos.

DISEÑO DE LOS DISPOSITIVOS DE SOMBREADO

PANTALLAS SOLARES FIJAS

Las pantallas perforadas ofrecen beneficios visuales para un diseño minimalista frente a las aletas o las persianas salientes. Su efectividad depende del material, la relación de perforación, la profundidad, la geometría y la ubicación, así como de elementos arquitectónicos tradicionales que mejoran aún más el confort térmico en climas cálidos (Alhmoud y Alhmoud, 2024). Este estudio posiciona una pantalla plana a 20 cm del plano de acristalamiento. El panel cortina base mide 4 m × 2 m y tiene una altura de suelo de 4 m. La pantalla cubre la parte superior e inferior del panel, dejando un espacio de visualización central. El área de la pantalla varía en tres configuraciones: 60%, 80% y 100% (Figura 2).

ALETAS DIAGRID FIJAS

Diagrids, que surgieron en la construcción moderna de acero alrededor de 2003, emplean refuerzos diagonales en soportes exteriores enmarcados (Brake, 2011). Este sistema de sombreado diagonal de cajas de huevos gestiona eficazmente la captación de luz diurna, el control del deslumbramiento y la visibilidad hacia el exterior. Esta investigación emplea una rejilla de 4 m × 4 m colocada a 20 cm del panel acristalado, con profundidades de aleta de 400, 500 y 600 mm. Las aletas diagonales se colocan a nivel del piso y en el centro de la rejilla del panel (Figura 3).

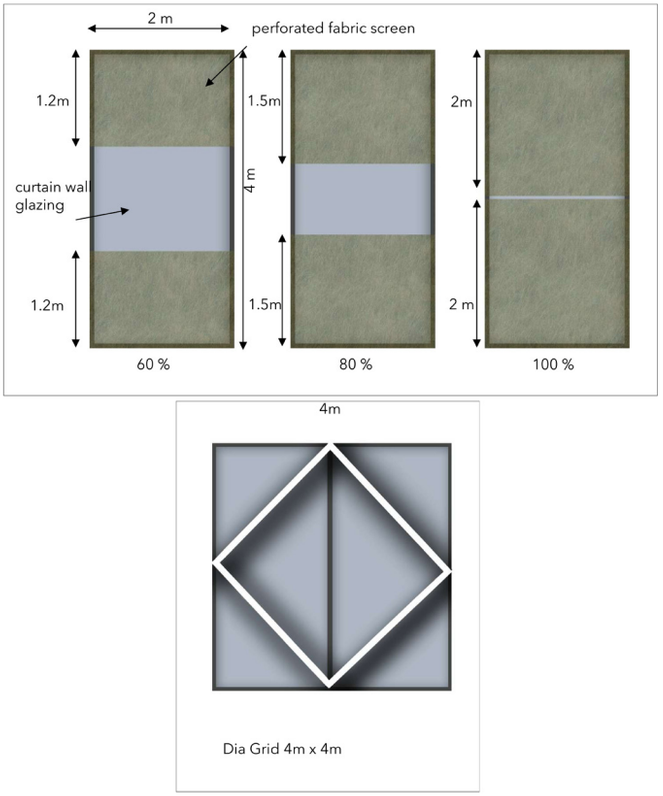


Figura 2. Opciones de pantalla solar: 60%, 80% y 100% del área del panel de acristalamiento y de la vista frontal del diagrid. Fuente: Preparación por los autores.

DISPOSITIVO DE SOMBREADO DINÁMICO

Los sistemas de sombreado dinámico mejoran la comodidad de los ocupantes al adaptarse en tiempo real a las condiciones ambientales (Sorooshnia et al., 2023). Los mecanismos de rotación cinética y de plegado pueden reducir las demandas de energía de enfriamiento e iluminación entre un 19% y un 24% en las regiones tropicales (Shi, Tablada y Wang, 2020). Este estudio utiliza una pantalla solar dinámica con perforaciones y un mecanismo de plegado tipo paraguas. Operado por un pistón neumático central, el dispositivo se extiende o se retrae de manera similar a la del sistema de la torre Al-Bahr. El panel de 4 m × 4 m contiene cuatro brazos diagonales que se pliegan en siete etapas (Figura 3). Modelado en Revit mediante una familia de paneles de cortina basados en patrones, el sistema se abre o se cierra al ajustar la altura del eje central. Las siete etapas operativas varían de 20° a 80° a intervalos de 10°

DESEMPEÑO ENERGÉTICO

Las simulaciones energéticas anuales se realizaron utilizando un modelo estándar de oficina de planta abierta de un piso, consistente con los utilizados en investigaciones anteriores (Thalfeldt, Kurnitski y Voll, 2015). Los tres tipos de dispositivos de sombreado se aplican sólo a las orientaciones este, oeste y sur. Esta investigación no consideró el ángulo de las aletas, las propiedades térmicas del material de sombreado ni la transmitancia solar a través de este.

Revista Hábitat Sustentable Vol. 16, N°. 1. ISSN 0719 - 0700 / Págs. 126 - 141
https://doi.org/10.22320/07190700.2026.16.01.08

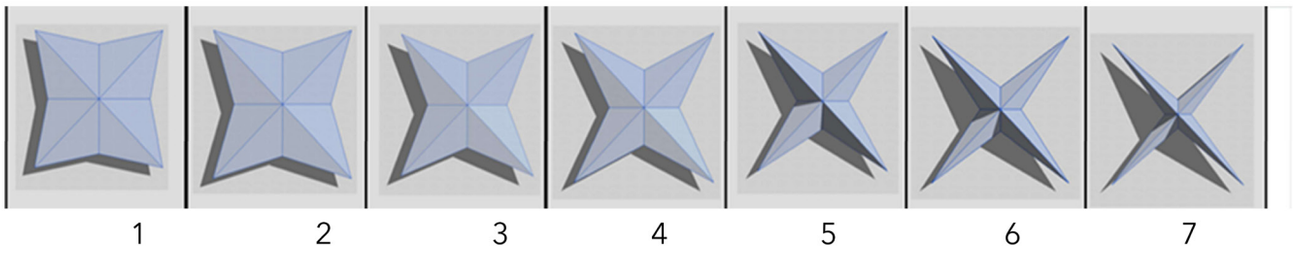


Figura 3. Imagen de la geometría de sombreado dinámico y de 7 etapas de plegado. Fuente: Preparación por los autores.

PERÍODO DE ANÁLISIS

- Un día al mes: la fecha utilizada para la simulación es el día 21 de cada mes (Coakley et al., 2014). Como el sombreado dinámico se basa en datos horarios, sería complejo considerar todos los días del año en el análisis. Los datos de un día por mes se recopilan para obtener los resultados anuales.
- Horas de análisis de sombreado: para evaluar la influencia del diseño de sombreado en la energía, se toman entre las 10:00 y las 16:00, ya que son las horas pico de radiación solar en el plano de la fachada.

Cubre 12 días a 7 horas diarias, lo que suma 84 horas de las 2880 horas diurnas.

MODELO DE ENERGÍA DEL CASO BASE

Según los hallazgos de investigaciones previas, es necesario un elemento de sombreado para un piso típico en Chennai, donde la superficie acristalada supera el 25% de la superficie de la oficina (Chockalingam, 2021). El modelo del caso base se crea en E-Quest con más del 25% del área de acristalamiento de la oficina. El edificio de oficinas es un bloque rectangular de 30 m x 45 m, con el lado más largo orientado de este a oeste y una altura de 60 metros. El edificio fue construido con 15 pisos y una altura entre pisos de 4 m. La simulación se ejecutó en modo multiplicador de piso para los pisos intermedios (entre la planta baja y el piso superior). La superficie total construida es de 13.500 m² y el área total de oficinas con aire acondicionado es de 10.800 m². Cada piso estándar tiene 1350 m², con un área de oficinas de 1080 m² en cada piso, cuatro zonas por orientación y un área central sin aire acondicionado, como se muestra en la Figura 4.

Los siguientes son los supuestos para el análisis energético basados en datos predeterminados y en estudios de casos (Chockalingam, 2021):

- Ubicación y clima : Chennai y datos meteorológicos*. Archivo E.P.W.
- Proyección norte : Norte verdadero
- Planificación de espacios de oficina/zonas de actividad : 50% de plan de oficina abierta, con 25% de cubículos, 10% de pasillos, 5% de vestíbulo y 10% de servicios públicos.
- Altura de piso a piso : 4 metros
- Altura del suelo al cielo falso : 3 metros
- Patrón de zonificación : perímetro y área central
- Zonas con A/C: el área de la oficina tiene un 80% con aire acondicionado y un 20% de área central sin aire acondicionado
- Tasa de ocupación : 12,5 personas por metro cuadrado
- Horario de ocupación : de 9:00 a 18:00 y 6 días a la semana.
- Muros : bloque A.A. de 150 mm sin aislación.
- Acristalamiento : individual transparente teñido de gris de 6 mm de grosor en una estructura de aluminio

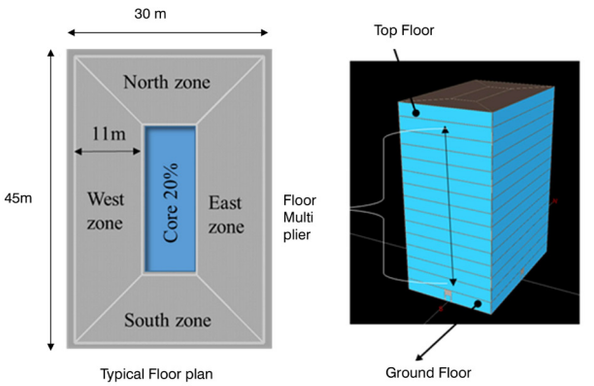


Figura 4. Modelo de caso base en E-Quest. Fuente: Preparación por los autores.

- Acristalamiento no 1205 según DOE glass
- Biblioteca con SHGC : 0,59
- Transmitancia visual : 0,43
- % relación ventana-pared : 95% en todas las orientaciones.
- Tamaño de la ventana : 2 m x 4 m.
- Carga de iluminación : 1 vatio / m²
- Carga de potencia : 2 watts/m²
- Punto de ajuste de enfriamiento : 23,3 °C
- Tipo HVAC : VAV con sistema de agua fría por piso.
- Temperatura del aire de suministro : 12 °C
- Humedad relativa (HR) : 50%
- Ganancia de calor latente por persona : 58 W
- Ganancia de calor sensible por persona : 73 W

El modelo del caso base de energía se crea mediante un asistente de diseño detallado para obtener resultados de SCL y EUI por hora. Los resultados simulados para cada hora del día suman un total de 3000 horas (de 9:00 a 18:00, 6 días a la semana, con una densidad de SCL de 96,5 kWh/m² y un EUI de 219 kWh/m²).

ANÁLISIS DE ENERGÍA PARA PANTALLA DE TELA SOLAR

La norma EN 13363-1 ofrece un enfoque sencillo para evaluar el SHGC del acristalamiento de fachadas. Los hallazgos de laboratorio demuestran una reducción del SHGC en tipos específicos de acristalamiento cuando se combinan con pantallas solares específicas. En E-quest, los componentes de fachada de medida de eficiencia energética (EEM) se crean incorporando un tipo de acristalamiento adicional con un valor SHGC más bajo, según lo

Descripción	Valor	Unidades
Stg (transmitancia solar de acristalamiento)	0,46	
St (transmitancia solar de la tela)	0,29	
g (SHGC de vidrio)	0,59	
Sa (absorbancia solar de la tela)	0,35	
Ug - factor U de acristalamiento	1,19	w/m2
G	1,14	w/m2
G2	10	w/m2
G1	5	w/m2
g tot	0,23	
No. acristalamiento igual a gtot	1403	

Tabla 2. Método EN 13363-1 para el acristalamiento seleccionado y valor SHGC revisado según las ecuaciones. Fuente: Preparación por los autores.

establecido en el método EN13363-1 (Carletti et al., 2014). Para determinar el SHGC ajustado del vidrio tintado simple elegido de la biblioteca de vidrio del DOE, específicamente el no. 1205 (SHGC = 0,59) (Lawrence Berkeley National Laboratory – James J. Hirsch & Associates, 2009), se deben usar la Ecuación 1 y Ecuación 2.

$$g_{tot} = S_{tg} + S_a (G/G_2) + St((1- g)G/G_1)$$

(Ecuación 1)

Donde g_{tot} es el SHGC revisado agregando una pantalla exterior sobre el acristalamiento, S_{tg} es la transmitancia solar del acristalamiento, S_t es el valor de transmitancia solar de la pantalla, S_a es la absorbencia solar de la pantalla, G_1 y G_2 son valores fijos definidos por los estándares, g es el SHGC del acristalamiento y G se deriva de la Ecuación 2.

$$G = (1/Ug)+(1/G_1) +(1/G_2)$$

(Ecuación 2)

Donde U_g es el valor U del acristalamiento. El área de la pantalla solar se revisa en el modelo del caso base para incluir otro tipo de vidrio con un SHGC de 0,23, según la biblioteca de vidrio DOE no. 1405. En la EEM del modelo del caso base en E-Quest, el acristalamiento de la ventana se reemplaza por una pantalla solar (60% del área de la pantalla), como se muestra en la Figura 2. Las 84 horas del período de análisis se comparan con el caso base en la Tabla 2.

ANÁLISIS DE ENERGÍA PARA EL DISPOSITIVO DE SOMBREADO DIAGRID

En E-Quest no se pueden crear aletas complejas como la caja diagonal de huevos. Por lo tanto, hemos creado aletas horizontales y verticales equivalentes basadas en la fracción de sombra de las aletas diagrid. El comando Dynamo se usa para calcular el área de sombra mediante el método P & C (Murta, 2015) para diagrid, como se muestra en la Figura 2, y la profundidad equivalente de la aleta de la caja de huevos, como se muestra en la Tabla 3. En E-Quest se creó el sombreado de ventanas usando la tabla y se ejecutó EEM para obtener el consumo de energía de enfriamiento del espacio.

ANÁLISIS DE ENERGÍA PARA EL DISPOSITIVO DE SOMBREADO DINÁMICO

El dispositivo de sombreado dinámico combina aletas y una pantalla que se transforma según el ángulo del sol. El comando de Dynamo calcula el ángulo solar de los paneles de sombreado y el ángulo abierto correspondiente. Para simplificar, se tomaron solo 7 posiciones, que oscilaban entre 10° y 80° en intervalos de 10°. Mediante los cálculos geométricos de las elevaciones, se puede determinar el área de la pantalla y la profundidad de las aletas para cada paso, como se muestra en la Tabla 5. Los cálculos de esta información se realizan durante el período de análisis de 84 horas. Para cada hora, el modelo de caso base se actualiza con una profundidad de aleta específica revisada y un área de pantalla, como en la simulación EEM. Posteriormente, se suman y se evalúan los resultados de 84 simulaciones de EEM en comparación con el caso base para el mismo período de análisis. El ahorro de energía supera el de los sin sombreado en todos los tipos de dispositivos con sombreado, como se muestra en la Figura 6.

Como se ilustra en la Tabla 4, se presenta el ángulo incidental calculado para cada hora y orientación del 21 de marzo. Con base en esto, se asignaron los pasos del dispositivo dinámico y se asignaron su % de relación ventana-pared y su profundidad de aleta equivalentes en las ejecuciones de EEM. Por ejemplo, en la etapa 1, el % de la relación ventana-pared es 20 y la profundidad de la aleta en el cálculo del área de sombra es 400 mm, n.° 2, como se muestra en la Tabla 5. Y para la etapa 7, la relación ventana-pared es del 80% con una profundidad de aleta de 200 mm (n.° 2), como se muestra en la Tabla 4. La trayectoria del sol, el vector del sol y el ángulo incidente del comando de cálculo del panel dinámico en Dynamo se muestran en la Figura 5.

DIAGRID 4m x 4m	Hora	Orientación	SF% diagrid			SF% aleta equivalente		
Día de simulación			600	500	400	800	660	520
21 de marzo	11:00	Este	55	47	37	52	44	33
	15:00	Oeste	42	35	28	40	34	25
	11:00	Sur	72	60	48	74	62	46
	15:00	Sur	72	60	48	82	69	51
21 de junio	11:00	Este	70	59	47	49	41	31
	15:00	Oeste	49	41	33	35	30	22
21 de septiembre	11:00	Este	65	54	43	61	52	38
	15:00	Oeste	37	31	25	35	29	22
	11:00	Sur	73	61	49	71	66	44
	15:00	Sur	73	61	49	88	74	55
21 de diciembre	11:00	Este	55	46	37	69	58	43
	15:00	Oeste	37	31	25	45	38	28
	11:00	Sur	27	22	18	29	24	18
	15:00	Sur	24	20	16	32	27	20
TOTAL			751	628	503	762	648	476
Promedio			53,6	44,9	35,9	54,4	46,3	34,0

Tabla 3. Tabla de profundidad H F. y V.F. equivalentes según SF% de las opciones de diagrid. Fuente: Preparación por los autores.

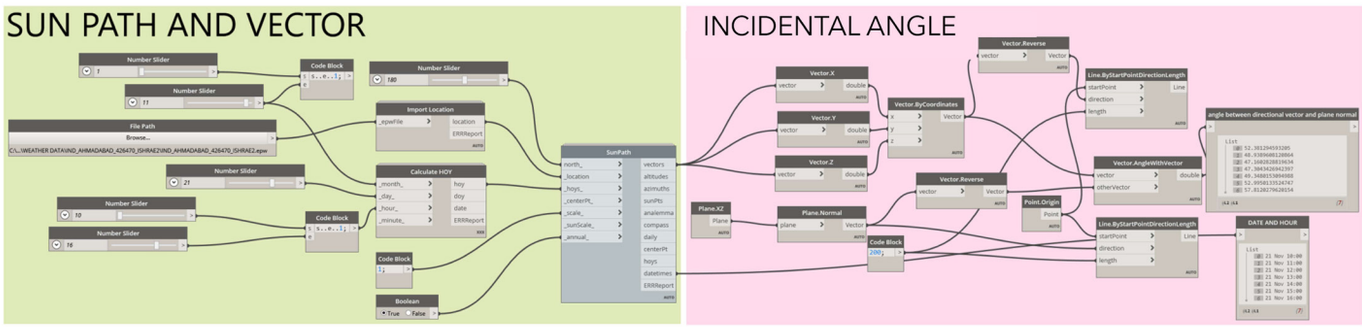


Figura 5. Trayectoria solar, vector solar y ángulo de incidencia del comando de cálculo del panel dinámico en Dynamo. Fuente: Preparación por los autores.

21 de marzo	Hora - Número de paso del dispositivo dinámico						
	10am	11am	12pm	1pm	2pm	3pm	4pm
Este / Oeste	42	27	0	4	19	24	49
Sur	17	21	23	23	22	19	15
Este / Oeste	5	3	1	1	2	3	5
Sur	2	3	3	3	3	2	2

Tabla 4. Ángulo incidente del 21 de marzo y número de paso del dispositivo de sombreado dinámico para cada hora y orientación. Fuente: Preparación por los autores.

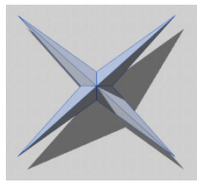
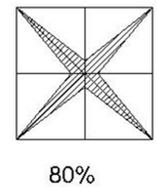
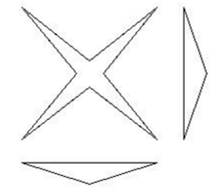
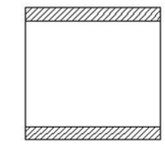
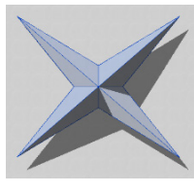
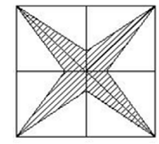
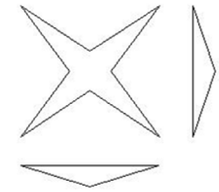
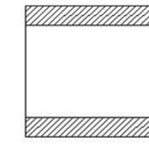
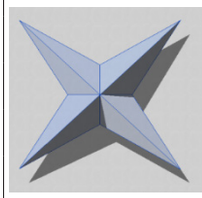
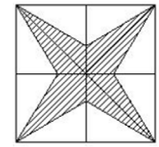
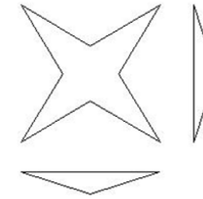
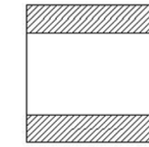
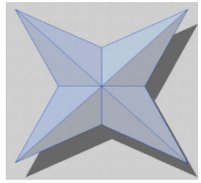
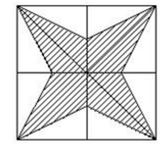
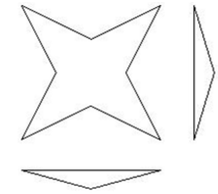
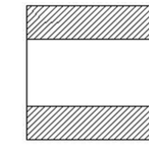
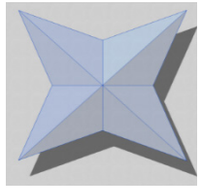
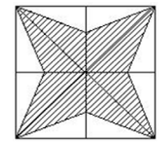
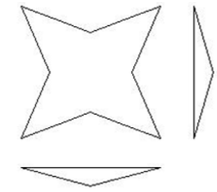
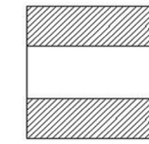
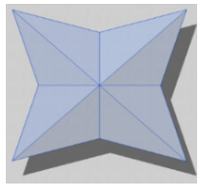
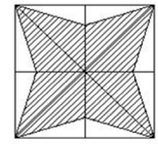
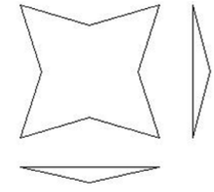
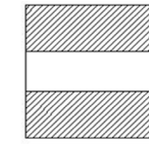
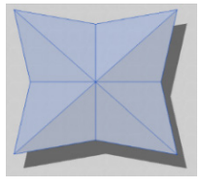
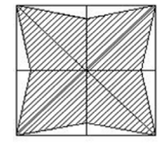
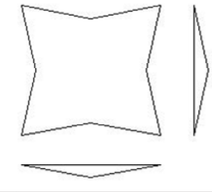
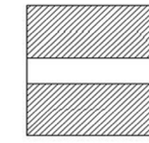
Etapa	Imagen	Descripción	Valores	Vista de planta	Vista de la zona de aletas	vista del área de la pantalla
1		Etapa	8	 80%		
		Relación ventana-pared	20%			
		Proyección	650			
		G2	400 x 2			
		Prof. HF/VF	375			
2		Etapa	7	 70%		
		Relación ventana-pared	30%			
		Proyección	630			
		G2	600 x 2			
		Prof. HF/VF	315			
3		Etapa	6	 60%		
		Relación ventana-pared	40%			
		Proyección	610			
		G2	800 x 2			
		Prof. HF/VF	305			
4		Etapa	5	 50%		
		Relación ventana-pared	50%			
		Proyección	575			
		G2	1000 x 2			
		Prof. HF/VF	287			
5		Etapa	4	 40%		
		Relación ventana-pared	60%			
		Proyección	532			
		G2	1200 x 2			
		Prof. HF/VF	266			
6		Etapa	3	 30%		
		Relación ventana-pared	70%			
		Proyección	475			
		G2	1400 x 2			
		Prof. HF/VF	237			
7		Stage	2	 20%		
		WWR	80%			
		Projection	400			
		G2	1600 x 2			
		HF/VF dep	200			

Tabla 5. Los 7 pasos del dispositivo de sombreado dinámico y su respectiva profundidad de aleta y porcentaje de área de pantalla para las ejecuciones E.E.M. de E-Quest. Fuente: Preparación por los autores.

OBSERVACIONES

1. La energía ahorrada por la pantalla solar es la más alta para los dispositivos de sombreado, seguida de las opciones dinámica y diagrid, como se muestra en la Figura 6
2. El ahorro de energía de la pantalla solar del 60% del área acristalada es casi igual al sombreado dinámico del 50% del área acristalada, como se muestra en la Figura 6
3. El mayor ahorro de energía se obtiene con el área de la pantalla más que con la profundidad de la aleta diagrid, como se muestra en la Figura 6.

RENDIMIENTO DE LA LUZ DIURNA

Los análisis anuales de la luz diurna se realizaron mediante un modelo de oficina de planta abierta para cada tipo de dispositivo de sombreado. Las propiedades visuales y ópticas de la tela se especificaron en el modelo de Revit, con una transmitancia de luz visible (VLT) del 29%. El análisis de la luz diurna se realizó mediante el complemento Insight de análisis de iluminación para Revit. Se empleó la iluminancia diurna útil (UDI) como métrica; el análisis se realizó el 21 de cada mes (García-Martín et al ., 2025), ya que el sombreado dinámico utiliza datos horarios. El rendimiento del sombreado se evaluó a las 10:00 y a las 15:00. (Ahmed, 2021), 10:00 para el este, 15:00 para el oeste y, en ambas, para las orientaciones sur. El análisis se adhirió a un rango umbral de 200-2000 lux según la ECBC (NRDC y ASCI, 2017), abarcando 24 horas de un total de 2880 horas de ocupación.

MODELO DE LUZ DIURNA DEL CASO BASE

La geometría del caso base se desarrolló en Revit, incorporando opciones de dispositivos de sombreado para cada piso. Los supuestos de simulación son los siguientes:

- No hay cubiertas de ventanas ni tabiques interiores.
- La reflectividad se establece en 80% para cielos falsos, 20% para pisos y 50% para paredes.
- El acristalamiento se especifica como el n.° 1205 de la biblioteca de vidrios D.O.E., con una transmitancia visual de 0,43.
- El plano de análisis se coloca a 0,8 metros, con un tamaño de cuadrícula de 0,6 x 0,6 metros
- Los análisis se realizan a las 10:00 y a las 15:00.
- La tela de sombreado tiene una transmitancia de luz visual (VLT) de 0,29 y una reflectancia óptica de 30%.
- El componente cielo se basa en datos meteorológicos anuales de Chennai.

Se realizan doce análisis un día al mes a las 10:00 y a las 15:00, con los resultados promediados y presentados en la Figura 7.

OBSERVACIONES

1. La configuración diagrid demuestra un rendimiento superior, como se muestra en la Figura 7.
2. La pantalla solar funciona por debajo de la línea de base sin sombra, mientras que el sombreado dinámico logra resultados equivalentes a la condición sin sombra, como se muestra en la Figura 7.
3. El sombreado controla eficazmente el deslumbramiento por encima del umbral de 2000 lux, superando el escenario sin sombra, como se muestra en la Figura 7.

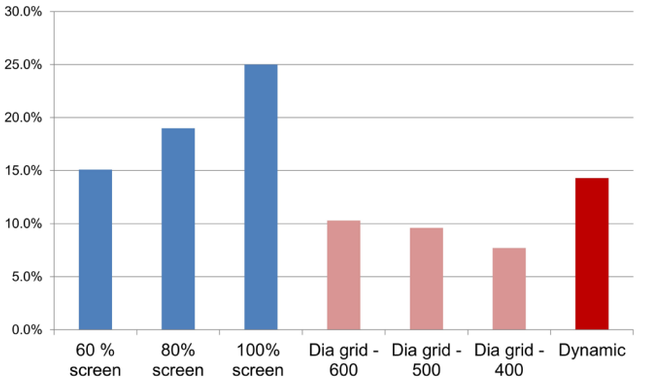


Figura 6. El ahorro de energía es mejor que no sombrear en absoluto con los tipos de dispositivos de sombreado. Fuente: Preparación por los autores.

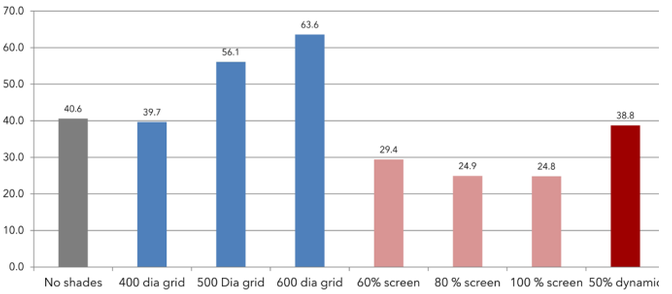


Figura 7. Análisis de la luz diurna mediante un rango personalizado de 200-2000 lux para el porcentaje del área de piso utilizable a las 9:00 y 15:00. Fuente: Preparación por los autores.

PERÍODO DE RECUPERACIÓN DE LA INVERSIÓN

El período de recuperación de la inversión es un método eficiente para evaluar la viabilidad económica de las soluciones en las etapas iniciales de diseño (Malatji et al., 2013; Chidiac et al., 2011). Representa el tiempo necesario para que una iniciativa recupere su inversión inicial a través de reducciones de costos. Esta investigación muestra que solo la conservación de energía para el enfriamiento de espacios supera el escenario de referencia. El cálculo del período de recuperación de la inversión representa el costo de la inversión inicial del dispositivo de sombreado, según lo determinado por los datos del estudio de caso y por la Ecuación 3.

$$Pb = IIC - Ofa / AES-Ofa$$

(Ecuación 3)

Opciones de dispositivo de sombreado	Costo por panel	ICC para un piso en las fachadas este, oeste y sur, área de 600 m²	Costo ICC por área de piso de oficina en R/m²	ASE por m² de área de oficina kWh/m²/ año	Período de recuperación de la inversión en años
400 Diagrid	36250	978750	725	63,2	11,48
500 Diagrid	41650	1124550	833	78,7	10,58
600 Diagrid	46600	1258200	932	84,5	11,03
pantalla del 60%	20800	561600	416	123,9	3,36
pantalla del 80 %	26400	712800	528	155,8	3,39
pantalla del 100%	32000	864000	640	205,1	3,12
Dinámico	98000	2646000	1960	117,3	16,71

Tabla 6. Costo del panel de sombreado en USD, con instalación y otros costos, por metro cuadrado del piso de la oficina y su ahorro de energía. Fuente: Preparación por los autores.

Donde: Pb = período de recuperación de la inversión; IIC-Ofa = costo de inversión inicial por metro cuadrado de área de piso de oficina para las opciones de modernización; AES-Ofa = ahorro anual de energía por metro cuadrado de área de piso de oficina para el enfriamiento de espacios. Los costos de inversión iniciales se basaron en los precios comerciales promedio nacionales de la India y en los profesionales de la construcción de Chennai. Los costos del dispositivo de sombreado por m² del área de fachada (Tabla 6) se calculan con una tasa de conversión de $1 = ₹78 (IRS, 2022). Este costo, multiplicado por el área de fachada y dividido por el área de oficinas, da IIC por opción. Utilizando la tasa comercial TNEB de Rs. 8,5 / kWh (Comisión Reguladora de Electricidad de Tamil Nadu [TNERC], 2017), se calcula el ahorro anual de energía en el enfriamiento de espacios por m². La Figura 8 muestra el período de recuperación de la inversión para todas las opciones en función del ahorro de energía y de los costos de inversión.

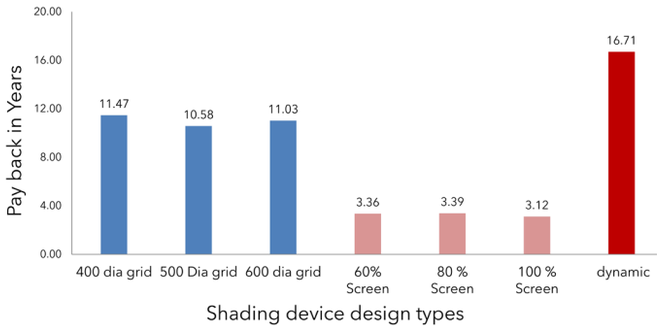


Figura 8. Período de recuperación de la inversión en años para todos los tipos de dispositivos de sombreado seleccionados. Fuente: Preparación por los autores.

RESULTADOS Y DISCUSIÓN

Los hallazgos indican que la eficacia de los sistemas de sombreado externo en climas cálidos y húmedos está influenciada no solo por la presencia de sombreado, sino también por la interacción entre las propiedades del material, la configuración geométrica y el comportamiento operativo. Investigaciones anteriores han subrayado las ventajas medioambientales de las membranas textiles, en particular su naturaleza liviana, alta reflectancia solar, adaptabilidad y características semitransparentes (Al-Masrani y Al-Obaidi, 2019; Nurazzi et al., 2021). Este estudio avanza en la comprensión al comparar cuantitativamente pantallas solares fijas, sistemas de sombreado dinámico y sombreado diagrid, utilizando el mismo material de membrana Frontside View 381 de Serge Ferrari en el contexto climático de Chennai. Al mantener la consistencia del material, el estudio aísla el impacto de la tipología de sombreado y del comportamiento del sistema en el rendimiento energético de enfriamiento.

Entre las tres tipologías examinadas, el sistema de pantalla solar logró la reducción más significativa de la demanda de energía para el enfriamiento, de aproximadamente un 25%. Este hallazgo corrobora investigaciones anteriores de Ciampi et al. (2022), que identificaron las cortinas de tela Frontside View 381 como altamente efectivas para mitigar la ganancia de calor solar en climas cálidos. Sin embargo, este estudio avanza en la literatura al demostrar que el rendimiento de la membrana mejora cuando se integra con una geometría de pantalla continua y uniformemente distribuida. Los resultados también se alinean con Kirimtat y Manioğlu (2024), quienes sostienen que las cubiertas perforadas estáticas pueden superar a los sistemas adaptativos más complejos en

Revista Hábitat Sustentable Vol. 16, N°. 1. ISSN 0719 - 0700 / Págs. 126 - 141
https://doi.org/10.22320/07190700.2026.16.01.08

latitudes tropicales debido a su protección constante frente a la radiación solar de alto ángulo. Por lo tanto, el estudio sugiere que en climas cálidos y húmedos, la capacidad de respuesta climática y la estabilidad geométrica pueden influir más que la sofisticación tecnológica. Además, el costo relativamente bajo y el período de recuperación de la inversión más corto mejoran la viabilidad de los sistemas de sombreado fijo en aplicaciones comerciales a gran escala.

El enfoque de simulación basado en materiales también resalta la importancia de la alta reflectancia solar de la membrana textil para minimizar la absorción de calor superficial en comparación con materiales convencionales de alta masa térmica, como el hormigón o el aluminio. Sin embargo, dado que los tres sistemas de sombreado emplearon el mismo material de membrana, la variación del rendimiento energético puede atribuirse principalmente a diferencias en la configuración geométrica y en el comportamiento del sistema. Esto demuestra que la forma de la fachada debe entenderse como un parámetro ambiental activo en lugar de una mera decisión estética.

El sistema de sombreado dinámico logró una reducción moderada del consumo de energía de enfriamiento, de aproximadamente 15%. La literatura existente destaca con frecuencia la adaptabilidad y la capacidad de respuesta de las fachadas cinéticas y de los sistemas móviles basados en textiles (Gonçalves et al., 2024). Sin embargo, los hallazgos presentes indican que la capacidad de adaptación no equivale necesariamente a una mayor eficiencia energética en climas tropicales. Aunque el sistema respondió eficazmente a las cambiantes condiciones solares, su rendimiento general fue inferior al de la pantalla fija debido a una cobertura de sombreado inconsistente y una mayor complejidad operativa. Este hallazgo aborda una brecha significativa identificada en la revisión de la literatura, según la cual los sistemas dinámicos de sombreado de membranas no se habían evaluado previamente en comparación con los sistemas fijos en climas cálidos y húmedos.

Por el contrario, el sistema de sombreado diagrid logró ahorros de energía inferiores al 10%, lo que indica que una mayor apertura y permeabilidad visual pueden reducir el rendimiento térmico. Si bien investigaciones anteriores han enfatizado el potencial estético y visual de las fachadas textiles (Procaccini et al., 2024), el presente estudio aclara la compensación entre el acceso a la luz diurna, la visibilidad hacia el exterior y la reducción de la carga de enfriamiento. Aunque es menos eficiente térmicamente, el sistema facilita una mayor penetración de la luz diurna y vistas al exterior, alineándose con las prioridades arquitectónicas respecto de la experiencia de los ocupantes y de la calidad espacial (Sawyer et al., 2022). En general, el estudio sugiere que los sistemas de pantallas solares fijas ofrecen la solución más equilibrada para edificios de oficinas cálidos y húmedos al integrar la eficiencia térmica, la viabilidad económica y la calidad ambiental interior. Más importante aún, los hallazgos avanzan en la investigación sobre fachadas sensibles al clima al desafiar la suposición de que las tecnologías adaptativas complejas superan de manera invariable a las estrategias de diseño pasivo.

CONCLUSIÓN

Este estudio enfatiza el papel esencial de incorporar el diseño del sistema de sombreado en las etapas iniciales del desarrollo arquitectónico, particularmente en edificios de oficinas completamente acristalados y con aire acondicionado en climas cálidos y húmedos como el de Chennai. Los hallazgos indican que las decisiones en la etapa inicial afectan significativamente la demanda de energía de enfriamiento, lo que subraya la necesidad de enfoques de diseño orientados al rendimiento en lugar de la optimización posterior al diseño. Mediante un marco computacional paramétrico, la investigación evaluó sistemáticamente múltiples estrategias de sombreado externo empleando materiales de membrana textil. Entre las opciones evaluadas, la pantalla solar perforada, colocada paralela a la fachada acristalada, resultó ser la solución más efectiva, ofreciendo un equilibrio óptimo entre eficiencia energética, rendimiento de la luz diurna y viabilidad económica. Por el contrario, aunque los sistemas de sombreado dinámico proporcionan un control adaptativo, su alto costo de capital inicial, la complejidad del sistema y los períodos prolongados de recuperación de la inversión limitan su aplicabilidad práctica en economías en desarrollo como la India.

El estudio contribuye al campo al introducir una metodología de simulación basada en materiales que permite realizar comparaciones consistentes entre diferentes tipologías de sombreado utilizando el mismo material de membrana textil. Este enfoque aísla la influencia de la geometría y el comportamiento del sistema, proporcionando así información más clara sobre los resultados de rendimiento. Los resultados confirman que las cortinas solares bien diseñadas pueden reducir significativamente el consumo de energía, al tiempo que mantienen una iluminación natural y un confort visual adecuados, todo ello con costos de inversión relativamente bajos. Sin embargo, el alcance de esta investigación se limita a materiales específicos de membranas textiles, tres orientaciones de fachadas y tres tipos de dispositivos de sombreado, con un enfoque principal en el control de la radiación solar directa en superficies acristaladas. La investigación futura debería ampliar este marco para incluir una gama más amplia de materiales, configuraciones geométricas alternativas, variables climáticas adicionales y parámetros de rendimiento integrados, como la ventilación y la energía incorporada. En general, el estudio destaca el potencial sustancial de los sistemas de fachadas de membranas textiles como una estrategia sostenible y rentable para reducir el consumo de energía en los edificios. Establece una base para una mayor exploración de soluciones de sombreado basadas en membranas, contribuyendo al avance del diseño arquitectónico sensible al clima y orientado al rendimiento.

CONTRIBUCIÓN DEL AUTOR CRediT

Conceptualización: C. C.; Curación De Datos: C. C.; Análisis Formal: C. C.; Investigación: C. C.; Metodología: C. C.; Administración De Proyectos: C. C.; Recursos: A. M.; Software: C. C.; Supervisión: C. C.; Validación: A. M.; Visualización: A. M.; Escritura – Borrador Original: A. S. K. S.; Escritura – Revisión y Edición: N. M.; Escritura – Revisión y Edición: M. N.

AGRADECIMIENTOS

Los autores agradecen a los revisores anónimos por sus comentarios constructivos, que contribuyeron a mejorar el manuscrito. Los autores no recibieron apoyo financiero para la investigación, la autoría y/o la publicación de este artículo.

REFERENCIAS BIBLIOGRÁFICAS

Ahmed, E.B. (2021). Utilizing dynamic shading system to achieve daylight performance according to LEED standards V.4: case study, university classrooms in Egypt. *HBRC Journal, 17*(1), 177-200. http://doi.org/10.1080/16874048.2021.1920138

Alhmoud, S.H., & Alhmoud, H.H. (2024). Analysis of thermal comfort techniques for the performance conserving of buildings and interior spaces. *International journal of sustainable development & planning*, *19*(11), 4193-4201. https://doi.org/10.18280/ijsdp.191109

Al-Masrani, S.M., & Al-Obaidi, K. M. (2019). Dynamic shading systems: A review of design parameters, platforms and evaluation strategies. *Automation in construction*, *102*, 195-216. http://doi.org/10.1016/j.autcon.2019.01.014

Arumugam, P., & Ramalingam, V. (2024). Thermal comfort enhancement of office buildings located under warm and humid climate through phase change material and insulation coupled with natural ventilation. *Sustainable energy technologies and assessments*, *63*, 103657. http://doi.org/10.1016/J.SETA.2024.103657

Barozzi, M, Lienhard, J., Zanelli, A., & Monticelli, C. (2016). The Sustainability of Adaptive Envelopes: Developments of Kinetic Architecture. *Procedia Engineering, 155*, 275-284. http://doi.org/10.1016/j.proeng.2016.08.029

Bhatia, A., Dontu, S., Garg, V., & Singh, R. (2024). Approach for energy efficient building design during early phase of design process. *Energy Informatics*, *7*(1), 122. https://doi.org/10.1186/s42162-024-00426-z

Brake, T. M. (2011). *Understanding Steel Design: An Architectural Design Manual.* Birkhäuser

Carletti, C., Sciurpi, F., & Pierangioli, L. (2014). The Energy Upgrading of Existing Buildings: Window and Shading Device Typologies for Energy Efficiency Refurbishment. *Sustainability*, *6*(8), 5354-5377. https://doi.org/10.3390/su6085354

Chockalingam, C. (2021). Envelope Performance Analysis of Office Buildings in Warm and Humid Climate: From Case Studies of Multi-storied Office Buildings in Chennai. In K. Thirumaran, G. Balaji, N.D. Prasad (eds) *Sustainable Urban Architecture* (vol. 114). Springer Singapore. https://doi.org/10.1007/978-981-15-9585-1

Chi, D. A., Moreno, D., & Navarro, J. (2018). Impact of perforated solar screens on daylight availability and low energy use in offices. *Advances in Building Energy Research, 15*(1), 117–141. https://doi.org/10.1080/17512549.2018.1550439

Chidiac, S.E., Catania, E.J.C., Morofsky, E. & Foo, S. (2011). Effectiveness of single and multiple energy retrofit measures on the energy consumption of office buildings. Energy, 36(8), 5037-5052. https://doi.org/10.1016/j.energy.2011.05.050

Ciampi, G., Spanodimitriou, Y., Nocente, A., Scorpio, M., & Sibilio, S. (2022). Energy performances of tensile material in building renovation in the Nordic region. *E3S Web of Conferences, 362,* 05003. https://doi.org/10.1051/e3sconf/202236205003

Coakley, D., Raftery, P., & Keane, M. (2014). A review of methods to match building energy simulation models to measured data. *Renewable and Sustainable Energy Reviews, 37,* 123–141. https://doi.org/10.1016/j.rser.2014.05.007

Comitti, A., Vijayakumaran, H., Nejabatmeimandi, M. H., Seixas, L., Cabello, A., Misseroni, D., Penesa, M., Paech, C., Bessa, M., Bown, A.C. Dal Corso, F., & Bosi, F. (2024). Ultralight membrane structures toward a sustainable environment. In A. Bahrami (eds) *Estructuras y edificios sostenibles* (pp. 17-37). Springer. https://doi.org/10.1007/978-3-031-46688-5_2

Dynamo. (n.d.). Dynamo forum. http://dynamobim.com

García-Martín, G., Campano, M. Á., Acosta, I., & Bustamante, P. (2025). New approaches in dynamic metrics for lighting control systems: A critical review. *Applied sciences*, *15*(15), 8243. https://doi.org/10.3390/app15158243

Gonçalves, M., Figueiredo, A., Almeida, R.M.S.F., & Vicente, R. (2024). Dynamic façades in buildings: A systematic review across thermal comfort, energy efficiency and daylight performance. *Renewable and Sustainable Energy Reviews, 199*, 114474. https://doi.org/10.1016/j.rser.2024.114474

Hwang, R.-L., & Chen, W.-A. (2022). Creating glazed facades performance map based on energy and thermal comfort perspective for office building design strategies in Asian hot-humid climate zone. *Applied Energy, 311*, 118689 https://doi.org/10.1016/j.apenergy.2022.118689

IRS (2022). Yearly average exchange rates for Indian Rupee to US $. https://www.irs.gov/individuals/international-taxpayers/yearly-average-currency-exchange-rates

Kirimtat, A., & Manioğlu, G. (2024). A simulation-based performance evaluation of new generation dynamic shading devices with multi-objective optimization. *Journal of Building Engineering, 90,* 109322. https://doi.org/10.1016/j.jobe.2024.109322

Lawrence Berkeley National Laboratory – James J. Hirsch & Associates. (2009). DOE- 2.2 Building Energy Use and Cost

Analysis Program. Volume 4: Libraries & Report. March 2009. James J. Hirsch

Malatji, E.M., Zhang, J., & Xia, X. (2013). A multiple objective optimisation model for building energy efficiency investment decision. *Energy and Buildings, 61*, 81–87. http://doi.org/10.1016/j.enbuild.2013.01.042

Mollaert, M. & De Laet, L. (2017). Novel Structural Skins: Improving sustainability and efficiency through new structural textile materials and designs – COST Action. *Impact, 2017*(5), 46-48. http://doi.org/10.21820/23987073.2017.5.46

Murta, A. (2015). *GPC: General Polygon Clipper library, Astrophysics Source Code Library, record ascl:1512.006.* SciX Transition Resource. https://ui.adsabs.harvard.edu/abs/2015ascl.soft12006M

Natural Resources Defense Council [NRDC] & Administrative Staff College of India [ASCI]. (2014). *Transforming Cities: Building Efficiency Lessons from Hyderabad*. https://tgredco.telangana.gov.in/PDFs/ECBC/6_Transforming_Cities_Building_Efficiency_Lessons.pdf

Nurazzi, N.M., Asyraf, M.R.M., Khalina, A., Abdullah, N., Aisyah, H.A., Rafiqah, S.A., Sabaruddin, F.A., Kamarudin, S.H., Norrrahim, M.N.F., Ilyas, R.A., & Sapuan, S.M. (2021). A Review on Natural Fiber-Reinforced Polymer Composite for Bullet Proof and Ballistic Applications. *Polymers*, *13*(4), 646. https://doi.org/10.3390/polym13040646

Procaccini, G., Prieto, A., Knaack, U., Monticelli, C., & Konstantinou, T. (2024). Textile membrane for façade retrofitting: exploring fabric potentialities for the development of innovative strategies. *Buildings*, *14*(1), 86. http://doi.org/10.3390/buildings14010086

S. A. Industries BEC, (2014). *Stamisol FT 381*. http://www.bec.es/en/fabrics-for-curtains-blinds-screens-and-textil-architecture/textile-meshes/stamisol-ft-381

São João, L., Carvalho, R., & Fangueiro, R. (2016). A Study on the Durability Properties of Textile Membranes for Architectural Purposes. *Procedia Engineering,* 155, 230-237. https://doi.org/10.1016/j.proeng.2016.08.024

Sawyer, A. O., Navvab, M., Weissman, D., & Guanzhou, J. (2022). Facade photometry: Linking annual daylight performance to facade design. *Buildings, 12*(10), 1556. https://doi.org/10.3390/buildings12101556

Serge Ferrari group. (n.d.a) Projects Serge Ferrari.https://www.sergeferrari.com/us-en/references/largest-textile-facade-netherlands-serge-ferrari

Serge Ferrari group. (n.d.b). Tenseo. Frontiside 381. https://www.sergeferrari.com/en-nz/productsfrontside-range/frontside-view-381

Shi, X., Tablada, A., & Wang, L. (2020). Influence of two motion types on solar transmittance and daylight performance of dynamic façades. *Solar Energy, 201*, 561-580. https://doi.org/10.1016/j.solener.2020.03.017

Sorooshnia, E., Rahnamayiezekavat, P., Rashidi, M., Sadeghi, M., & Samali, B. (2023). Passive intelligent kinetic external dynamic shade design for improving indoor comfort and minimizing energy consumption. *Buildings*, *13*(4), 1090. https://doi.org/10.3390/buildings13041090

TensiNet. (n.d.). https://www.tensinet.com/index.php

Thalfeldt, M., Kurnitski, J. & Voll, H. (2015). Comparison of Simplified and Detailed Window Models in Office Building Energy Simulations. Energy Procedia, 78, 2076-2081. http://doi.org/10.1016/j.egypro.2015.11.235

Tian, G-J., Fan, Y-S., Zhang, X., Wang, H., Xie, W., & Peng, K. (2020). Analysis of solar radiation heat transfer of architectural fabric membrane material. *Journal of Engineered Fibers and Fabrics*, 15. https://doi.org/10.1177/1558925020911005

Tamil Nadu Electricity Regulatory Commission [TNERC]. (2017). Determination of Tariff for Generation and
Distribution. Order in T.P. No.1 of 2017 DT:11.08.2017. Government of Tamilnadu. https://tecaonline.in/pdfupload/Files/TNERC%20Tariff%20Order-TANGEDCO%20dtd-11-08-2017.pdf

Wang, J., Huang, X., Wang, W., Han, H., Duan, H., Yu, S., & Zhu, M. (2022). Effects of PTFE coating modification on tribological properties of PTFE/aramid self-lubricating fabric composite. Materials Research Express, 9(5), 055302. http://doi.org/10.1088/2053-1591/ac587a

Revista Hábitat Sustentable Vol. 16, N°. 1. ISSN 0719 - 0700 / Págs. 126 - 141
https://doi.org/10.22320/07190700.2026.16.01.08

Revista Hábitat Sustentable Vol. 16, N°. 1. ISSN 0719 - 0700 / Págs. 142 - 155
https://doi.org/10.22320/07190700.2026.16.01.09

Recibido 28/01/2026
Aceptado 27/06/2026

AIR TIGHTNESS OF PRECARIOUS HOUSING IN INFORMAL SETTLEMENTS IN LIMA, PERU

HERMETICIDAD AL AIRE DE VIVIENDAS PRECARIAS EN BARRIOS INFORMALES DE LIMA, PERÚ

HERMETICIDADE AO AR DE HABITAÇÕES PRECÁRIAS EM ASSENTAMENTOS INFORMAIS DE LIMA, PERU

Martín Wieser
Doctor en Arquitectura
Docente investigador, Departamento de Arquitectura
Pontificia Universidad Católica del Perú
Lima, Perú
https://orcid.org/0000-0002-4556-3507
mwieser@pucp.edu.pe

Ronald Mas
Doctor en Ingeniería
Docente investigador, Departamento de Ingeniería
Pontificia Universidad Católica del Perú
Lima, Perú
https://orcid.org/0000-0003-1507-462X
rmas@pucp.edu.pe

Enrique Barrantes
Magíster en Ingeniería
Docente investigador, Departamento de Ingeniería
Pontificia Universidad Católica del Perú
Lima, Perú
https://orcid.org/0000-0002-9037-3358
ebarran@pucp.edu.pe

Enrique Mejía-Solis
Magíster en Ingeniería
Docente investigador, Departamento de Ingeniería
Pontificia Universidad Católica del Perú
Lima, Perú
https://orcid.org/0000-0002-5512-1286
enrique.mejia@pucp.edu.pe

Alessandra Gonzales
Bachiller en Arquitectura
Asistente de investigación, Facultad de Arquitectura y Urbanismo
Pontificia Universidad Católica del Perú
Lima, Perú
https://orcid.org/0009-0004-5184-1907
a20201689@pucp.edu.pe

Jimena Valdivia
Bachiller en Arquitectura
Asistente de investigación, Facultad de Arquitectura y Urbanismo
Pontificia Universidad Católica del Perú
Lima, Perú
https://orcid.org/0009-0007-5170-5245
a20200320@pucp.edu.pe

Luis-Ricardo Chirinos-García
Doctor en Ciencias Ambientales
Docente investigador, Departamento de Ingeniería
Pontificia Universidad Católica del Perú
Lima, Perú
https://orcid.org/0000-0002-5620-3312
lchirin@pucp.edu.pe

CC BY SA

Revista Hábitat Sustentable Vol. 16, N°. 1. ISSN 0719 - 0700 / Págs. 142 - 155
https://doi.org/10.22320/07190700.2026.16.01.09

ABSTRACT

The level of air tightness in a dwelling directly affects its thermal, acoustic, and health-related conditions. Due to the lack of studies providing such data at a local level, this research aimed to determine both the values and the contributing factors that condition the level of air tightness in precarious housing built in informal settlements in Lima. Using the blower door method, measurements were conducted in five dwellings, revealing air change rates between 40 and 280 ACH (Air Changes per Hour) at a differential pressure of 50 pascals, which are remarkably high and indicate poor airtightness. These findings constitute the first empirical approach to airtightness in precarious housing, providing preliminary data useful for analyzing thermal comfort in contexts of high urban vulnerability.

Keywords
sloping construction, sustainable development, thermodynamics

RESUMEN

El nivel de hermeticidad al aire de una vivienda influye directamente en las condiciones térmicas, acústicas y de salubridad que se presentan en su interior. Ante la ausencia de estudios que abordan el tema en el ámbito local, la presente investigación tuvo como objetivo identificar el valor y los factores que condicionan el nivel de hermeticidad de viviendas precarias construidas en barrios informales de la ciudad de Lima. Mediante el método de 'puerta sopladora', se realizaron mediciones en cinco viviendas que evidenciaron tasas de renovación de aire de entre 280 y 40 ACH (renovaciones de aire por hora) a una presión diferencial de 50 pascales, valores considerablemente altos que reflejan la baja hermeticidad de estas viviendas. Estos hallazgos constituyen una primera aproximación empírica a la hermeticidad al aire en viviendas precarias, al aportar datos preliminares útiles para el análisis del confort térmico en contextos de alta vulnerabilidad urbana.

Palabras clave
construcción en pendiente, desarrollo sustentable, termodinámica

RESUMO

O nível de hermeticidade ao ar de uma habitação influencia diretamente as condições térmicas, acústicas e de salubridade que se apresentam em seu interior. Diante da ausência de estudos que abordem o tema no âmbito local, a presente pesquisa teve como objetivo identificar o valor e os fatores que condicionam o nível de hermeticidade de habitações precárias construídas em assentamentos informais da cidade de Lima. Por meio do método da "porta ventiladora" (blower door), realizaram-se medições em cinco habitações, que evidenciaram taxas de renovação de ar entre 280 e 40 ACH (renovações de ar por hora) a uma pressão diferencial de 50 pascals — valores consideravelmente elevados, que refletem a baixa hermeticidade dessas edificações. Estes resultados constituem uma primeira abordagem empírica sobre a hermeticidade ao ar em habitações precárias, ao fornecerem dados preliminares úteis para a análise do conforto térmico em contextos de alta vulnerabilidade urbana.

Palavras-chave
construção em encosta, desenvolvimento sustentável, termodinâmica

Revista Hábitat Sustentable Vol. 16, N°. 1. ISSN 0719 - 0700 / Págs. 142 - 155
https://doi.org/10.22320/07190700.2026.16.01.09

INTRODUCTION

Airtightness is a key property of the energy and environmental performance of buildings, directly related to uncontrolled air leakage between the outdoor and indoor environments. This characteristic significantly affects energy consumption, thermal comfort, and indoor air quality. High airtightness helps minimize unwanted air flows, reducing energy losses associated with heating or cooling (Ambrosio Alfano et al., 2012). Similarly, the airflow and temperature differences caused by these leaks can lead to local thermal discomfort for occupants (Kalamees, 2007). On the other hand, the entry of outdoor air from these leakages can negatively affect indoor air quality, as it is not subject to the filtering and control processes typical of mechanical ventilation systems (Buonanno, Morawska & Stabile, 2009).

STUDIES ON THE AIR TIGHTNESS OF BUILDINGS

The first studies on airtightness in buildings highlighted the importance of controlling leakage as part of efficient building design. Hutcheon (1953) was one of the pioneers in highlighting the need to limit the flow of unwanted air through the envelope. Since the energy crisis of the 1970s, airtightness has acquired a more prominent role, particularly due to its potential to reduce winter heat losses and, therefore, the energy consumption associated with heating (Etheridge, 2015).

In 1998, the first airtightness limit values were established in Germany through the DIN V 4108-7 standard, which set a maximum of 3.5 air changes per hour (ACH) for buildings with natural ventilation and 1.5 ACH for those with mechanical ventilation (Guyot, Schild & Carrié, 2010). At the same time, in the United States, ASHRAE regulations included procedures for evaluating airtightness using the 'blower door' pressurization test. This regulation also classified the levels of airtightness in homes: 2 ACH was considered an excellent value, 5 ACH represented an average level, 10 ACH a common value, and above 20 ACH was classified as a house with low airtightness; all evaluated under a standard differential pressure of 50 Pa (Persily, 1998).

In recent decades, in industrialized countries, airtightness control has become increasingly important, driven mainly by the need to reduce energy consumption for both economic and environmental reasons (Zheng et al., 2019). In the particular case of residential buildings, typical airtightness values, measured under a differential pressure of 50 Pa, currently range between 1 and 3 ACH, depending on the type of ventilation, natural or mechanical (Poza-Casado et al., 2020). In this context, some high-energy-performance certifications, such as Passivhaus in Germany and Minergie in Switzerland, establish even stricter criteria requiring airtightness values below 0.6 ACH.

In contrast, in the Global South, the approach to airtightness has been more closely tied to the need to build habitable shelters and reduce health risks (Kulshreshtha, Khare & Seetharaman, 2008; Lambert et al., 2023). Inadequate ventilation can lead to high concentrations of particulate matter, polluting gases such as CO, SO_2, and NO_2, and toxic compounds emitted by stoves and cooking systems, increasing the incidence of respiratory diseases (Kulshreshtha et al., 2008). In addition, poor ventilation control can foster mold growth, a problem especially prevalent in low-income housing (Choi et al., 2020). In general, ventilation conditions are not a priority in the design of informal housing, exposing occupants to health risks from both insufficient and excessive uncontrolled ventilation.

Despite differences in regional priorities, experimental studies on airtightness using the 'blower door' pressurization method have also been conducted in the Global South. 189 homes were evaluated in different climatic zones of Chile, obtaining an average airtightness of 12.9 ACH at 50 Pa (Bobadilla et al., 2014). In this study, light wooden buildings were the least airtight (24.6 ACH), whereas massive concrete buildings were the most airtight (9 ACH). Based on these results, Chile updated its "Thermal Regulation" in November 2025, establishing airtightness limits ranging from 4 to 8 ACH at 50 Pa, depending on the bioclimatic zone. On the other hand, in Uruguay, heavy traditional masonry buildings (fired ceramics) were analyzed, reporting ACH values of 3.5 and 5.2 at 50 Pa for two houses (Rodríguez Muñoz et al., 2020). These results are comparable with European studies carried out in various typologies and materials: in Estonia, an average of 4.9 ACH was reported in detached single-family houses of light construction with wooden frames (Kalamees, 2007); in Lithuania, an average of 4.73 ACH in single-family houses built with bricks or masonry blocks (Sfakianaki et al., 2008); and in Greece, a value of 7.0 ACH in stone, concrete and brick single-family dwellings (Šadauskienė et al., 2016). Finally, in multifamily masonry typologies, averages of 7.26 ACH have been recorded in apartments in Spain (Feijó-Muñoz et al., 2018), and 6.25 ACH in a concrete-and-brick apartment in Montenegro (Tombarević, Vušanović & Šekularac, 2023).

In this study, airtightness measurements were conducted using the pressurization method with a blower door in informal housing built with limited resources in a peri-urban area of Lima, Peru. According to our review of the literature, no previous studies have applied this technique in homes with similar characteristics. This work seeks to address this space by

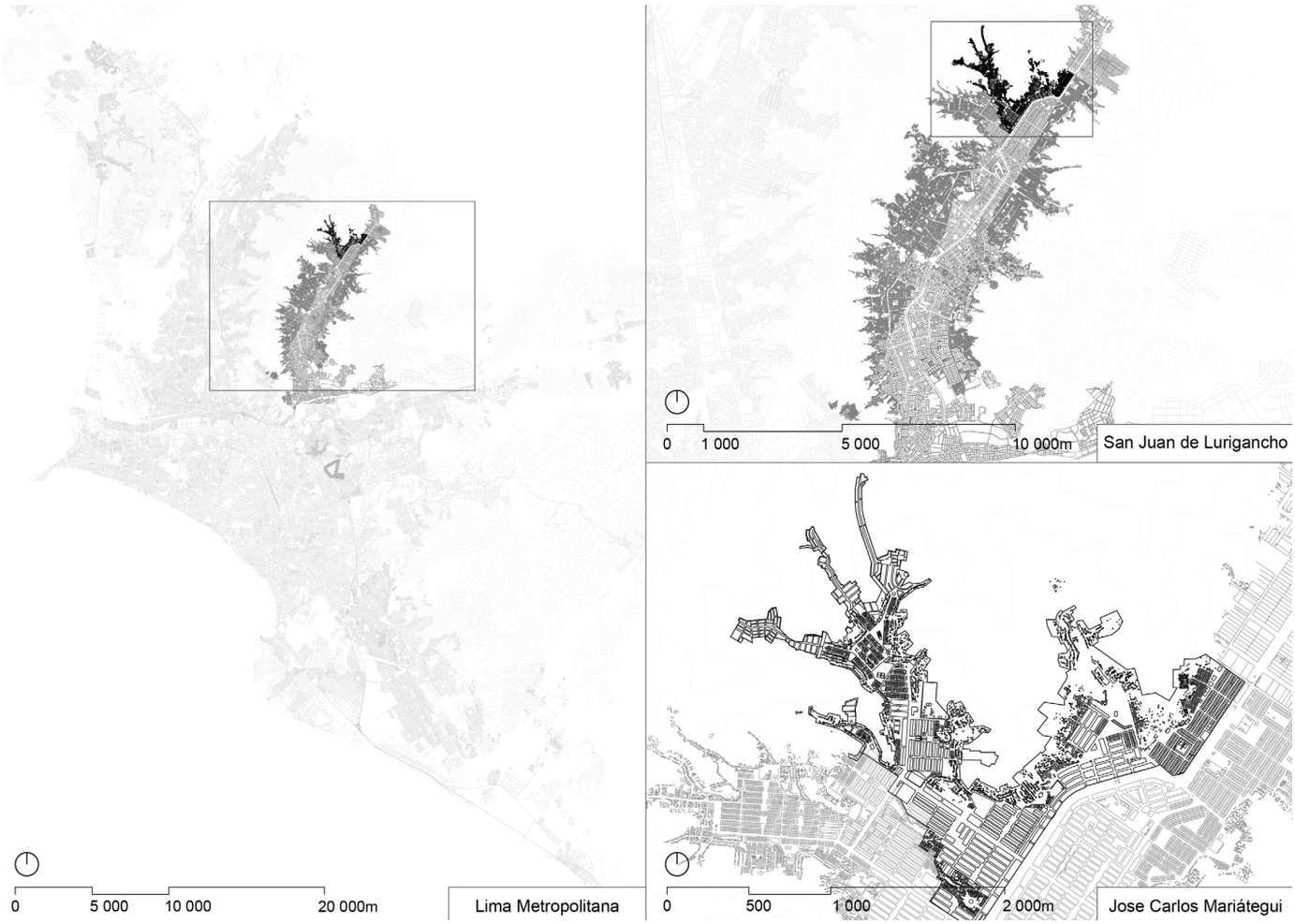


Figure 1. Location of the José Carlos Mariátegui neighborhood in the San Juan de Lurigancho district of Lima. Source: Prepared by the Authors.

exploring airtightness in unconventional buildings. The importance of generating this evidence lies in the fact that, by providing initial empirical data on infiltrations in precarious contexts, starting points for the study of thermal comfort and habitability (Oraiopoulos et al., 2023) can be established. Consequently, these findings could offer a first empirical approach to feed the debate on informal housing retrofitting strategies and the relevance of applying international standards in highly vulnerable contexts.

CASE STUDY

THE NEIGHBORHOOD OF JOSÉ CARLOS MARIÁTEGUI

The neighborhood of José Carlos Mariátegui, located in the district of San Juan de Lurigancho, Lima, originated as an informal settlement in the mid-1980s on flat, arid land lacking basic infrastructure. Located between the Andean foothills, approximately 15 kilometers from the center of Lima and at an altitude of 400 masl (Figure 1), this neighborhood has experienced progressive, unplanned growth, based mainly on self-construction. Over time, new settlements have occupied increasingly elevated areas on the slopes surrounding the original esplanade.

This growth pattern reflects a common dynamic in the urban peripheries of many Latin American cities, where informal urban expansion has been the primary driver of housing stock growth. In the specific case of Lima, it is estimated that about 2 million people live in homes with roofs built from light, precarious materials such as wood, calamine, or similar materials, representing approximately 20% of the population (National Institute of Statistics and Informatics [INEI], 2018). These precarious conditions tend to persist for an average of 10 to 15 years before housing reaches some level of consolidation in both construction and the provision of basic services (Lambert et al., 2023).

Revista Hábitat Sustentable Vol. 16, N°. 1. ISSN 0719 - 0700 / Págs. 142 - 155
https://doi.org/10.22320/07190700.2026.16.01.09



Figure 2. Overview of the José Carlos Mariátegui neighborhood. Source: Prepared by the Authors.



Figure 3. Location of the houses tested on a satellite image. Source: Prepared by the Authors using an image from Google Earth.

Revista Hábitat Sustentable Vol. 16, N°. 1. ISSN 0719 - 0700 / Págs. 142 - 155
https://doi.org/10.22320/07190700.2026.16.01.09

Equipment	Brand	Model
Blower door equipment, pressure gauge (integrated), and airflow meter (orifice plate).	The Energy Conservatory	Minneapolis Blower Door with differential-pressure sensor, DG-700. Software TECLOG 4 version 4.2.0.37
Signal recorder	Yokogawa	MW100
Differential pressure sensors	Yokogawa	EJX110A
Temperature and relative humidity recorders	Onset	Hobo data logger U12-006
Micro weather station	Onset	Hobo data logger Microstation H21-002

Table 1. Instruments used to measure leakage levels. Source: Prepared by the Authors.

The lower degree of consolidation of both housing and infrastructure in the higher areas of informal neighborhoods is readily identifiable. It is usually associated with an increased risk of landslides and difficulties in accessing and providing basic services. The initial precariousness of the buildings is manifested in the use of light materials, such as board or *triplay* walls and corrugated metal plate roofs (Figure 2). These constructive conditions, combined with the desert, coastal, and temperate climates of Lima, generate extremely uncomfortable indoor environments, characterized by overheating in summer and very low temperatures in winter (Wieser, Verdiere & Fennell, 2022). Mild and moderate breezes are constant throughout the year (usually between 1 and 2 m/s). However, they do not mitigate the effects of intense summer solar radiation (5.7 kWh/m^2 per day on average), high relative humidity (60% in summer and 80% in winter on average), or frequent winter fog (Oraiopoulos et al., 2025).

METHODOLOGY

Airtightness tests were carried out in five dwellings (Figure 3) using the blower door method in accordance with the ASTM E779-19 standard, Standard Test Method for Determining Air Leakage Rate by Fan Pressurization (Advanced Standards Transforming Markets [ASTM], 2019). This procedure, widely applied in conventional buildings (Hsu et al., 2021), quantifies air leakage through the building envelope by creating a controlled pressure difference with a fan to pressurize and depressurize the indoor space. The instrumentation used in the tests is detailed in Table 1. Although the number of homes evaluated is small, this limitation is inherent to the exploratory nature of the study and the difficult conditions of the context: accessibility, safety, and availability of families. The study is conceived as an exploratory approach that provides initial empirical background on airtightness in this type of building, a gap in the literature to date. The values obtained are not intended to be statistically representative of the universe of informal housing in Lima, but to provide initial empirical data that guide future research and serve as input for energy modeling and the formulation of public policies, in line with similar studies in hard-to-access contexts (Rodríguez Muñoz et al., 2020; Oraiopoulos et al., 2023).

The envelope of the studied dwellings consisted of corrugated metal plate roofs (zinc calamine) and walls built of wood, drywall, Oriented Strand Board (OSB), or brick (Figure 4). For house selection, convenience sampling was used, subject to families' willingness and geographical proximity. The aim was to document the actual condition of the houses in the neighborhood, where imperfections and deterioration in the structures are a common result of self-construction and economic constraints. However, four of the five homes were located on hillsides, approximately 300 meters from the vehicle access point, and at a height difference of nearly 90 meters, which posed an additional challenge for transporting the equipment needed for the tests. For the equipment to work properly, an additional electric generator capable of providing a starting current of 8-10 amps was needed, since the local network in the upper parts of José Carlos Mariátegui is unstable and supplies only 4-5 amps.

Prior to the tests, a thorough inspection was carried out in each dwelling, making sure that doors and windows remained completely closed and that there were no additional openings that could affect the accuracy of the measurements. The blower door equipment was then installed, preliminary tests were carried out, and a pressure of 10 Pa was applied, increasing it in 5 Pa increments until reaching 50 Pa.

Revista Hábitat Sustentable Vol. 16, N°. 1. ISSN 0719 - 0700 / Págs. 142 - 155
https://doi.org/10.22320/07190700.2026.16.01.09



Figure 4. Tested housing. Floor plans and features. Source: Prepared by the authors.

It should be noted that in dwellings with high leakage due to poor construction, achieving the required pressure differences was challenging. To ensure the reliability of the data obtained, the readings from the pressure gauge integrated into the blower door equipment were compared with measurements from four additional calibrated pressure gauges.

During the tests conducted in each house, the blower door system fan generated a pressure difference ΔP throughout the building envelope. To characterize this condition, differential pressure measurements were recorded at three strategic points inside the house. Simultaneously, the equipment measured the airflow rate (Q) required to maintain the pressure difference. From these data, the air leakage coefficient (C) and the pressure exponent (n) were determined by fitting the obtained values to the airflow model equation as a function of pressure (Equation 1).

$$Q = C(\Delta P)^n \qquad \text{(Equation 1).}$$

The number of air changes per hour (ACH) was calculated by multiplying the airflow rate (Q) by 3600 (the number of seconds in an hour) and dividing the result by the dwelling's interior volume (V), according to the conventional formula used in airtightness studies (Equation 2).

$$ACH = \frac{Q \times 3600}{V} \qquad \text{(Equation 2).}$$

Additionally, both indoor and outdoor environmental parameters were recorded during the tests. The detailed list of instruments used is presented in Table 1. Figure 5 and Figure 6 illustrate the installation and operation of the equipment in the field.

Dwelling V01 was used as a reference case to compare the pressure-difference measurements recorded by the blower-door pressure gauge with those obtained by the other four pressure gauges used in the experiments

Revista Hábitat Sustentable Vol. 16, N°. 1. ISSN 0719 - 0700 / Págs. 142 - 155
https://doi.org/10.22320/07190700.2026.16.01.09





Figure 5. Left. Blower door installed in Dwelling V03. Source: Prepared by the Authors.
Figure 6. Right. Sensors installed in Dwelling V02. Source: Prepared by the Authors.

(Figure 7). Throughout the entire pressure range tested, no significant differences were observed between the instruments. This allowed validating the reliability of the measurements.

RESULTS AND DISCUSSION

The leakage airflow and air change values recorded in the evaluated dwellings far exceeded the ranges commonly reported in the specialized literature (Figure 8 and Figure 9). At a differential pressure of 50 Pa, leakage rates ranged from 40 to 285 ACH. In the particular case of dwellings V02, V03 and V04, it was not possible to reach the target pressure of 50 Pa due to the high leakage rates, typical of highly permeable constructions; in those cases, these values were estimated from the extrapolation of the airflow curve, by applying the equation of the power law model ($Q=C(\Delta P)^n$) with the coefficients C and n

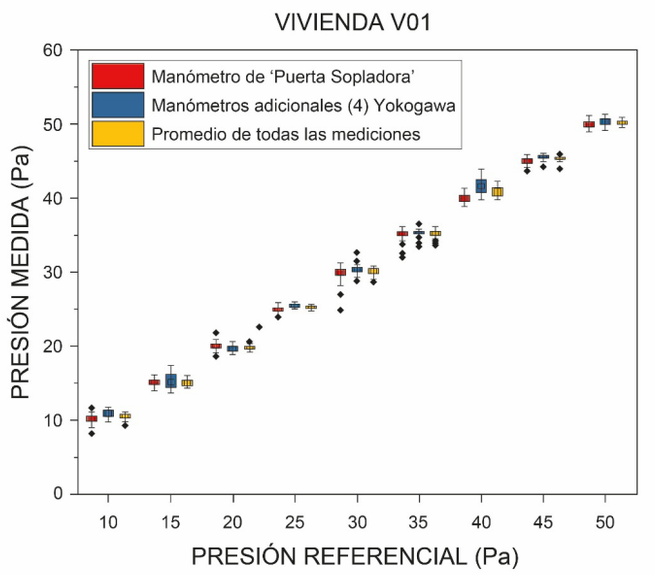


Figure 7. Average pressure measurements in dwelling V01. Source: Prepared by the Authors.

Revista Hábitat Sustentable Vol. 16, N°. 1. ISSN 0719 - 0700 / Págs. 142 - 155
https://doi.org/10.22320/07190700.2026.16.01.09

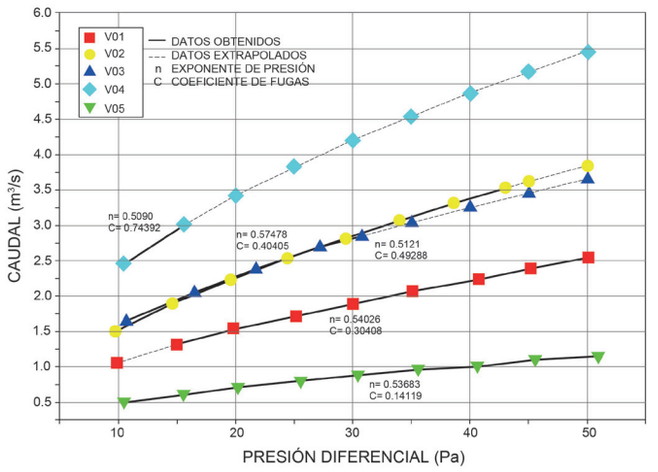


Figure 8. Air leakage in each dwelling. The dashed lines indicate the values extrapolated when the desired pressure difference could not be reached during the experiment. Source: Prepared by the Authors.

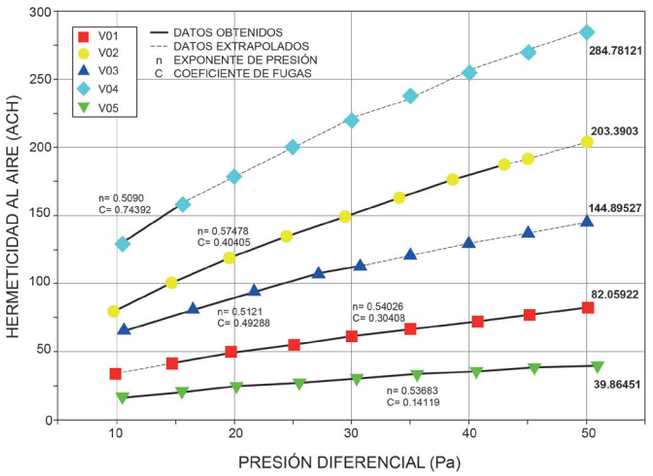


Figure 9. Air renewal per hour in each dwelling. The dashed lines indicate values that were extrapolated to facilitate comparison. Source: Prepared by the Authors.

derived from the least squares adjustment of the measured points. However, it should be noted that in the V04 dwelling, due to its extreme permeability, only two measurement points could be obtained; therefore, the result is presented as an indicative estimate, as it did not meet the minimum of five points required by the ASTM E779-19 standard.

These unusually high leakage levels reflect the structural deficiencies typical of the informal housing analyzed. For reference, the highest values reported in the literature were 24.6 ACH in Chilean wooden houses (Bobadilla et al., 2014) and 23.3 ACH in an Italian building built in 1950 (Ambrosio Alfano et al., 2012). The main causes identified were the presence of visible interstices in both the openings and the joints between the walls and the corrugated iron roof. In the sample, the houses with wooden slatted walls (V02 and V04) and drywall (V03) had significantly higher leakage levels than those built with masonry walls (V01) and OSB panels (V05). This difference is explained by construction systems based on assembled elements, such as boards or drywall sheets, which create multiple potential leakage points that tend to expand over time due to wear, weather exposure, and material expansion, thereby accentuating the loss of airtightness.

The logarithms of the measured leakage airflow (Q) and pressure difference (ΔP) values were closely related across all dwellings, with coefficients of determination (R^2) near 1 (Figure 10 and Table 2). This makes it possible to identify the predictability of air-leak behavior, which, in turn, allowed the extrapolation of data in cases where the desired pressure difference could not be generated during the experiments. The air leakage graph (Figure 10) shows, for each dwelling, the fan-generated air inflow relative to the applied air pressure. For example, in Dwelling V01, the airflow varies between 1.3 and 2.5 m^3/s depending on the pressure exerted. However, it should be noted that for dwelling V04, the values obtained are indicative estimates, as the property's extreme permeability prevented the collection of the minimum of five points required by the ASTM E779-19 standard. In this specific case, the R^2 coefficient lacks interpretative value, and the results should be read with the caution typical of findings under conditions of extreme constructive precariousness.

During fieldwork, in test preparations, and during instrument placement, it was possible to identify in all the dwellings conditions that foreshadowed very high levels of leakage. Interstices, grooves, perforations, inaccuracies in the joints of the constructive components, and even gaps without enclosing capacity were identified (Figure 11). In the case of dwelling V02, the identified opening in the ceiling is an intentional design feature for ventilation and lighting. During the survey of information in the area, it was observed that this type of solution is part of the spontaneous constructive logic of several inhabitants, which allows considering this case as an example of how certain habitability practices severely impact airtightness. That which, in formal contexts, would be classified as a defect or constructive damage in precarious housing, represents a habitual condition derived

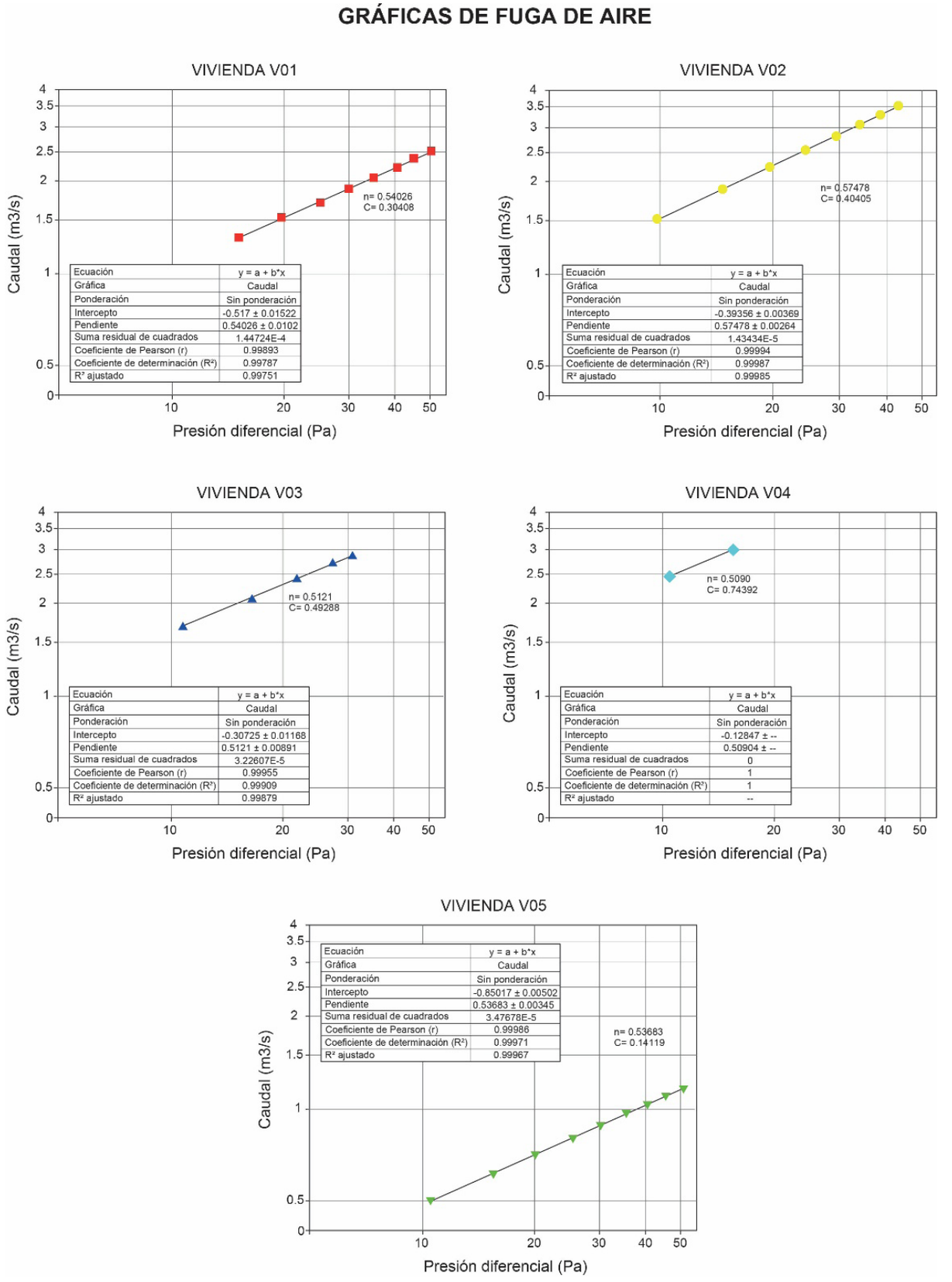


Figure 10. Air leakage results in the five tested dwellings. For dwelling V04, the values represent indicative estimates, as the property's extreme permeability prevented obtaining the minimum of five points required by the ASTM E779 standard. Source: Prepared by the Authors.

Revista Hábitat Sustentable Vol. 16, N°. 1. ISSN 0719 - 0700 / Págs. 142 - 155
https://doi.org/10.22320/07190700.2026.16.01.09

Housing	Material	Air leakage exponent, n	Leakage coefficient, C	Flow rate (m3/s) at 50 Pa	ACH to 50 Pa	R2
V01	Brick	0.540	0.304	2.5	82	0.99787
V02	Wooden panel	0.575	0.404	3.8	203	0.99987
V03	Drywall	0.512	0.493	3.7	145	0.99909
V04	Wooden panel	0.509	0.744	5.4	285	1.00000 a
V05	OSB	0.537	0.141	1.1	40	0.99971

*Value obtained with only two measuring points because the building's extreme permeability prevented the required pressure differentials from being reached by the equipment. In this case, the R2 coefficient has no interpretative value for the quality of the adjustment, and the results should be considered indicative estimates rather than validated against the minimum criteria (5 points) of the ASTM E779 standard.

Table 2. Values obtained from the tests. Source: Prepared by the Authors.

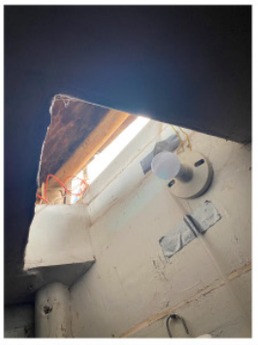
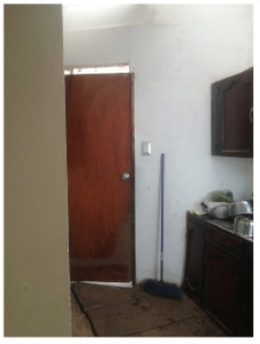
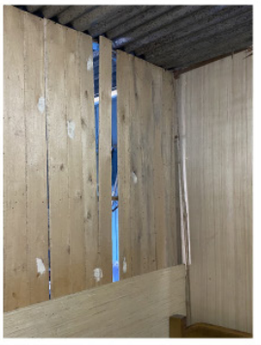
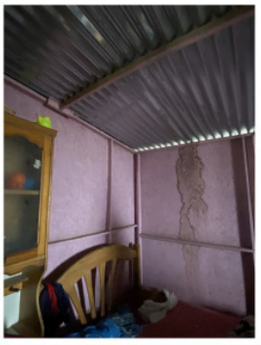
	V01	V02	V03	V04	V05
FOTOGRAFÍA					
AMB.	Dormitorio	Baño	Cocina	Dormitorio	Dormitorio
INTERSTICIOS	-Vanos con partes sin cerramiento vidriado -Ladrillos con orificios debido a rajadura	-Abertura en el techo del baño -Intersticio entre el cerramiento y la calamina	-Aberturas en la puerta de entrada	-Rotura de listones de madera -Intersticio entre el muro del baño y de los dormitorios	-Intersticio entre el cerramiento y la calamina

Figure 11. Images of situations that reduce the level of airtightness of homes. Source: Prepared by the Authors.

from self-construction and lack of maintenance due to economic limitations. The observed constructive precariousness aligns with previous socio-economic diagnoses in these informal settlements (Wieser et al., 2022), which show that income constraints in self-construction limit families' ability to invest in appropriate technical solutions and to improve their homes' envelopes.

These extreme leakage levels have significant implications for the thermal comfort, health, and indoor air quality of the occupants. On the one hand, the presence of air currents, leaks, and loss of thermal control of the living space can generate severe thermal discomfort, especially during winter. In addition, the high, uncontrolled air change makes it difficult to maintain stable indoor temperatures, which negatively impacts the dwelling's overall habitability. Consequently, the continuous, unfiltered entry of outdoor air can introduce pollutants, moisture, and suspended particles, which increase the risk of respiratory diseases, aggravate pre-existing conditions such as asthma, and promote mold growth. This problem is exacerbated by the large presence of sand outside.

The relevance of this study lies not only in being the first to perform systematic measurements of airtightness in informal housing in the Peruvian context, but also in its potential to nurture future energy and thermal comfort simulations. The availability of empirical airtightness data for self-

Revista Hábitat Sustentable Vol. 16, N°. 1. ISSN 0719 - 0700 / Págs. 142 - 155
https://doi.org/10.22320/07190700.2026.16.01.09

built and precarious homes is essential for calibrating models that estimate energy losses, habitability, and intervention scenarios. In contexts where data collection is difficult and expensive, these results allow the definition of realistic infiltration ranges for comparative studies, impact evaluations, or improvement proposals in retrofitting programs and public policies.

To assess the magnitude of the recorded results, note that a dwelling with 100 ACH at 50 Pa — an intermediate value within the recorded range — experiences an involuntary air renewal rate several times higher than the recommended rate to ensure minimum conditions of habitability and comfort. In practical terms, this implies that any passive thermal conditioning strategy—such as the use of mass or insulation—would have a marginal effect without a prior intervention on the envelope that reduces such leakage. Similarly, the identified leakage levels make the eventual efficient use of active heating systems practically infeasible, since the generated heat would dissipate almost immediately to the outside.

All these considerations are especially relevant in the context of Lima's winter, characterized by temperatures that, although not extreme in absolute terms, are difficult to cope with indoors without thermal control, due to the combination of high relative humidity, little direct solar radiation, and the inability to finance heating systems (Wieser et al., 2022). Consequently, improving the airtightness of homes in this context should be considered a priority and a relatively low-cost intervention before other comfort and energy-efficiency improvements.

CONCLUSIONS

Based on the values obtained, it is seen that air leakage levels in precarious housing in informal neighborhoods in Lima are extremely high compared to international regulations and even to housing in other countries in the region. This lack of airtightness, combined with the enclosure's lightness and low insulation, leaves the inhabitants exposed to extreme conditions, reducing thermal comfort, especially during the winter months. Taking into account the identified material characteristics and the sector's economic vulnerability, which limits the viability of autonomous, rigorous interventions by the inhabitants, improving the airtightness of these homes suggests the need to implement public support programs.

Additionally, the results suggest that possible simple and low-cost interventions aimed at increasing airtightness in these homes, such as sealing interstices and improving the fit of doors and windows, would have a significant thermal impact, making it necessary to consider them in the design of eventual improvement programs and public housing policies aimed at these populations. The results obtained constitute a fundamental input for the development of regulations and intervention strategies to improve habitability in contexts of urban vulnerability.

Given the recognized direct relationship between airtightness and thermal comfort in naturally ventilated, non-active-thermal-conditioning buildings, greater attention is needed to include these aspects in the local academic and public debate. Finally, there is a need to significantly expand the number of measurements to establish a baseline that covers the different types of construction in the country's housing stock, across both the formal and informal sectors. This baseline will support the development of technical regulations adapted to local realities and calibrate energy simulation models applicable to housing contexts in other cities in the country and the region.

CONTRIBUTION OF AUTHORS CRediT

Conceptualization, M.W.; Data curation, M.W., R.M., E.B., E.M., A.G., J.V., LC; Formal analysis, M.W., R.M., E.B., E.M., L.C.; Acquisition of M.W. funding; Research, M.W., R.M., E.B., E.M., A.G., J.V., L.C.; Methodology, M.W., R.M., E.B., E.M., A.G., J.V., L.C.; Project Management, M.W.; Supervision, M.W., R.M., E.B., E.M., A.G., J.V.; Validation, M.W., R.M., E.B., E.M., L.C.; Writing – original draft, M.W.; Writing – revision and editing, M.W., R.M., E. B., E.M., A.G., J.V., L.C.

ACKNOWLEDGMENTS

This study has been carried out thanks to the financing of the following units of the Pontifical Catholic University of Peru: Department of Architecture, CIAC Architecture and City Research Center, Energy Laboratory of the Department of Engineering, and the Academic Direction of Social Responsibility DARS. We are grateful to the families who allowed us to conduct measurements in their homes and to the NGO CENCA for support with fieldwork and engagement with the community.

Revista Hábitat Sustentable Vol. 16, N°. 1. ISSN 0719 - 0700 / Págs. 142 - 155
https://doi.org/10.22320/07190700.2026.16.01.09

BIBLIOGRAPHIC REFERENCES

Ambrosio Alfano, F., Dell'Isola, M., Ficco, G., & Tassini, F. (2012). Experimental analysis of air tightness in Mediterranean buildings using the fan pressurization method. *Building and Environment*, 53, 16-25. https://doi.org/10.1016/j.buildenv.2011.12.017

Advancing Standards Transforming Markets [ASTM]. (23 de enero de 2019). *ASTM 779-19. Standard Test Method for Determining Air Leakage Rate by Fan Pressurization*. ASTM International. https://doi.org/10.1520/E0779-19

Bobadilla, A., Díaz, M., Figueroa, R., & Arriagada, R. (2014). Proposal of Acceptable Air Tightness Classes for Buildings in Chile. *Revista de la construcción, 13*(1), 15-23. https://doi.org/10.4067/S0718-915X2014000100002

Buonanno, G., Morawska, L., & Stabile, L. (2009). Particle emission factors during cooking activities. *Atmospheric Environment, 43*(20), 3235-3242. https://doi.org/10.1016/j.atmosenv.2009.03.044

Choi, Y., Lim, Y., Kim, J., & Song, D. (2020). Why Does a High Humidity Level Form in Low-Income Households Despite Low Water Vapor Generation? *Sustainability, 12*(18), 7563. https://doi.org/10.3390/su12187563

Etheridge, D. (2015). A perspective on fifty years of natural ventilation research. *Building and Environment*, *91*, 51-60. https://doi.org/10.1016/j.buildenv.2015.02.033

Feijó-Muñoz, J., Poza-Casado, I., González-Lezcano, R. A., Pardal, C., Echarri, V., Assiego De Larriva, R., Fernández-Agüera, J., Dios-Viéitez, M. J., Del Campo-Díaz, V. J., Montesdeoca Calderín, M., Padilla-Marcos, M. Á., & Meiss, A. (2018). Methodology for the Study of the Envelope Airtightness of Residential Buildings in Spain: A Case Study. *Energies*, *11*(4), 704. https://doi.org/10.3390/en11040704

Guyot, G., Schild, P. G., & Carrié, R. (abril de 2010). *Stimulation of good building and ductwork airtightness through EPBD*. ASsessment and Improvement of the EPBD Impact [ASIEPI]. https://www.aivc.org/resource/stimulation-good-building-and-ductwork-airtightness-through-epbd

Hsu, Y.-S., Zheng, X., Cooper, E., Gillott, M., & Wood, C. J. (2021). Evaluation of the indoor pressure distribution during building airtightness tests using the pulse and blower door methods. *Building and Environment*, *195,* 107742. https://doi.org/10.1016/j.buildenv.2021.107742

Hutcheon, N. B. (1953). Fundamental considerations in the design of exterior walls for buildings. Technical Report No.13 of the Division of Building Research Ottawa. *NRC, 2057*(37), 1-25. https://publications-cnrc.canada.ca/eng/view/object/?id=e03a98e6-9755-42d8-a9ea-f8b34680bded

Instituto Nacional de Estadística e Informática [INEI]. (2018). *Resultados definitivo de los Censo Nacional 2017. Región Lima*. XII de Población, VII de Vivienda y III de Comunidades Indígenas. https://www.inei.gob.pe/media/MenuRecursivo/publicaciones_digitales/Est/Lib1550/

Kalamees, T. (2007). Air tightness and air leakages of new lightweight single-family detached houses in Estonia. *Building and Environment*, *42*(6), 2369-2377. https://doi.org/10.1016/j.buildenv.2006.06.001

Kulshreshtha, P., Khare, M., & Seetharaman, P. (2008). Indoor air quality assessment in and around urban slums of Delhi city, India. *Indoor Air*, 18(6), 488-498. https://doi.org/10.1111/j.1600-0668.2008.00550.x

Lambert, R., Escalante, C., De los Rios, S., Verdiere, M., & Wieser, M. (2023). *Dignified housing and energy justice: Learning from low-income neighbourhoods in Lima*. University College London (UCL). https://discovery.ucl.ac.uk/id/eprint/10181093/

Oraiopoulos, A., Wieser Rey, M., Verdiere, M., Fennell, P., & Ruyssevelt, P. (September 4–6, 2023). *Thermal comfort in low-income housing in informal settlements in Lima, Peru. Towards a localised adaptive comfort standard* [Conference paper]. Building Simulation 2023: 18th Conference of International Building Performance Simulation Association [IBPSA], Shanghai, China. https://doi.org/10.26868/25222708.2023.1474

Oraiopoulos, A., Wieser, M., Verdiere, M., Lambert, R., Fennell, P., & Ruyssevelt, P. (2025). Improving habitability in informal settlements in the Global South: Exploring the impact of community urban green infrastructure on outdoor heat stress. *Building and Environment, 287*(Part A), 113787. https://doi.org/10.1016/j.buildenv.2025.113787

Persily, A. K. (December 6–10, 1998). *Airtightness of commercial and institutional buildings: Blowing holes in the myth of tight buildings*. Thermal Performance of the Exterior Envelopes of Buildings VII: proceedings of the Conference. Clearwater, Florida, EE.UU. https://www.aivc.org/sites/default/files/airbase_13149.pdf

Poza-Casado, I., Cardoso, V. E. M., Almeida, R. M. S. F., Meiss, A., Ramos, N. M. M., & Padilla-Marcos, M. Á. (2020). Residential buildings airtightness frameworks: A review on the main databases and setups in Europe and North America. *Building and Environment*, *183*, 107221. https://doi.org/10.1016/j.buildenv.2020.107221

Rodríguez Muñoz, J. M., Sevrini, A., Gil, G., & Bove, I. (2020). Estudio experimental de la permeabilidad al aire de edificios en Uruguay. ENERLAC. *Revista de energía de Latinoamérica y el Caribe*, 4(2), 76-91. https://enerlac.olade.org/index.php/ENERLAC/article/view/119

Šadauskienė, J., Šeduikytė, L., Paukštys, V., Banionis, K., & Gailius, A. (2016). The role of air tightness in assessment of building energy performance: Case study of Lithuania. *Energy for Sustainable Development*, *32*, 31-39. https://doi.org/10.1016/j.esd.2016.02.006

Sfakianaki, A., Pavlou, K., Santamouris, M., Livada, I., Assimakopoulos, M.-N., Mantas, P., & Christakopoulos, A. (2008). Air tightness measurements of residential houses in Athens, Greece. *Building and Environment, 43*(4), 398-405. https://doi.org/10.1016/j.buildenv.2007.01.006

Revista Hábitat Sustentable Vol. 16, N°. 1. ISSN 0719 - 0700 / Págs. 142 - 155
https://doi.org/10.22320/07190700.2026.16.01.09

Tombarević, E., Vušanović, I., & Šekularac, M. (2023). The Impact of Windows Replacement on Airtightness and Energy Consumption of a Single Apartment in a Multi-Family Residential Building in Montenegro: A Case Study. *Energies, 16*(5). https://doi.org/10.3390/en16052208

Wieser, M., Verdiere, M., & Fennell, P. (December 13-14, 2022). *The impact of built environment on thermal comfort in informal settlements. The case of José Carlos Mariátegui, Lima, Perú* [Conference paper]. Sixth Building Simulation and Optimisation Virtual Conference. Hosted by University of Bath, UK. https://publications.ibpsa.org/proceedings/bso/2022/papers/bso2022_52.pdf

Zheng, X., Cooper, E. W., Mazzon, J., Wallis, I., & Wood, C. J. (2019). Experimental insights into the airtightness measurement of a house-sized chamber in a sheltered environment using blower door and pulse methods. *Building and Environment, 162*, 106269. https://doi.org/10.1016/j.buildenv.2019.106269

Comparative thermal evaluation of a vegetative shading structure and a synthetic shade net in Parral, Chile
Nelson Arias-Jiménez, Rodrigo Figueroa-San-Martín, Diego Cárdenas-Merino
Revista Hábitat Sustentable Vol. 16, N°. 1. ISSN 0719 - 0700 / Págs. 156 - 169
https://doi.org/10.22320/07190700.2026.16.01.10

COMPARATIVE THERMAL EVALUATION OF A VEGETATIVE SHADING STRUCTURE AND A SYNTHETIC SHADE NET IN PARRAL, CHILE

Recibido 28/01/2026
Aceptado 27/06/2026

EVALUACIÓN TÉRMICA COMPARATIVA DE UNA ESTRUCTURA DE SOMBREADO VEGETAL Y UNA MALLA DE SOMBREADO ARTIFICIAL EN PARRAL, CHILE

AVALIAÇÃO TÉRMICA COMPARATIVA DE UMA ESTRUTURA DE SOMBREAMENTO VEGETAL E DE UMA TELA DE SOMBREAMENTO ARTIFICIAL EM PARRAL, CHILE

Nelson Arias-Jiménez (Autor de Correspondencia)
Doctor en Arquitectura y Urbanismo
Académico, Facultad de Arquitectura, Construcción y Diseño,
Departamento de Diseño y Teoría de la Arquitectura
Universidad del Bío-Bío
Concepción, Chile
https://orcid.org/0000-0003-1782-7314
narias@ubiobio.cl

Rodrigo Figueroa-San-Martín
Doctor en Arquitectura y Urbanismo
Académico, Facultad de Arquitectura, Construcción y Diseño,
Departamento de Ciencias de la Construcción
Universidad del Bío-Bío
Concepción, Chile
https://orcid.org/0000-0002-4382-3782
rfiguero@ubiobio.cl

Diego Cárdenas-Merino
Magíster en Arquitectura
Estudiante de doctorado, Facultad de Arquitectura, Construcción y Diseño,
Departamento de Diseño y Teoría de la Arquitectura
Universidad del Bío-Bío
Concepción, Chile
https://orcid.org/0000-0003-3093-6996
diegocardenasarquitecto@gmail.com

CC BY SA

ABSTRACT

This study comparatively evaluates the thermal performance of a grapevine pergola and a shade net as conditioning strategies for intermediate outdoor spaces in a temperate climate. An in situ experiment was conducted in Parral, Chile, using environmental measurements collected over a 14-day summer period as part of an exploratory approach. Air temperature, relative humidity, wind speed, and globe temperature were recorded, and mean radiant temperature and the Universal Thermal Climate Index (UTCI) were calculated for the period between 11 am and 4 pm. The results indicate the grapevine pergola performed better, with a lower UTCI and mean radiant temperature values than those recorded under the shade net. The greatest difference between the two conditions was observed for the second parameter, with daily variations ranging from 2.6 to 4.3 °C. It is concluded that the grapevine pergola constitutes a more effective passive strategy for improving outdoor thermal comfort.

Keywords
overheating, grapevine pergola, outdoor thermal comfort, transitional spaces

RESUMEN

Este estudio evalúa comparativamente el comportamiento térmico de un parrón y una malla de sombreo como estrategias de acondicionamiento de espacios exteriores intermedios en clima templado. Se desarrolló un experimento in situ en la ciudad de Parral, Chile, mediante mediciones ambientales durante 14 días de verano, con un enfoque exploratorio. A partir del registro de temperatura del aire, humedad relativa, velocidad del viento y temperatura de globo, se calcularon la temperatura radiante media y el índice UTCI entre las 11:00 y las 16:00 h. Los resultados evidencian un mejor desempeño del parrón, con valores menores de UTCI y de temperatura radiante media que los de la malla. La mayor diferencia entre ambas condiciones se observó en este último parámetro, con variaciones diarias de 2,6 a 4,3 °C. Se concluye que el parrón constituye una estrategia pasiva más efectiva para mejorar el confort térmico exterior.

Palabras clave
sobrecalentamiento, parrón, confort térmico exterior, espacios intermedios

RESUMO

Este estudo avalia comparativamente o comportamento térmico de um pergolado com parreira e de uma tela de sombreamento como estratégias de condicionamento de espaços exteriores intermediários em clima temperado. Desenvolveu-se um experimento in situ na cidade de Parral, Chile, com medições ambientais ao longo de 14 dias de verão, adotando-se uma abordagem exploratória. A partir do registro da temperatura do ar, da umidade relativa, da velocidade do vento e da temperatura de globo, calcularam-se a temperatura radiante média e o índice UTCI entre 11h e 16h. Os resultados evidenciam um melhor desempenho do pergolado com parreira, com valores mais baixos de UTCI e de temperatura radiante média em comparação à tela. A maior diferença entre as duas condições foi observada neste último parâmetro, com variações diárias de 2,6 a 4,3 °C. Conclui-se que o pergolado com parreira constitui uma estratégia passiva mais eficaz para melhorar o conforto térmico exterior.

Palavras-chave
Superaquecimento, pergolado com parreira, conforto térmico exterior, espaços intermediários



Figure 1. Two examples of grapevine pergolas and their deciduous behavior. Source: Prepared by the authors.

INTRODUCTION

The environmental conditioning of outdoor spaces is a growing challenge amid climate change and the intensification of the urban heat island (Intergovernmental Panel on Climate Change [IPCC], 2023). In cities and regions with temperate climates, rising temperatures and increased solar radiation have worsened thermal comfort in outdoor spaces, affecting their inhabitability and everyday use (Liu et al., 2025; Wang et al., 2023). In this scenario, passive climate mitigation strategies, particularly those based on vegetation, have become relevant as sustainable alternatives to energy-intensive technological solutions (Gherri, 2023).

In this sense, the literature has extensively addressed the role of green infrastructure across different scales, from urban trees to plant-based construction systems (Bowler et al., 2010). On the latter, it has been shown that the incorporation of vegetation in enclosures can significantly reduce the mean radiant temperature in outdoor environments (Perini & Magliocco, 2014) and the surface temperature of walls exposed to direct solar radiation, depending on variables such as leaf density and vegetation cover (Nasr et al., 2024).

For cooling outdoor spaces, in addition to incorporating vegetation on walls, facades, or roofs, there are vegetative shades, built with horizontal structures that control solar radiation using climbing species, typically seen on pergolas. In these cases, vegetation acts as an effective climate mediator through two main mechanisms: reducing incident solar radiation via shading and evaporative cooling associated with evapotranspiration (Salonen et al., 2022; Wu et al., 2024). These processes reduce both surface and air temperatures, improving thermal comfort in outdoor spaces and mitigating the urban heat island effect.

Recent evidence agrees that the shade generated by vegetation tends to offer a better thermal performance than artificial devices, both in reducing temperature and improving outdoor thermal comfort (Kusaka, Asano & Kimura, 2022). In contrast, there is less systematization of knowledge regarding traditional devices that, in local contexts, have fulfilled similar roles in environmental conditioning. In this context, the grapevine pergola—a vegetation-based structure associated with grape cultivation—is a characteristic element of vernacular architecture in temperate climates, particularly in Mediterranean regions and Chile's central valley. The grapevine pergola can provide habitable intermediate spaces by generating shade and favorable microclimates. Its use has been documented in rural and domestic practices in the country, where it is part of everyday life (Aravena Alvarado, 2015).

From an environmental perspective, its trait as a deciduous species (Figure 1) enables efficient seasonal adaptation, providing shade in summer and allowing solar radiation to enter in winter, as in other deciduous species (Zhang et al., 2022). From the physical point of view, the grapevine pergola acts as a thermal regulation system that combines shading and evapotranspiration. Despite its presence in both rural and urban environments, the grapevine pergola has been progressively replaced by solutions with rapid, economical implementation, such as high-density polyethylene shading meshes. These provide immediate control of solar radiation and generate cooling effects that enhance thermal comfort (Lopez-Cabeza et al., 2022; Zhao et al., 2024).

This replacement of an ancestral solution by an artificial element is not solely a matter of technical criteria, but also part of broader standardization dynamics driven by public policies and the market, which tend to displace vernacular strategies. Similar phenomena have been documented in other contexts, where the incorporation of industrialized solutions has contributed to the homogenization of vernacular built environments (Arias Tapiero, Ortega & Vasconcelos, 2025). Consequently, a progressive loss of the relevance of identity is observed in the configuration of outdoor spaces, particularly in rural areas (Figure 2).



Figure 2. People in front of a grapevine pergola and mesh shading system. Source: Prepared by the Authors.

Although there is a consolidated body of research on the role of vegetation as a climate mediator, recent research on the thermal performance of vegetation has mainly concentrated on contemporary systems, such as walls (Jim, 2015; Zheng et al., 2025), facades (MacIvor & Margolis, 2015) and green roofs (From Christ et al., 2025), so a specific gap is identified in the study of plant shaders as environmental conditioning devices. In this context, this study aims to analyze the effect of the grapevine pergola on the thermal behavior of outdoor spaces, as a representative case of vegetative shading, and compare it with a contemporary solution based on shading mesh, to evaluate its effects on micro-meteorological conditions and its potential as an environmental conditioning strategy.

METHODOLOGY

STUDY SITE

The study was conducted in the city of Parral, located in Chile´s central valley (36°08′ S, 71°49′ W), an area characterized by a temperate climate with Mediterranean influence (Csb), according to the Köppen–Geiger classification. This climate has hot, dry summers with high solar radiation and large daily temperature ranges, and colder, wetter winters.

These conditions allow evaluating the performance of shading strategies in scenarios representative of everyday life in south-central Chile, particularly in contexts with high summer sun exposure. According to the historical records of the nearest weather station, average maximum air temperatures during the warm months reach 28.1 °C in December, 30.6 °C in January, 30.0 °C in February, and 26.5 °C in March. Specifically for this last month, in which the measurements were made, the absolute maximum temperatures recorded range from 31.4 °C to 34.3 °C (Servicios Climáticos, 2026).

EXPERIMENTAL DESIGN

The design adopts an exploratory experimental approach, based on in situ measurements, to analyze the thermal behavior of a pre-existing plant shading system (grapevine pergola) compared with a localized surface covered with high-density polyethylene shading mesh (mesh). The study was conducted in a single intervened space, in which a limited mesh surface (1.0 × 1.2 m) was introduced, allowing localized micro-meteorological variations within the same environment. This approach considers operational constraints specific to the case study and is proposed as an exploratory strategy to identify initial comparative trends (Figure 3).

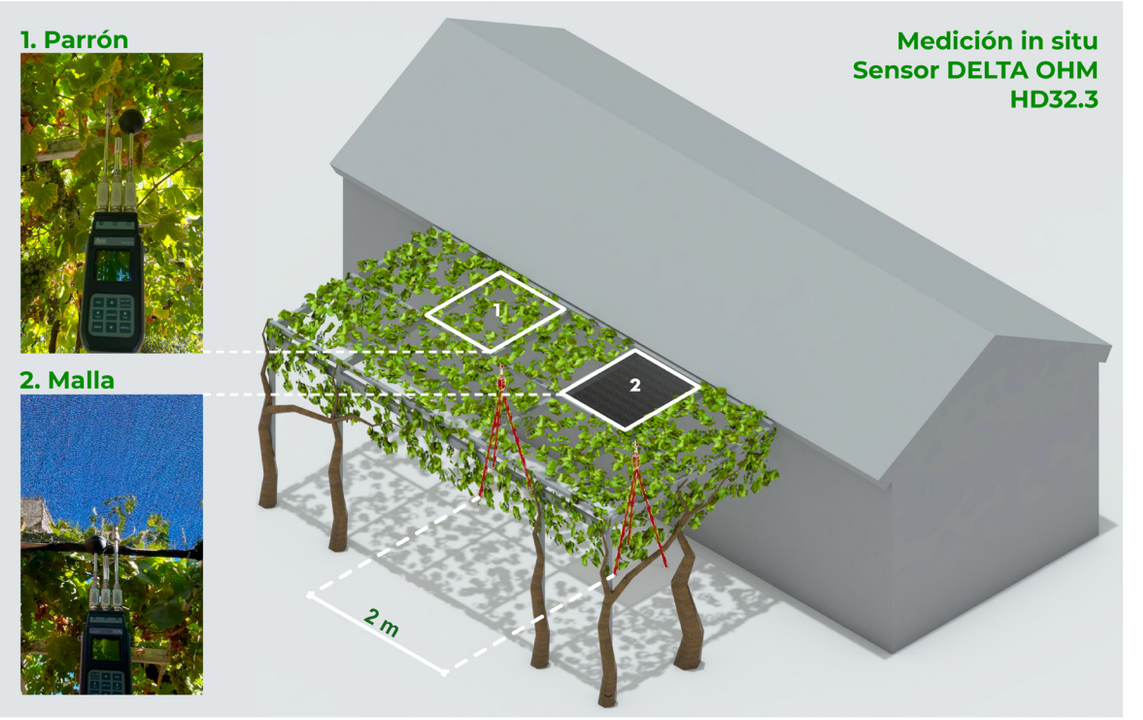


Figure 3. Layout of shading strategies studied. Source: Prepared by the Authors.

Measurements were taken at specific positions under both conditions to capture variations in thermal behavior on a micro-meteorological scale. In particular, the globe temperature was recorded beneath the mesh, approximately 75 cm from the shading surface and 1.55 m above ground level, representative of the exposure height of the human body in a standing position (Zhao et al., 2024). Data loggers and sensors were used, positioned at the center of the shading systems studied, 2 meters apart.

The measurement campaign was conducted over a continuous 14-day period during the summer season. This duration allows for the recording of daily thermal cycles and reduces the influence of specific meteorological events, improving the representativeness of the data, in line with methodological recommendations for environmental field studies (Arias-Jimenez et al., 2026; Guerrero-Blond et al., 2017; Umishio et al., 2024).

The measurements were taken by sensors installed in the study space, with a 10-minute recording interval during each 24-hour period. In similar research, the analysis time window has been restricted to capture the critical peaks of thermal stress and avoid distortions caused by low solar altitude (Elgheznawy & Eltarabily, 2021; Lee et al., 2018; Zhao et al., 2024). In accordance with this criterion, a sunlight study was run using a georeferenced digital replica of the experimental site in Archicad to identify the period

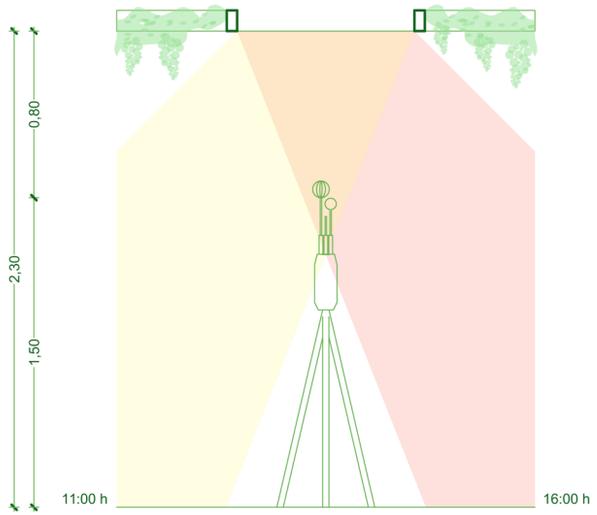


Figure 4. Period of incident solar radiation on the sensor. Source: Prepared by the Authors.

of greatest solar exposure over the analyzed area. Based on this procedure, the interval from 11 am to 4 pm was defined as the study window (Figure 4). This made it possible to evaluate the shading performance under consistent sunlight conditions and concentrate the analysis on the hours of greatest thermal demand. In this way, the sensors recorded the variables of the outdoor thermal environment necessary for thermal evaluation of the space in the shade (Table 1 and Table 2).

Variable	Unit
t_a	Air temperature (°C)
t_g	Globe temperature (°C)
v_a	Wind speed (m/s)
RH	Relative humidity (%)

Table 1. Measured meteorological variables. Source: Prepared by the Authors.

Component / Probe	Type of Sensor	Operating Range	Accuracy / Tolerance Class	Resolution
Base Unit (HD32,3)	Processor with SICRAM inputs	*T*: -5 to 50 °C *RH*: 0 to 90%	±1 digit at 20 °C	N/A
Globe thermometer	Pt100 (Ø = 50 mm / 150 mm)	-10 to 100 °C	Class 1/3 DIN	0.1 °C
Combined Thermohygrometer	Pt100 (*T*) Capacitive (*RH*)	*T*: -40 to 80 °C *RH*: 0 to 100%	*T*: Class 1/3 DIN *RH*: ±1,5% (0-90%) / ±2% (90-100%) at 15-35 °C	*T*: 0.1 °C *RH*: 0.1%
Omnidirectional Anemometer	Hot wire (NTC 10 kΩ)	*v*: 0.1 to 5 m/s *T*: 0 to 80 °C	±0.2 m/s (0.1 to 1 m/s) ±0.3 m/s (1 to 5 m/s)	0.01 m/s

Table 2. Technical specifications and operating ranges of the DELTA OHM HD32,3 microclimatic monitoring system. Source: Prepared by the Authors.

To evaluate the outdoor thermal conditions, two complementary indicators were established. The mean radiant temperature (T_r) was used as a physical variable to characterize the radiative load of the environment on the human body, accounting for solar, reflected, and long-wave radiation emitted by surrounding surfaces. In outdoor spaces, this variable is especially relevant for analyzing the physical-radiative performance of shading systems and their influence on the thermal perception of the environment (López-Cabeza et al., 2022; Mihalakakou & Romeos, 2026). The Universal Thermal Climate Index [UTCI] (COST European Cooperation in Scientific and Technical Research, 2026) was also used as a biometeorological index of external thermal stress, which expresses an equivalent temperature derived from a thermophysiological model that integrates air temperature, relative humidity, wind speed, and thermal radiation to represent the human physiological response to the environment (Błażejczyk et al., 2013; Bröde et al., 2012). Its use is relevant to comparative studies of outdoor comfort under sunny, built-shade, and vegetative-shading conditions (Watanabe et al., 2014). Thus, the t_r allowed comparing the radiative performance of the shading system, while the UTCI allowed evaluating its effects on thermal comfort conditions at the pedestrian scale.

CALCULATION OF MEAN RADIANT TEMPERATURE

The mean radiant temperature (T_r) is calculated by the sensor from the measured parameters: globe temperature (T_g), air temperature (t_a), and wind speed (v_a); the following formulas were used, as established in the standard ISO 7226:2025.

When the air speed is less than 0.2 m/s, (Equation 1).

$$t_r = \left[\left(t_g + 273\right)^4 + \frac{0.25 \times 10^8}{\varepsilon_g} \left(\frac{\left|t_g - t_a\right|}{D} \right)^{1/4} \times \left(t_g - t_a\right) \right]^{1/4} - 273$$

(Equation 1)

When the air speed is greater than or equal to 0.2 m/s, (Equation 2).

$$t_r = \left[\left(t_g + 273\right)^4 + \frac{1.1 \times 10^8 \times v_a^{0.6}}{\varepsilon_g \times D^{0.4}} \left(t_g - t_a\right) \right]^{1/4} - 273$$

(Equation 2)

Where D = diameter of the globe thermometer; E_g = 0.95, the presumed emissivity of the globe thermometer; t_g = globe temperature; t_a = air temperature; and v_a = air speed.

Measurement condition	Convection regime (ISO 7726)	Average combined uncertainty (u_c) [°C]	Minimum uncertainty ($u_{c\,max}$) [°C]	Maximum uncertainty (u_{cmax}) [°C]
t_r mesh	Natural	± 0.155	± 0.077	± 0.179
	Forced	± 0.747	± 0.105	± 2.215
t_r grapevine pergola	Natural	± 0.146	± 0.082	± 0.167
	Forced	± 0.516	± 0.105	± 1.198

Table 3. Comparative analysis of the uncertainty of the calculation of tr. Source: Prepared by the Authors

CALCULATION OF THE UTCI INDEX

The UTCI index, defined as a multivariate function of air temperature, mean radiant temperature, air velocity, and water vapor pressure, is defined by (Equation 3):

$$UTCI=\int(t_a, t_r, v_a, P) \quad \text{(Equation 3)}$$

Where t_a is the air temperature, t_r is the mean radiant temperature, v_a is the air speed, and P is the water vapor pressure (hPa). The values of t_a and RH were obtained directly by the Delta OHM HD32.3 sensor, while *P* was calculated by means of (Equation 4):

$$P = \left(\frac{HR}{100}\right) \text{ x } 0{,}6108 \text{ x} \exp\left(\frac{(17{,}27 \times t_a)}{(t_a + 237.3)}\right) \quad \text{(Equation 4)}$$

Where *P* is expressed in hectopascals, (Equation 5):

$$hP = \frac{P}{100} \quad \text{(Equation 5)}$$

As far as the v_a is concerned, although the classic formulation of the UTCI uses the wind speed referred to 10 m high (Bröde et al., 2012), in this study, the speed measured in situ at 1.55 m above ground level was used, since the evaluation was carried out on a pedestrian scale under the shading systems. Recent studies indicate that the standard wind treatment may not adequately represent the airflow in the urban pedestrian layer and that the meteorological variables used in its calculation should originate from that same scale of human exposure (Read et al., 2025). The UTCI values were calculated using a computational implementation available on the UTCI-COST Action 730 web platform, based on the formulation proposed by Bröde et al. (2012).

DATA VALIDATION AND ANALYSIS

The quantification of the combined uncertainty margin for t_r and the UTCI was performed in accordance with international guidelines (Bureau International des Poids et Mesures [BIPM], 2008). The standard uncertainties of each input variable were determined from the maximum allowable errors specified in the manufacturer's technical datasheets (Table 2), assuming a rectangular probability distribution.

Because the equations of t_r from the norm ISO 7726:2025 and the UTCI polynomial are complex and non-linear formulas, the error propagation was solved as a coupled system. This approach links the UTCI directly to the instrument's primary readings, avoiding duplication of variance when evaluating the intermediate variables. The sensitivity coefficients for each parameter were numerically approximated, point by point, for the 478 observations in the database using the central finite-difference method. Finally, the total combined uncertainty was obtained by the quadrature total of the weighted individual errors.

Regarding the measurements, since they were carried out in the same environment and under simultaneous conditions, the data were analyzed as paired time series, which allows direct comparison of the values recorded at each instant. Firstly, a descriptive analysis of the measured variables was conducted, considering the average and maximum values and their hourly evolution within the study period (11 am to 4 pm), to identify thermal behavior patterns under high solar radiation exposure. Secondly, variations between paired measurements over time were evaluated using paired comparisons, which allow the identification of systematic variations associated with vegetation-based and artificial shading. Finally, differences between the tr values recorded and the UTCI index values were analyzed, due to their relevance in the characterization of outdoor thermal comfort.

MARGIN OF UNCERTAINTY

Based on the metrological analysis of coupled propagation (BIPM, 2008) applied to the 478 observations of each measurement condition, the final standard combined uncertainty ($u_{c)}$ [°C] for

Measurement condition	Average combined uncertainty (c) [°C]	Minimum uncertainty (uc max) [°C]	Maximum uncertainty (ucmax) [°C]	Final expanded uncertainty (U) 95% Confidence [°C]
UTCI mesh	± 0,115	± 0,284	± 0,412	± 0,230
UTCI grapevine pergola	± 0,137	± 0,089	± 0,076	± 0,274

Table 4. Comparative analysis of the uncertainty in UTCI calculations. Source: Prepared by the Authors.

the results of t_r and of the UTCI can be reviewed in Table 3 and Table 4. The analysis of the margin of error shows that the accuracy of t_r depends on the chosen method. The natural convection model (calm air) is highly stable, with an average error of ±0.150 °C, while the forced convection model (with wind) raises the average error to between ±0.516 °C and ±0.747 °C due to the wind sensor. The latter method becomes unstable in absolute calm (less than 0.1 m/s), the point error being triggered at ±2.215 °C. Despite this, the UTCI maintains an average error of less than ±0.137 °C and a definitive total error of less than ±0.274 °C (with 95% confidence). This stability occurs because the system compensates for errors internally: the direct cooling of the wind on the human body is opposed by the indirect effect on the globe thermometer, which balances the sensor's deviations in the final result. This supports the instrumental relevance and the calculation procedure for the comparative analysis developed within the study's exploratory scope.

RESULTS AND DISCUSSION

INITIAL METEOROLOGICAL DATA

During the monitoring period (March 01-14, 2024), the meteorological conditions recorded between 11 am and 4 pm show relatively stable behavior, with limited variation between days and consistent differences between the two measurement conditions (Table 5). The t_a under the mesh has daily average values ranging from 22.6 °C to 28.3 °C, while under the grapevine pergola, it varies from 21.1 °C to 26.5 °C. On all recorded days, the air temperature under the grapevine pergola is lower than that under the mesh, with differences ranging from approximately 1.3 °C to 2.0 °C. The differences between the two conditions were consistently maintained throughout the period, with higher values in the mesh condition.

Regarding the RH, the values recorded under the shading mesh are between 31.2% and 46.8%, while under the grapevine pergola, they range between

Day	ta (°C) mesh	tg (°C) mesh	va (m/s) mesh	HR (%) mesh	ta (°C) grapevine pergola	tg (°C) grapevine pergola	va (m/s) grapevine pergola	HR (%) grapevine pergola
01-03-2024	28,2	30,4	0,3	32,3	26,5	27,7	0,3	36,5
02-03-2024	26,5	28,3	0,4	31,2	25,0	26,1	0,4	34,8
03-03-2024	24,5	26,7	0,3	33,7	22,9	24,2	0,3	37,8
04-03-2024	26,2	28,4	0,2	35,0	24,5	25,8	0,2	38,8
05-03-2024	28,3	30,3	0,3	35,0	26,5	27,6	0,3	39,1
06-03-2024	26,8	28,9	0,2	42,8	25,3	26,5	0,2	47,2
07-03-2024	23,6	25,3	0,3	38,3	22,3	23,3	0,3	41,4
08-03-2024	24,1	25,8	0,3	38,9	22,9	23,8	0,3	42,0
09-03-2024	25,3	27,1	0,3	35,3	23,8	24,9	0,3	39,5
10-03-2024	22,6	24,2	0,2	46,8	21,1	22,1	0,2	51,1
11-03-2024	25,7	27,5	0,3	37,3	24,1	25,1	0,3	41,2
12-03-2024	26,2	27,7	0,3	40,5	24,7	25,6	0,3	44,0
13-03-2024	24,1	26,0	0,3	41,6	22,2	23,4	0,3	46,8
14-03-2024	25,0	26,6	0,4	36,2	23,2	24,3	0,4	40,7

Table 5. Average day values for each variable recorded. Source: Prepared by the Authors.

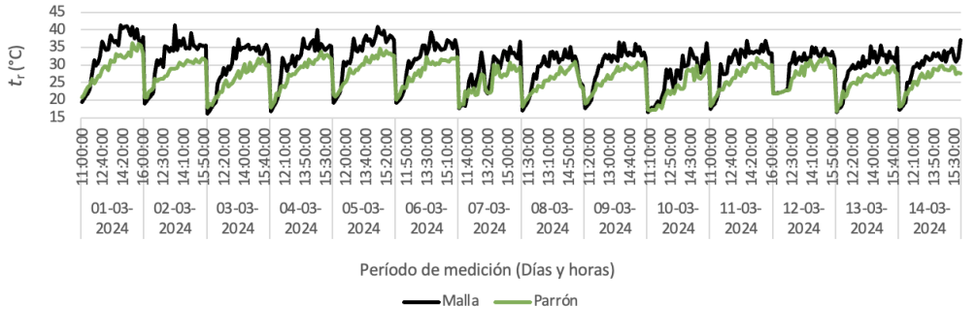


Figure 5. tr throughout the analyzed measurement period. Source: Prepared by the Authors.

Day	Mesh	Grapevine Pergola	Difference Mesh - Grapevine Pergola
01-03-2024	34.0	29.8	4.2
02-03-2024	32.3	28.1	4.2
03-03-2024	30.2	26.1	4.1
04-03-2024	31.2	27.9	3.3
05-03-2024	33.6	29.3	4.3
06-03-2024	32.0	28.3	3.7
07-03-2024	28.0	25.1	2.9
08-03-2024	28.6	25.3	3.3
09-03-2024	30.4	26.7	3.7
10-03-2024	26.6	23.4	3.1
11-03-2024	30.6	26.9	3.8
12-03-2024	30.0	27.4	2.6
13-03-2024	29.4	25.5	3.9
14-03-2024	29.7	26.2	3.5

Table 6. Daily average tr (°C) values of the analyzed schedule. Source: Prepared by the Authors.

34.8% and 51.1%. In all cases, relative humidity is higher under the grapevine pergola, with differences ranging from approximately 3% to 5%. v_a presents low and practically constant values in both conditions, between 0.2 and 0.4 m/s, with no appreciable differences between the measurement points due to the proximity of the sensors in both cases.

On the other hand, the t_g ranges from 24.2 °C to 30.4 °C under the shading mesh and from 22.1 °C to 27.7 °C under the grapevine pergola. The differences between the two conditions were consistently maintained throughout the period, with higher values under the mesh. Overall, the recorded meteorological conditions indicate higher temperatures and lower RH under the shading mesh, whereas the grapevine pergola shows lower temperatures and higher RH, with similar wind speeds in both configurations.

AVERAGE RADIANT TEMPERATURE BEHAVIOR

During the analysis period, t_r has constant differences between the two evaluated conditions. The maximum temperature was reached on 01-03-2024 at 2:10 pm, with 41.3 °C under the mesh, while the space under the grapevine pergola was 33 °C, a difference of 8.3 °C. Meanwhile, the maximum temperature under the grapevine pergola was recorded one hour later, at 3:10 pm, at 36.2 °C, while the mesh recorded 40.8 °C, a difference of 4.6 °C (Figure 5). On the other hand, the maximum average daily value under the mesh reaches 34 °C, while under the grapevine pergola it is 29.8 °C, resulting in a difference of 4.2 °C, both observed on 01-03-2024. Consistently lower values are presented under the grapevine pergola throughout the period (Table 6).

Measurement time	Mesh	Grapevine Pergola	Difference Mesh - Grapevine Pergola
11:00:00	18.0	19.0	-1.0
11:30:00	20.2	21.8	-1.6
12:00:00	27.8	23.5	4.3
12:30:00	30.1	25.3	4.8
13:00:00	31.3	26.6	4.7
13:30:00	33.5	27.8	5.7
14:00:00	33.8	29.1	4.7
14:30:00	34.7	29.8	4.9
15:00:00	34.3	30.3	4.0
15:30:00	34.6	30.7	3.9
16:00:00	33.8	29.8	3.9

Table 7. tr (°C) values every 30 minutes on an average day. Source: Prepared by the Authors.

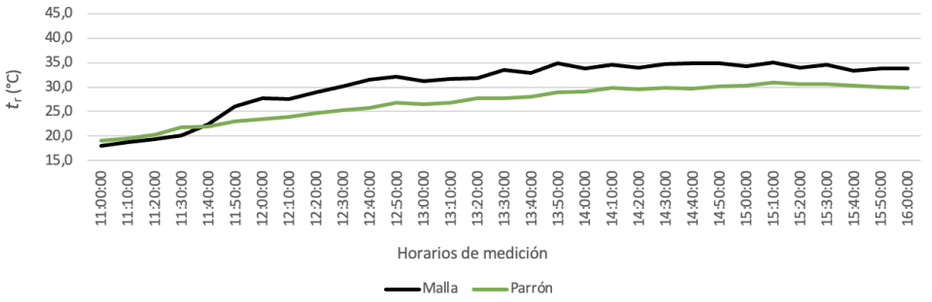


Figure 6. Behavior of tr on an average day. Source: Prepared by the authors.

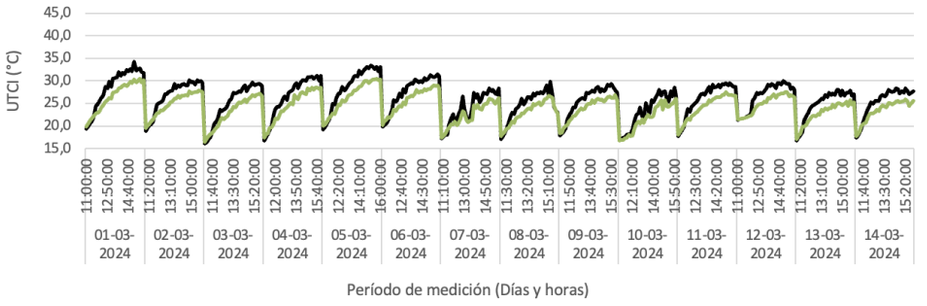


Figure 7. UTCI index over the analyzed measurement period. Source: Prepared by the authors.

The analysis of the average day (Table 7 and Figure 6) reveals clear time dependence. In the early morning intervals (11 am - 11:30 am), the t_r under the mesh is slightly lower than that recorded under the grapevine pergola (up to 1.7 °C). From 12 pm, this relationship is reversed in a sustained way: the t_r under the mesh consistently exceeds that of the grapevine pergola, with differences that scale to reach values between 4 and 5.9 °C between 1 pm and 3 pm, coinciding with the highest incidence of direct solar radiation. From 3:20 pm to 4 pm, the gap narrows, dropping to a difference between 3.9 and 3.1 °C.

UTCI INDEX BEHAVIOR

During the analysis period, the UTCI presents constant differences between the two evaluated conditions. The maximum temperature was reached on 01-03-2024, with 34.2 °C under the mesh at 3:10 pm, while the space under the grapevine pergola was at 30.3 °C,

Day	Mesh	Grapevine Pergola	Difference Mesh - Grapevine Pergola
01-03-2024	28,7	26,5	2,2
02-03-2024	26,8	25,0	1,9
03-03-2024	25,0	23,1	1,9
04-03-2024	26,7	24,6	2,1
05-03-2024	28,8	26,6	2,2
06-03-2024	27,7	25,8	1,9
07-03-2024	24,0	22,5	1,5
08-03-2024	24,6	23,0	1,6
09-03-2024	25,7	23,9	1,8
10-03-2024	23,3	21,7	1,7
11-03-2024	26,2	24,2	2,0
12-03-2024	26,7	24,9	1,8
13-03-2024	25,0	22,9	2,1
14-03-2024	25,4	23,4	1,9

Table 8. Average UTCI (°C) values of the analyzed daily times. Source: Prepared by the Authors.

Day	Mesh	Grapevine Pergola	Difference Mesh - Grapevine Pergola
11:00:00	18,1	18,4	-0,4
11:30:00	19,6	20,1	-0,5
12:00:00	23,1	21,5	1,7
12:30:00	25,0	22,8	2,2
13:00:00	26,1	23,8	2,3
13:30:00	27,4	24,8	2,6
14:00:00	28,3	25,7	2,6
14:30:00	29,1	26,3	2,7
15:00:00	29,4	26,8	2,6
15:30:00	29,4	27,1	2,4
16:00:00	28,7	26,9	1,9

Table 9. UTCI (°C) every 30 minutes on an average day. Source: Prepared by the Authors.

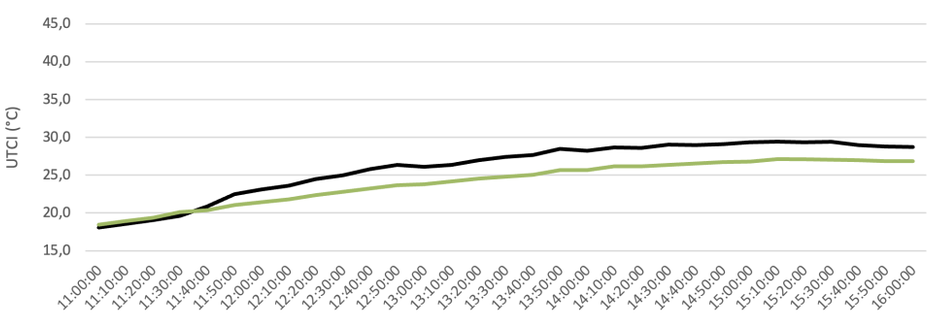


Figure 8. UTCI behavior on an average day. Source: Prepared by the Authors.

a difference of 3.9 °C. Meanwhile, the maximum reached under the grapevine pergola was recorded 30 minutes later, at 3:40 pm, at 30.5 °C, while the mesh recorded 32.8 °C, a 2.3 °C difference (Figure 7). On the other hand, the average value under the shading mesh is 26.0 °C, while under the shade is 24.1 °C. The average difference between the two conditions is 1.9 °C, with lower values consistently recorded under the grapevine pergola throughout the analyzed period.

In terms of maximum average daily values, the UTCI reaches 28.8 °C under the mesh and 26.6 °C under the grapevine pergola. The maximum observed difference between the two conditions is about 2.2 °C, observed on 05-03-2024 (Table 8).

The analysis of the average day (Table 9 and Figure 8) reveals a clear time dependence. In the first intervals of the morning (11:00 – 11:30 am), the UTCI under the mesh is slightly lower than that recorded under the grapevine pergola, by values between 0.4 and 0.5 °C. From 11:40 am onward, this relationship is reversed in a sustained way: the UTCI under the mesh consistently exceeds that of the grapevine pergola, with differences of over 2°C in 67.74% of the average records, reaching a maximum of 2.9 °C at 13:50. The gap begins to decrease from 15:50, which makes a difference of 1.9 °C.

The hourly behavior of the UTCI shows an increasing trend between 11:00 am and 3:30 pm, followed by stabilization or a slight decrease toward 4:00 pm in both conditions. The differences between the grapevine pergola and the mesh are maintained throughout the hourly interval, with a relatively constant separation between the curves. The greatest differences are observed in the central section of the analyzed period, coinciding with the hours when the t_r recorded higher values, between 12:30 and 2:30 pm.

Depending on the UTCI index ranges, the values recorded under the shading mesh are mostly in the thermal stress range due to heat during the study period, reaching strong thermal stress in some cases. On the other hand, the values under the grapevine pergola are distributed between the categories “thermal stress due to heat” and “without thermal stress”, with a higher frequency of values in the latter (Figure 9).

The data collected are consistent with those indicated by Watanable et al. (2014), Kusaka et al. (2022), and Chàfer et al. (2020), who agree on the high efficiency of horizontal vegetation-based covers to mitigate thermal stress on a human scale by controlling the radiative environment and evaporative cooling, which reinforces the

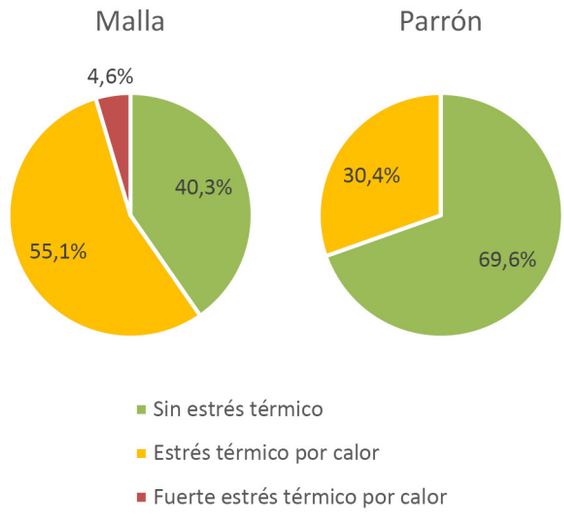


Figure 9. UTCI thermal stress frequencies. Source: Prepared by the Authors.

potential of the grapevine pergola as a passive thermal conditioning and climate adaptation strategy for intermediate spaces and backyards in temperate climates.

CONCLUSION

The results of this study show that the grapevine pergola creates an outdoor space that is thermally more favorable than the artificial shading mesh. During the analyzed period, the grapevine pergola systematically recorded lower t_a (reductions of between 1.3°C and 2.0°C) and higher RH levels (between 3% and 5% more) compared to the mesh. In terms of thermal comfort, the grapevine pergola maintained an average UTCI of 24.1 °C, compared to 26.0 °C for the mesh, representing an average reduction of 1.9 °C and maximum daily differences of up to 2.2 °C. These differences were interpreted in light of the uncertainty analysis incorporated into the study, which allowed for contextualizing the margins of error associated with instrumental measurements and the calculation of derived indicators such as the mean radiant temperature and the UTCI.

The decrease in the t_r is identified as the determining factor in improving comfort. Under the grapevine pergola, the t_r was consistently lower, with average daily differences between 2.6 °C and 4.3 °C relative to the mesh, reaching up to 5.9 °C during the hours of greatest radiative load. These findings suggest that not all shades offer the same performance: while the mesh acts as an inert system limited to solar obstruction, the grapevine pergola functions as an

active thermal regulator that combines shading with bioclimatic processes such as evapotranspiration and lower surface temperatures.

These results reinforce the potential of the grapevine pergola as a passive thermal-conditioning and climate-adaptation strategy for intermediate spaces and backyards in temperate climates. However, its implementation faces practical limitations such as growing time, the need for structural support, and the dependence on foliage density. Also, given the study's exploratory experimental approach, a methodological limitation is the proximity of the measurement points, which could lead to slight moisture transfer from the grapevine pergola to the mesh area. In addition, the mesh condition may have been partially influenced by the vegetation of the immediate environment. Therefore, the results should be understood as localized evidence for two nearby shading conditions, avoiding generalizations not supported by the experimental design.

As future lines of research, it is suggested to analyze the impact of these shaders on adjacent indoor enclosures and to evaluate how plant species variability influences the magnitude of cooling, in order to optimize their use as a tool for urban resilience at a domestic scale. Also, it should be considered that the measurements were made in March; future studies should evaluate warmer summer periods, during which the observed differences could be more pronounced, especially in the UTCI. It is also recommended to consider more physically independent shading scenarios, equivalent shading surfaces, and greater separation between measurement points to strengthen comparability between vegetation-based and inert setups.

CONTRIBUTION OF AUTHORS CRediT

Conceptualization, N.A.; Data curation, R.F.; Formal analysis, N.A.; Acquisition of financing, N.A.; Research, N.A., R.F., DC; Methodology, N.A., R.F, DC; Project management, N.A.; Resources, N.A., R.F.; Software. R.F.; Supervision, N.A.; Validation, N.A., R.F.; Visualization, R.F., D.C.; Writing - original draft, N.A., R.F., D.C.; Writing - revision and editing, N.A., D.C.

ACKNOWLEDGMENTS

This research was conducted within the framework of the Research Group on Environmental Comfort and Energy Poverty (CO-PE) of the University of Bio-Bio (GI2310945 code).

BIBLIOGRAPHIC REFERENCES

Aravena Alvarado, R. (Ed.). (2015). *Patrimonio vitivinícola: aproximaciones a la cultura del vino en Chile*. Ediciones Biblioteca Nacional. https://centropatrimonio.uc.cl/wp-content/uploads/2023/01/Patrimonio-vitivinicola-aproximaciones-a-la-cultura-del-vino-en-Chile-1.pdf

Arias-Jiménez, N., Trebilcock-Kelly, M., Figueroa-SanMartín, R., & González-Cáceres, A. (2026). Experimental evaluation of the impact of roofing materials and natural ventilation on attic overheating in a temperate Chilean climate. *Building Research & Information*, *54*(5), 573–587. https://doi.org/10.1080/09613218.2025.2607633

Arias Tapiero, J. C., Ortega, J., & Vasconcelos, G. (2025). A methodology for analysing the impact of contemporary transformation processes in vernacular built environments. Built Heritage, 9(1), 51. https://doi.org/10.1186/s43238-025-00220-0

Błażejczyk, K., Jendritzky, G., Bröde, P., Fiala, D., Havenith, G., Epstein, Y., Psikuta, A., & Kampmann, B. (2013). An introduction to the Universal Thermal Climate Index (UTCI). *Geographia Polonica, 86*(1), 5–10. https://doi.org/10.7163/GPol.2013.1

Bowler, D. E., Buyung-Ali, L., Knight, T. M., & Pullin, A. S. (2010). Urban greening to cool towns and cities: A systematic review of the empirical evidence. *Landscape and Urban Planning*, *97*(3), 147–155. https://doi.org/10.1016/j.landurbplan.2010.05.006

Bröde, P., Fiala, D., Błażejczyk, K., Holmér, I., Jendritzky, G., Kampmann, B., Tinz, B., & Havenith, G. (2012). Deriving the operational procedure for the Universal Thermal Climate Index (UTCI). *International Journal of Biometeorology*, *56*(3), 481–494. https://doi.org/10.1007/s00484-011-0454-1

Bureau International des Poids et Mesures [BIPM]. (2008). *Evaluation of Measurement Data - Guide to the Expression of Uncertainty in Measurement*. JCGM 100. https://www.bipm.org/documents/20126/2071204/JCGM_100_2008_E.pdf

Chàfer, M., Pisello, A. L., Piselli, C., & Cabeza, L. F. (2020). Greenery System for Cooling Down Outdoor Spaces: Results of an Experimental Study. Sustainability, 12(15), 5888. https://doi.org/10.3390/su12155888

COST European Cooperation in Scientific and Technical Research. (20 de abril de 2026) *COST Action 730 on UTCI*. UTCI. https://www.utci.org/utci_calc.php

De Cristo, E., Evangelisti, L., Barbaro, L., De Lieto Vollaro, R., & Asdrubali, F. (2025). A Systematic Review of Green Roofs' Thermal and Energy Performance in the Mediterranean Region. *Energies*, *18*(10), 2517. https://doi.org/10.3390/en18102517

Servicios Climáticos (20 de marzo de 2026) Temperatura Histórica Mensual de la Estación. Dirección General de Aeronáutica Civil. https://climatologia.meteochile.gob.cl/application/historico/temperaturaHistoricaMes/360047/3

Elgheznawy, D., & Eltarabily, S. (2021). The impact of sun sail-shading strategy on the thermal comfort in school courtyards. *Building and Environment, 202*, 108046. https://doi.org/10.1016/j.buildenv.2021.108046

Gherri, B. (2023). The Role of Urban Vegetation in Counteracting Overheating in Different Urban Textures. *Land*, *12*(12), 2100. https://doi.org/10.3390/land12122100

Guerrero-Rubio, J., Sendra, J. J., Fernández-Agüera, J., & Oteiza, I. (2017). Modelos predictivos del consumo energético de climatización asociado a soluciones de fachadas en Madrid a partir de la monitorización en módulos de ensayo. *Informes de La Construcción*, *69*(548), e225. https://doi.org/10.3989/id.54794

Intergovernmental Panel on Climate Change [IPCC]. (2023). Technical Summary. In *Climate Change 2021 – The Physical Science Basis: Working Group I Contribution to the Sixth Assessment Report of the Intergovernmental Panel on Climate Change* (pp. 35–144). frontmatter, Cambridge: Cambridge University Press. https://doi.org/10.1017/9781009157896.002

Jim, C. Y. (2015). Thermal performance of climber greenwalls: Effects of solar irradiance and orientation. *Applied Energy*, *154*, 631–643. https://doi.org/10.1016/j.apenergy.2015.05.077

Kusaka, H., Asano, Y., & Kimura, R. (2022). Wisteria trellises and tents as tools for improved thermal comfort and heat stress mitigation: Meteorological, physiological, and psychological analyses considering the relaxation effect of greenery. *Meteorological Applications*, *29*(1), e2046. https://doi.org/10.1002/met.2046

Lee, H., Park, S., & Mayer, H. (2025). Approach for the vertical wind speed profile implemented in the UTCI basics blocks UTCI applications at the urban pedestrian level. *International Journal of Biometeorology*, *69*(3), 567–580. https://doi.org/10.1007/s00484-024-02835-x

Lee, I., Voogt, J. A., & Gillespie, T. J. (2018). Analysis and Comparison of Shading Strategies to Increase Human Thermal Comfort in Urban Areas. *Atmosphere, 9*(3), 91. https://doi.org/10.3390/atmos9030091

Liu, T., Wang, Y., Zhang, L., Xu, N., & Tang, F. (2025). Outdoor Thermal Comfort Research and Its Implications for Landscape Architecture: A Systematic Review. *Sustainability*, *17*(5), 2330. https://doi.org/10.3390/su17052330

López-Cabeza, V. P., Diz-Mellado, E., Rivera-Gómez, C. A., & Galán-Marín, C. (2022). Shade and Thermal Comfort in Courtyards: Experimental versus Simulation Results. *Buildings*, *12*(11), 1961. https://doi.org/10.3390/buildings12111961

MacIvor, J. S., & Margolis, L. (2015). Cooling of a south-facing wall using a double-skin green façade in a temperate climate. *ISHS Acta Horticulturae*, *1085,* 185–194. https://doi.org/10.17660/ActaHortic.2015.1085.30

Mihalakakou, G., & Romeos, A. (2026). Mean radiant temperature in outdoor urban environments: From radiative physics to data-driven and hybrid modelling frameworks. *Building and Environment*, *297*, 114595. https://doi.org/10.1016/j.buildenv.2026.114595

Nasr, Y., El Zakhem, H., Hamami, A. E. A., El Bachawati, M., & Belarbi, R. (2024). Comprehensive Assessment of the Impact of Green Roofs and Walls on Building Energy Performance: A Scientific Review. *Energies*, *17*(20), 5160. https://doi.org/10.3390/en17205160

Perini, K., & Magliocco, A. (2014). Effects of vegetation, urban density, building height, and atmospheric conditions on local temperatures and thermal comfort. *Urban Forestry & Urban Greening*, *13*(3), 495–506. https://doi.org/10.1016/j.ufug.2014.03.003

Salonen, T., Hollands, J., Sesto, E., & Korjenic, A. (2022). Thermal Effects of Vertical Greening in Summer: An Investigation on Evapotranspiration and Shading of Façade Greening in Vienna. *Buildings*, *12*(10), 1705. https://doi.org/10.3390/buildings12101705

Umishio, W., Ikaga, T., Fujino, Y., Ando, S., Kubo, T., Nakajima, Y., Kagi, N., Hoshi, T., Suzuki, M., Kario, K., Yoshimura, T., Yoshino, H., & Murakami, S. (2024). Spatial and temporal indoor temperature differences at home and perceived coldness in winter: A cross-sectional analysis of the nationwide Smart Wellness Housing survey in Japan. *Environment International*, *186*, 108630. https://doi.org/10.1016/j.envint.2024.108630

Wang, Y., Zhao, N., Yin, X., Wu, C., Chen, M., Jiao, Y., & Yue, T. (2023). Global future population exposure to heatwaves. *Environment International*, *178*, 108049. https://doi.org/10.1016/j.envint.2023.108049

Watanabe, S., Nagano, K., Ishii, J., & Horikoshi, T. (2014). Evaluation of outdoor thermal comfort in sunlight, building shade, and pergola shade during summer in a humid subtropical region. *Building and Environment*, *82*, 556–565. https://doi.org/10.1016/j.buildenv.2014.10.002

Wu, Z., Shi, Y., Ren, L., & Hang, J. (2024). Scaled outdoor experiments to assess impacts of tree evapotranspiration and shading on microclimates and energy fluxes in 2D street canyons. *Sustainable Cities and Society*, *108*, 105486. https://doi.org/10.1016/j.scs.2024.105486

Zhang, Y., Yang, Y., Zhang, L., Zhao, C., Yan, J., Liu, M., & Zhao, L. (2022). Seasonal variation in leaf area index and its impact on the shading effects of vertical green facades in subtropical areas. *Building and Environment*, *225*, 109629. https://doi.org/10.1016/j.buildenv.2022.109629

Zhao, Y., Zhao, K., Zhang, X., Zhang, Y., & Du, Z. (2024). Assessment of combined passive cooling strategies for improving outdoor thermal comfort in a school courtyard. *Building and Environment*, *252*, 111247. https://doi.org/10.1016/j.buildenv.2024.111247

Zheng, X., Wang, W., Chen, J., Chen, Q., Luo, S., Wang, H., Hu, W., & Pan, L. (2025). Influence of vertical greenery systems with different greenery coverage ratios on microclimate improvement in street canyons by scaled outdoor experiments. *Building and Environment*, *267*(Part B), 112158. https://doi.org/10.1016/j.buildenv.2024.112158

Edificio de Innovación
Universidad del Bío-Bío
Pego von Ellrichshausen
2021



BANMA 2025

Objeto singular Concepción